

**Alma Mater Studiorum – Università di Bologna**

Dottorato di Ricerca in

Meccanica e Scienze Avanzate dell'Ingegneria

Progetto n° 4 - Meccanica dei materiali e processi tecnologici

Ciclo XXIII

Settore scientifico disciplinare di appartenenza: ING-IND/18

**Integrated approaches for designing and  
optimizing thermal plasma processing for  
metal cutting and material treatment**

Presentata da: Alessia Concetti

Coordinatore Dottorato

Prof. Giangiacomo Minak

Relatore

Prof. Vittorio Colombo

Esame finale anno 2011



# Contents

0.1 Introduction.....	6
Part I.....	11
Plasma arc cutting .....	11
Evolution of the plasma arc cutting technology.....	11
The plasma arc cutting process .....	13
Main issues in plasma arc cutting technology .....	16
Cutting quality.....	16
Electrode erosion.....	22
Double arcing.....	26
References.....	29
Chapter 1 .....	30
Design Oriented Simulation and experimental tests of Plasma Arc Cutting torches.....	30
1.1 Physical-Mathematical Model .....	33
1.2 Optimization of plasma arc cutting of mild steel thin plates through experiments and 2D simulations .....	35
1.2.1 Description of the experiments .....	35
1.2.2 Results.....	36
1.3 Optimization of the consumables service life of a mono-gas plasma torch through experiments and 2D simulations .....	51
1.3.1 Experimental set-up .....	51
1.3.2 Torch and process design.....	52
1.3.3 Results and discussion .....	52
1.4 Optimization of the components design of a mono-gas plasma torch through experiments and 3D simulations.....	61
1.4.1 Experimental set-up .....	61
1.4.2 Results.....	61

Conclusions and future developments .....	65
References .....	68
Chapter 2 .....	71
2.1 Experimental analysis of the behaviour of high current electrodes in plasma arc cutting during first cycles .....	77
2.1.1 Experimental set-up .....	78
2.1.2 Experimental procedure .....	79
2.1.3 High speed imaging analysis of the behaviour of Hf cathodes .....	80
2.1.4 Behaviour and analysis of electrodes with no initial recess .....	81
2.1.5 Behaviour of electrodes with initially optimized recess .....	83
Conclusions and future developments .....	89
References .....	91
Chapter 3 .....	92
High Speed Camera Imaging and Schlieren Imaging diagnostic in plasma arc cutting .....	92
3.1 Diagnostic based on high-speed video imaging and flow visualization techniques .....	95
3.2 Literature analysis and first results on High Speed Imaging in Plasma Arc Cutting .....	96
Review on high speed imaging and flow visualization methods in plasma arc cutting .....	96
3.2.1 Visualization of phenomena that take place at the plasma cutting front .....	96
3.2.2 Visualization of shock waves at the nozzle exit, dross formation, arc root attachment in the <i>kerf</i> , double arcing phenomena .....	99
3.2.3 Visualization of cathode erosion phenomena .....	102
New developments .....	104
3.2.4 Experimental setup and HSC operating conditions .....	104
3.2.5 Effects of different operating parameters on pilot arc behavior .....	106
3.2.6 Cathode surface images during pilot arcing .....	107
3.2.7 Images of non-destructive double arcing during the transferring phase .....	110
3.2.8 Tracking of ejected particles from the nozzle orifice .....	111
3.2.9 Piercing phase .....	112

3.3 High speed imaging investigation of transition phenomena in the pilot arc phase in Hf cathodes for PAC .....	130
3.3.2 Experimental set-up .....	132
3.3.3 Results.....	134
3.3.4 Comments on the results .....	137
3.4 Multiple View and Tomographic Reconstruction of Pilot Arcing Transients .....	139
3.4.1 Experimental set - up .....	139
3.4.2 Results.....	139
3.5 Schlieren Imaging experimental set-up.....	142
3.6 Statistical Analysis of High-Speed Schlieren Imaging in PAC .....	147
3.6.1 Experimental set-up .....	147
3.6.1Results.....	147
Conclusions and future developments .....	150
References.....	152
Part II.....	155
RF induction coupled plasma torches .....	155
Working principle .....	155
Plasma discharge ignition .....	156
RF torch operation parameters.....	156
Modern architecture of the RF torch.....	164
The Inductively Coupled Plasma System installed at the UNIBO - DIEM laboratories ....	167
References.....	168
Chapter 1 .....	169
Thermal plasma in-flight waste treatment .....	169
1.1 RF thermal plasma treatment of waste glass and its reutilization in composite materials.	171
1.1.2 Pre-treatment of waste glass and chemical-physical analysis.....	171
1.1.3 Inductively coupled thermal plasma treatment of waste-glass .....	172
1.1.4 Reuse of purified and spheroidized waste glass in thermoplastic polymers.....	173

1.2 RF thermal plasma vitrification of incinerator bottom and fly ashes with waste glasses from fluorescent lamps .....	178
1.2.1 Experimental set-up .....	180
1.2.3 Plasma treatment .....	181
1.2.4 Characterization of the obtained glassy slags .....	183
Conclusions and future developments .....	187
References .....	188
Chapter 2 .....	190
Scaling-up of ICP technology for continuous production of Metallic nanopowders for Battery Applications .....	190
2.1 The SIMBA project.....	190
2.2. Characterization of the lab-scale ICPT system at EMPA .....	191
Conclusions and future developments .....	196
References .....	197

## 0.1 Introduction

The activities reported in this thesis have been performed during my three years Ph.D. course, as a member of the Group for Industrial Applications of Plasmas, and are focused on the design and optimization of thermal plasmas devices and thermal plasmas assisted processes by means of an integrated approach that jointly uses experiments, diagnostics and numerical simulation.

The first part of this work concerns plasma arc cutting (PAC) torches, studied in different geometric configurations and operating conditions, and their application cutting of metallic plates.

After an introduction on plasma arc cutting devices, the first chapter is about 2D and 3D modeling of plasma arc cutting devices, used in conjunction with experimental test, for their design and optimization. The results here described has been presented in the following congresses:

- V. Colombo, A. Concetti, E. Ghedini, F. Rotundo, P. Sanibondi, S. Dallavalle, M Vancini, Plasma arc cutting technology: simulation and experiments, Proceedings of the XVIII International Conference on Gas Discharges and Their Applications-GD 2010, (Editor Prof. K.-D. Weltmann), GD 2010 Local Organizing Committee, Greifswald, 2010, pp. 18-25 (ISBN: 0-9539105-4-7).
- G. Cantoro, V. Colombo, A. Concetti, E. Ghedini, P. Sanibondi, F. Zinzani, F. Rotundo, S. Dallavalle, M. Vancini. (2011). Plasma arc cutting technology: simulation and experiments. JOURNAL OF PHYSICS. CONFERENCE SERIES. 11th European Conference on High-Technology Plasma Processes (HTPP 11). Brussels, Belgium. 27 June–2 July 2010. vol. 275, pp. 012008-1 - 012008-10 ISSN: 1742-6588.
- Colombo, A. Concetti, E. Ghedini, S. Dallavalle, M. Vancini. (2008). Modelling and comparison of different design solutions and experimental results for dc transferred arc plasma cutting torches. Invited talk. *4th International Scientific Conference of the Military Technical College - 13th International Conference on Applied Mechanics and Mechanical Engineering*. Il Cairo - Egitto. 27-29 May 2008.
- V. Colombo, A. Concetti, E. Ghedini, S. Dallavalle, M. Vancini, Optimization of plasma arc cutting of mild steel thin plates, 15-19 June 2008 Congress 35th IEEE International Conference on Plasma Science (ICOPS2008), Karlsruhe, Germany.
- V. Colombo, A. Concetti, E. Ghedini, S. Dallavalle, M. Vancini, Optimization of plasma arc cutting of mild steel thin plates, 7-11 July 2008 Congress 10th Biennial European Plasma Conference (HTTP-10), Patras, Greece.
- V. Colombo, A. Concetti, E. Ghedini, S. Dallavalle, M. Vancini. (2007). Understanding Plasma Fluid Dynamics Inside Plasma Torches Through Advanced Modeling. *16th IEEE International Pulsed Power Conference*. 16th IEEE International Pulsed Power Conference. Albuquerque, New Mexico. June 17-22, 2007.
- V. Colombo, A. Concetti, E. Ghedini, S. Dallavalle, M. Vancini. (2007). Modelling and Comparison of Different Design Solutions for DC Transferred Arc Plasma Cutting Torches. *18th*

*International Symposium on Plasma Chemistry Abstract and Full-Papers CD*. 18th International Symposium on Plasma Chemistry - ISPC18. Kyoto University, Japan. 26-31 August 2007.

- V. Colombo, A. Concetti, E. Ghedini, F. Rotundo, P. Sanibondi, S. Dallavalle, Plasma arc cutting technology: simulation and experiments, XVIII International Conference on Gas Discharges and Their Applications-GD 2010, Greifswald, 2010. Invited talk.
- G. Cantoro, V. Colombo, A. Concetti, E. Ghedini, P. Sanibondi, F. Zinzani, Plasma arc cutting technology: simulation and experiments, High Technology Plasma Processes – HTPP11, Brussels, 2010.
- V. Colombo, A. Concetti, E. Ghedini. (2011). Design oriented simulation of the behavior of PAC consumables and experimental validation of results. Planned publication on *Proceedings ISPC 20, Philadelphia, July 24-29, 2011*. 20th International Symposium on Plasma Chemistry.

and published as articles in:

- Vittorio Colombo, Alessia Concetti, Emanuele Ghedini, Silvano Dallavalle, Mauro Vancini *Understanding Plasma Fluid Dynamics Inside Plasma Torches Through Advanced Modeling*, IEEE Transaction on Plasma Science, Vol. 36, No.2, pp. 389-402 (2008)
- Colombo V, Concetti A, Ghedini E, Dallavalle S, Fazzioli R, and Vancini M *Optimization of plasma arc cutting of mild steel thin plates*, Journal of High Temperature Material Processes, 13 (2009) 267-285.
- V Colombo, A Concetti, E Ghedini *Design oriented simulation of consumables in PAC and experimental validation of results* in press on Plasma Sources Sci. Technol., 2011.
- V Colombo, A Concetti, E Ghedini *3D design oriented simulation of plasma arc cutting phenomena* Submitted for publication on IEEE Trans. Plasma Sci, 6th Triennial Special Issue on Images in Plasma Science.

Moreover, three patents have been deposited on this topic:

- Colombo Vittorio, Ghedini Emanuele, Dallavalle Silvano, Vancini Mauro, Concetti Alessia, Fazzioli Riccardo, “DIFFUSORE PER TORCE PER IL TAGLIO AL PLASMA” Cebora S.P.a. BO2010A000223 (2010)
- Colombo Vittorio, Ghedini Emanuele, Dallavalle Silvano, Vancini Mauro, Concetti Alessia, Fazzioli Riccardo, “TORCIA PER IL TAGLIO AL PLASMA” Cebora S.P.a. BO2010A000224 (2010)
- Colombo Vittorio, Ghedini Emanuele, Dallavalle Silvano, Vancini Mauro, Concetti Alessia, Fazzioli Riccardo, “TORCIA MONOGAS PER IL TAGLIO AL PLASMA” Cebora S.P.a. BO2010A000492 (2010)

In the second chapter innovative technological processes for the optimization of the electrodes performance, in terms of its service life, are presented. Some of the results here described has been presented in the following congresses:

- V. Colombo, A. Concetti, E. Ghedini, S. Dallavalle, M. Vancini, F. Rotundo, C. Chiavari. (2009). Experimental analysis of the behaviour of high current electrodes in plasma arc cutting during first cycles. *Proceedings ISPC 19, Bochum, 2009*. 19th International Symposium on Plasma Chemistry. Ruhr-University Bochum, Germany. July 27 - 31 2009. (pp. P1.5.30). BOCHUM: International Plasma Chemistry Society.
- V. Colombo, A. Concetti, E. Ghedini, S. Dallavalle, M. Vancini, F. Rotundo, C. Martini. (2009). Recent advancements in Plasma Arc Cutting Research at UNIBO. Part II: Experimental Analysis of the Behaviour of High Current Electrodes During First Cycles. *International Round Table on the Characterization of Thermal Plasmas for Industrial Applications - Book of Abstracts*. International Round Table on the Characterization of Thermal Plasmas for Industrial Applications. Alexandria, Egypt. 24-28 October 2009.

and published as articles in:

- V Colombo, A Concetti, E Ghedini, F Rotundo, S Dallavalle *Experimental analysis of the behaviour of high current electrodes in plasma arc cutting during first cycles* Plasma Sources, Science and Technology, Vol. 19 doi: 10.1088/0963-0252/19/6/065023 (2010)

The third chapter is about high speed and schlieren imaging in plasma arc cutting; after a literature review on this field, some new studies are presented. The results here described has been presented in the following congresses:

- V. Colombo, A. Concetti, E. Ghedini, S. Dallavalle, M. Vancini. (2009). High Speed Imaging of transient phenomena in PAC. *Proceedings ISPC 19, Bochum, 2009*. 19th International Symposium on Plasma Chemistry. Ruhr-University Bochum, Germany. July 27 - 31 2009. (vol. 1, pp. O2.09).
- V. Colombo, A. Concetti, E. Ghedini, S. Dallavalle, M. Vancini. (2008). High Speed Imaging of Pilot Arcing and Piercing in Plasma Arc Cutting. ISFV13 - 13th International Symposium on Flow Visualization FLUVISU12 - 12th French Congress on Visualization in Fluid Mechanics. Nice, France. July 1-4, 2008.
- V. Colombo, A. Concetti, E. Ghedini, S. Dallavalle, M. Vancini, High Speed Imaging of Pilot Arcing and Piercing in PAC, 7-11 luglio 2008 Congress 10th Biennial European Plasma Conference (HTTP-10), Patraso, Grecia.
- V. Colombo, A. Concetti, E. Ghedini, V. Nemchinsky, High speed imaging investigation of transition phenomena in the pilot arc phase in hf cathodes for PAC, Gordon Conference on Plasma Processing Science, New London, NH, USA, 2010.
- Colombo, A. Concetti, E. Ghedini, P. Sanibondi, S. Dallavalle, M. Vancini. (2009). Recent Advancements in Plasma Arc Cutting Research at UNIBO. Part I: High Speed Imaging of Transients Phenomena and Schlieren Photography. *International Round Table on the*

*Characterization of Thermal Plasmas for Industrial Applications - Book of Abstracts.* International Round Table on the Characterization of Thermal Plasmas for Industrial Applications. Alexandria, Egypt. 24-28 October 2009.

- V. Colombo, A. Concetti, E. Ghedini, P. Sanibondi, F. Rotundo, S. Dallavalle, M. Vancini. (2011). Advances in plasma arc cutting technology: the experimental part of an integrated approach. Invited talk. Submitted for publication on *Proceedings ISPC 20, Philadelphia, July 24-29, 2011*. 20th International Symposium on Plasma Chemistry.

and published as articles in:

- Vittorio Colombo, Alessia Concetti, Emanuele Ghedini, Silvano Dallavalle, Mauro Vancini *High-Speed Imaging of Pilot Arcing and Piercing in PAC*, IEEE Trans. Plasma Sci, **36**, 4 part 1, 1042-1043, 5th Triennial Special Issue on Images in Plasma Science (2008).
- V Colombo, A Concetti, E Ghedini, S Dallavalle and M Vancini *High speed imaging in plasma arc cutting: a review and new developments*, Review Paper, Plasma Sources Science and Technology, Vol. 18, doi:10.1088/0963-0252/18/2/023001 (2009).
- V Colombo, A Concetti, E Ghedini, V Nemchinsky *High speed imaging investigation of transition phenomena in the pilot arc phase in Hf cathodes for PAC* Plasma Sources, Science and Technology, Vol. 19 doi:10.1088/0963-0252/19/6/065025 (2010)
- G Cantoro, V Colombo, A Concetti, E Ghedini, P Sanibondi, F Zinzani *Statistical Analysis of High-Speed Schlieren Imaging in PAC* Submitted for publication on IEEE Trans. Plasma Sci, 6th Triennial Special Issue on Images in Plasma Science.
- V Colombo, A Concetti, E Ghedini, P Sanibondi, M Gherardi, M Bodelli and G Cantoro *High-Speed Imaging in PAC: Multiple View and Tomographic Reconstruction of Pilot Arcing Transients* Submitted for publication on IEEE Trans. Plasma Sci, 6th Triennial Special Issue on Images in Plasma Science.

Inductively coupled plasma torch (ICPTs) for treatment of materials and waste vitrification are considered in the second part of this work. After an outline of the RF ICPTs and their industrial applications, the first chapter is about waste treatment. Some of the results here described has been presented in the following congresses:

- Barbieri, L., Lancellotti, I., Pellacani, G.C. ; “Vitrification of municipal waste incinerator bottom ash and product properties”, (1998), Proceedings of XVIII International Congress on Glass, The American Ceramic Society, 21-30
- V. Colombo, A. Concetti, E. Ghedini, F. Andreola, L. Barbieri, E. Fabbri, I. Lancellotti, P. Pozzi. (2007). RF Thermal Plasma Treatment of Waste Glass: Design of the Experiment with 3D Modelling and Glass Reutilization in Composite Materials. *18th International Symposium on Plasma Chemistry Abstract and Full-Papers CD*. 18th International Symposium on Plasma Chemistry - ISPC18. Kyoto University, Japan. 26-31 august 2007.

- V. Colombo, E. Ghedini, G. Masini, D. Russo, F. Andreola, L. Barbieri, E. Fabbri, I. Lancellotti, P. Pozzi. (2006). RF Thermal Plasma Treatment of Waste Glass and its Reutilization in Composite Materials. *High Technology Plasma Processes 9 - HTPP9, St. Petersburg*
- V. Colombo, A. Concetti, E. Ghedini, M. Gherardi, P. Sanibondi, B. Vazquez, D. Zanini, L. Barbieri, I. Lancellotti. (2011). RF thermal plasma vitrification of incinerator bottom and fly ashes with waste glasses from fluorescent lamps. Submitted for publication on *Proceedings ISPC 20, Philadelphia, July 24-29, 2011*. 20th International Symposium on Plasma Chemistry.

and published as articles in

- V. Colombo, E. Ghedini, G. Masini, D. Russo, F. Andreola, L. Barbieri, E. Fabbri, I. Lancellotti, P. Pozzi. (2006). *Journal of High Temperature Material Processes*, 10, 2, 207
- V Colombo, A Concetti, E Ghedini, M Gherardi and P Sanibondi (2011) *3D Time-Dependent Large Eddy Simulation of Turbulent Flows in an Inductively Coupled Thermal Plasma Torch with Reaction Chamber* Submitted for publication on IEEE Trans. Plasma Sci, 6th Triennial Special Issue on Images in Plasma Science.

The second chapter is about design oriented modeling of ICPTs devices for the production of Si nano - powders. Some of the results here described will be presented in the following congress:

- V. Colombo, A. Concetti, E. Ghedini, M. Gherardi, P. Sanibondi, M. Leparoux, C. Descheaux, C. Jaeggi. (2011). Validation of 3D modelling of an inductively coupled thermal plasma reactor through enthalpy probe measurements. Submitted for publication on *Proceedings ISPC 20, Philadelphia, July 24-29, 2011*. 20th International Symposium on Plasma Chemistry.

and published as articles in

- V Colombo, A Concetti, E Ghedini, M Gherardi and P Sanibondi (2011) *3D Time-Dependent Large Eddy Simulation of Turbulent Flows in an Inductively Coupled Thermal Plasma Torch with Reaction Chamber* Submitted for publication on IEEE Trans. Plasma Sci, 6th Triennial Special Issue on Images in Plasma Science.

## Part I

### Plasma arc cutting

Plasma arc cutting is a widely used industrial process for the cutting of different types of metals in several operating conditions. The process is characterized by a transferred electric arc that is established between a negative electrode (cathode) that is part of the cutting torch and a positive electrode (anode) that is the metallic work-piece to be cut [1]. Plasma arc cutting is considered a challenging technology when compared to its main competitors: oxy-fuel and laser cutting, in particular for cutting of mild steel in the thickness range 8-40 mm.

Among all the technologies for cutting metallic materials, plasma cutting has taken a leading role in recent decades, becoming a significant market and competing directly with other technologies for thermal cutting such as laser cutting and oxy-acetylene flame. The plasma technology was officially born in 1955 as an evolution of TIG (Tungsten Inert Gas) with a patent of Robert Gage [1]. The purpose of the Gage research at the Union Carbide was to improve the directional stability of the arc of free plasma used in TIG welding. To achieve this, Gage used a metal nozzle to force the plasma arc and he found that the forced arc underwent a significant increase in temperature, electric voltage and its directional stability. This last feature in particular, made the new technology particularly suitable for cutting metal and was immediately used for cutting aluminum and stainless steel, using nitrogen as plasma gas or a mixture of argon and hydrogen. In its 55 years of history, the plasma cutting technology has greatly developed both in the technology of components and materials, and in the understanding of physical phenomena behind it, however, the working principle of a plasma arc cutting torch was unchanged .

#### **Evolution of the plasma arc cutting technology**

The architecture of a current plasma arc cutting torch does not differ significantly from the first model of the '50 previously shown. Nevertheless, important innovations have followed over the years that have carried the torch to become a mechanical component with very high technological value added. In his review article [2], Nemchinsky summarizes the evolution of technology through some milestones:

1. In 1964, the use of air as plasma gas was introduced. The innovation allowed to significantly increase the cutting speed for mild steel and greatly improved the cut quality. However, the presence of oxygen in the cathode area involved a fast wear of tungsten, which was replaced by a zirconium cathode, much more resistant to oxidizing environments.
2. In 1974, the torches that used  $N_2$  were introduced, with injection of water. In these torches, about one or two liters per minute of water were injected within the plasma jet, whose heat

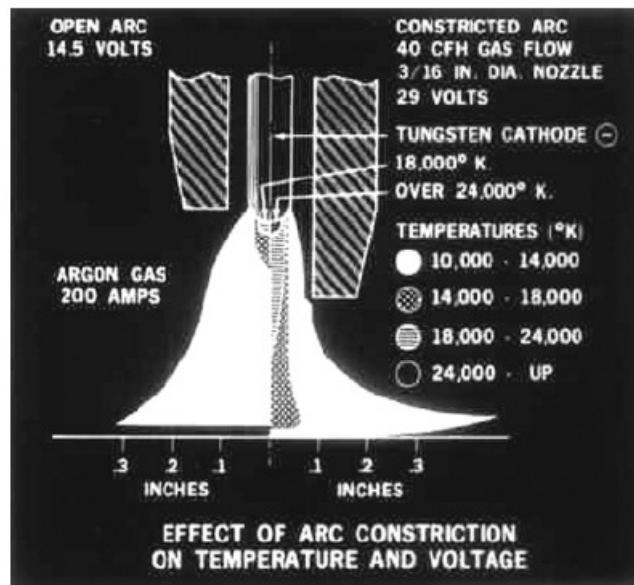


**Figure 1.1** Comparison of the temperature distribution in the open arc (left) and in the arc constricted by the nozzle (right). Taken from [2].

enabled to evaporate or dissociate about half of the injected water. This process produced extremely squared cuts with very little top edge rounding. Plasma arc cutting quickly became the dominant technology for cutting material thinner than 75mm, and remained so for over two decades.

3. In the early '80s oxygen torches with water injection were introduced, they led at great improvements in the quality of cutting mild steel with thickness less than 25mm.
4. Subsequently, it was discovered that even small-amplitude oscillations in the electric arc current significantly increased the electrode erosion rate. The introduction of power generators so-called "low-ripple" led immediately to further improve the electrode service life. Moreover, the introduction of slope-up ramps for the increase of the current level and the removal of "overshoots" further contributed to improving the service life of the nozzle and the electrode.
5. Another great technological step was the substitution of zirconium with the hafnium as electrons emitter material. According to Nemchinsky[1], hafnium electrodes have a service life about 1.5 times with respect to the that of zirconium; however, the physical reasons behind these phenomenon are not fully understood. The majority of the electrodes for plasma arc cutting of mild steel actually commercialized have hafnium as emitter material. This type of electrode is used with currents up to 100A in air-cooled torches and with currents up at 400A in liquid-cooled torches. This invention revolutionized the market for plasma torches in the '80s, together with the introduction of current source inverter. In particular, the market of the manual torches experienced an increase extreme.
6. Finally, in the '90s the so-called "dual-gas" torches were perfected. In these torches a secondary gas surrounds the column of the plasma jet greatly improving the cutting quality and protecting the torch during the piercing, or piercing. This technology had already been

invented in the '60s, but in the precision plasma torches were produced and commercialized. Plasma arc cutting technology was able to compete with laser cutting, until then the market leader for thermal cutting of steel thin plates.

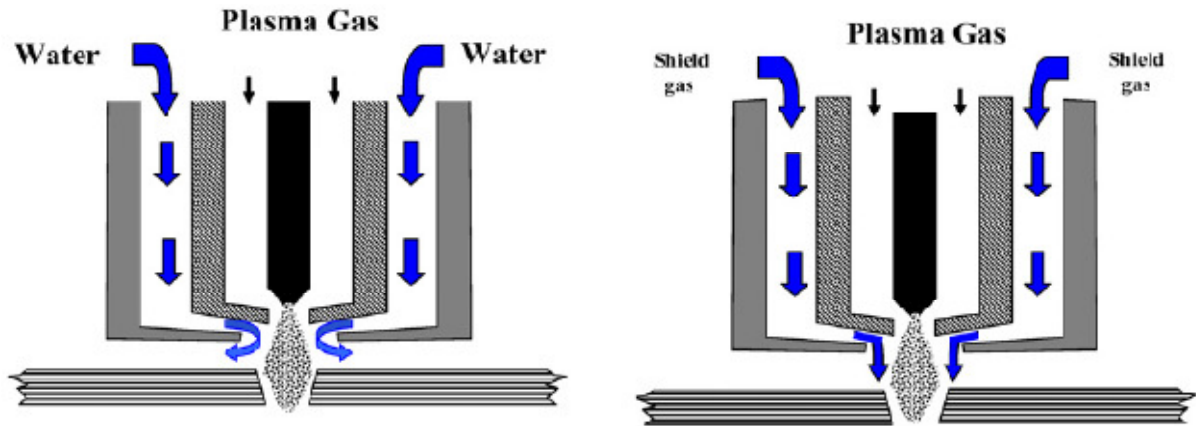


**Figure 1.2** comparison between water injection and dual-gas plasma torches. Taken from [2].

Nowadays, plasma arc cutting systems are industrially widely used for cutting metal. In fact, they are in many cases a good alternative to the two main competitors in the thermal cutting of metallic materials: laser and oxy-fuel cutting. Among the three processes, the oxy-fuel is the oldest and the most economically both in terms of fixed and variable costs. However, it produces poor quality and it is able to cut only mild steel as it exploits the reaction of oxidation of iron, so it is not effective either on stainless steel or aluminum. In contrast, laser cutting ensures excellent cutting quality and excellent precision. It is however limited to thin plates and requires significant investment in equipment and causes high operating and maintenance costs. It is therefore an appropriate technology only in the case of large volumes of production, making it possible to recover their costs. Plasma cutting is a compromise between these two extremes, as the latest developments in technology have allowed it to achieve excellent cutting quality, comparable to that of the laser, even when cutting thin materials. In addition, it requires much lower investment and variable costs while still providing comparable and similar services, both in terms of speed and cutting quality, than laser. Plasma cutting compete in particular with the laser cutting of mild metal with thickness of 8-40 mm and stainless steel with thickness of 3-30 mm.

### **The plasma arc cutting process**

The plasma arc cutting, with the laser cutting and the oxyacetylene flame, belongs to the category of thermal cuts. Common to these three technologies is in fact the principle of operation, except minor variations peculiar to each one. In particular, in plasma arc cutting, a jet of ionized gas at very high pressure and temperature affects the metal and melt it in a very localized area. The same gas jet also removes the molten metal from the work-piece, leaving a *kerf*.

A plasma torch, in its most basic form, consists of a cylindrical pipe in which flows a gas, called plasma gas. At the center of this tube is located a copper electrode, whose tip is engaged with a  $\rho$ ellet of hafnium, a material with high termoionical emissivity. The electrode is connected to an electrical circuit which constitutes the negative pole, or cathode. The anode, or positive, is the metal piece to be cut. Because the arc is transferred to the workpiece, this type of torch is called "transferred arc", in contrast with "not transferred arc" torches, in which the positive is the nozzle of the torch. However, this second type of torches cannot find applications in the cutting of metallic materials and is therefore irrelevant to this discussion.

From the tip of the electrode body, an electrical arc that closes the circuit between the torch and the work-piece ionize the surrounding gas, creating a column of plasma flowing through a nozzle, which gives it a very stable thermal fluid dynamics. The forced plasma jet melts the metal and removes the molten material, leaving a groove, called the "*kerf*". The directional stability of the jet is further enhanced by the presence of a peripheral layer of non-ionized gas. It keeps separate the gas from the arc nozzle walls. The column of plasma from the nozzle outlet, in fact, consists of an inner zone at very high temperatures, which conducts the electricity, and an outer zone colder and that protects the inner wall of the nozzle from direct contact with the plasma hot. Furthermore, due to constriction, upstream of the nozzle a pressure will form, which significantly accelerates the motion of the fluid in the axial direction: the speed increases with decreasing cross section. The jet thus obtained is then able to remove the molten material during the drilling and cutting.

As was mentioned above, the cutting process begins with the creation of an electrical arc that turns the swirling flow of gas injected into the plasma chamber in plasma arc. There are two main methods for injecting the arc:

- in the first mode, the anode and cathode are initially in contact and are crossed by an electric current. By opening a solenoid valve, the gas is let flow into the plasma chamber, the electrode is disconnected from the nozzle. This detachment causes the electrical arcing, which is called "pilot arc";
- in a second mode, the pilot arc between the electrode and nozzle is generated after a short pulse of electrical current in high frequency. This will create an electrical arc that connects the two closest points of the electrode and nozzle.

During this first phase, the electric current and the gas flow are relatively low compared to the nominal values taking into real cutting phase. Sometimes, the plasma gas used at this stage may be different from what will then be used for cutting, in order to reduce the electrode erosion.

Once ignited the pilot arc, the arc is blown-out of the nozzle by the plasma gas flow. When the arc has been blown-out of the nozzle, it folds back on itself and takes on a hook shape. The arc is then transferred to the workpiece, which becomes the anode, while the nozzle is removed from the circuit and electrically insulated. The electric current increases then gradually from relatively low levels with respect to the operating value. Simultaneously, the gas flow rate increases gradually to the nominal value for the cut. Finished cutting, the values of pressure and current are gradually reduced to zero, as shown in figure 1.3.

The cutting process can be started in two ways: from the edge of the plate (edge cut), or breaking through the slab at a point (piercing). In order to protect the torch, it is always preferable to start cutting from the edge, however, for the construction of several pieces of particular shape the direct piercing of the piece cannot be avoided. The stage backdrop, or piercing, is particularly critical because the torch will remain virtually motionless, while the plasma arc creates a hole deeper and deeper into the work-piece. During this phase, the molten material coming from the hole edge dates back to the torch and can in some cases weld the nozzle to the work-piece. During this phase, moreover, the torch can be damaged by drips and splashes of molten metal that might reach its tip. To avoid these side effects another stream of gas, called "secondary gas, is used which has the function to wrap the primary flow of gas and to reject any splashes. In addition, during the break, the so-called "stand-off ", i.e. the distance between the torch and the work-piece is usually greater than that used during the cutting phase.

After the piercing, the torch is lowered at the optimal cutting-height and begins to move along the cutting path. In order to obtain a high quality cutting, it is necessary to maintain the stand-off constant, corresponding to the optimal distance, defined in terms of the arc current, the used gases and the thickness of the piece to be cut.

The torch height can be managed by a mechanical control or with a voltage control. With the mechanical control, the torch is physically rested to the work-piece and the pantograph stores the zero height level, then it is raised up to the optimal work height. However, sometimes the surface of the metal is not perfectly flat, then, if the torch keeps the initially determined height, on many occasions it could not be more the optimal distance from the work-piece. This problem is overcome by the voltage control. In fact, modern pantographs for automatic cutting manage the torch height by measuring the electrical voltage drop that is established between the torch head and the work-piece. With this control system, the torch height is adjusted so as to maintain a constant tension drop between the torch and the work-piece. However, the gradual erosion of the electrode create a recess in the emitter surface of the hafnium pellet, which can reach several millimeters in depth. This phenomenon brings to an optimal voltage higher than that which was initially registered. If the electronic control system does not adjust the voltage level, the torch will fall gradually and would be at a less distance of than optimal.

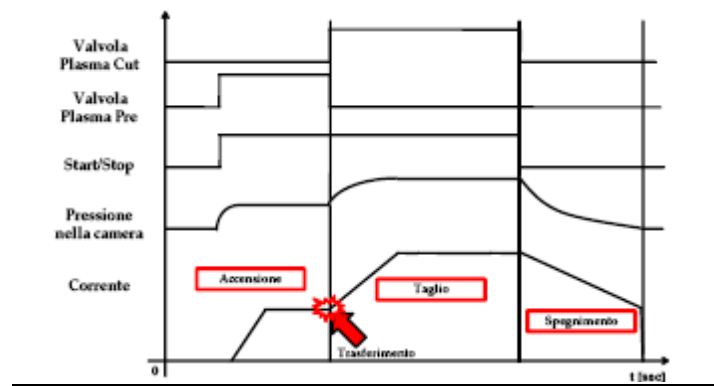


**Figure 1.3** Scheme of a cutting cycle

### **Main issues in plasma arc cutting technology**

Despite the considerable scientific and technological effort, there are many unsolved problems that affect the technology of plasma cutting, in terms of cutting quality and consumables service life. In this section, the cutting quality, as described by international standards, will be primarily defined, and then we will discuss in detail two of the major unsolved problems of plasma arc cutting technology, namely the electrode erosion and the double arcing.

### **Cutting quality**

The concept of "quality of cut" is defined in a rigorous and unique by international standards ISO 9013 of 2002 [3]. The ISO is not only related to plasma cutting, but it refers to materials cut with oxyacetylene flame, laser and plasma cutting. The standard prescribes some objective parameters that can be experimentally measured:

1. Perpendicularity or angular tolerance  $u$ : distance between two parallel lines tangent to the two extremes of the cut edge (figure 1.4)
2. Drag  $n$ : projection of the distance between the two extreme points of the drag line in the direction of cutting (figure 1.5)
3. Rounding of the top edge  $r$ : characteristic size of the upper edge (figure 1.6)
4. Mean height of the profile  $Rz5$ : arithmetic mean of the single profile elements of five bordering single measured distances (figure 1.7)

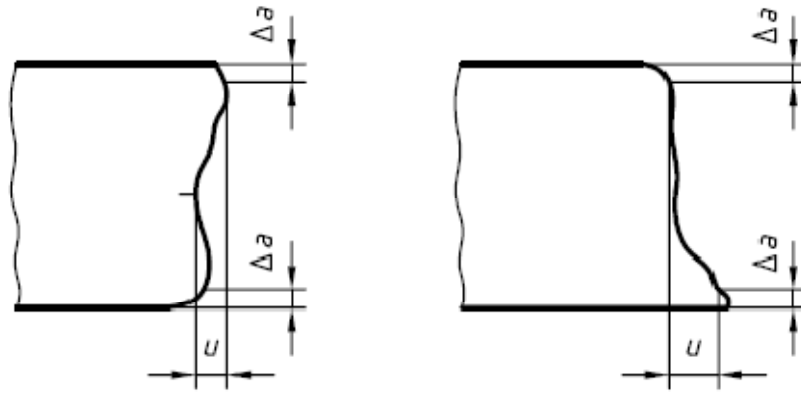


**Figure 1.4** Perpendicularity and angularity tolerances for vertical cuts. Taken from [3]

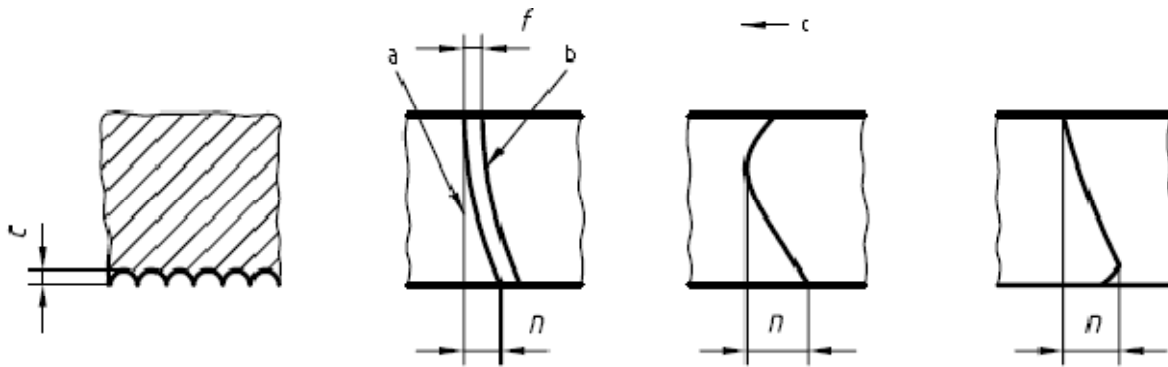


**Figure 1.5** Drag lines n. Taken from [3]

In addition to the parameters, the international standard also prescribes the instrumentation and experimental conditions in which the measures must be carried out. Using the characteristic variables  $u$ ,  $n$ , re Rz5 is therefore possible to define the quality of the intervals, or ranges, which are then reported in the tables.

#### *Perpendicularity or angular tolerance*

The profile cut by the plasma is never perfectly normal to the surface of the slab. In fact, the amplitude of the *kerf* in the upper surface of the plate is always greater than on the lower surface. Moreover, the two sides of the *kerf* does not have the same inclination to the vertical but one is always more inclined of the other. Which of the two sides is more inclined depends on the direction of the cut and on the direction of the swirl rotation of the plasma gas.

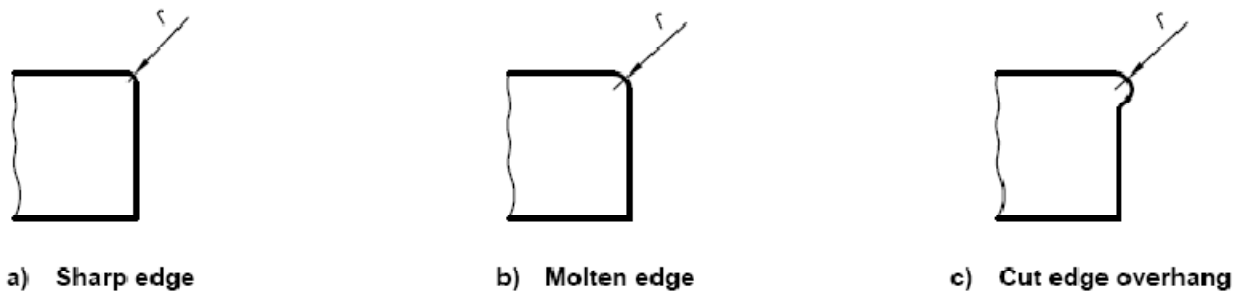


**Figure 1.6** Melting of the top edge. Taken from [3]

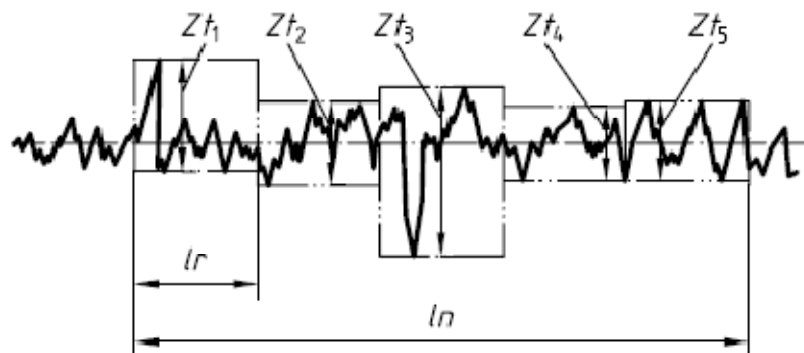


**Figure 1.7** Mean height of the profil. Taken from [3]

The nature of the phenomenon is not known with certainty, but one possible explanation is proposed by Nemchinsky in his review article [2]. Figure 1.9 shows two orthogonal views of the cutting area, a horizontal section of the plasma jet and a vertical section and the piece of metal. If the gas flows with a swirl in a clockwise direction, as shown in the figure, the coldest part of the jet is identified by point C, because before you reach that point, the column has been in contact for a longer time with the cold metal. On the other hand, the hottest part is represented by point A, which is the point where the plasma meets the metal. The vertical section shows that the plasma melts the metal with more intensity in the hot side, corresponding to point A. The asymmetry of the *kerf* is therefore the result of the asymmetry of the plasma fluid dynamics. Also, since the swirl speed decreases in the terminal part of the jet, the thermal asymmetry decreases with the depth of the cut and therefore, also the geometric one decreases.

However, as shown in [15], this approach would be unsuccessful in explaining the positive effects of anticlockwise secondary swirl on cut quality. In fact, by taking into account the whole radial extension of the plasma jet as a means for cutting the workpiece, with anticlockwise secondary swirl, one should experience a left bevel angle that is smaller than the right one; however, that is not the case in real life - in many operating conditions and materials. On the contrary, one can conclude from the analysis of the simulative results presented in [15] that the main effect of anticlockwise secondary swirl is a relevant reduction of plasma-swirl velocity in the post-nozzle region of the jet, which is radially limited to the *kerf* core.

The perpendicularity of the *kerf* is lower when the cutting speed is high, in fact, the jet plasma cools gradually as it penetrates deep into the *kerf*: consequently the plasma column cannot be at the same speed that it has at the top of the piece . This decreasing effect of *kerf* width at the bottom of the plate has a dual effect. A narrow *kerf*, implies a low energy consumption for cutting, with obvious consequences on the economy of the process. However, when the *kerf* is narrow, the thickness of molten layer that builds up is greater and tends to separate the plasma from the solid material and consequently reduces the efficiency of the jet in melting the metal. Finally, the surface tensions are heightened in the molten metal in a very narrow *kerf*. These forces oppose the flow of molten metal and make it much more difficult the separation from the lower edge of the piece.

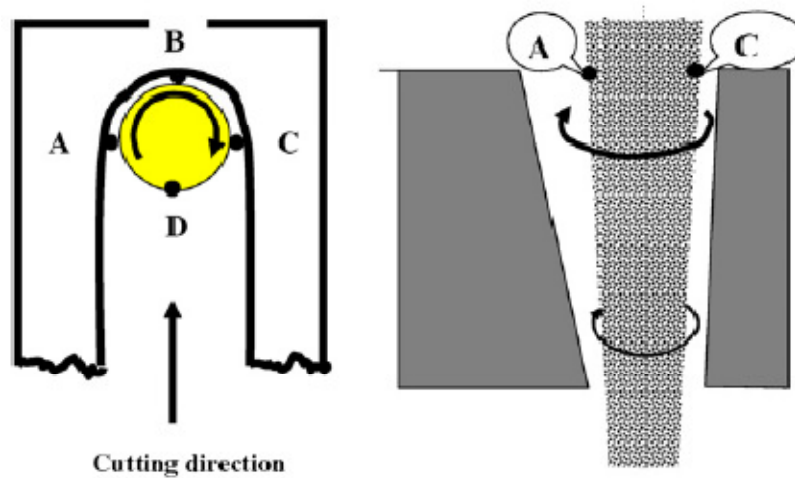


**Figure 1.9.** Top view and side view of the *kerf* during cutting. Taken from [2].

The optimization of the cutting process can be obtained by acting on several parameters, such as:

- operating current;
- plasma gas;
- cutting speed;
- plasma and secondary gas flows;
- swirl velocity;
- stand-off distance.

The optimization of the cutting process, however, cannot ignore the many considerations related to the erosion of the consumable components, which have direct implications on the economy of the process. The optimization is thus always a trade-off between solutions that maximize the quality of the cut and those that minimize the operating costs.

### *Dross formation*

Among the issues still unsolved in plasma arc cutting technology, the dross formation plays a key role. In fact, the plasma arc, not only has to provide thermal energy to heat and bring to melt the metal, but must also give a momentum sufficient to eject the molten metal from the cutting area (*kerf*). During cutting, the thermal energy supplied by the plasma is absorbed by the surrounding metal, so if there is an imbalance between the power transferred from the plasma arc and the power absorbed by the work-piece, the metallic material solidify creating dross. Dross have a direct impact on the economy of the process because they require subsequent machining to be removed, and then they greatly increases the overall operating costs of the process.

Nemchinsky discusses the physical phenomenon of dross formation [2], identifying two main groups of forces:

- driving forces: gravity and aerodynamic drag
- braking forces: surface tension and viscosity

The experimental evidence showed that the contribution of viscosity is negligible compared to other forces and that the gravity is significant only during the cutting of very thin material. The aerodynamic drag is therefore the force that contributes mainly to the removal of molten material from the *kerf*. Nemchinsky identifies a minimum gas flow that allows to supply a sufficient drag on the material.

$$G_{\min} = \pi R^2 \sqrt{\frac{4\rho_g}{\pi C_f H} \left( \gamma + \rho_m \frac{U^3 H^2}{\alpha} \right)} \quad (1.1)$$

Equation (1.1) expresses the flow rate ( $G_{\min}$ ) according to the radius of the nozzle orifice ( $R$ ), the gas density ( $\rho_g$ ), the thickness of the piece ( $H$ ), the cutting speed ( $U$ ), the surface tension ( $\gamma$ ), the coefficient of drag ( $C_f$ ),  $\alpha$  and  $\rho_m$  are the thermal diffusivity and density of the molten material.

Depending on the cutting speed of the torch, two different types of dross can be identified: dross of high and low speed. There is a range of cutting speed so-called “dross-free” that allows to obtain pieces free of dross. At high current levels the required cutting speed to obtain dross-free cut increases while it decreases with the thickness of the piece. However, when cutting very thin plates, the dross-free interval have a very limited or nonexistent extension.

The surface tension is the main source of dross cuts at low speed, then it is necessary to implement all possible measures to reduce this physical quantity. For example, it is useful to use oxygen as plasma gas, because it dissolves in the iron and extends the range of cutting speeds that produce dross free parts. Nemchinsky still claims that this beneficial effect is caused by all the elements of Group VI (oxygen, sulfur, selenium and tellurium). However, even low concentrations of alloying elements can significantly affect the surface tension. Silicon, for example, reacts with oxygen by reducing its surface tension-lowering effect in iron.

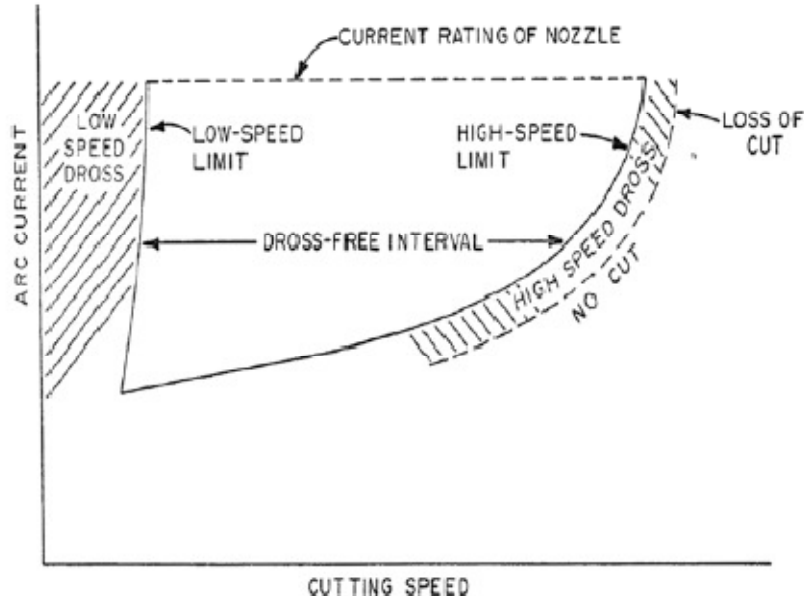


**Figure 1.10** Dross free window conditions. Taken from [2].

In the same article [2] Nemchinsky presents a mathematical model to estimate the limits of the range for which you produce parts without low speed dross. The model is derived considering the interaction of two forces: the surface tension that holds the dross and the drag of the plasma jet, which tends to drag it on. The interaction between these two forces is effectively expressed by a dimensionless parameter, the Weber number,  $We = \rho V^2 \delta / 2\gamma$ , expressed as a function of the plasma density ( $\rho$ ), its average speed ( $V$ ), the thickness of molten metal ( $\delta$ ), and the surface tension coefficient  $\gamma$ . Nemchinsky assumes the existence of a critical value  $We_{crit}$ , such that if  $We > We_{crit}$  the surface tension is negligible. In these operating conditions, the molten material would separate spontaneously from the piece and there would not be dross formation. Based on this hypothesis, Nemchinsky derives the formula for the minimum cutting speed that can produce dross free cuts ( $U_{lsd}$ ) and presents the formula in order to highlight a characteristic dimensionless parameter ( $A$ ).

$$\left( \frac{U_{max}}{U_{lsd}} - 1 \right) \left( \frac{U_{max}}{U_{lsd}} \right)^2 = \frac{\rho U_{max}^3 H^2}{4\gamma\alpha We_{crit}} = A \quad (1.2)$$

In equation (1.2),  $U_{max}$  is the maximum cutting speed under the operating conditions given by the thickness of the piece ( $H$ ), the arc current and the gas flow. The other parameters maintain the significance previously discussed, while  $\alpha$  is the thermal diffusivity of the metal. Then, the ratio  $U_{max} / U_{lsd}$  can be plotted as a function of the dimensionless parameter  $A$ , as exemplified in the figure 1.11 for a value of  $We = 2$ , where it is also compared to experimental data. It is clearly evident that the experimental points follow the theoretical trend of the curve for all values of the parameter  $A$ .

In contrast, the phenomenon of high-speed dross is not yet fully understood. The high-speed dross are formed when the torch goes with a speed close to the maximum cutting speed. Under these operating conditions, the arc assumes a very inclined configuration and therefore, the molten

material flows in the direction almost tangential to the lower edge of the piece, giving thermal energy to the slab and solidifying itself.

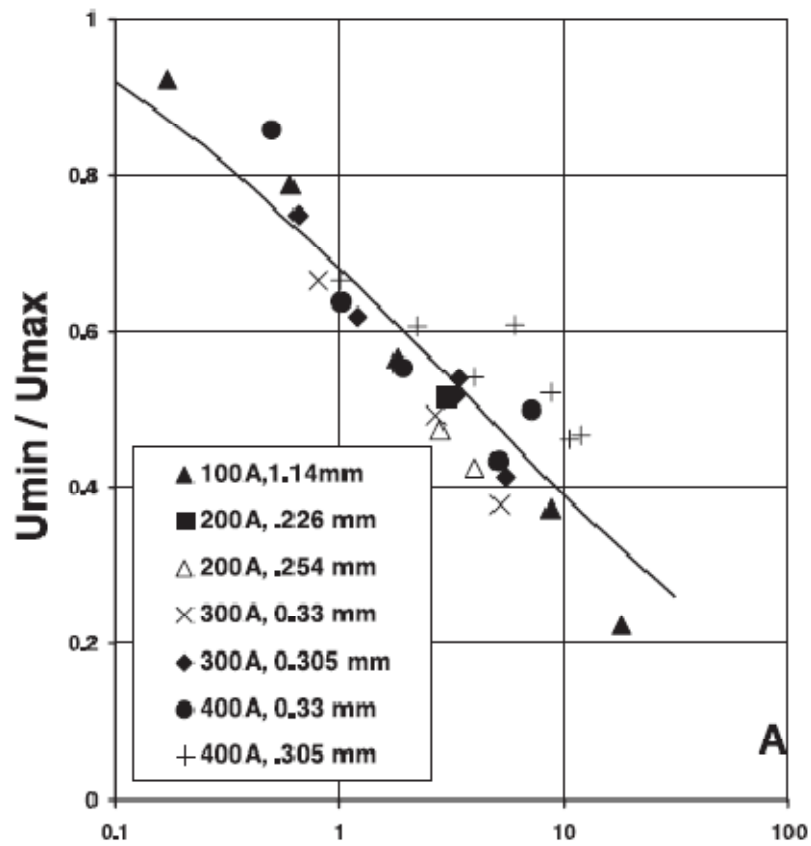


**Figure 1.11** Plot of the ratio  $U_{min}/U_{sd}$  as a function of the dimensionless parameter  $A$ . Taken from [2].

An experimental study on the formation of dross was carried out by Bemis and Settles [4] using a high-speed camera with an acquisition rate of 1000 frames per second (fps). The authors also interposed a UV filter to highlight the radiative emission of molten iron oxide in the ultraviolet spectrum. The results obtained by Bemis and Settles will be described in chapter 3.

### Electrode erosion

In the early years of plasma cutting technology, the plasma gas most commonly used were nitrogen, or a mixture of argon and hydrogen. Tungsten (W) was used as emitter material, whose erosion rate was relatively low in inert atmospheres. Tungsten in fact causes no erosion problems, except in cases of very high currents or insufficient cooling.

In subsequent years, however, air or oxygen began to be used as plasma gas, creating a strong oxidant atmosphere inside the plasma chamber, and making inappropriate tungsten, which was replaced by other emitter materials such as hafnium (Hf) or zirconium (Zr). These materials were placed inside a copper body to significantly improve cooling.

Hafnium and zirconium resist much better than tungsten in oxidizing atmospheres; however, their oxidation rate is still much higher than that of tungsten in an inert atmosphere.

To increase the cutting speed it is necessary to increase the arc current and the gas pressure, however, it is experimentally validated that these operating conditions also induce to an increase in the hafnium erosion rate. This phenomenon leads to a strong technological problem because it puts a limit on the maximum power for the plasma arc. In addition, a fast erosion of the electrode frequently forces to interrupt the cutting process to replace the consumable, with an obvious increase in operating costs.

The research showed that in the electrode service life there is no single erosion phenomenon, but there are very different erosion phenomena during the cutting process and during the arc on and arc off transients.

In [5] Nemchinsky studied in detail the phenomenon of electrode erosion during cutting and he explained it through a combination of several factors, including the plasma chamber pressure, the arc current and the path to the gas flow close to the electrode emitter surface. In addition, Nemchinsky verified experimentally that the erosion rate increases linearly increasing the plasma chamber pressure.

The influence of the current arc is more complex. Since the cathode surface is finished, the cathodic attachment of the arc cannot be extended indefinitely increasing the current level. Consequently, it generates a very localized increase in temperature in the cathodic attachment point that significantly accelerates the rate of erosion.

It was found that the erosion rate at this stage is relatively low, because much of the melted material vaporizes and returns to the cathode, where it solidifies again. In fact, the vaporized metal atoms have an ionization potential much lower than that of the surrounding gas, so they are immediately ionized and referred to the electrode by the electric field, which is particularly intense near the cathode. But there is a "point of no return" because, with the increase of the distance from the cathode, the velocity of the plasma gas increases, and reaches a value sufficient to give a fluid-dynamic drag more intense of the attraction electrostatic. If the vaporized atoms reach that distance, they are taken away by the flow of plasma.

In this stage, a key role in the erosion process is then filled by the velocity field near the cathode, because this determines the possibility that the hafnium vaporized ions are able to escape the electric field. The velocity tangential component, the swirl, mainly contributes to the electrode wear, despite having many beneficial effects, such as increased stability of the plasma jet, as well as having a protective function for the nozzle. In the presence of swirl, a small vortex is created in the area near the cathode, which tends to expel the vapors of hafnium in a region where the electric field is too weak to address them.

However, as abovementioned, the electrode wear occurs mainly during arc-on and arc-off transients, both for the nature of these phenomena, and for the high numbers of starts and stops of the torch that take place during a real cutting process. The erosion phenomena in these phases has been studied also by Heberlein [7]. In particular, Heberlein showed that the morphology of emitted particles is not constant but it changes at different stages of the cutting process. During the arc-on

transient, the ejected particles are characterized by small dimensions, while the diameter of the particles emitted during the shutdown is greater by several orders of magnitude.

Both Heberlein and Nemchinsky devoted much attention to the interpretation of these phenomena and gave a full description of them [6,7]. In recent years, some new insight in this field have been made by experimental studies shown in some scientific works [8,9].

Nemchinsky in [6] presented a model describing the behavior of the cathodic attachment during arc-on transient. When using oxygen as plasma gas, after the first ignition the electrode emitter surface is covered with a thin layer of hafnium oxide ( $\text{HfO}_2$ ) that at the solid-state behaves as a perfect insulator both electrical and thermal. This oxide layer is formed at the end of each cutting stage and is always present at the beginning of a cutting cycle.

During the arc-on transient, a pilot arc is ignited between the electrode and nozzle, the cathodic arc attachment gradually proceeds from the periphery of the electrode toward the center of the hafnium surface, carried by the flow of gas injected into the chamber plasma. Once it has reached the center, the cathodic attachment is expanded during the growth of current and stays there during the cutting phase. However, during his path to the center of the electrode, the cathodic arc attachment meets the oxide layer not yet melted, causing its cracking and the consequent emission of  $\text{HfO}_2$  solid particles.

This phenomenon can be reduced by avoiding a too rapid expansion of the arc on the hafnium pellet, and thus limiting the thermal stress on the layer of  $\text{HfO}_2$ . This objective can be achieved by implementing a gradual growth of the arc current, leaving to the oxide the time to melt before coming into contact with the arc and thus avoiding the violent break.

Recent studies [9] showed that during the pilot arc ignition transient, the moving from the periphery to the center of the surface is not characterized by a gradual path, but by a massive and instantaneous event, as more fully described in the second chapter.

Erosion mechanism during shutdown transient is understood with less clarity. Nemchinsky proposed a theoretical model in [6]. During cutting, the plasma gas at high pressure and temperature is in contact with a layer of molten emitter material at the tip of the electrode. In these physical conditions, the diffusivity of gas in the liquid is particularly strong, and a high concentration of particles in the molten pool is created. After the arc off the physical conditions inside the plasma chamber rapidly change; in particular, a strong pressure drop takes place. In this new environment, some of the gas trapped in the molten pool exits from it in the form of bubbles, and drag away with it drops of molten material. This phenomenon becomes particularly evident if gases with low atomic radius are used as plasma gas, and then high solubility, for example, hydrogen. Moreover, the microscopic observation of the cathode surface after the arcing process shows the presence of characteristic craters generated by gas bubbles leaving the molten pool.

Heberlein [7] however noted that the erosion during arc off transient is not so much dependent on the type of gas used as on the current slope-down ramp profile. If the current is reduced very gradually, the molten pool is very stable and the emission of particles is very limited. Otherwise, if the slope down is very sudden, many particles are carried away by the plasma gas flow. In particular, in [7] Heberlein carried out a survey using high-speed camera to film the cathode surface

during the different phases of an operating cycle whose results will be described in detail in the following chapter.

### *Industrial property*

The electrode wear is a phenomenon of primary importance that not only has encouraged academic research but has also given rise to several patents that propose different approaches to the problem solution. In general, the proposed solutions can be divided into two macro-categories. On the one hand an attempt has been to optimize the pressure and current profiles during transients. On the other, an attempt has been to optimize the geometry of the plasma chamber introducing specific modifications to the electrode, the nozzle and the diffuser.

In the first category is the patent US5166494 (1992) by Hypertherm Inc. "Process and apparatus for Reducing electrode wear in a plasma arc torch" [10], which claims to enter a flow of plasma gas during pilot arc, known as "pre-flow" clearly distinguished from a different flow during the cutting phase, called "cut-flow". The second flow is delivered in conjunction with the growth of current during the arc transfer. The patent does not just claim the distinction between the two flow rates but also claims the change in direction of the plasma gas flow within the plasma chamber, first granted in the radial direction, then provided with a tangential component.

Other two patents by Hypertherm try to optimize the consumables geometry. The first of these is the patent US5310988 (1994) "Electrode for high current density plasma arc torch" [11] that claims the optimum size of the diameter of the emitter pellet. The use of this optimal size would allow on one hand to not reach the boiling point of hafnium through a good cooling, and secondly to support the arch and prevents its attachment on the copper body because the pellet diameter must be slightly larger than the emission spot, or cathodic attachment of the arc. Set a maximum current that the electrode can support, the diameter of the pellet should be reduced to the point corresponding to the maximum current density. It is important to note that if the diameter of the emitting surface is reduced, the current density increases and then, usually, other parameters being equal, the quality of cut increases. In addition, one other important claim of the patent refers to the internal cooling of the electrode. In the electrode design claimed by Hypertherm, the coolant comes into direct contact with the hafnium pellet and then descends through an annular passage to cool the side surfaces of the insert.

The second of these is the patent US 5464962 (1995) "Electrode for plasma arc torch" [12]. The idea of the patent starts from the observation that during the first starts, a significant portion of emitter material is ejected, creating a concave recess in the emitter pellet. Hafnium ejected tends to deposit on the inner walls of the nozzle and to act as a trigger for potential double arches. The patent claims the artificial creation of a recess, concave or cylindrical, on the emission surface of the hafnium pellet. This solution greatly reduces the amount of hafnium that is deposited on the inner walls of the nozzle and consequently reduces the risk of establishing double arches, without acting directly on reducing the electrode erosion rate. The phenomena of the electrode erosion during first starts has been studied in detail in the last year [9], some of the obtained results will be described in chapter 2.

## Double arcing

The plasma cutting process is affected by another problem still unresolved: the double arcing. During normal operation of a transferred arc torch, the arc connects the electrode and the workpiece passing through the nozzle orifice without touching it, because the nozzle is electrically neutral. The double arch takes place when the arc moves on the surface of the nozzle and simultaneously split itself in two parts, one connecting the electrode and the nozzle, the other connecting the nozzle and the workpiece. The occurrence of double arches is a phenomenon very damaging for the electrode and the nozzle, and can quickly cause damage to all components of the torch. Recent studies showed, as detailed in chapter 3, that also non - destructive double arching can occur in specific conditions [13].

Experimentally, we observe that double arches are established when one or more of these anomalous conditions occur:

- the arc current is too high;
- the nozzle orifice is too narrow;
- the nozzle orifice is too long;
- the gas flow is too low;
- the gas flow not have enough tangential component;
- consumables are excessively wear.

Nemchinsky investigated the double arching phenomenon [14], starting from the observation that the potential drop within the nozzle is particularly high, especially when the operating current values are particularly high and the nozzle orifice is characterized by small cross section and are too long .

Nemchinsky observed that the diameter of the plasma column that is formed on the electrode surface tends to increase with distance by it. When the column reaches the nozzle inlet, it occupies only the central part of the orifice, and there is a surrounding annulus through which the colder gas flows.

During the crossing of the nozzle, the plasma is gradually heated and the heat can be divided into three parts: the first part of the heat is used to increase the enthalpy flux, the second part is irradiated but the remaining is transmitted by conduction directly to the nozzle surfaces.

At the nozzle orifice output, the plasma column is located extremely close to the nozzle wall. However, it is still separated from the walls through the cold gas ring which, however, is characterized by a minimum thickness.

As explained by Nemchinsky, fixed a cartesian axis  $d$  on the torch axis of symmetry, and identified as  $d = 0$  the electrode tip, it can be seen as the potential difference between the metallic nozzle and the plasma arc increases with the coordinate  $d$ . In particular, at the nozzle exit this difference in potential can take a value very similar to the plasma potential drop through the nozzle.

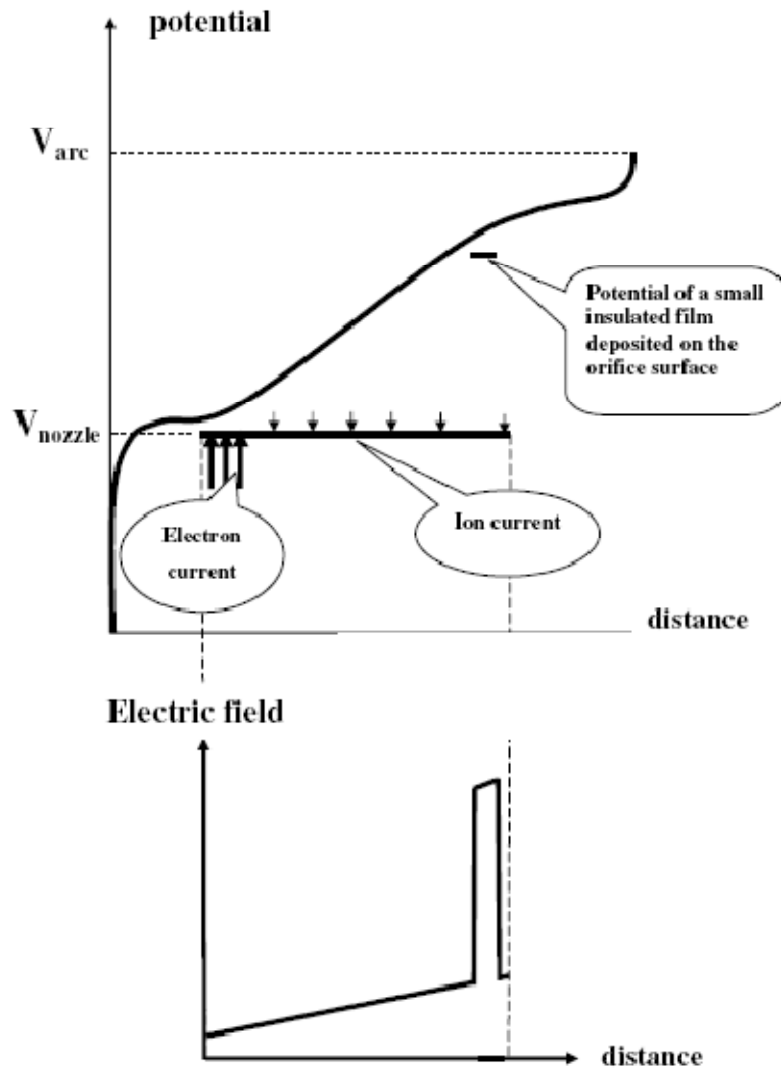


**Figure 1.11** Potential distribution in the plasma inside the nozzle orifice (top). Distribution of the radial electric field at the orifice surface when a small insulated film is deposited on the orifice surface (bottom).

Taken from [2].

It is important to understand that this potential difference is applied across the thin annulus of cold gas that surrounds the plasma column and that isolates the column itself from the nozzle.

In this area, the concentration of electrons is very low compared to the central area of the flow so the cold gas in the layer has a Debye length greater than that of the plasma. Under these conditions, the electric field can penetrate deeply into the thin neutral gas annular layer because there does not exist the quasi-neutrality of the plasma. If in a point the electric field becomes strong enough to cause the breakdown of dielectric (electrical breakdown), it triggers an electronic cascade (electron avalanche) culminating in the establishment of a double arch. In addition, a non-symmetrical erosion of the emissive surface brings the cathodic attachment to move from the center of the emissive surface, resulting in a loss of axial symmetry of the plasma column. The absence of axial symmetry has the direct consequence of the further thinning of the cold annular layer, whose thickness decreases further close to the nozzle orifice outlet, facilitating the triggering of an

electronic cascade. Finally, especially in connection with what previously discussed, the electrode wear, including deposits of eroded material on the inner surface of the nozzle, disturb the axial symmetry of the plasma and help to thin the thickness of the annular protective layer.

Moreover, the electrode erosion products further contribute to the establishment of double arches because they increase the electric field. A drop of hafnium oxide on the inner surface of the nozzle exit orifice leads to an electric potential almost equal to that of the layer of cold gas. However, given to the size and morphology of the inclusion of  $\text{HfO}_2$ , the electric field on its top can be much higher than the field normally present in the cold layer: this peak of the electric field may be sufficient to trigger a cascade and a subsequent dielectric breakdown. Finally, it should be noted that despite the small thickness of the cold annular layer is the cause of the establishment of double arches, if it becomes too thin it would be completely transparent to electrons, and not being able to establish a high voltage, it could not generate double arches.

## References

- [1] Gage R M 1957, "Arc torch and process", US Patent 2,806,124 10 September
- [2] Nemchinsky V A and Severance W S 2006, "What we know and what we do not know about plasma arc cutting" J. Phys. D: Appl. Phys. 39 R423-R438
- [3] International standard ISO 9013 2002 "Thermal cutting – Classification of thermal cuts – Geometrical products specification and quality tolerances"
- [4] Bemis B L and Settles G S 1998 "Visualization of liquid metal, arc, and jet interactions in plasma cutting of steel sheet" 8th Inter. Symp. On Flow Visualization (Sorrento, Italy)
- [5] Nemchinsky V A and Showalter M S 2003, "Cathode erosion in high current high-pressure arc" J. Phys. D: Appl. Phys. 36 704-712
- [6] Nemchinsky V A 2003, "Cyclic erosion of a cathode in high-pressure arcs" J. Phys. D: Appl. Phys. 36 1573-1576
- [7] Peters J, Yin F, Borges C F M, Heberlein J and Hackett C 2005 "Erosion mechanisms of hafnium cathodes at high current". J. Phys. D: Appl. Phys. 38 1781-179
- [8] V Colombo, A Concetti, E Ghedini, F Rotundo, S Dallavalle *Experimental analysis of the behaviour of high current electrodes in plasma arc cutting during first cycles* Plasma Sources, Science and Technology, Vol. 19 doi: 10.1088/0963-0252/19/6/065023 (2010)
- [9] V Colombo, A Concetti, E Ghedini, V Nemchinsky *High speed imaging investigation of transition phenomena in the pilot arc phase in Hf cathodes for PAC* Plasma Sources, Science and Technology, Vol. 19 doi:10.1088/0963-0252/19/6/065025 (2010)
- [10] Luo L, Sanders NA and Couch RW Jr 1992, "Process and apparatus for reducing electrode wear in a plasma arc torch", Hypertherm Inc. Patent 5,166,494
- [11] Couch RW Jr et al 1994, "Electrode for high current density plasma arc torch" Hypertherm Inc., Patent 5,310,988
- [12] Luo L, Couch R W Jr 1997, "Electrode for a plasma arc torch", Hypertherm Inc., US Patent 5,601,734
- [13] V Colombo, A Concetti, E Ghedini, S Dallavalle and M Vancini *High speed imaging in plasma arc cutting: a review and new developments*, Review Paper, Plasma Sources Science and Technology, Vol. 18, doi:10.1088/0963-0252/18/2/023001 (2009)
- [14] Nemchinsky V A 1998, "Plasma flow in a nozzle during plasma arc cutting" J. Phys. D: Appl. Phys. 31 3102
- [15] Colombo V, Concetti A, Dallavalle S, Ghedini E and Vancini M 2008 Understanding plasma fluid dynamics inside plasma torches through advanced modelling *IEEE Transactions on Plasma Science* **36** 389-402

## Chapter 1

### Design Oriented Simulation and experimental tests of Plasma Arc Cutting torches

Transferred arc plasma torches are widely used in industrial processes for cutting of metallic materials because of their ability to cut a wide range of metals with very high productivity [1]. The process is characterized by a transferred electric arc established between an electrode inside the torch (the cathode) and another electrode, the metallic work-piece to be cut (the anode). In order to obtain a high quality cut and a high productivity, the plasma jet must be as collimated as possible and must have the higher achievable power density. Plasma modeling, numerical simulation and diagnostics can be very useful tools for designing and optimizing these devices and they should be used in conjunction in order to obtain significant added value from an integrated approach to design, but research is still in the making for finding a link between simulation of the plasma arc and a consistent prevision of cut quality.

Numerical simulation may be very useful tool for the investigation of the characteristics of the plasma discharge and for the optimization of industrial cutting torches [2-9]. Experimental evidences can be integrated with simulative results in order to avoid a try & fail approach, often too expensive, to validate models and to identify innovative design solutions, addressing specific issues that cannot be fully investigated through experimental tests.

Most of the activities that I carried out in this field have been done in the framework of the research contract between the DIEM and Cebora Spa. My contribution consisted in taking part in studies, by numerical simulation and experimental tests, aimed at optimizing the performance of plasma arc torches for cutting metals, involving members of the Group for Industrial Applications of Plasma of the University of Bologna and the members of R & D section of the Cebora Spa Company. Some of the activities related to optimization of the performances of consumable electrode and nozzle, in terms of their service life, were carried out in collaboration with the Metallurgy Group of the Department SMETEC of the University of Bologna.

Within the project for the development and the optimization of the high definition multi-gas plasma torch CEBORA CP250G, critical details were encountered in optimizing the performances of the torch when cutting thin plates of mild steel (1-3mm) with O<sub>2</sub> as plasma gas and secondary gas and operating current of 30-40A. The study that have been carried out to address these critical issues has been described in paragraph 1.2. The approach is based on an integrated study of the influence of variations in different operative parameters and different consumables geometry on the torch performances, both in terms of cut quality and expected life of consumables. Reported results concern operative parameters values and geometry of consumables fit for optimizing the process, overcoming its intrinsic critical aspects and reaching cutting performances that can be usefully compared to those obtainable from laser technology. All experimental tests have been supported by simulative studies in aimed at understanding physical phenomena that take place inside the plasma chamber during cutting.

My collaboration for the activities for the development of the mono-gas torch Cebora CP161 manual and automatic cutting of metallic materials with a maximum current of 160A consisted in participating both in the first phase of design of the components of the new torch and in the subsequent phases of development and optimization of the overall torch performances, as explained in the 1.3 paragraph. In this context, my activities focused on both participating in several experimental campaigns carried out during the performance optimization in terms of cutting and wear of consumable components, and the new flashlight models and developing 2D and 3D models of the new torch prototype that I subsequently implemented in FLUENT carrying out numerical simulations to study the influence of changes in operating conditions and consumable components geometry on the behavior of the plasma discharge inside the chamber and on the interaction between the plasma discharge and the secondary gas jet.

The main problems encountered in the development of the torch, and on which I focused in both experimental tests and simulations have been:

- adequate cooling of the consumable components, in particular the electrode and nozzle, for which it was necessary to develop multiple head configurations that differ in the different ways for the passage of air gas inside the torch;
- service life of the electrode; this problem, present in all the torches that operate with oxidizing plasma gas, is particularly important in torches that are used manually as it is not possible to work on optimizing the current and pressure profiles transients in shutdown in order to reduce the expulsion of Hf based material from the emitter melted pool. It was therefore necessary to study the effects of internal and external geometry of the electrode and the nozzle, and of the plasma gas inlet swirl velocity component on the plasma gas swirl velocity field inside the plasma chamber;
- interaction of the secondary gas with the plasma discharge under different operating conditions and different geometries of the shield and its consequences on the performances of the torch in terms of cut quality.

My collaboration for the development of the mono-gas plasma torch Cebora CP101 for both manual and automatic cutting of metallic materials with a maximum current of 100A consisted in participating both in the first phase of the design of the new torch components and in the subsequent phases of development and optimization of the overall performances, as explained in the 1.4 paragraph. In this context, my activities focused on participating in several experimental campaigns carried out during the performances optimization in terms of cut speed and quality and of consumable components wear, and on the achieving 2-D and 3D models of the new torch prototype which I then implemented in FLUENT in order to study the influence of changes in operating conditions and consumable geometry on the behavior of the plasma discharge inside the chamber and on the interaction between the plasma discharge and the secondary gas flow.

The main problems encountered in the development stage of the torch, and on which I focused in both experimental test and numerical simulations have been:

- service life of the electrode; this problem, present in all the torches that operate with oxidizing plasma gas, is particularly important in torches that are used manually as it is not possible to

work on optimizing the current and pressure profiles transients in shutdown in order to reduce the expulsion of Hf based material from the emitter melted pool. It was therefore necessary to study the effects of internal and external geometry of the electrode and the nozzle, and of the plasma gas inlet swirl velocity component on the plasma gas swirl velocity field inside the plasma chamber;

- interaction of the secondary gas with the plasma discharge under different operating conditions and different geometries of the nozzle and its consequences on trajectories of the molten metal droplets coming from the *kerf* during the piercing phase;
- optimization of the shape and of the size of the spacer component in terms of minimization of its influence on the behavior of the secondary, in particular, for minimizing the formation of recirculating vortices between the nozzle tip and the surface of the work-piece;
- study of the behaviour of Hf cathodes, with high speed camera (HSC) imaging techniques, during the ignition transient, to highlight the different behaviour of the cathodic attachment in torches with retract starting and high frequency pulse pilot arc ignition, with electrodes for plasma arc cutting (PAC) of mild steel plates.

## 1.1 Physical-Mathematical Model

2D and 3D computational models for transferred arc plasma torch requires the solution of the fluid-dynamic, electromagnetic, and energy-transfer equations, as done in [3]–[6].

The details of the plasma chamber, of the nozzle outer surfaces and of the work-piece are included in the computational domain. The plasma chamber is bounded by the inner wall of the nozzle, the outer wall of the cathode and the Hf emission surface. The injection of the plasma gas is achieved by a pressure inlet fixed on the upper boundary of the plasma chamber. The area of the plasma gas inlet boundary is equivalent to the real cross section of the considered plasma diffuser holes, allowing us to obtain, together with a properly definition of the pressure value at the inlet, realistic values of the velocity magnitude in the plasma chamber. At the same time, the properly definition of the direction vector components allowed us to take into account the real plasma gas flow direction.

The electrical potential boundary condition on the cathode has been implemented by means of a parabolic current density profile fixed on the Hf emitter surface. The shape of the profile does not significantly influence the plasma quantities for a fixed total current, as stated also in [7]. The *kerf* has been modeled by a hole, at the center of the work-piece upper surface, regarded as a pressure outlet boundary.

Turbulence phenomena are taken into account by means of a  $\kappa$ - $\varepsilon$  realizable model [8]. The capability of this turbulence model to predict experimentally measured pressure in the plasma chamber and flow rates was verified. Flow inside the plasma torch presents a transitional regime: turbulent in the region close to the inlet, nearly laminar inside the nozzle, and turbulent again at the nozzle exit. Boundary layer meshing is performed by using a very fine grid near the walls, of about 20  $\mu\text{m}$ , in order to capture the details of the flow field and the mechanisms of turbulence generation. The main simplifying assumptions are: stationary discharge, optically thin plasma, and local thermodynamic equilibrium. Taking into account the previous assumptions, the equations for the species diffusion and momentum take the following form:

$$\nabla \cdot (\rho \bar{v} Y_i) + \nabla \cdot \bar{J}_i = 0$$
$$\nabla \cdot (\rho \bar{v} \bar{v}) = -\nabla p + \nabla \cdot \bar{\tau} + \bar{j} \times \bar{B}$$

where  $Y_i$  is the mass fraction of the species  $i$ ,  $\bar{J}_i$  represents the diffusive fluxes of the species  $i$ ,  $\rho$  is the density of the fluid,  $\bar{v}$  is the velocity of the fluid,  $p$  is the pressure,  $\bar{\tau}$  denotes the viscous stress tensor, and the last term is the Lorentz force due to the interaction of the conductive fluid and the electromagnetic field.

The energy equation is solved taking into account the viscous dissipation and including the kinetic energy term

$$\nabla \cdot \left[ \rho \vec{v} \left( h + \frac{v^2}{2} \right) \right] = \nabla \cdot (k \nabla T) - \frac{5}{2} \frac{k_B}{e} \left( \vec{j} \cdot \frac{1}{C_p} \nabla h \right) + Q_J - Q_R$$

where  $h$  is the enthalpy of the fluid,  $k$  is the thermal conductivity of the fluid,  $k_B$  is the Boltzmann constant,  $e$  is the electron charge,  $j$  is the current density, and  $C_p$  is the specific heat of the fluid at constant pressure.  $Q_J$  is the energy dissipated in the discharge by the Joule effect, and  $Q_R$  represents the radiation losses. Compressibility is taken into account as in [9]. The main effects of pressure on the plasma properties regard density and radiation emission; in this model, we assume a linear dependence of these properties on the pressure. Maxwell equations are solved using electrostatic potential  $V$  and vector potential  $A$  in the form:

$$\nabla \cdot \sigma \nabla V = 0$$

$$\nabla^2 \vec{A} + \mu_0 \vec{j} = 0$$

$$\vec{j} = \sigma \vec{E} = -\sigma \nabla V$$

where  $\sigma$  is the temperature dependent electrical conductivity of the plasma,  $\vec{j}$  represents the current density, and  $\mu_0$  is the magnetic permeability of the vacuum. The electromagnetic equations are solved by the FLUENT solver by means of a user-defined scalar. The thermodynamic and transport coefficients of gas used for the numerical simulations are those given in [10-12]; the radiation properties are those given in [13].

## **1.2 Optimization of plasma arc cutting of mild steel thin plates through experiments and 2D simulations**

Plasma arc cutting processes (PAC) of mild steel thin plates through a Cebora HQC Plasma Prof 164 plasma source, operating in the range 25-120A, with a Cebora CP250G plasma torch have been studied. Plasma arc cutting of mild steel thin plates (thickness in the range 1-3mm) is characterized by low current levels (25-45A) and the use of O<sub>2</sub> both as plasma gas and secondary gas. Intrinsic critical aspects initially pointed out concern both cut quality (unevenness of the cut, inclination of the cut surfaces and dross formation) and performance of the consumables (rapid and severe nozzle wear). The aim of the work is to report on the optimization procedure of PAC of mild steel thin plates, carried out with respect to both cut quality and, to achieve high cut quality standards, high performances of the consumables and productivity levels otherwise obtainable with laser cutting processes through the simultaneous planning and analysis of experimental tests and numerical simulations. Experimental tests have allowed a better design of consumables (in particular nozzle, electrode and gas diffusers) and the optimization of current profiles (in particular current levels during pilot arcing); on the other side, modeling and numerical simulation have allowed a better understanding of the physical phenomena evidenced by experimental results and to suggest successful design solutions. The integration of the results of these two activities has allowed the overcoming of the critical aspects initially pointed out, improving plasma jet constriction and reducing plasma jet instabilities, to obtain better cut quality and better performance of the consumables.

### **1.2.1 Description of the experiments**

The plasma cutting system used for experiments comprises the power supply Cebora Plasma Prof 164 HQC, equipped with the remote high frequency unit HV18 and the Gas Console PGC1-2 for manual gas settings, together with the multi-gas plasma torch CP250G (Fig. 1.2.1). The system can operate in the current range 25-120A. Torch motion is accomplished by means of a CNC cutting table 1000x1000 mm. During experimental tests several quantities have been continuously monitored through a digital oscilloscope LeCroy Waverunner LT374M, namely: arc current, pressure and flow of plasma and secondary gas, voltage between electrode and work-piece and voltage between electrode and nozzle. Measurements of the squareness of the cut and of the roughness of cut surfaces to define cut quality in accordance with the International Standard ISO 9013 [14] have been done on samples cut under each operative condition and for each set of consumables.

All the accomplished experimental tests had the aim of evaluating how cut quality and consumables erosion can be influenced by a change in operative conditions or in geometry of the consumables. In particular, experimental observations have focused on the investigation of phenomena typically considered to be critical for the cutting process in those conditions: unevenness of the *kerf* surface, inclination of the cut surfaces and dross formation. Moreover, in spite of the presence of an oxidizing plasma gas, electrode erosion is not a critical aspect in this case, due to the low operative

current levels, while wear phenomena concern particularly the nozzle. In fact, during experimental tests, in some operating conditions, after very few piercings (<100) a severe wear process can involve nozzle orifice inlet and outlet regions, also inducing a deterioration of the cut quality: in fact, under these cutting conditions the nozzle is characterized by diameter of its orifice less than 1mm, and rapid wear can take place in case of minimal arc instabilities. So, maximization of arc stability becomes a priority objective, to be obtained through modifications of both operative parameters and geometry of the consumables. The influence of operative parameters on critical phenomena has been studied, mainly changing secondary gas flow and the plasma gas inlet pressure. Also, modifications of the geometry of the consumables have been carried out, for nozzle, electrode and gas diffusers.

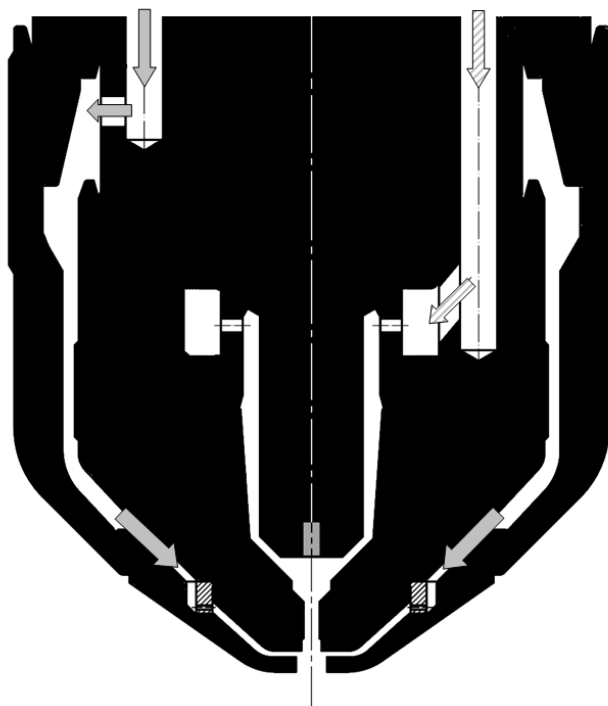


**Fig. 1.2.1** schematic of the Cebora CP250G torch head with plasma and secondary gas flow injection points.

Taken from [6].

## 1.2.2 Results

### *Effects of variations in secondary gas flow*

Experimental tests showed that the secondary gas flow strongly influences the level of unevenness of the *kerf* surface, while it has not influence on other aspects of the cut quality and on the performance of consumables. In particular, it has been verified that with a secondary gas flow lower than 9 lpm the unevenness of the *kerf* surface disappears, independently from other cutting parameters and from geometry of the consumables. Different electrode geometries have been tested (changing the length of the copper holder and the diameter of the hafnium insert) together with different nozzle geometries (changing the diameter of the nozzle orifice, the internal shape of the plasma chamber and the internal shape of the nozzle orifice exit) and different shield geometries (changing the diameter of the shield orifice and the distance from the nozzle tip) to highlight their influence on the unevenness of the cut. Moreover, in addition to the secondary gas flow, other

cutting parameters have been studied, in terms of their influence on the unevenness of the cut: cutting velocity, distance between the torch and the work-piece and cutting pressure of the plasma gas. In every tested condition, only the secondary gas flow had influence on the unevenness of the *kerf* (Fig.1.2.2).

With the conventional torch configuration, to obtain a very low secondary gas flow rate (<9 lpm) it is necessary to set a secondary gas pressure which is too low (< 40 kPa) to guarantee a correct functioning of the pressure regulator in the gas console. In order to obtain the best compromise between these two opposite needs, a modified secondary diffuser has been designed and tested, with a number of the holes suitably set to obtain a plasma flow rate lower than 9 lpm with a secondary gas pressure value sufficiently high for the gas console.

Simulation analysis wasn't used to study the influence of the secondary gas flow rate on the unevenness of the cut surfaces because this phenomenon is related to the interaction between the plasma jet and the workpiece and it has no relationship with phenomena that taking place inside the nozzle.

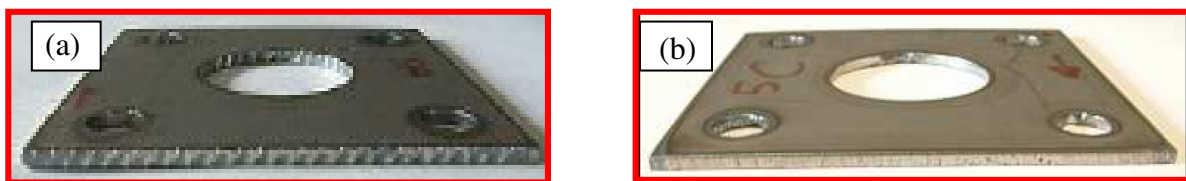


**Fig. 1.2.2** mild steel piece of 2 mm thickness cut with secondary gas flow rate (a) higher than 9 lpm and (b) lower than 9 lpm. Taken from [6].

#### *Effects of variations in plasma gas inlet pressure*

Modelling and numerical simulation results showed that the maximum value of plasma temperature moves toward the cathode (Fig. 1.2.3) and that plasma swirl velocity increases in the plasma chamber and along the nozzle orifice wall (Fig. 1.2.4), when plasma gas pressure increases. These results can be related to an improved constriction of the plasma jet and to an improved cooling of the nozzle orifice exit region. On this basis, experimental test with different levels of the plasma gas pressure have been accomplished. Experimental results were in agreement with simulation results, showing that an increase in the plasma gas inlet pressure, and so in the plasma flow rate, brings to an improvement of cut quality and to a reduction of nozzle wear. Finally, the operative plasma pressure level was brought from 450 kPa (corresponding to a plasma flow rate of about 4 lpm) to 540 kPa obtaining a plasma flow rate of about 5.4 lpm.

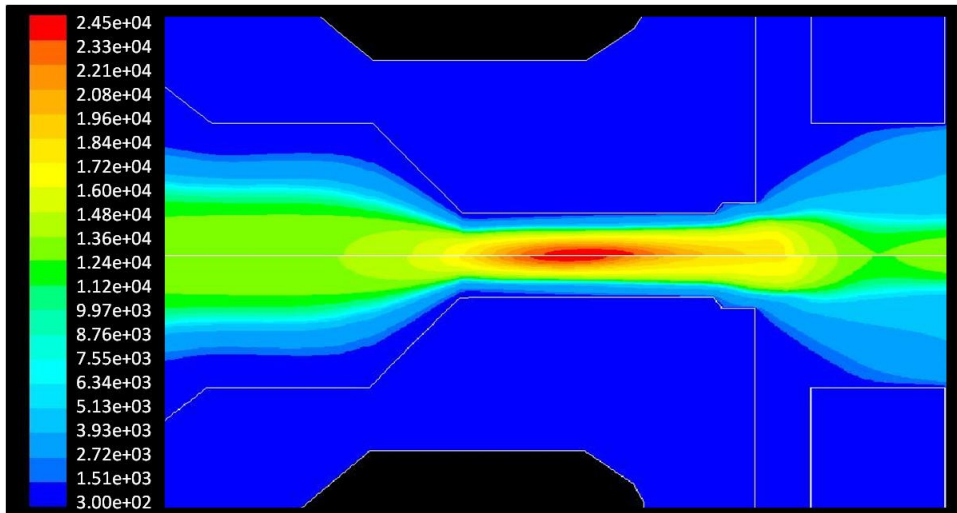


**Fig. 1.2.3** Plasma temperature field [K] for the simulation of the Cebora plasma torch under the following operating conditions: 40 A; plasma gas pressure (O<sub>2</sub>): 540 kPa (upper half) and 590 kPa (lower half); secondary gas pressure (O<sub>2</sub>): 40 kPa; nozzle diameter: 0.8 mm. Taken from [6].

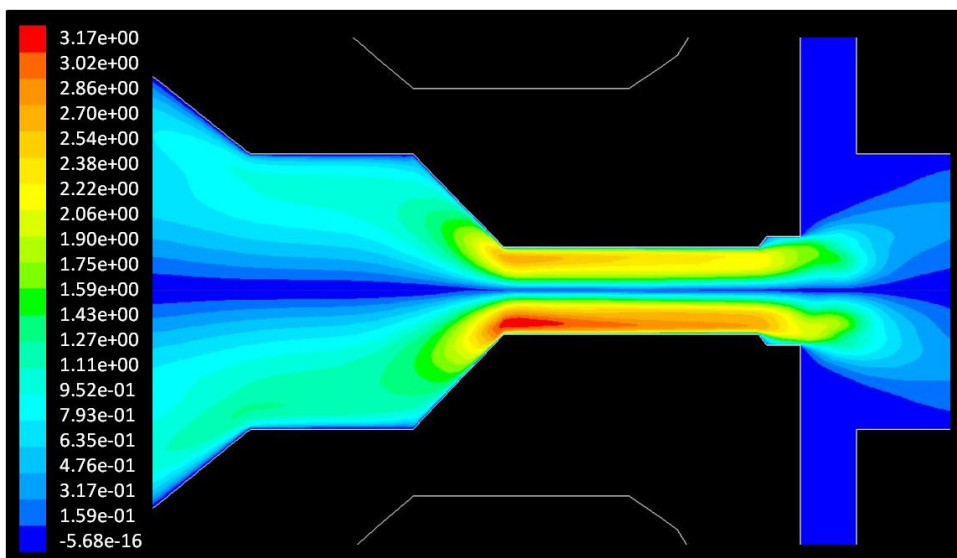


**Fig. 1.2.4** Plasma swirl velocity [m/s] for the simulation of the Cebora plasma torch under the following operating conditions: 40 A; plasma gas pressure (O<sub>2</sub>): 540 kPa (upper half) and 640 kPa (lower half); secondary gas pressure (O<sub>2</sub>): 40 kPa; nozzle diameter: 0.8 mm. Taken from [6].

### *Effects of changes in nozzle internal geometry*

One of the intrinsic critical aspects initially pointed out concern the severe and rapid wear of the internal area of the nozzle orifice, with consequent deterioration of the cut quality. Changes in nozzle internal geometry have been tested in order to reduce the arc instabilities and to improve plasma arc constriction. The geometry of the conventional Cebora nozzle orifice for cutting mild steel plates thicker than 3 mm, is characterized, in its end portion, by the enlargement of the hole diameter with a conventional cylindrical shape. Changes to the geometry of this end portion of the

nozzle orifice with the introduction of a conical shape have been accomplished and tested (Fig. 1.2.5).

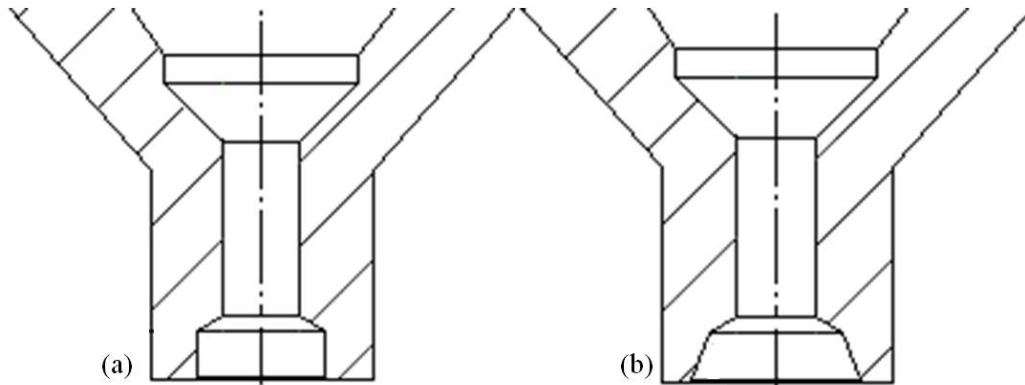


**Fig. 1.2.5:** (a) 2D scheme of a conventional Cebora nozzle with a cylindrically shaped orifice end and (b) 2D scheme of a modified Cebora nozzle with a conically shaped nozzle orifice end. Taken from [6].

Experimental results showed that, alone, the introduction of the modified nozzle induces an increase of plasma gas flow rate: maintaining the plasma pressure reference value of 540 kPa, the plasma flow rate becomes about 7.2 lpm, while with the standard nozzle it was about 5.4 lpm, as abovementioned (Table 1). This result can be correlated to the abovementioned effects deriving from the improvement of the plasma gas pressure and consequently of the plasma flow rate.

Plasma pressure [kPa]	450		520		540	
	Cilindrical	Conical	Cilindrical	Conical	Cilindrical	Conical
Plasma flow rate [lpm]	4.00	5.30	5.00	6.70	5.40	7.20

**Table 1.2.1** Plasma flow rate for different values of the plasma pressure and for different shapes of the nozzle orifice end. Taken from [6].

In fact, modelling and numerical simulation results showed that the introduction of a conical shape in the nozzle orifice end brings to a further increasing of the plasma swirl velocity in the nozzle orifice region (Fig. 1.2.6). Moreover, modelling and numerical simulation results shows how the introduction of the described modified nozzle induces some relevant effects: the disappearing of a turbulent vortex on the nozzle orifice exit wall with improved cooling of the nozzle (Fig. 1.2.7), the reduction of the static temperature of nozzle wall along its orifice, together with a shift of its maximum value towards a more internal axial coordinate (Fig. 1.2.8). These results describe a

further improvement of the plasma arc constriction and of the nozzle efficient cooling, with respect to the ones obtainable through the previously described increase of the plasma pressure.

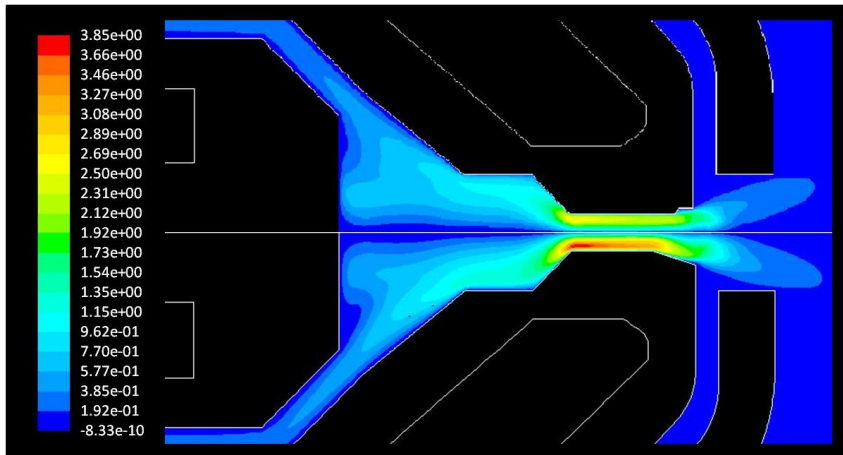


**Fig. 1.2.6** Plasma swirl velocity [m/s] for the simulation of the Cebora plasma torch under the following operating conditions: 40A; plasma gas pressure ( $O_2$ ): 540 kPa; secondary gas pressure ( $O_2$ ): 40 kPa; nozzle diameter: 0.8mm with a nozzle orifice end cylindrically shaped (upper half) and conically shaped (lower half). Taken from [6].

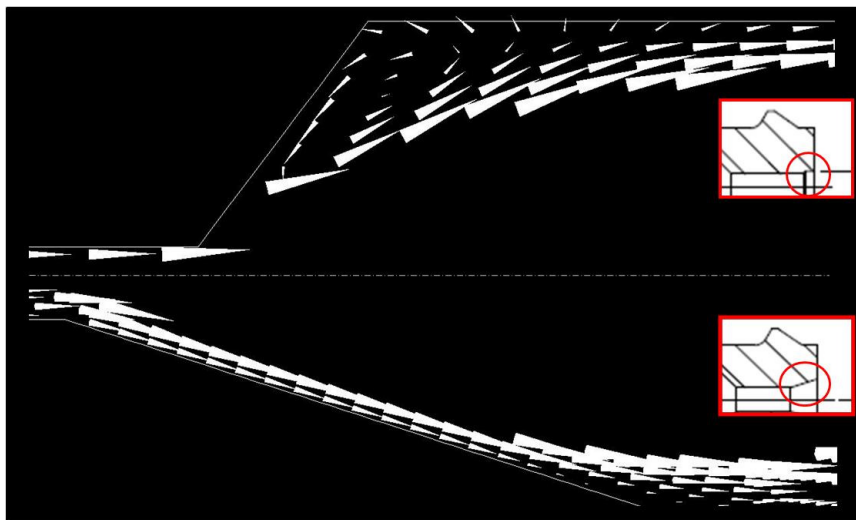


**Fig. 1.2.7** Plasma velocity [m/s] for the simulation of the Cebora plasma torch under the following operating conditions: 40 A; plasma gas pressure ( $O_2$ ): 540 kPa; secondary gas pressure ( $O_2$ ): 40 kPa; nozzle diameter: 0.8 mm with the nozzle orifice end cylindrically shaped (upper half) and conically shaped (lower half). Taken from [6].

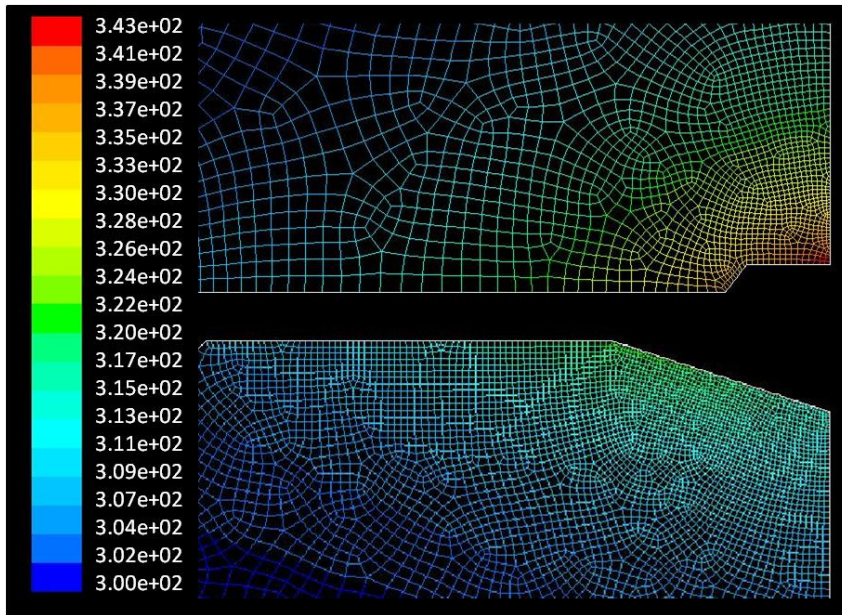


**Fig. 1.2.8** Temperature of the nozzle wall [K] for the simulation of the Cebora plasma torch under the following operating conditions: 40A; plasma gas pressure ( $O_2$ ): 540 kPa; secondary gas pressure ( $O_2$ ): 40 kPa; nozzle diameter: 0,8mm with a nozzle orifice end cylindrically shaped (upper half) and conically shaped (lower half). Taken from [6].

Finally, experimental results showed that the introduction of the modified nozzle brings to a considerable increase of the cutting quality with respect to the original configuration, reaching a “range 1” cut as defined by the ISO 9013-2002. Moreover, the introduction of the modified nozzle involved the improvement of the nozzle service life (up to about 500-600 piercings) delaying the occurrence of two destructive phenomena that initially used to eventually affect the nozzle after few piercings (about 100): the deformation of the inlet region of the nozzle orifice, due to arc instabilities and the corrosion of the exit end of the nozzle orifice, due to overheating (Fig. 1.2.9).

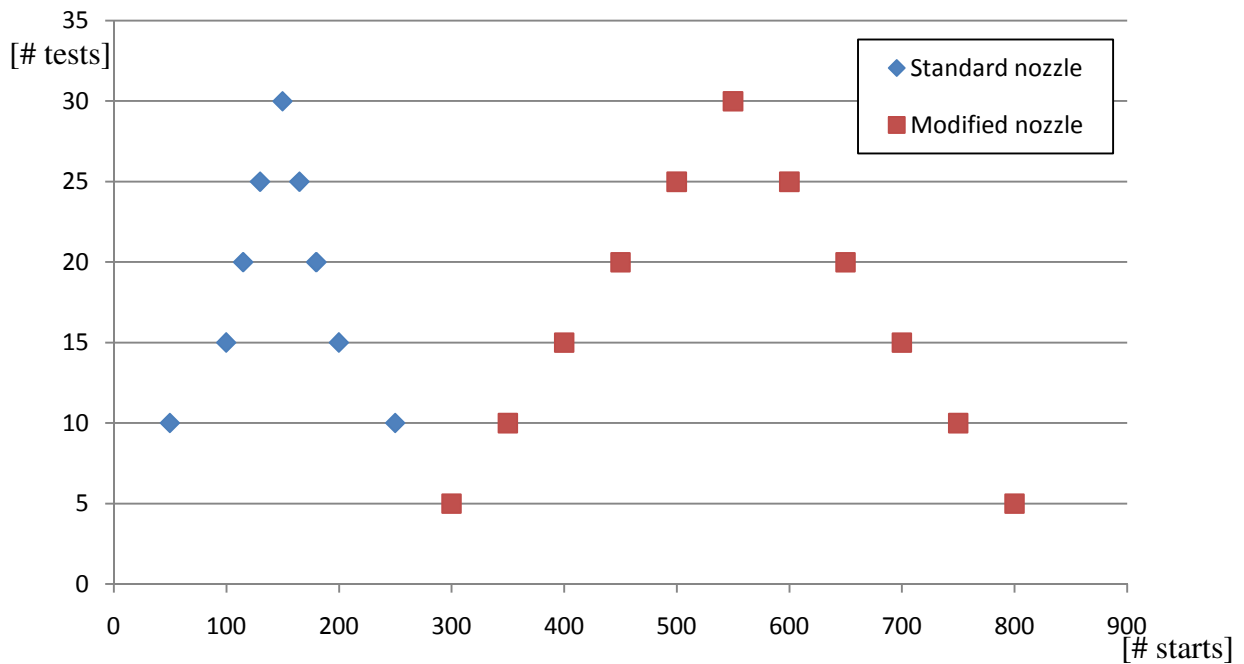


**Fig. 1.2.9** graph of the distribution of nozzle wear for a standard nozzle (blue) and for a nozzle with a conically shaped orifice end (red). Taken from [6].

*Effects of variations in the depth of the conical area in the nozzle orifice end*

After the introduction of a conical shape in the nozzle orifice end, different depths of this conical area have been tested to better understand its influence on cutting performance. The depth level of the conical area in the nozzle orifice end has been evaluated through measurements of the penetration depth of a 1 mm diameter pin inserted into the nozzle through the nozzle tip (Fig. 1.2.10).

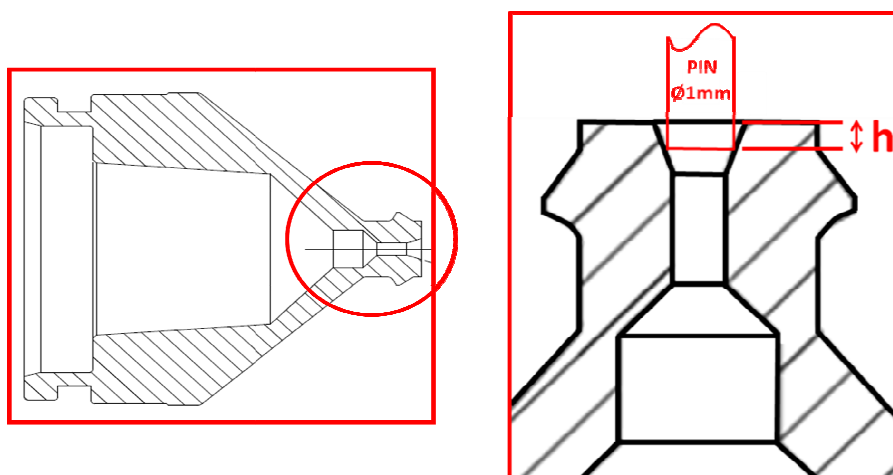


**Fig. 1.2.10** scheme of the experimental set-up to measure the depth  $h$  of the conical area in the nozzle orifice end. Taken from [6].

Experimental tests showed a deterioration of the cutting quality both increasing and decreasing the penetration depth value around 0.6 mm (Fig. 1.2.11). The cutting quality has been evaluated as the perpendicularity of the cut surface, through the indicator “angularity tolerance” as defined in the ISO 9013-2002. The same trend has been identified for what concern the correlation between the depth of the conical area in the nozzle orifice end and the nozzle wear phenomena. Best results, in terms of nozzle service life, have been obtained with nozzles whose depth level of the conical area was in the range 0.59-0.62 mm (Fig. 1.2.12). In this conditions the expected nozzle service life reaches about 600-800 piercings. With nozzles whose depth of the conical area in the orifice end was outside abovementioned range, more quick wear phenomena have been taken into account. Finally, the penetration depth value of 0.6 mm has been identified as the reference value since it enabled to obtain both the best cut quality and the highest nozzle expected life.

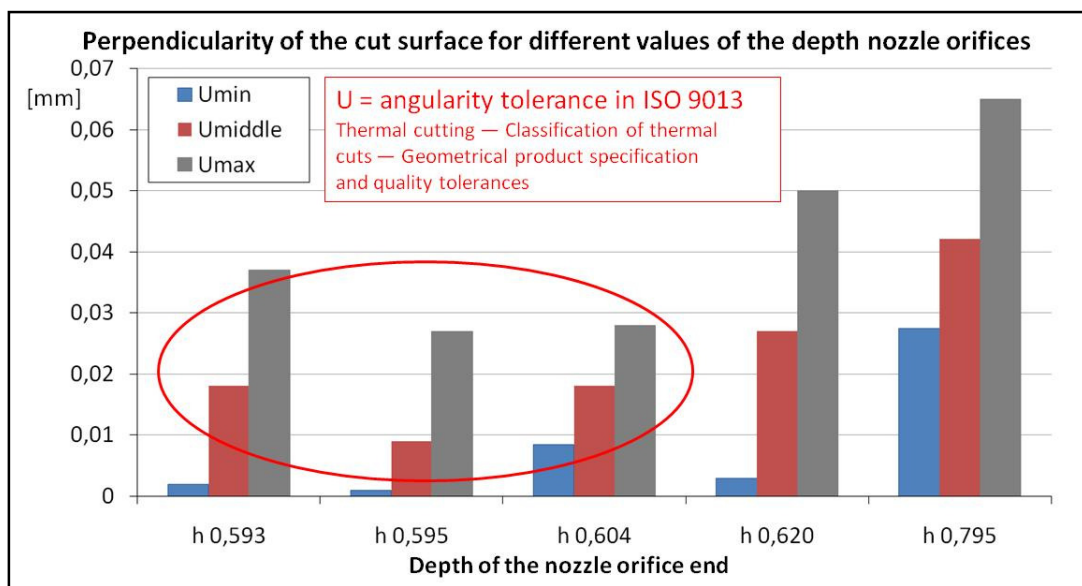


**Fig. 1.2.11** graph of the perpendicularity of the cut surface for different values of the depth of the conical area in the nozzle orifice end. Taken from [6].

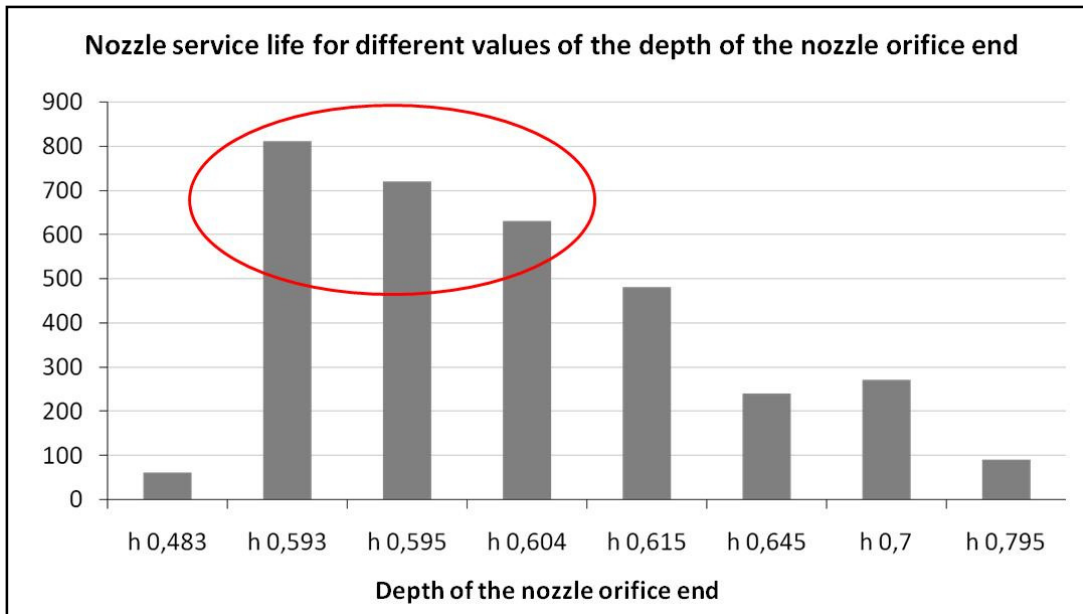


**Fig. 1.2.12** graph of the nozzle service life for different values of the depth of the conical area in the nozzle orifice end. Taken from [6].

Numerical simulations have been carried out for different values of the depth of the conical area in the nozzle orifice end. They showed as, with the increasing of the depth of the conical area in the nozzle orifice end, the maximum value of the plasma temperature moves toward the cathode (Fig. 1.2.13), the values of axial plasma velocity show a reduction, while its maximum value shifts toward the cathode (Fig. 1.2.14); also, the swirl velocity linearly increases everywhere (Fig. 1.2.15) while the temperature of the nozzle wall linearly decreases everywhere (Fig. 1.2.16).

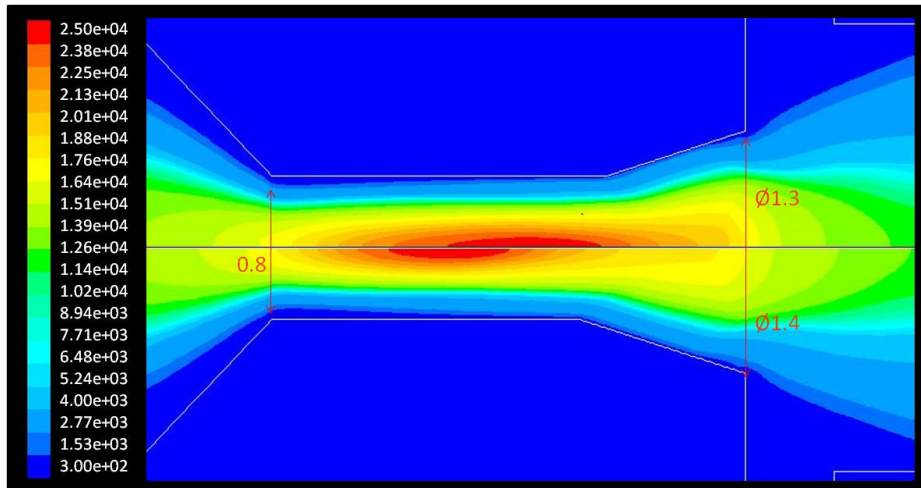


**Fig. 1.2.13** Plasma temperature [K] for the simulation of the Cebora plasma torch under the following operating conditions: 40 A; plasma gas pressure ( $O_2$ ): 540 kPa; secondary gas pressure ( $O_2$ ): 40 kPa; nozzle diameter: 0.8 mm with a diameter of the nozzle orifice outlet of 1.3 mm (upper half) and 1.4 mm (lower half). Taken from [6].

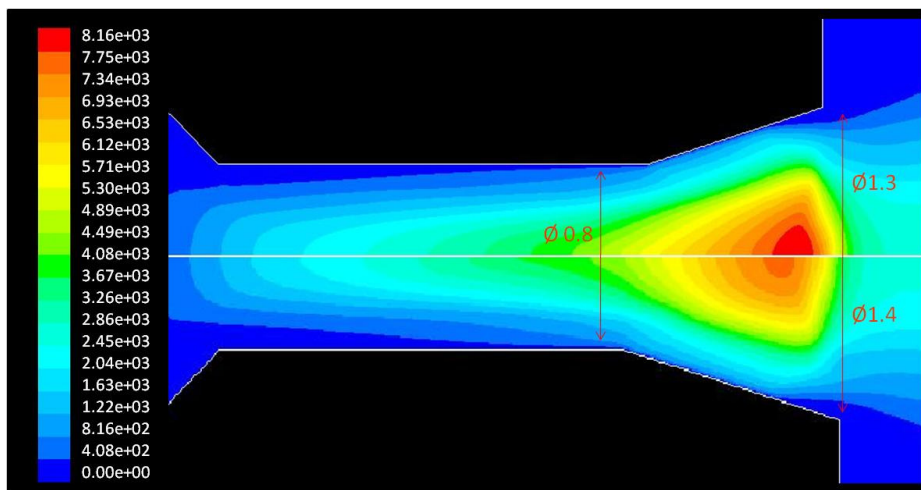


**Fig. 1.2.14** Plasma axial velocity [m/s] for the simulation of the Cebora plasma torch under the following operating conditions: 40 A; plasma gas pressure ( $O_2$ ): 540 kPa; secondary gas pressure ( $O_2$ ): 40 kPa; nozzle diameter: 0.8 mm with a diameter of the nozzle orifice outlet of 1.3 mm (upper half) and 1.4 mm (lower half). Taken from [6].

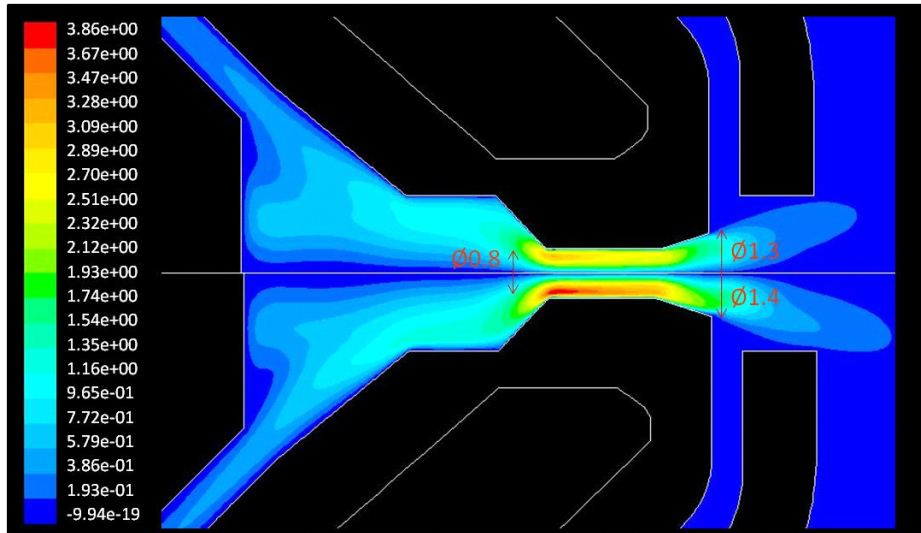


**Fig. 1.2.15** Plasma swirl velocity [m/s] for the simulation of the Cebora plasma torch under the following operating conditions: 40 A; plasma gas pressure ( $O_2$ ):540 kPa; secondary gas pressure ( $O_2$ ): 20 kPa; nozzle diameter: 0.8 mm with a diameter of the nozzle orifice outlet of 1.3 mm (upper half) and 1.4 mm (lower half). Taken from [6].

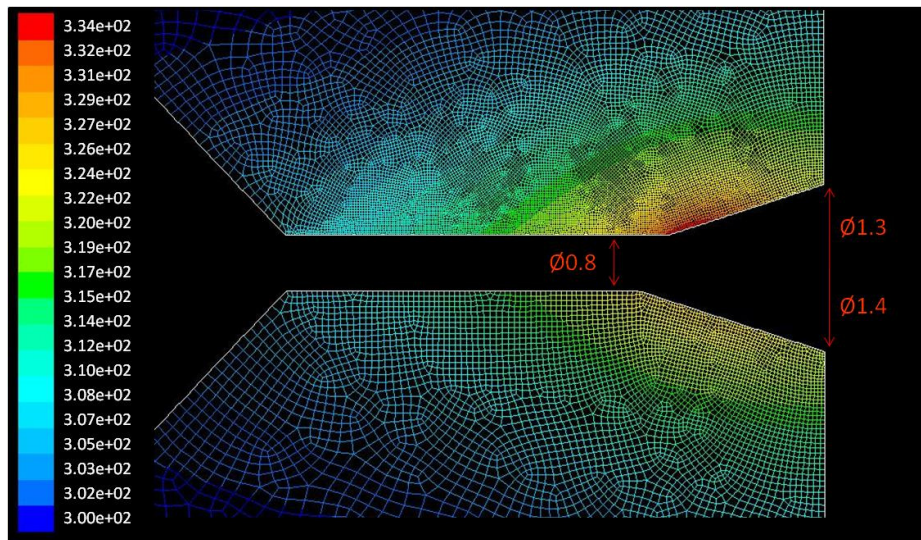


**Fig. 1.2.16** Temperature of the nozzle wall [K] for the simulation of the Cebora plasma torch under the following operating conditions: 40 A; plasma gas pressure ( $O_2$ ): 540 kPa; secondary gas pressure ( $O_2$ ): 80 kPa; nozzle diameter: 0.8 mm with a diameter of the nozzle orifice outlet of 1.3 mm (upper half) and 1.4 mm (lower half). Taken from [6].

### *Effects of variations in the plasma gas diffuser geometry*

The plasma diffuser design is fundamental to obtain the correct amount of plasma gas flowing the plasma chamber. Experimental tests have been carried out with several plasma gas diffusers, differing from one another for the diameter of the holes that allow the passage of the plasma gas. In particular, three diffusers with (three) holes of different diameter have been tested: 1.1 mm, 0.75

mm and 0.4 mm, respectively. Experimental results showed that a reduction of the diameter of the holes induces an increase in arc constriction, thus improving cut quality and reducing nozzle internal surfaces deterioration. However, too small diameters of the holes do not guarantee suitable levels of plasma flow rate into the nozzle, so increasing the probability of arc instabilities. Therefore, it is necessary to identify the better compromise between these two opposing needs. In the considered cutting conditions, the previously described increase in the plasma pressure and the introduction of the modified nozzle, brought to the presence of a very high plasma flow rate into the nozzle (about 7.2 lpm); then, the plasma diffuser characterized by three holes of 0.4 mm, that has been defined as the best solution for arc constriction, maintains a suitable plasma flow rate into the nozzle, about 6.5 lpm (Table 2).

Plasma Diffuser	Plasma gas flow rate [slpm]					
	P-plasma: 450 kPa		P-plasma: 520 kPa		P-plasma: 540 kPa	
	Standard nozzle	Conical nozzle	Standard nozzle	Conical nozzle	Standard nozzle	Conical nozzle
Ø 1,1 mm	4,00	5,30	5,00	6,70	5,40	7,20
Ø 0,75 mm	3,90	5,20	4,90	6,60	5,20	7,10
Ø 0,4 mm	3,80	4,80	4,60	6,00	5,00	6,50

**Table 1.2.2** Values of plasma gas flow rate for different plasma diffusers, different plasma pressure levels and different nozzle type. Taken from [6].

#### *Effects of variations in the hafnium insert diameter*

Experimental tests evaluating both cut quality and nozzle wear have been carried out with three different types of cylindrical hafnium insert with equal axial length but with different diameters: 0.8 mm, 1.07 mm and 1.6 mm, respectively.

Experimental results show that the insert with 1.6 mm diameter does not assure a suitable stability of the plasma arc root attachment on the emitter surface, causing a rapid wear of the nozzle internal surface. The morphological analysis of the emitter surface shows that the emission spot (the melted hafnium based puddle) is not axially centred, leaving a portion of the hafnium insert surface unattached (Fig. 1.2.17). This configuration of the electrode emitter surface can lead to arc root attachment instabilities, increasing the probability of double arcing, and can reduce the cooling efficiency of the hafnium insert, with consequent reduction of the electrode expected life.

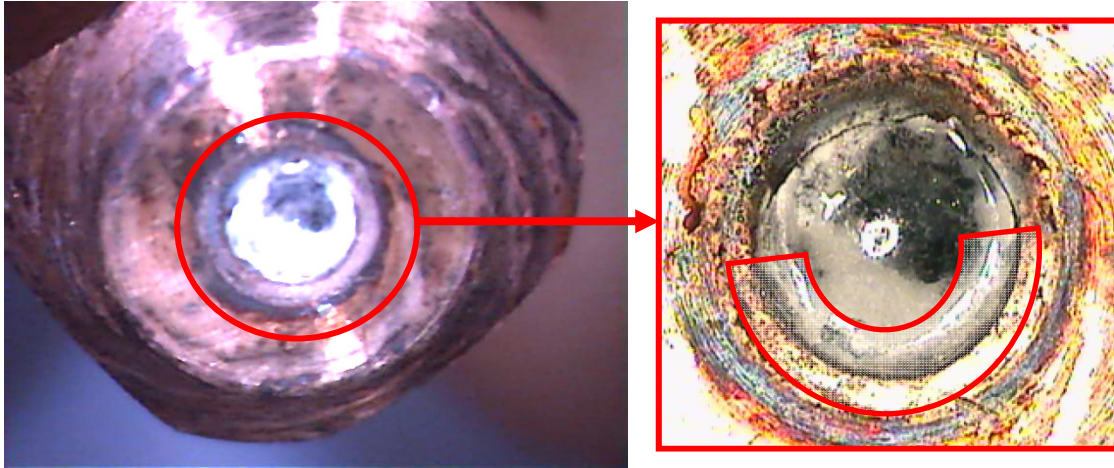


**Fig. 1.2.17** Image of an electrode tip with diameter of the hafnium insert equal to 1.6 mm with evidence of non axially centred attachment. Taken from [6].

On the other side, the hafnium insert with a 0.8 mm diameter induces, in spite low current level used, a considerable overheating of the copper holder in the area around the hafnium insert due to a the melted hafnium based puddle extending on the whole insert area, leading to a rapid deterioration of the electrode due to the increased probability of arc attaching on the copper holder. The morphological analysis of the electrode tip in these conditions shows the presence of discharge marks that go from the emitter surface towards the copper surface (Fig. 1.2.18). Finally, the hafnium insert with 1.07 mm diameter has been proved as the better compromise between the need for suitable arc attachment stability and that of maintaining a sufficient portion of solid hafnium around the emitter spot that surrounds its melted puddle, avoiding the arc attachment moving from the hafnium to the copper surface.

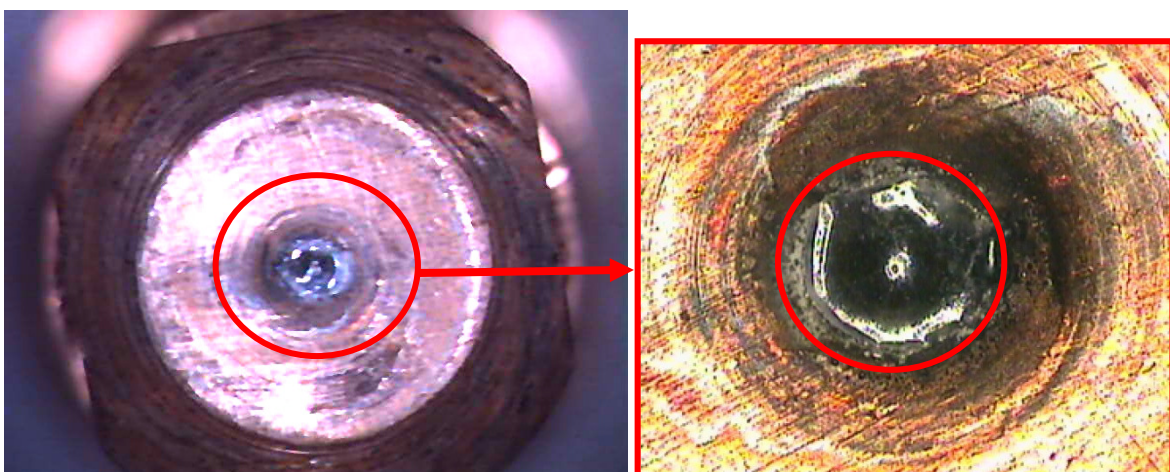


**Fig. 1.2.18** Image of an electrode tip with the diameter of the hafnium insert equal to 0.8 mm with evidence of damaging of the copper holder. Taken from [6].

### *Effects of variations in current profile during pilot arcing*

The plasma arc cutting process is characterized by an initial phase of pilot arcing, in which the arc connects the electrode to the nozzle, which works as anode. This phase starts with the ignition of a low current arc discharge between the electrode and the nozzle; after ignition of the arc, current increases to a pilot arcing level (about 25-45 A) and the particular set of plasma gas operative conditions induces the arc to be blown out of the nozzle and to attach to the workpiece; when the arc is transferred to the workpiece, the nozzle is isolated and the cutting phase starts (Fig. 1.2.19).

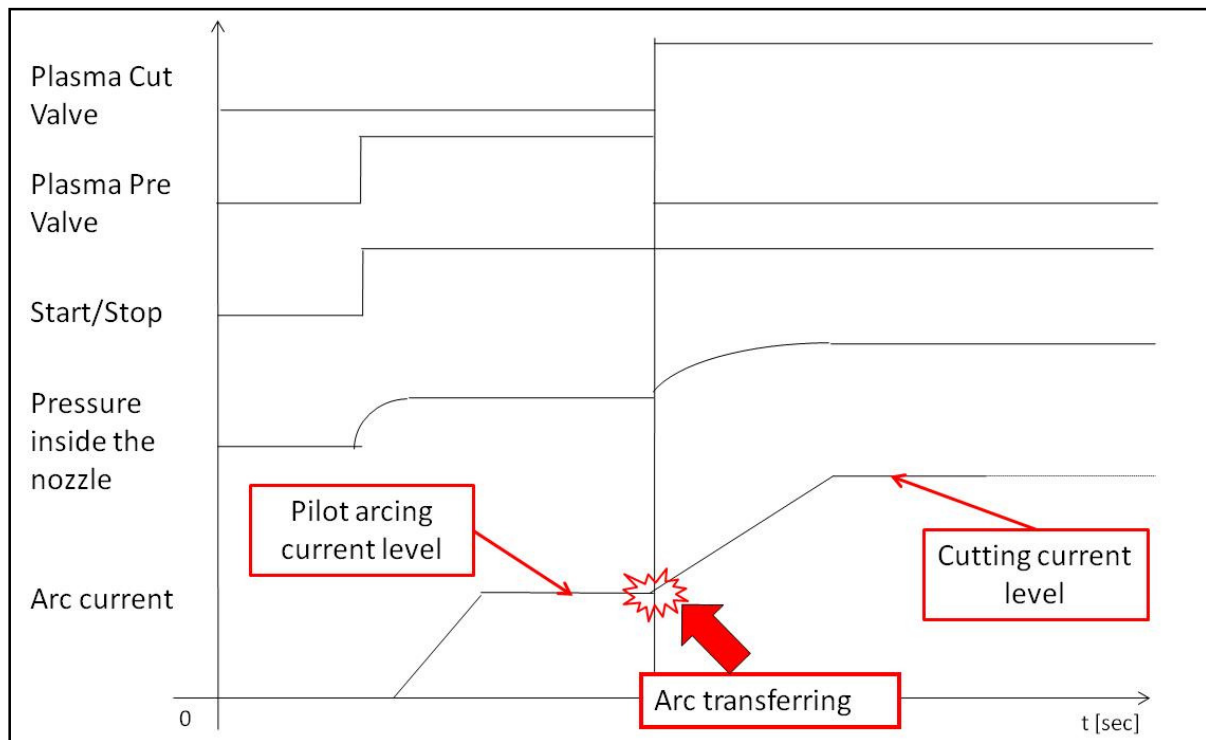


**Fig. 1.2.19** scheme of the waveform of arc current and plasma pressure during the first part of the plasma arc cutting process. Taken from [6].

During pilot arcing phase the internal surfaces and the tip of the nozzle are particularly stressed by the anode arc root attachment [15-16]. In our experiments, the optimization of the current profile in this initial phase of the process had the final aim of minimizing damaging of the nozzle internal surfaces and tip; the deformation of the internal profile of the nozzle can, in fact, lead to a loss of the axial-symmetry of the plasma discharge and consequently to a loss of arc stability. On the other side, in the low current range used for cutting thin plates, the influence of the pilot arcing current profile on electrode erosion phenomena is not a relevant issue. Before optimization, as an effect of pilot arcing, the nozzle internal surface and its tip showed pronounced damaging due to arc attachment points (Fig. 1.2.20). Experimental tests have been aimed at selecting the pilot arcing current level as the best compromise between two opposite needs: the maximization of arc transfer speed and the minimization of nozzle damaging.

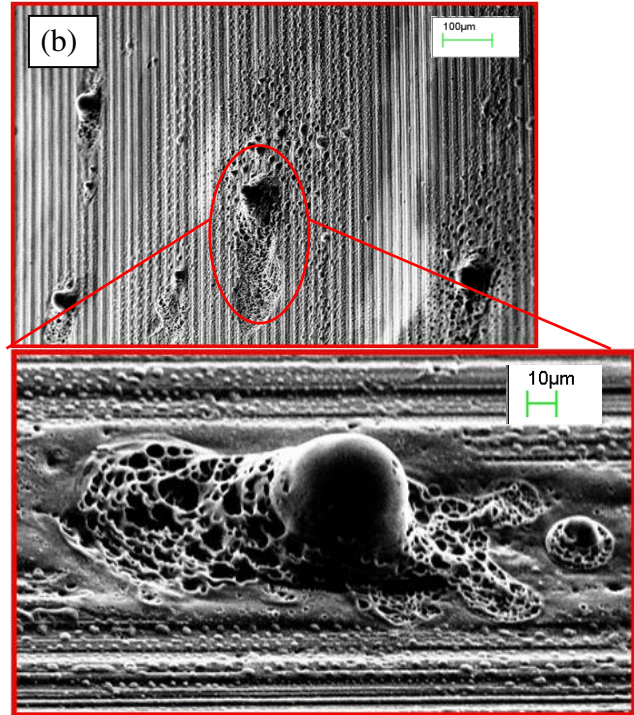
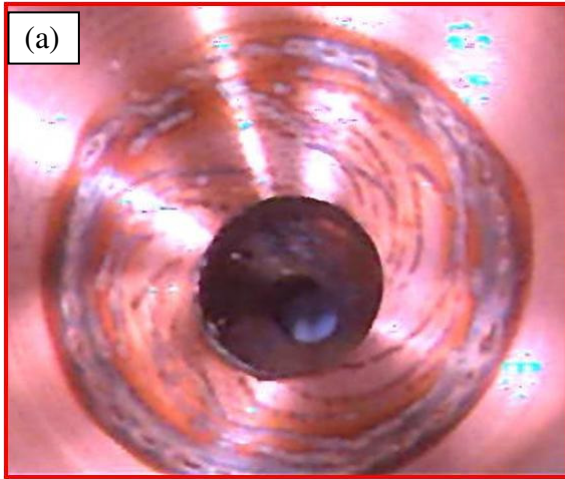


**Fig. 1.2.20** (a) magnified image of the internal surface of the nozzle after pilot arcing with high current level, (b) SEM image of the internal surface of the nozzle. Taken from [6].

### **1.3 Optimization of the consumables service life of a mono-gas plasma torch through experiments and 2D simulations**

Cathode erosion phenomena put still a limit to performance improvement in PAC process; in particular for operative conditions in which oxidizing plasma gases (oxygen and air) and high current levels (above 200 A) are used in presence of an Hafnium (Hf) emitter.

In recent years several studies [1, 17-20] have been accomplished in order to understand phenomena that give rise to Hf erosion in different phases of the PAC operative cycle, at the same time numerical simulation has become increasingly widespread as a tool for torch design, and a lot of papers have been published on this topic ([2]-[9] just to name a few). But none of the works done up to now address numerical simulations able to predict the electrode and nozzle wear mechanisms in realistic operating conditions.

Electrode and nozzle erosion mechanisms in plasma arc cutting (PAC) processes of mild steel have been studied while designing a prototype mono-gas plasma torch, operating in the range 25-160A. The correlation between the distribution of different quantities inside the plasma chamber and the erosion mechanisms of the hafnium emitter surface and of the nozzle inner surfaces have been investigated by means of a 2D FLUENT-based numerical model, with the final aim of optimizing the overall performances of the prototype. Modelling and numerical simulation have allowed a better understanding of the physical phenomena evidenced by experimental results and have suggested successful design solutions for consumables (in particular nozzle, electrode and primary gas diffusers). The correlation between the results of experimental tests and numerical simulations has proven useful in overcoming the critical aspects initially pointed out, significantly improving the expected lifetime of consumables. Results have been analyzed with respect to plasma behaviour, and conclusions have been drawn, concerning the powerfulness of numerical simulation as a tool for designing plasma cutting torches.

The aim of this paper is to investigate the correlation between some distributions of different quantities inside the plasma chamber and the erosion mechanisms of the hafnium emitter surface and of the nozzle inner surfaces by means of a 2D FLUENT-based numerical model.

Using numerical simulation as a tool for torch design implies to define the best compromise between highly realistic modelling (costly) and reliable and accurate results; correspondence between simulation results and experimental evidence must be also obtained.

#### **1.3.1 Experimental set-up**

Experimental tests have been accomplished through a prototype Cebora mono-gas plasma torch, able to operate in the current range 25-160 A both for manual and automated cutting. Experiments have been accomplished at 160 A under operative conditions typically used in cutting of MS plates thicker than 20 mm, with air as both plasma and shield gas. Electrodes have a press fit Hf insert with a 1.6 mm diameter flat emission surface, associated to a 1.8 mm diameter nozzle.

### 1.3.2 Torch and process design

The first experimental tests done with the torch prototypes during design process helped to reveal the major weaknesses in terms of system performance; major critical aspects that have been identified dealt with both electrode and nozzle wear and in particular:

- too small values of the hafnium maximum depth “at death”;
- high average hafnium erosion rates;
- rapid wear of the nozzle orifice inlet.

Average hafnium erosion rates have been evaluated using the ratio between the total depth “at death” and the total number of Cutting Cycles (in the following CCs); it has been measured in mm/20 CCs, as customarily in the plasma cutting experimental practice.

In order to define a strategy for torch prototype optimization, the correlation between simulation results for some quantities inside the plasma chamber and the experimental evidence in terms of electrode and nozzle wear was studied, by means of the abovementioned 2D FLUENT-based code. In particular the following correlations were identified:

- a possible correlation between the intensity of plasma swirl velocity at the nozzle orifice inlet and maximum hafnium erosion depth “at death”;
- a possible correlation between swirl velocity field near the Hf based emission surface of the cathode and its erosion rate;
- influence of the axial component of the plasma gas inlet velocity on the swirl velocity field;
- evaluation of the “real” arc current density taking into account the effective radial extension of the cold boundary region near the wall of the nozzle orifice.

The identified correlations allowed making suitable modifications to the consumables of the new torch prototypes, in particular electrode, nozzle and primary gas diffuser, overcoming the initially highlighted critical aspects.

### 1.3.3 Results and discussion

The importance of the study of swirl velocity in PAC has been highlighted in the past [4, 21]; in this section, results obtained in studying the influence of the plasma gas tangential and axial components on the electrode erosion are showed. The evaluation of the real arc current density inside the nozzle orifice is also presented.

#### *Maximum value/intensity of the plasma swirl velocity at the nozzle orifice inlet*

Erosion tests with a first version of the torch prototype (figure 1.3.1) showed that the electrode death would take place for about 0.8 mm Hf erosion depth (well before the 3.5 mm total axial length of the pellet) and with a quite high average Hf erosion rate (about 0.27 mm/20 CCs). The

overall electrode service life in that case would be about 60 CCs (test1), as shown in figure 1.3.2 and it is unacceptable with respect to any market standard.

Simulative results showed that the geometry of this first version prototype was characterized by reduced values of gas swirl velocity at the exit of the orifices of the primary gas diffuser and by a significant drop of the swirl velocity between the exit of the primary gas diffuser orifices and the nozzle orifice inlet; both phenomena led to very low values of the plasma swirl velocity in the region of the nozzle orifice inlet.

It can be hypothesized that the plasma swirl velocity field in the region of the nozzle orifice inlet influences the constriction and stability of the plasma arc root on the emissive surface, conditioning also the Hf erosion depth “at death”: with the same Hf pellet diameter, a more constricted arc root induces to lower thermal end electric stresses to copper body of the electrode and to the Hf/Cu boundary interface region, leading to higher values of the Hf erosion depth “at death”. For this reason, at first the effects of changes of some design parameters of the torch geometry on the swirl velocity field in the nozzle orifice inlet region have been studied through modelling; subsequently, the correlation between these simulative values and the Hf erosion depth “at death” was found through experimental tests.

In particular, the following torch design parameters were modified:

- number and diameter of the primary gas diffuser holes, together with the Ra size, as shown in figure 1.3.1, in order to increase plasma swirl velocity at the exit of the primary gas diffuser orifices and consequently at the nozzle orifice inlet region;
- the distance between the exit of the primary gas diffuser orifices and the inlet of the nozzle orifice (Ha size, as shown in figure 1.3.1), in order to reduce the drop of the plasma swirl velocity.

As reported in figure 1.3.3, simulative results showed that, changes in the primary gas diffuser geometry gave rise to a significant increase in the maximum value of the plasma swirl velocity at the nozzle orifice inlet: from 20 m/s (figure 1.3.3(a)) to 47 m/s (figure 1.3.3(b)); while the reduction of the Ha size - from 21,74 mm to 15,48 mm - gave rise to a significant reduction of the plasma swirl velocity drop and consequently to an increase of the maximum value of the plasma swirl velocity at the nozzle orifice inlet up to 73 m/s (figure 1.3.3(c)). Erosion tests (test 2 and test 3) have been accomplished under these same torch geometries and operating conditions; experimental evidences showed, as reported in figure 4, that the increase in the maximum value of the plasma swirl velocity at the nozzle orifice inlet corresponds to an increase in the Hf erosion depth “at death” from 0,8 mm (test 1) to 0,9 mm (test 2) and finally to 1,6 mm (test 3), without obtaining significant results on the reduction of the Hf erosion rate in association with the increase of the Hf erosion depth “at death”. As a consequence, a significant increase of the electrode service life has been evidenced: from 60 CCs to 120 CCs. In figure 1.3.5, the correlation between the maximum value of the plasma swirl velocity at the nozzle orifice inlet and the Hf erosion depth “at death” is shown.

### *Swirl velocity field near the emission surface*

In order to design torch geometry and operating conditions aimed at a further increase of electrode service life, a study of the parameters influencing the Hf erosion rate has been accomplished. In particular, the swirl velocity field near the cathode emission surface has been analyzed, taking into account the swirl velocity radial profile at three axial levels (figure 1.3.6): at 0.5 mm (line 1), 1.0 mm (line 2) and 1.5 mm (line 3) from the emitter surface, respectively. By linking simulation and experimental results hitherto obtained, a direct correlation has been found between the Hf erosion rate and what has been called “Hf erosion rate predictor”, that’s to say the ratio between the plasma swirl velocity values on line 1 and the ones at the nozzle orifice inlet (figure 1.3.7). In order to reduce the Hf erosion rate a reduction of the “Hf erosion rate predictor” has been tried, by modifying some design parameters; in particular through the increase of the value of the distance between the Hf emitter surface and the nozzle orifice inlet (Hb size, as shown in figure 1.3.6) from 2.9 mm (test 3) to 3,6 mm (test 4) and to 4,3 mm (test 5), respectively. Simulative results showed that the maximum value of the swirl velocity at the nozzle orifice inlet remained almost unaffected by the modifications applied to the Hb size, while its extension was slightly reduced, as shown in figure 1.3.8; the “Hf erosion rate predictor” values were significantly reduced, as shown in figure 1.3.9. At the same time, erosion tests results showed a significant reduction of the Hf erosion rate, from 0.26-0.29 mm/20 CCs to 0.24 mm/20 CCs, even if the electrode service life remained almost constant, due to a slight reduction of the Hf erosion depth at death, as shown in figure 1.3.10. The torch geometry configuration of test 5 has not been applied in practice because the Hb value of 4.3 mm was considered too critical in terms of arc stability.

### *The axial component of the plasma gas inlet velocity*

In order to further increase the electrode performances, the design of the primary gas diffuser geometry has been changed, to introduce an axial component in the velocity of the plasma gas entering the plasma chamber, while maintaining the same values for its tangential component with respect to the primary gas diffuser of the first version prototype.

Simulative results showed that, the introduction of the axial component in the plasma gas velocity gave rise to an increase of the maximum value of the plasma gas swirl velocity at the nozzle orifice inlet (figures 1.3.11(a) and 1.3.11(b)) from 73 m/s (test 3) to 83 m/s (test 6), with a slight increase of the plasma swirl velocity values on line 1. The combination of these two changes in the plasma swirl velocity field gave rise to a quite similar “Hf erosion rate predictor” for the test 3 and test 6 cases (figure 1.3.12), confirmed by a quite similar experimental value of the Hf erosion rate too (about 0.26 mm/20 CCs).

In order to reduce the “Hf erosion rate predictor”, while maintaining the maximum value of the plasma gas swirl velocity at the nozzle orifice of 83 m/s, an increase of the Hb size from 2.9 mm to 3.6 mm has been introduced (test 7). Simulative results showed that the maximum value of the swirl velocity at the nozzle orifice inlet remained almost unaffected (figure 1.3.11(c)), while the “Hf erosion rate predictor” values were significantly reduced, as shown in figure 1.3.12.

On the side of experiment, erosion test results evidenced both a reduction of the Hf erosion rate to 0.24 mm/20 CCs and an increase in the maximum erosion depth “at death” up to 1.7 mm, with a final significant increase in the electrode service life of 140 CCs (figure 1.3.13).

#### *Evaluation of the real arc current density*

Torch and process design can be supported by the study of suitable parameters, in order to avoid progressive wear of the nozzle orifice due to thermal stress on its inner walls, also inducing significant degradation of cut quality, the parameters inducing been accomplished. For example, the evaluation of the “real” arc current density in the orifice region, taking into account the effective radial extension of the central hot region in which the current flows, as ideally separate from the cold boundary region near the nozzle wall. For this purpose, the temperature radial profile inside the nozzle orifice at different axial levels has been studied (figure 1.3.14), for the torch geometry of test case 7. Figures 1.3.15 and 1.3.16 show the radial behaviour of temperature and current density at the nozzle orifice inlet and at its exit, respectively. The matching of the two curves shows that the current density is significantly different from zero in the region where plasma temperature is above 7500 K. Around this temperature nitrogen dissociation occurs and electrical conductivity increases significantly due to ionization. Therefore, the temperature value of 7500 K has been ideally taken as the transition between hot and cold regions in the plasma jet and its radial location as representative of the arc radius. This type of approach is not new, if one considers the description proposed by Robert Gage in his 1957 patent that started PAC technology [22]: “[...] much of the flowing gas becomes part of the arc and must be heated to arc temperatures [...]” we can describe the hot and cold regions on the whole as gas jet and the central hot region as the current - carrying arc stream. In figure 1.3.17 the arc radius is plotted as function of axial position along the nozzle orifice. Figure 1.3.18 shows the axial profiles of the air mass flow rate in the hot and cold plasma regions. The air plasma flow rate in the hot region is always significantly lower with respect to the one in the cold region; moreover when the arc radius increases, the air mass flow rate in the hot region increases and the air mass flow rate in the cold region decreases, respectively. This analysis allows the study of the temperature field of the cold region (figure 1.3.19) and it could be useful to predict nozzle wear phenomena.

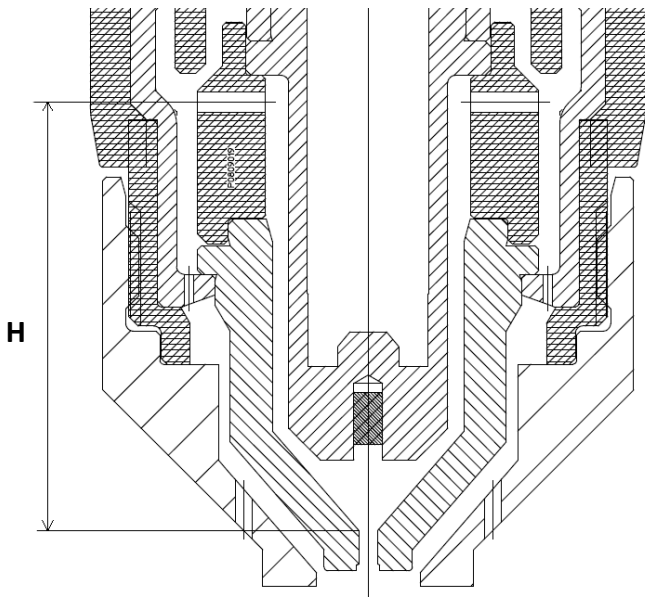


**Figure 1.3.1** 2D schemes of the torch and of the primary gas diffuser of the *first version* prototype (test 1). Taken from [23].

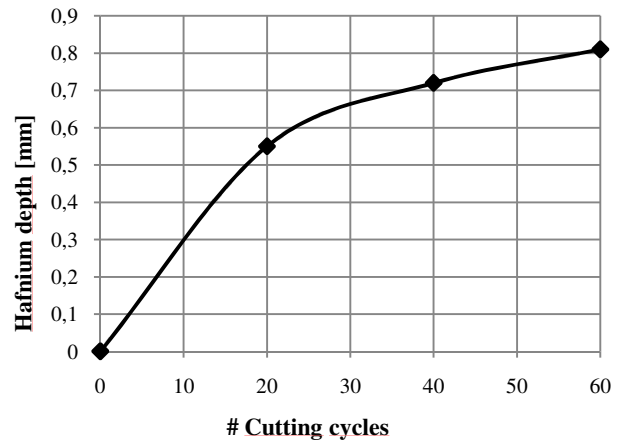
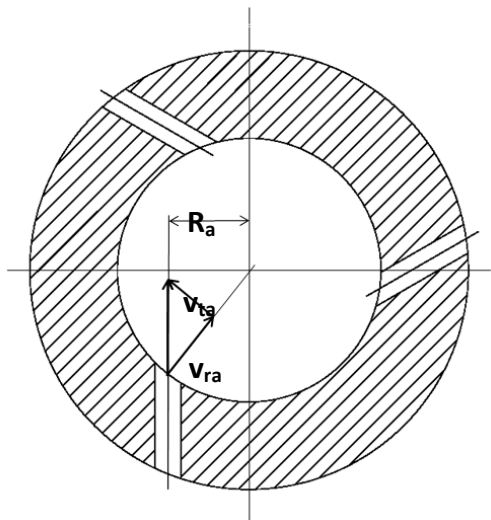


**Figure 1.3.2** Hafnium erosion depth at different CCs for the torch geometry of test case 1. Taken from [23].

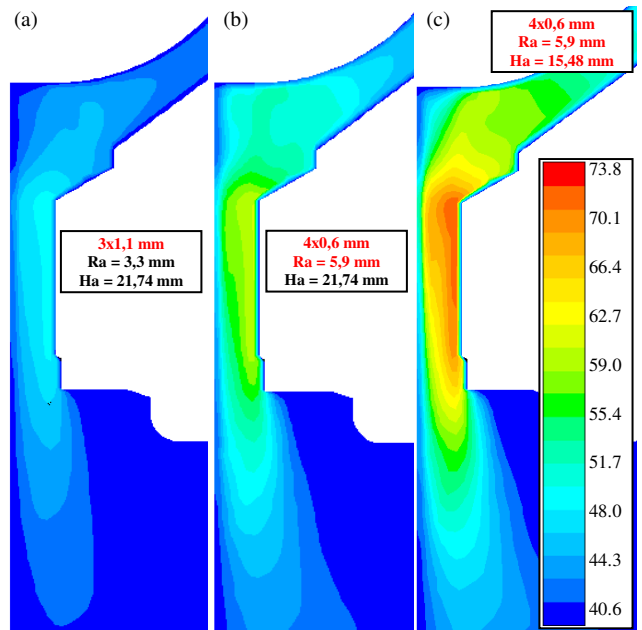


**Figure 1.3.3** Comparison of the plasma swirl velocity field [m/s] from the simulations of the torch geometry of (a) test case 1, (b) test case 2 and (c) test case 3. Taken from [23].

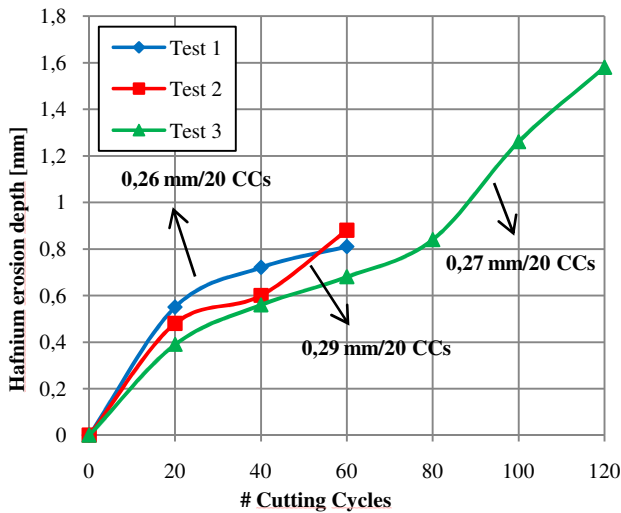


**Figure 1.3.4** Hafnium erosion depth [mm] at different CCs for the torch geometry of test cases from 1 to 3. Taken from [23].

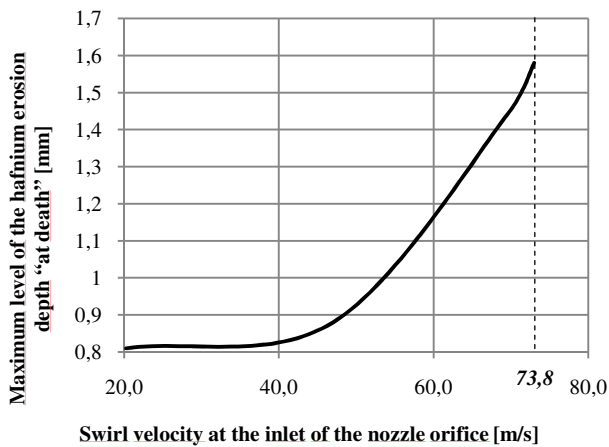


**Figure 1.3.5** Correspondence between numerical results (swirl velocity at the inlet of the nozzle orifice [m/s]) and experimental evidences (maximum level of the hafnium erosion depth “at death” [mm]). Taken from [23].

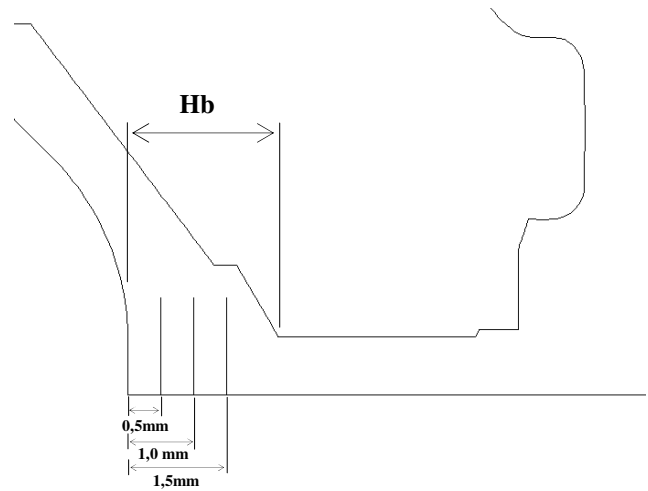


**Figure 1.3.6** Design parameters for the study of the plasma swirl velocity field near the Hf emitter surface. Taken from [23].

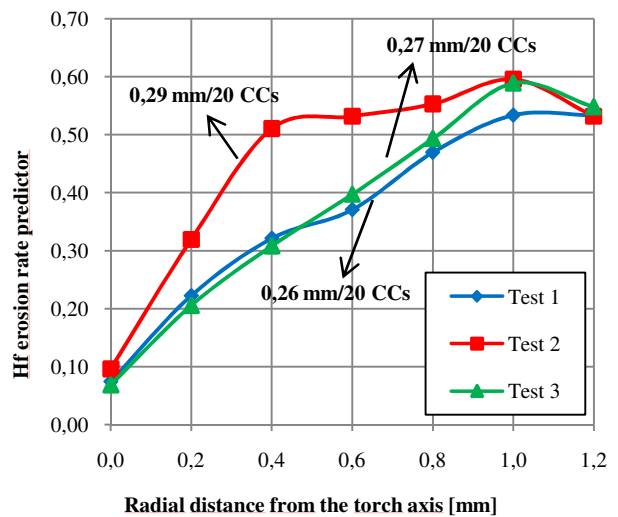


**Figure 1.3.7** Radial trend of the ratio between the swirl velocity profile at the axial level of LINE 1 and the maximum swirl velocity at the nozzle orifice inlet for the torch geometry of test cases from 1 to 3. Taken from [23].

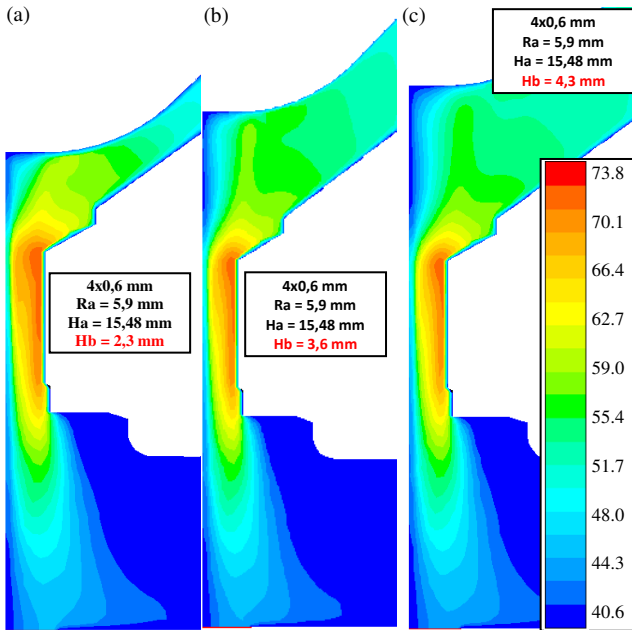


**Figure 1.3.8** Comparison of the plasma swirl velocity field [m/s] from the simulations of the torch geometry of (a) test case 3, (b) test case 4 and (c) test case 5. Taken from [23].

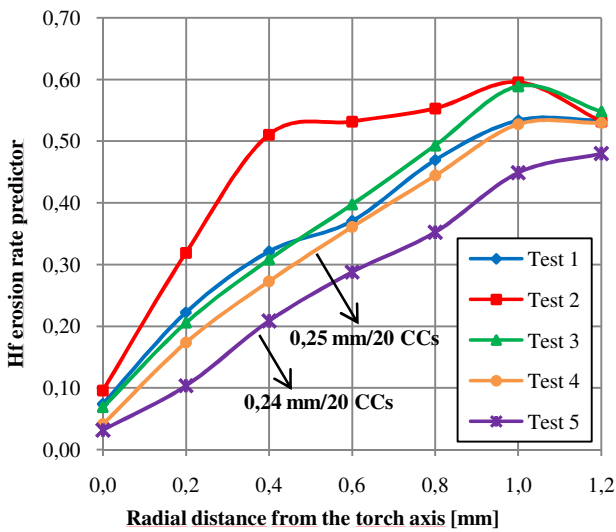


**Figure 1.3.9** Radial trend of the ratio between the swirl velocity profile at the axial level of LINE 1 and the maximum swirl velocity at the nozzle orifice inlet for the test cases from 1 to 5. Taken from [23].

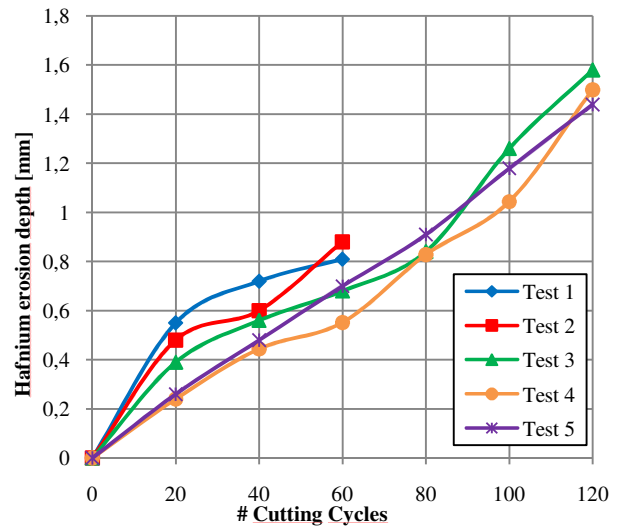


**Figure 1.3.10** Hafnium erosion depth [mm] at different CCs for the test cases from 1 to 5. Taken from [23].

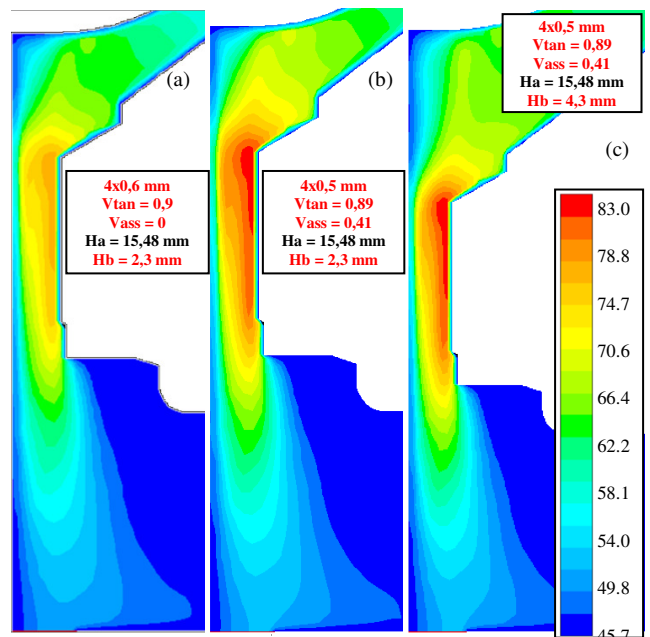


**Figure 1.3.11** Comparison of the plasma swirl velocity field [m/s] from the simulations of the torch geometry of (a) test case 3, (b) test case 6 and (c) test case 7. Taken from [23].

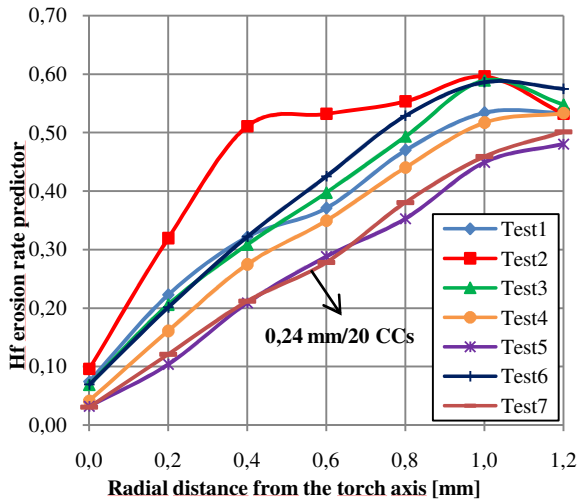


**Figure 1.3.12** Radial trend of the ratio between the swirl velocity profile at the axial level of LINE 1 and the maximum swirl velocity at the nozzle orifice inlet for the test cases from 1 to 7. Taken from [23].

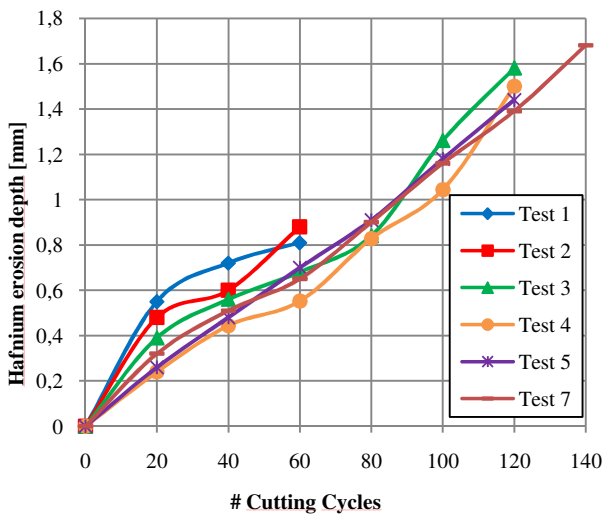


**Figure 1.3.13** Hafnium erosion depth [mm] at different CCs for the test cases from 1 to 7. Taken from [23].

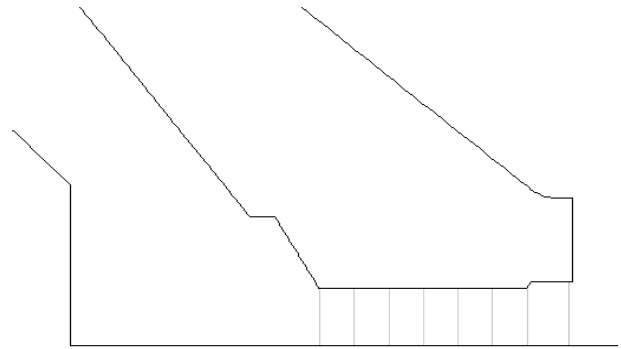


**Figure 1.3.14** Axial levels of the considered temperature radial profiles inside the nozzle orifice, from the simulation of the torch geometry of test case 7. Taken from [23].

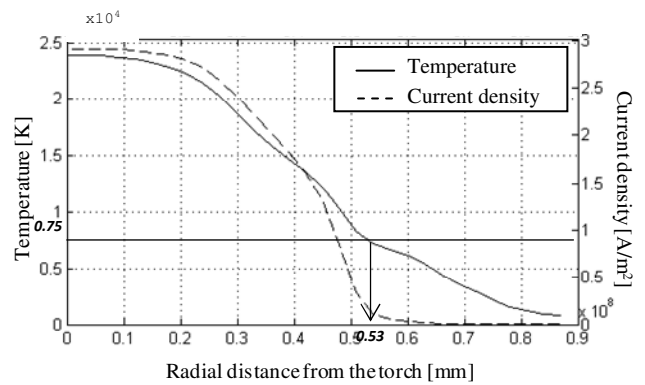


**Figure 1.3.15** Radial trend of the temperature [K] and of the current density [A/m<sup>2</sup>] at the nozzle orifice inlet, from the simulation of the torch geometry of test case 7. Taken from [23].

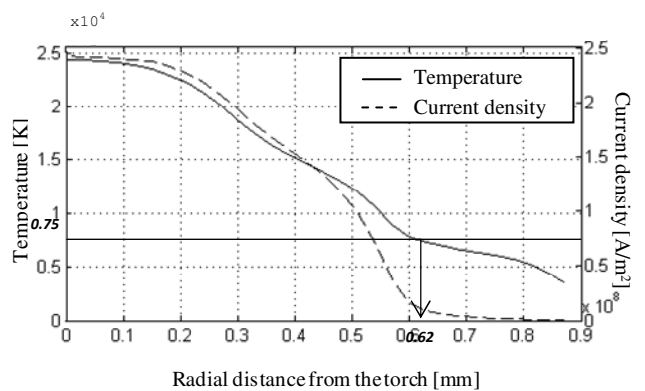


**Figure 1.3.16** Radial trend of the temperature [K] and of the current density [A/m<sup>2</sup>] at the nozzle orifice exit, from the simulation of the torch

geometry of test case 7. Taken from [23].

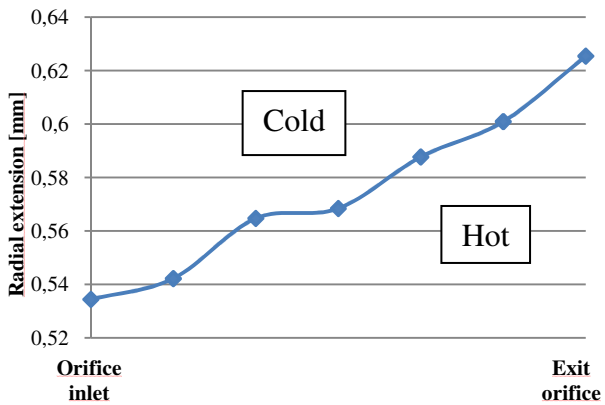


**Figure 1.3.17** Axial profile of the arc radius [mm], from the simulation of the torch geometry of test case 7. Taken from [23].

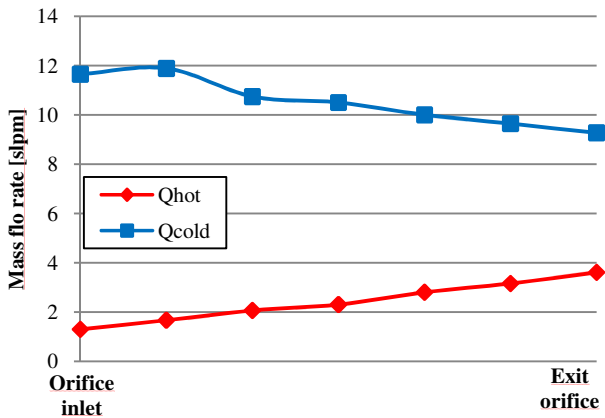


**Figure 1.3.18** Axial profile of the air mass flow rate in the hot plasma region and in the cold region [slpm], from the simulation of the torch geometry of test case 7. Taken from [23].

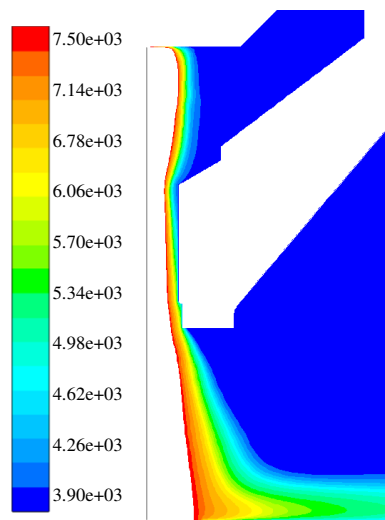


**Figure 1.3.19** Temperature field [K] of the cold region from the simulation of the test 7 torch geometry case. Taken from [23].

## **1.4 Optimization of the components design of a mono-gas plasma torch through experiments and 3D simulations**

Three dimensional phenomena, related to the fluid dynamic behavior of the plasma and secondary gas in the region between the torch tip and the work-piece, have been studied by means of a 3D FLUENT-based numerical model, with the final aim of optimizing the design of a prototype mono-gas plasma arc cutting torch, operating in the range 25-100A. The details of the spacer for contact cutting geometry and of the metallic substrate with the keyhole, are included in the computational domain. The development of a 3D model was necessary to solve specific design issues that cannot be properly studied by two-dimensional models, providing also useful results to be compared with experimental evidences coming from diagnostic and cut quality/erosion tests.

### **1.4.1 Experimental set-up**

Experimental tests have been accomplished through a prototype Cebora mono-gas plasma torch, able to operate in the current range 25-100 A both for manual and automated cutting. Experiments have been accomplished at 100 A under operative conditions typically used in cutting of MS plates thicker than 20 mm, with air as both plasma and shield gas. Electrodes have a press fit Hf insert with a 1.6 mm diameter flat emission surface, associated to a 1.35 mm diameter nozzle.

### **1.4.2 Results**

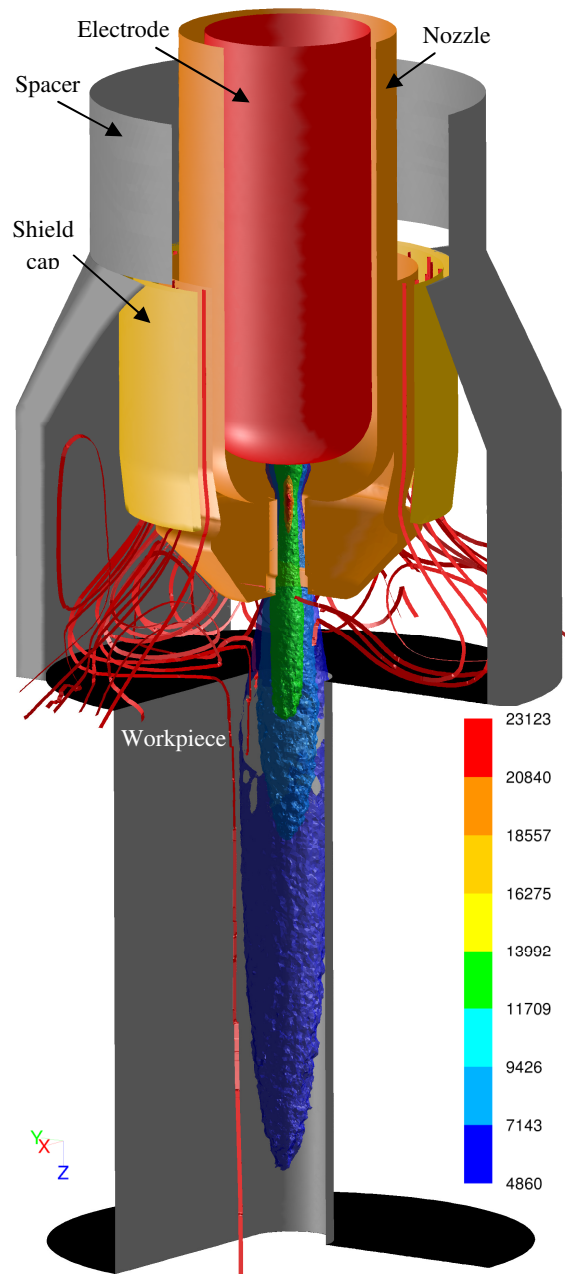
A 3D numerical model within a customized version of the code FLUENT [3-4, 10] has been developed in the design phase of a new Cebora mono-gas plasma torch, operating in the current range 25-100 A, for both manual and automated cutting have been obtained. The development of a 3D model was necessary, despite the greater computational effort required, compared to a 2D model, to address specific design issues: experimental evidences, as rapid wear of the nozzle tip with a consequent decrease of cut quality performances, led to approach the optimization of the geometry of the spacer for contact cutting as well as the fluid dynamic behavior of the secondary gas in the region between the torch tip and the work-piece.

The metallic substrate and the keyhole are included in the computational domain in order to take into account their effects on the flow field of the discharge in the region between the nozzle and the work-piece, and to better understand the interaction between the secondary gas and the molten metal in the *kerf* front. The detailed geometry of the spacer is included in the computational domain as well, in order to realistically study its effect on the flow field of the secondary gas in the region between the work-piece and the nozzle tip. Experimental measurements were performed in order to evaluate the keyhole shape for the considered operating conditions, to use them as input for the numerical simulation.

Simulations results are here presented for the prototype geometry and operating conditions fit for cutting mild steel at 90 A (plasma/secondary gas: air; nozzle diameter: 1.37 mm; gas inlet pressure:

3,5 bar). Fig. 1 shows the temperature iso-surfaces of the plasma jet extending from the emitter surface to the *kerf* region, together with the flow pattern of the secondary gas streamlines. The maximum temperature of 23'100 K is located inside the plasma chamber, near the nozzle orifice inlet; the 7'500 iso-surface can be considered as the external limit of the conducting plasma arc region. Figs 2a and 2b show the velocity versors coloured by log scale velocity magnitude [m/s] on two perpendicular planes passing through the axis of the system. The secondary gas flow is characterized by several eddies located in the region between the metallic substrate and the spacer inner side walls. These selected results highlight the influence of the particular relative position of the work-piece and of the spacer on the behavior of the secondary gas flow with possible implications in terms of cut quality performances and nozzle tip integrity.

In conclusion, 3D simulation results can lead to a more in-depth understanding of some of the phenomena otherwise experimentally observed during the development of a torch prototype; in this particular case, a relationship can be evidenced between the formation of secondary gas eddies in the region close to the *kerf*, where some molten metal can be entrained and then deposited of the nozzle tip, with its consequent rapid damage and wear. Such a detailed and realistic description of the interaction of the secondary gas flow and of the plasma jet with the work-piece and the *kerf* might be used for optimizing plasma cutting systems and for efficiently designing plasma torch components. Due to their complexity, the development and use of 3D models, can hardly be compatible with the typical temporal requirements of an industrial project. For this reason, 3D design oriented simulation should be addressed only when torch design issues involve specific phenomena that cannot be properly studied by 2D models.



**ig. 1** Iso-temperature surfaces [K] with the flow pattern of the secondary gas streamlines. Taken from [24].

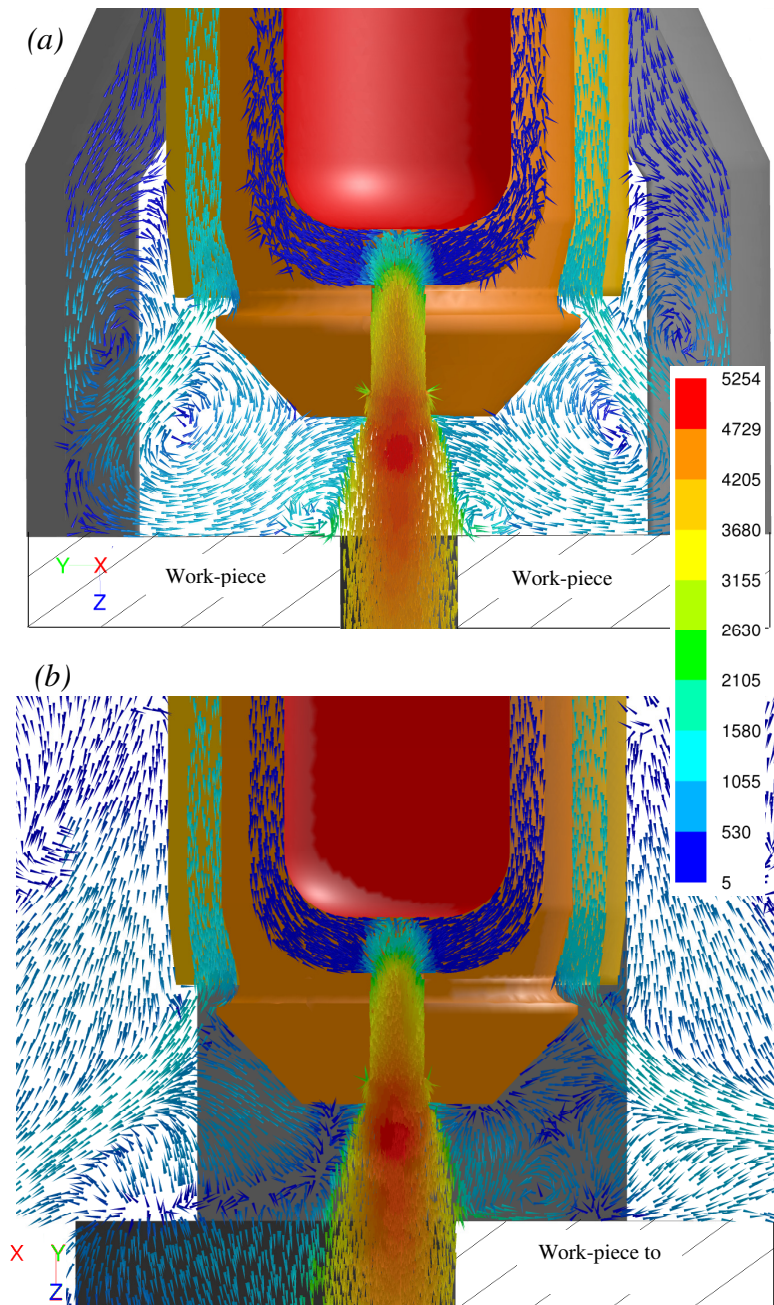


**Fig. 2.** Velocity versors colored by log scale velocity magnitude [m/s] on (a) yz and (b) xz planes passing through the axis of the torch. Taken from [24].

## **Conclusions and future developments**

Results presented in chapter 1 showed that plasma modeling, as a part of an integrated approach comprising also experimental tests and diagnostics, can be a very useful tool for designing and optimizing plasma arc cutting torches

The study presented in paragraph 1.1 enabled to analyze in-depth the influence of several operative parameters and consumables geometries on the performance of the considered high definition plasma cutting system, in the particular condition of cutting of mild steel thin plates. Information coming from numerical simulations results has been used together with experimental results in order to better understand physical phenomena that take place into the plasma chamber and in the *kerf* region of the workpiece.

The experimental and simulative study of the influence of operative and geometrical conditions on the cutting process performances lead to the definition of optimal process and technological parameters, both in terms of cutting quality and in terms of consumables service life. Modifications that have been introduced to the operative parameters and to the torch configuration are:

- the reduction of the secondary gas flow rate (lower than 9 lpm);
- a considerable improvement of the plasma flow rate (from 4 lpm to 6.5 lpm);
- the introduction of a modified nozzle with the conical shape of the orifice end characterized by an optimum value of the depth of the conical area;
- the introduction of an optimized diameter of the hafnium insert (1.07 mm);
- a reduction of the diameter of the holes of the plasma gas diffuser (0.4 mm);
- the optimization of the current profile during pilot arcing.

Simulation results show that all modifications that have been introduced, both in terms of operating parameters and consumables geometry, lead to:

- an increase of the axial plasma temperature inside the nozzle;
- an increase of the plasma swirl velocity in the nozzle orifice region;
- the removal of turbulent vortexes in the nozzle orifice exit region.

In conclusion, the most important effects that have been obtained are: the increase of the plasma arc constriction and the improvement of the nozzle cooling that induced an improvement of cut quality and the reduction of erosion phenomena of the torch consumables, in particular of the nozzle.

In the study presented in paragraph 1.2, a direct correlation was found between simulation results and experimental evidences, in particular:

- swirl velocity at the nozzle orifice inlet and maximum erosion depth at electrode death;
- swirl velocity distribution near the emissive surface and hafnium erosion rate.

Some torch design parameters useful to increase the electrode service life were identified from the study of the swirl velocity field into the plasma chamber, in particular:

- the distance between the exit of the primary gas diffuser holes and the nozzle orifice inlet;
- the distance between the electrode emissive surface and the nozzle orifice inlet;
- the correct combination of axial component and tangential component in the velocity of the plasma gas entering the plasma chamber.

The estimate of the real arc current density inside the nozzle orifice as a useful predictor of the nozzle service life has been introduced.

Finally, a 2D model characterized by some simplifying assumptions enabled us to obtain, sufficiently accurate and reliable results, also satisfying the typical temporal requirements of an industrial project. Numerical simulation has been used to predict electrode erosion phenomena. Numerical simulation results helped in identifying design parameters for a new commercial plasma torch and enabled us to suggest successful design solutions.

The study presented in paragraph 1.3 showed that 3D simulation results can lead to a more in-depth understanding of some of the phenomena otherwise experimentally observed during the development of a torch prototype; in that particular case, a relationship was evidenced between the formation of secondary gas eddies in the region close to the *kerf*, where some molten metal can be entrained and then deposited of the nozzle tip, with its consequent rapid damage and wear. Such a detailed and realistic description of the interaction of the secondary gas flow and of the plasma jet with the work-piece and the *kerf* might be used for optimizing plasma cutting systems and for efficiently designing plasma torch components. Due to their complexity, the development and use of 3D models, can hardly be compatible with the typical temporal requirements of an industrial project. For this reason, 3D design oriented simulation should be addressed only when torch design issues involve specific phenomena that cannot be properly studied by 2D models.

Even if the conjunction use of numerical modeling, experimental tests and diagnostics enable to obtain significant added value from an integrated approach to design, research is still in the making for finding a link between simulation of the plasma arc and a consistent prevision of cut quality.

Future developments will be devoted to:

- an effort towards the generalization of this type of procedure for the design of new plasma torches;
- experimental validation of simulation results concerning the potential correlation between the real arc current density and nozzle wear phenomena;

- investigation of new correlations between simulation parameters and plasma torch performances, with special regards to cut quality optimization.

## References

- [1] V. A. Nemchinsky and W. S. Severance, “What we know and what we know not about plasma arc cutting”, *J. Phys. D: Appl. Phys.*, 39, R423-R438, (2006)
- [2] V. A. Nemchinsky, “Plasma flow in a nozzle during plasma arc cutting” *J. Phys. D, Appl. Phys.* **31**, 3102–3107 (1998)
- [3] Colombo V, Dallavalle S, Ghedini E, Mentrelli A, and Vancini M 2005 3D fluiddynamic and plasma characterization of DC transferred arc plasma torches for metal cutting *Proc. International Symposium on Plasma Chemistry - ISPC-17 (Toronto, Canada, 7-12 August 2005)*
- [4] Colombo V, Dallavalle S, Ghedini E, Masini G, Russo D and Vancini M. 2006 2D and 3D fluiddynamic and plasma characterization of DC transferred arc plasma torches for metal cutting *J. High Temp. Mater. Process.* **10** 379–392
- [5] Colombo V, Concetti A, Dallavalle S, Ghedini E and Vancini M 2008 Understanding plasma fluid dynamics inside plasma torches through advanced modelling *IEEE Transactions on Plasma Science* **36** 389-402
- [6] Colombo V, Concetti A, Dallavalle S, Fazzioli R, Ghedini E and Vancini M 2009 Optimization of plasma arc cutting of mild steel thin plates *Journal of High Temperature Material Processes* **13** 267-285
- [7] Ghorui S, Heberlein JVR and Pfender E 2007 Non-equilibrium modelling of an oxygen-plasma cutting torch *J. Phys. D: Appl. Phys.* **40** 1966–1976
- [8] Shih T H, Liou W W, Shabbir A, Yang Z and Zhu J 1995 A new  $\kappa$ - $\epsilon$  eddy viscosity model for high Reynolds number turbulent flows *Comput. Fluids* **24** 227–238
- [9] P. Freton, “Etude d’un arc de découpe par plasma d’oxygène. Modélisation—Expérience,” Ph.D. dissertation, Université Paul Sabatier, Toulouse III, Toulouse, France, 2002. (in French).
- [10] A. B. Murphy and C. J. Arundell, “Transport coefficients of argon, nitrogen, oxygen, argon–nitrogen, and argon–oxygen plasmas,” *Plasma Chem. Plasma Process.*, vol. 14, no. 4, pp. 451–490, Dec. 1994.
- [11] Murphy A B 1995 Transport coefficients of air, argon-air, nitrogen-air, and oxygen-air plasmas *Plasma Chem. Plasma Process.* **15** 279-307
- [12] V. Colombo, E. Ghedini, P. Sanibondi, “Thermodynamic and transport properties in non-equilibrium argon, oxygen and nitrogen thermal plasmas”, *Progress in Nuclear Energy*, vol. 50, n. 8, pp.921-933, Nov. 2008.
- [13] Gleizes A, Cressault Y and Naghizadeh-Kashani Y 2002 Net emission coefficient of air thermal plasmas *J. Phys. D: Appl. Phys.* **35** 2925

- [14] International Standard ISO 9013 “Thermal cutting – Classification of thermal cuts – Geometrical product specification and quality tolerances” Second edition, 2002-09-15
- [15] V. Colombo, A. Concetti, S. Dallavalle, E. Ghedini, M. Vancini, “High Speed Imaging of Pilot Arcing and Piercing in PAC”. IEEE Transaction on Plasma Science, vol. 36, no. 4 part 1, pp. 1042-1043, Aug. 2008. 5th Triennial Special Issue on Images in Plasma Science.
- [16] V. Colombo, A. Concetti, S. Dallavalle, R. Fazzioli, E. Ghedini, M. Vancini, “High Speed Imaging of Pilot Arcing and Piercing in PAC”, *ISFV-13 – 13<sup>th</sup> International Symposium on Flow Visualization and FLUVISU12 – 12<sup>th</sup> French Congress on Visualization in Fluid Mechanics* (Nice, France), 2008.
- [17] Nemchinsky V A and Showalter M S 2003 Cathode erosion in high-current high-pressure arc *J. Phys. D, Appl. Phys.* **36** 704-712
- [18] Nemchinsky V A 2003 Cyclic erosion of a cathode in high-pressure arcs *J. Phys. D, Appl. Phys.* **36** 1573-1576
- [19] Peters J, Yin F, Borges C F M, Heberlein J and Hackett C 2005 Erosion mechanism of hafnium cathodes at high current *J. Phys. D, Appl. Phys.* **38** 1781-1794
- [20] V Colombo, A Concetti, E Ghedini, F Rotundo, S Dallavalle *Experimental analysis of the behaviour of high current electrodes in plasma arc cutting during first cycles* Plasma Sources, Science and Technology, Vol. 19 doi: 10.1088/0963-0252/19/6/065023 (2010)
- [21] Zhou Q, Yin H, Li H, Xu X, Liu F, Guo S, Chang X, Guo W and Xu P 2009 The effect of plasma-gas swirl flow on a highly constricted plasma cutting arc *J. Phys. D, Appl. Phys.* **42** doi: 095208
- [22] Gage R 1957 Arc Torch and Process *Union Carbide Corporation Patent* US 2,806,124
- [23] V Colombo, A Concetti, E Ghedini *Design oriented simulation of consumables in PAC and experimental validation of results* in press on Plasma Sources Sci. Technol., 2011.
- [24] V Colombo, A Concetti, E Ghedini *3D design oriented simulation of plasma arc cutting phenomena* Submitted for publication on IEEE Trans. Plasma Sci, 6th Triennial Special Issue on Images in Plasma Science.



## Chapter 2

### **Design and development of innovative technological processes aimed at optimizing the performances of plasma arc cutting torches' consumable components, in terms of their service life**

Cathode erosion phenomena put still a limit to performance improvement in PAC process; in particular for operative conditions in which oxidizing plasma gases (oxygen and air) and high current levels (above 200 A) are used in presence of an Hf emitter, typically set for cutting mild steel (MS) plates thicker than 20 mm. In PAC the cathode is made of an insert of high thermionic emissivity disposed with its surface exposed to the plasma chamber in the machined bore of an elongated body formed of high thermal conductivity material. Several studies [1-5] have been accomplished in order to understand phenomena that give rise to Hf erosion in different phases of the PAC operative cycle.

Cathode erosion is an outstanding challenge for many plasma arc cutting systems, in particular when operated in oxidizing atmospheres. Further than costs related to the consumables substitution and loss of working time, the low durability of the emissive insert limits the potential of such systems, since the erosion rates increase with arc current and pressure. The mechanism involved in the erosion phenomena still need to be fully investigated.

In plasma arc systems at high currents, the refractory cathode operates by means of thermionic emission enhanced by the Schottky effect [1, 6]. Temperatures achieved during the process are determined by a balance between the heating process due to ion bombardment and cooling due to heat conduction and electron emission. Conventional plasma electrodes comprise a water cooled tubular holder machined from a high thermal conductivity material, and an emissive insert facing the plasma chamber and characterized by a relatively low work function. Commonly used materials for the electrode body are copper (Cu), copper alloys, silver (Ag) and silver alloys. The conventional insert material for torches operating in inert atmospheres is tungsten (W). When cutting mild steels thicker than 20 mm, oxygen or oxidizing atmospheres are widely used to improve cutting speed and cutting quality. Under these conditions, tungsten electrodes erode dramatically [1], also due to the low melting point (MP) of its oxide ( $\text{WO}_2$ ,  $\text{MP} \approx 1500^\circ\text{C}$  [7]). Typical inserts for oxygen cutting consist of a refractory material, with a high MP and a relatively low work function ( $w_f$ ) at high temperatures, which forms high melting oxides, such as zirconium (Zr:  $w_f = 4.05 \pm 0.1$  eV [8],  $\text{MP} = 1852^\circ\text{C}$ ) or hafnium (Hf:  $w_f = 3.9 \pm 0.1$  eV [4],  $\text{MP} = 2222^\circ\text{C}$ ). At high temperature, Zr reacts with air faster than Hf: at  $740^\circ\text{C}$  they show approximately the same reaction rate, whilst already at  $900^\circ\text{C}$  Hf reacts with air at one-half the rate of Zr [9]. Although Hf inserts last approximately 1.5 times more than the Zr ones [1], their wear rate is still higher than that of electrodes containing tungsten when used in an inert gas.

Total cathode erosion results from the different contribution of constant current erosion in steady states and cyclic erosion during transients [1, 3, 4]. The former is due to the net flux of evaporated atoms which escape from the insert surface, due to its high temperature, and are not restrained to the emissive surface by the electric field. In particular, forces acting on the evaporated atoms (which

are almost immediately ionized due to the high ionization potential of the plasma) are the electric force, electron-ion drag and gas flow drag [1].

Cyclic erosion, which often is the predominant erosion mechanism, is due to the transients related to switching on and off of the arc [1, 4]. When Hf inserts are used with oxygen as working gas, the effective thermionic emitter is hafnium oxide ( $\text{HfO}_2$ ). This material behaves as a thermal and electrical insulator at room temperature, whilst in its molten state (i.e. at temperatures higher than  $2812^\circ\text{C}$ ) it shows good thermal and electrical conductivity, low work function and low vapour pressure. During the arc on transient, if the arc attachment is not slow enough to melt the Hf oxide, this insulating layer is removed by a series of thermal shocks [1]. On the other side, when shutting down the arc, the imbalance of the fluidynamic forces, gas and ion pressure on the molten surfaces causes relevant droplets ejection [4]. Another theory underlines the role of the working gas, which diffuses in the molten surface of the insert during state operations: when shutting down the arc, the steep pressure drop causes the ejection of this gas also in the forms of bubbles, dragging a relevant amount of emissive material out of the molten puddle [1, 3]. In both cases, thermal conduction plays an important role for the arc-off erosion. An efficient heat removal would reduce oxygen diffusion in liquid hafnium and allows the electrode surface to solidify faster, thus limiting droplets dragging from the molten pool and bubbles formation.

The different erosion contributions result in the formation of a concave cavity on the Hf emitter, whose deepening is particularly high during first cycles [4-5,10-11]. A significant amount of the emitted Hf oxide deposit on the electrode copper body and on the nozzle inner surface, negatively affecting both the cut quality and the consumables service life, as a consequence of the loss of axial symmetry in the plasma chamber, reduction of the boundary layer thickness and heat removal, the induction of destructive and non-destructive double arching phenomena [18].

Most of the activities that I carried out in this field have been done in the framework of the UniBo Strategic Project 2006-PLASMACUT involving members of the Group for Industrial Applications of Plasma of the Department DIEM of the University of Bologna, members of the Cebora Spa R & D section and members of the Metallurgy Group of the Department SMETEC of the University of Bologna. My contribution consisted in designing and carrying out experimental studies aimed at optimizing the performances of plasma arc torches in terms of consumables service life and in interpreting results coming from morphological and micro-structural characterization carried out by the Metallurgy Group of the Department SMETEC of the University of Bologna.. A summary of all activities carried out in this field is as follows.

Within the project the torch Cebora CP250G, a study on the influence of the consumable components centering on the variability of the quality attained on the cut pieces, in terms of inclination of the work piece side walls, has been carried out. The study involved the introduction of amendments to the draft of some components of the torch and to some stages of the assembling process of the torch. These modifications led to a concentricity level of the assembled torches less than 0.025 mm. Instruments for measuring the torches centering in various stages of the assembling process have been designed and built. Experimental tests for evaluating cut quality were also carried out with different cutting torches and different operating conditions in order to find a correlation between the centering level of the torches and the cut quality obtained on the work-

pieces. The cut quality was evaluated in terms of inclination of the side walls, in line with the international standard ISO 9013 2002.

In order to optimize the procedures for carrying out electrode erosion experimental tests, an automated system, called "rotating anode", has been developed. It comprises: a cylinder of graphite as anode of the circuit, a locking device of the torch, a cooling system for the graphite cylinder and two engines that produce, respectively rotary motion to the graphite cylinder and a linear movement to the locking of the torch. This system allows the simulation, under realistic conditions, of a cutting process in the transferred arc mode and it is used for carrying out electrode erosion tests ensuring, with respect to real cutting tests, increased efficiency of the process both in terms of time and costs spent to carry out a single erosion test. The system also ensures a high standardization of the process by providing high levels of repeatability and comparability of tests carried out.

An innovative process for the production of the electrode has been experimentally implemented. The new studied process involves the replacement of the traditional stage of turning the copper body of the electrode and the subsequent stage insertion the hafnium pellet in a specific hole in the copper body, with a single step of coining the piece. This change allows the production process, first, to improve the efficiency of the process itself in terms of time and money spent for the production of a single electrode and, secondly, to increase the performance of the electrode in terms of service life by improving the interface between the hafnium pellet and the copper body. This production process is still being tested and it will have to undergo a scaling-up process to be industrially implemented.

The microstructural modifications of the Hf insert in PAC electrodes operating at 250 A were experimentally investigated during first cycles to understand those phenomena occurring on and under the Hf emissive surface and involved in the electrode erosion process. Standard electrodes were subjected to an increasing number of cutting cycles (CCs) on mild steel plates in realistic operative conditions, with oxygen/air as plasma/shield gas. Microstructural analysis was performed for each electrode at different erosion stage by means of scanning electron microscopy (SEM) equipped with energy dispersive spectroscopy (EDS) and Raman spectroscopy. Electrodes cross sections were also observed by means of optical microscopy and polarised light after chemical etching. In the insert, three typical zones were found after cutting: monoclinic  $\text{HfO}_2$  layer; transition zone with  $\text{O}_2$ -Hf solid solution (possibly remelted) ; unmodified Hf. The erosion cavity and the oxide layer thickness increase with the number of cutting cycles. The oxide layer undergoes macrocracking, while the remelted Hf shows both a remarkable grain growth and the presence of microcracks which act as preferential oxidation paths. Detachment also occurs at the Hf/Cu interfaces worsening the heat dissipation and accelerating oxidation and erosion phenomena.

A combined optimization of the operating current and plasma gas flow profiles into the plasma chamber during the ignition and the shut-down transients was carried out, when using reactive gases ( $\text{O}_2$  and air) as the plasma gas with the consequent use of hafnium as emitter material. The objective of the optimization process was finding the best compromise between the need to minimize the excessive wear of the hafnium electrode, particularly important during the

abovementioned transients, and the need to ensure adequate stability at the plasma arc during the cutting process in order to prevent the occurrence of accelerated wear of the nozzle. This optimization procedure was standardized in order to be able to use it with the most efficiency during the design and development of every new plasma arc cutting torch prototype.

The behaviour of Hafnium (Hf) cathodes at the beginning of their service life when operating at high current levels (250A) in the plasma arc cutting (PAC) process has been experimentally investigated with the final aim of describing the phenomena that take place during those initial cutting cycles (CCs) and optimizing, with respect to expected service life, the initial shape of the electrode emissive surface, as detailed in paragraph 2.1. The experimental tests were carried out in realistic operative conditions for cutting mild steel plates with oxygen/air as plasma/shield gas. Starting with an electrode having a plane new emissive surface, subsequent CCs have been accomplished checking each time the dimension of the growing concave recess naturally created on the insert and the amount of Hf oxide ( $\text{HfO}_2$ ) collected on the nozzle surface and on the flat surface around the edge of the recess. Morphological and compositional analysis of the tested electrodes and nozzles led to a detailed description of Hf erosion mechanisms, modifications of the Hf insert morphological structure and effects of  $\text{HfO}_2$  deposits on the nozzle inner surface. High speed imaging during early stages of the transferred arc mode has been used to highlight the possible presence of non destructive double arcing phenomena taking place during the first few CCs as a consequence of deposition of  $\text{HfO}_2$  on the nozzle. Conclusions can be drawn concerning the optimization of dimension of the initial recess of the Hf insert fit to avoid massive deposition of material on the nozzle inner surface that would cause a strong reduction of electrode and nozzle service life and a rapid degrading of cut quality.

The introduction of innovative alloys to be used to replace pure hafnium as a raw material in the production of the electrode emitter used in the case of reactive plasma gas ( $\text{O}_2$  and air) has been evaluated. Two alloys were specifically studied: ZrCu and HfAg, evaluating different compositions for each of the two alloys. The introduction of these alloys would increase the performance of the electrode, in terms of its service life, providing a greater heat transfer between the hafnium pellet and the copper body and a greater cooling of the insert itself. Different techniques for the production of the considered alloys were evaluated, including:

- traditional process of melting of the alloy components (initially in solid form) in a graphite crucible and in inert atmosphere. The process was experimentally carried out obtaining the alloy Zr50Cu50. The alloy samples obtained by the experimental implementation of the melting process as described were subjected to micro-structural and compositional characterization by optical microscopy, SEM + EDS and X-ray diffraction (XRD). The characterization results revealed that the obtained samples were characterized by very poor quality because of strong differences in melting and vaporization temperatures of the used materials; then the subsequent phase of development of the melting process and prototyping of the electrodes was not accomplished;
- innovative processes that make use of powder metallurgy. Initially, the possibility of nano-structuring powders through high energy milling and subsequently sintering the powders

themselves, was evaluated only for the CuZr alloy. A first feasibility analysis of the described process was not followed by an experimental phase as it was found that the use of nanoscale powders to create the alloy would have caused the creation of intermetallic compounds during sintering, extremely reducing the alloy heat conductivity. The possibility of obtaining alloys by mechanical alloying of the starting powders, characterized by micrometer-sized, was subsequently evaluated. This second hypothesis led to a prototyping phase through the collaboration with Adma Products Inc., which provided us, according to our specifications, a sampling of powders of different compositions, obtained by mechanical alloying. In particular, for the CuZr alloy, three samples of powders with different composition were carried out (Zr30Cu70, Zr50Cu70, Zr69Cu29 (La2O3) 2), for the HfAg alloy, only a sample (Hf50Ag50) was carried out. The Adma Products Inc. also made some pellets with diameter 2.7 mm and length 5 mm consolidating the powders, with two alternative techniques (hot forming and sintering); so, for each sample of powders, two types of pellets were made, each one characterized by a different level of the obtained density. The powders and the pellet prototypes were characterized by XRD analysis. Being characterized by low density, they were not used for the construction of the electrodes.

Finally, the remaining powders provided by Adma products were used to produce some pellet with the so-called "Spark Plasma Sintering" which, compared to conventional sintering techniques, achieves 100% density with time and process temperature drastically reduced. The use of this technique was made possible thanks to collaboration with the Department DIMTI of the University of Trento. Among the obtained pellets samples, two types of samples, characterized by the best values of density, were chosen to produce some electrodes. The samples chosen were introduced in the copper body by means of the traditional production techniques, the obtained electrodes were subjected to erosion tests on the rotating anode. The wear tests were interrupted periodically in order to perform morphological and compositional analysis on the emission surface of the electrodes tested. The samples not used for erosion tests were used to perform diagnostic activities by means of High Speed Camera imaging. The video obtained revealed that the transitional phase of pilot arc ignition is characterized by the absence of transition phenomena in the discharge behavior, which are associated with expulsion of significant quantities of hafnium vapors and hafnium particles. The shut down transient of the pilot arc phase is also characterized by the absence of ejection of droplets of molten hafnium from the emission surface.

There is currently a first assessment of the possibility of introducing in the production process of the electrode, a warming of the piece (body copper + pellet) in order to provide better adhesion between the alloy that makes up the pellet and the body of copper electrode. This hypothesis would need to buy a system for induction heating of parts in a controlled atmosphere.

An innovative process of surface modification of the nozzles of the multi-gas plasma torch Cebora CP250G used for current levels of 200 and 250 A, has been carried out, in order to reduce electrical stress that the internal surfaces of the nozzles are subject to during the arc ignition. The implemented process involves the deposition of multilayer ACD Ni-P (~ 10µm) / PLC (~ 1 micron), i.e. the coating of the nozzle inner surface through a first layer of Ni (thickness of about 10 microns) in contact with the copper wall and a second outer layer coating (DLC Diamand Like Carbon) of a thickness of about 2 microns, obtained by PVD (Physical Vapour Deposition). The coating was carried out on two types of nozzles of the Cebora CP251G torch used for cutting mild steel by

O<sub>2</sub>/aria as plasma gas / secondary gas, respectively, and 200 A and 250 A as operating current. The nozzles were tested in realistic operating conditions. The microstructural characterization, morphology and composition in different stages of the tested nozzles service life has been performed by light microscopy, SEM + EDS and micro-Raman spectroscopy.

An innovative process of surface modification of electrodes used for the multi gas plasma torch Cebora CP250G, with current levels of 200 A and 250 A, has been carried out, to improve the interface between the insert of hafnium and the body of copper and thus increasing the heat exchange between the two components of the electrode. The implemented process involves the deposition of silver electrochemically on the side wall of the hafnium. The coating was carried out on hafnium rods with a diameter of 2 mm which were then cut and properly shaped in order to get the pellets to be inserted into the hole in the body of copper electrode. At a later stage some prototypes of the electrode will be produced both by the traditional technique of insertion of the coated pellets by interference and by the innovative technique, currently being tested, of coining of the electrode. The electrodes thus obtained will be then tested by means of specific erosion tests and in various stages of their service life, will be subjected to microstructural, morphology and composition characterization, in order to assess the behaviour of the interface between the hafnium pellet and copper body.

## **2.1 Experimental analysis of the behaviour of high current electrodes in plasma arc cutting during first cycles**

The behaviour of Hafnium (Hf) cathodes at the beginning of their service life when operating at high current levels (250A) in the plasma arc cutting (PAC) process has been experimentally investigated with the final aim of describing the phenomena that take place during those initial cutting cycles (CCs) and optimizing, with respect to expected service life, the initial shape of the electrode emissive surface. The experimental tests were carried out in realistic operative conditions for cutting mild steel plates with oxygen/air as plasma/shield gas. Starting with an electrode having a plane new emissive surface, subsequent CCs have been accomplished checking each time the dimension of the growing concave recess naturally created on the insert and the amount of Hf oxide (HfO<sub>2</sub>) collected on the nozzle surface and on the flat surface around the edge of the recess. Morphological and compositional analysis of the tested electrodes and nozzles led to a detailed description of Hf erosion mechanisms, modifications of the Hf insert morphological structure and effects of HfO<sub>2</sub> deposits on the nozzle inner surface. High speed imaging during early stages of the transferred arc mode has been used to highlight the possible presence of non destructive double arcing phenomena taking place during the first few CCs as a consequence of deposition of HfO<sub>2</sub> on the nozzle. Conclusions can be drawn concerning the optimization of dimension of the initial recess of the Hf insert fit to avoid massive deposition of material on the nozzle inner surface that would cause a strong reduction of electrode and nozzle service life and a rapid degrading of cut quality.

It is well known that the cavity deepening rate of the Hf emitter at high current level is high during the first arc ignitions, to successively decrease and become approximately constant [3, 5, 10-11]. The Hf-based materials emitted from the cathode at the beginning of its service life deposit both on the cathode itself and on the nozzle, so possibly inducing a loss of axial symmetry of the plasma chamber, a local perturbation of heat transfer conditions and a reduction of the boundary layer thickness, with important drawbacks both on cut quality and on consumables service life. Moreover, the Hf based droplets deposited on the inner nozzle surface have relative low work function, which makes the electrical breakdown even easier [1], so inducing more easily double arcing phenomena, both destructive and non destructive [12].

To avoid the negative effects induced by a natural deepening of the concave pit in an Hf insert initially flat, the emission surface can be otherwise shaped with a concave recess [10-11], so neatly removing a volume of emissive material that would anyhow be removed during the first few starts in a random or massively disordered way, also badly conditioning the subsequent erosion process. When used in a torch, this solution accounts for a minimal deposition of emissive material on the nozzle, so reducing nozzle wear and double arcing phenomena, together with an increase in arc stability and cut quality.

State of the art knowledge in PAC is defined more by the huge amount of patents literature than by journal papers; this fact induces a strong need for understanding the physical reasons behind industrially patented successful ideas that, due to patenting rules and strategies, are often not completely and correctly described.

On the side of patents and related technology aimed at the reduction of Hf cathode erosion at high current levels, Hypertherm published two patents strongly related to each other: “Improved electrode for high current density plasma arc torch” - US 5310988 (May 20, 1992) [10] and “Electrode for a plasma arc torch” - US 5464962 (July 29, 1994) [11]. The first patent is aimed at improving the electrode useful life through the optimization of the Hf insert diameter “as a function of the level of a current carried out by the electrode”. This patent gave rise to the European one EP 0641269 under the same title; finally revoked (in 21.11.2003) after a long and intricate opposition procedure started by the competitor Air Liquide. The second patent is a *continuation in part* of the first one and it is aimed at “minimizing the deposition of high emissivity material on the nozzle” due to massive ejection phenomena that take place at high current levels during first starts, by shaping the emission surface in order to define a concave recess in the Hf insert. This patent gave rise to the European one EP 0772957 under the same title; finally lapsed (11.07.2005) for non-payment of due fees in all European designated contracting states.

The evolution of patent *status* in the EPO (European Patent Office) environment on this specific subject has opened up the possibility of producing and commercializing at an industrial level in Europe high current electrodes with an optimized initial recess depth on the Hf emitter surface; together with the necessity of validating a general experimental procedure supporting the design of the electrodes for each particular plasma source, with its typical set of geometrical and operating conditions.

In order to define electrode design procedures, we investigated, in realistic operative conditions, Hf erosion phenomena on the emitter surface and modifications of the Hf insert morphological structure during first CCs. In particular, we analyzed the consequences of massive Hf ejections and the influence of the emissive surface initial shape on plasma arc behaviour and on Hf erosion rate. Experimental results enabled us to validate the iterative experimental procedure for the optimization of the shape of the initial recess of the Hf insert as a function of the operating conditions and for a particular plasma source (without losing generality of the approach), with the final aim of improving consumables service life and cut quality.

### **2.1.1 Experimental set-up**

The erosion tests on the electrodes have been accomplished through a Cebora plasma cutting system, comprising the power supply Plasma Prof 264 HQC, equipped with the remote high frequency unit HV18 and the Gas Console PGC1-2 for manual gas settings, together with the multi-gas plasma torch CP251G. The system can operate in the current range 25-250A. Experiments have been accomplished under operative conditions typically used in cutting of MS plates thicker than 20 mm, with O<sub>2</sub> as plasma gas and air as shield gas at 250 A.

For every cycle, piercing at the optimum torch piercing stand-off is followed by 20 seconds of linear cutting at the optimum torch stand-off and at reduced velocity (0.3 m/min vs. the optimum of 2.1 m/min); cutting velocity is known for affecting only slightly erosion rate and the use of a reduced velocity accounts for metallic material savings. The standard electrodes tested with an arc current of 250 A use a press fit Hf insert with an emission surface diameter of 2 mm associated to a nozzle with 1.9 mm orifice diameter.

Images aimed at detecting non destructive double arcing phenomena during few first piercing-cutting phases have been obtained using a NAC Memrecam K3R high speed camera with a maximum acquisition speed of 10.000 fps and a 180 mm focal-length lens, protected by a sacrificial neutral filter at a distance of 1 m from the plasma torch.

During all the experimental tests arc current, pressure and flow of plasma and secondary gas, voltage between electrode and work-piece and voltage between electrode and nozzle have been monitored through a digital oscilloscope LeCroy Waverunner LT374M. Images captured by the HS camera are time-correlated with the oscilloscope waveform synchronizing the start acquisition time of both instruments.

Morphological modifications of the tested electrodes at different *CCs* have been measured by means of a Hommelwerke T2000 contact profilometer. Moreover, mean profiles of each electrode at subsequent erosion stages were calculated by interpolating six radial profiles from every 3D topography. Both the Hf volume eroded from the initially plane emissive insert, and the HfO<sub>2</sub> volume deposited on the cathode surface, were detected. Scanning electron microscopy (SEM) of the tested electrodes has been performed to validate the topographies reconstruction. Qualitative evaluation of the HfO<sub>2</sub> deposition on the inner nozzle surface has been carried out by stereomicroscopy using a new nozzle at each *CC*.

### **2.1.2 Experimental procedure**

In this work we will present a modified experimental procedure, with respect to the one described in the abovementioned patents, highlighting the reasons for the proposed changes and their effect on the optimization process.

#### *Hypertherm Inc. experimental procedure*

In particular, the Hyperterm patent “Electrode for a plasma arc torch” - US 5464962 describes a try-and-fail experimental procedure that is to be carried out in order to optimize the initially concave shape of the emission surface “as a function of the operating current level, the diameter of the insert, and the plasma gas flow pattern in the torch”. The procedure starts with a first trial shaping of the emission surface to define a concave insert recess on it and testing the electrode with subsequent *CCs* in realistic operating conditions. The recess shape and the nozzle condition were checked after each *CC*. If double arcing consequent to massive Hf deposition on the nozzle took place, the erosion test was stopped and the experimental procedure was re-started with a deeper trail concave recess, until double arcing phenomena would disappear. The initial shape of the concave recess that gave inducing the absence of double arcing would be selected as optimal.

#### *Modified experimental procedure*

In general terms, the optimal shape of the initial recess of the Hf insert is strongly dependent upon “typical operating and geometric conditions” of the torch being optimized. Moreover, the recess

shape deriving from the Hypertherm experimental procedure could be significantly affected by the initial trial one.

For these reasons, a modified experimental procedure is proposed here, starting the investigation with an initially plane insert emission surface and analyzing the evolution of the recess depth naturally created during the first few *CCs* while using these information for defining subsequent optimization steps.

The proposed modified experimental procedure can be divided into different stages. The first stage is characterized by a series of tests accomplished on electrodes having an initially plane insert emission surface. The erosion tests were stopped after every *CC* to check the Hf eroded volume and the overall nozzle condition. Modifications of the Hf insert morphological structure were also monitored and this first test was stopped when the emissive surface morphology reached a stabilization phase as a function of the number of *CCs*; that's to say when massive Hf ejections stop and only slight ejections of Hf based solid particles take place; this phenomenon being related to the cyclic erosion process leading to constant deepening rate of the cavity for the entire electrode service life. The dimension of the recess that was naturally created on the emissive surface at the end of the first stage was taken as reference point to design some intermediate spherical recesses to be tested on erosion during *CCs* in the second stage of the procedure. The Hf eroded volume, the overall nozzle condition and the Hf insert morphological structure evolution over *CCs* were monitored, in order to identify the stabilization phase for each tested electrode. The modifications occurred on the emissive surface morphology of tested electrodes allowed to identify the optimal spherical recess.

### **2.1.3 High speed imaging analysis of the behaviour of Hf cathodes**

#### *Double arcing phenomena in new electrodes*

In a previous paper [12] some of the authors have investigated, through high speed imaging, non-destructive double arcing phenomena occurring during high current piercing, that probably take place as a consequence of the deposition of small amounts of  $\text{HfO}_2$  on the nozzle orifice wall, inducing a local increase of the radial electric field and an increase in the probability of double arcing. When double arcing occurs, rapid [ $<1$  ms] evaporation of the  $\text{HfO}_2$  with vapour emission from the nozzle restores the previous normal arc behaviour. The very short duration of the described phenomena is the reason for their being non-destructive. A detailed analysis of the correspondence between arc voltage instabilities between electrode and nozzle and plasma behaviour, led to a hypothesis of correlation between arc voltage isolated peaks and Hf vapours emissions and between arc voltage continuous spikes and arc attachment on the nozzle and the shield, respectively.

In the present work, the behaviour of optimized and non optimized brand new electrodes during a first arc ignition phase have been investigated through high speed imaging in order to observe the effects of Hf ejections from the emission surface (both Hf vapour and solid particles) on arc stability. Figure 1(a) shows a series of images of the first arcing process of a new electrode with planar emission surface associated, during the piercing phase, to a new nozzle. Images show how massive ejection of Hf vapours and solid particles are associated to arc instabilities and to arc

attachment on the nozzle, the arc having disappeared from its usual position along the torch axis. Figure 1(b) shows the waveform of the electrode-nozzle voltage drop during the piercing process of figure 1(a); it is characterized by the presence of significant spikes, that can be related, as described in [12], to the arc instabilities showed in figure 1(a). Figure 2(a) shows a series of images of the 14th arcing process of the electrode used during the test reported in figure 1(a) associated, during the piercing phase, to a new nozzle. In this condition the electrode is already characterized by a concave pit progressively created during previous arc ignitions. Images show that only slight ejections of Hf based solid particles take place; this phenomenon being probably related to the cyclic erosion process leading to constant deepening rate of the cavity. The image reported in figure 2(a) shows how the abovementioned Hf solid particles ejections don't induce arc instabilities. Figure 2(b) shows the waveform of the electrode-nozzle voltage drop between during the piercing process of figure 2(a); it is characterized by the absence of significant spikes.

#### **2.1.4 Behaviour and analysis of electrodes with no initial recess**

##### *Electrode erosion tests*

Erosion tests on electrodes with no initial recess have been accomplished in order to study the behaviour of the Hf insert during first ignitions in real cutting conditions. The current level has been set at 250 A; piercing and cutting (20 s) phases on a 25 mm thick MS plate have been accomplished in the optimum conditions for stand-off and gas inlet pressures.

At a first stage, 3 series of test were carried out. For each series, 5 tests have been accomplished, each characterized by an increasing number of *CCs* to which each electrode was subjected; each test has been started with a new electrode, associated to a new nozzle for each *CC*, in order to later investigate on the quantity of Hf-based particles deposited on the nozzle during each arcing process. On the whole, 15 electrodes and 45 nozzles have been used for each test. Unfortunately, the complexity of the phenomena involved in cathode erosion [1-5] during first cycles induces only a partial repeatability of the effects related to concave recess generation and morphological modifications in the Hf pellet.

Figure 3 shows the erosion cavity depth for each electrode of the abovementioned test series. These first results highlighted how the erosion morphology and cavity depth of each emissive insert after a certain number of *CCs* were strongly affected from the electrode status at the end of the previous *CC*. This strong dependence leads to difficulties in reconstructing the typical behaviour of one electrode over 5 *CCs*, using data coming from a limited number (for example, 5) of electrodes ideally identical at the beginning of their service life. Thus, in order to better understand the erosion mechanisms that each electrode underwent during first cycles, 4 more tests (*E1÷E4*) were accomplished with a different experimental procedure. For each test, 1 electrode with no initial recess underwent 5 *CCs*; a new nozzle was used for every *CC*. 3D topographies and volume measurements were accomplished for each electrode after every *CC* (figure 4).

### *Morphological and compositional analysis*

After the first arc ignition, all the tested electrodes evidenced the presence of a concave recess in the Hf emissive insert and an annular zone with Hf deposit surrounding the insert boundaries on the cathode surface, as shown for electrodes *E1* and *E2* in the topographies of figure 5. Moreover, SEM macrograph of figure 6 exhibits the presence of a fine dispersion of HfO<sub>2</sub> surrounding the massive Hf deposit, together with HfO<sub>2</sub> droplets. Finally, part of the Hf based particles ejected from the insert is deposited on the inner nozzle surface, as shown in figure 7(a).

Figure 8 reports the detailed evolution of the cross sectional mean profiles, calculated by interpolating six radial profiles from each topography, of all the tested electrodes, as a function of the number of *CCs*. Figure 9 reports the detailed evolution of the volume measurements, computed integrating the electrode surfaces from each topography, of all the tested electrodes, as a function of the number of *CCs*. In the histograms of figure 9, the erosion volume is a measure of the concave recess naturally established on the emitter surface, while the deposited one is the volume of the Hf deposited on the electrode surface, around the emitter surface; the net volume is the difference between the erosion volume and the deposited volume.

For *E3*, after 2 *CCs* and *E4*, after 1 *CCs*, the deposited volumes exceed the erosion ones; this result could be explained by taking into account the microstructure of the Hf insert after a few *CCs*, as shown in the cross sectional view of figure 10. It is possible to observe three zones: unmodified Hf, thermally affected Hf and HfO<sub>2</sub> layer. The latter can be interested by cracking and porosity, while the Hf affected by thermal cycling can be interested by cavities (as previously shown in [4]) due to the oxygen diffusion and oxide formation processes. These phenomena, together with the higher density of the pure Hf (13.31 g/cm<sup>3</sup> [13]) with respect to the one of monoclinic HfO<sub>2</sub> (9.7 g/cm<sup>3</sup> [14]) could affect the amount of hafnium oxide deposited on the cathode surface, leading to an increase both in the measured values of the deposited volumes and in the thickness of the superficial layer of the emissive insert, so decreasing the measured erosion volumes.

The evolution of the eroded volumes (figure 11(a)) of the four examined electrodes (which show a trend similar to the one of the maximum cavity depth, figure 11(b)) suggests how the erosion behaviour of each insert is only partially determined by the morphology of the emitting surface as measured at the previous step. For 3 out to 4 electrodes (*E1*, *E2*, *E4*), the deepening of the erosion cavity increases up to 2 *CCs*; between 2 and 3 *CCs* the maximum erosion depth tends to slightly decrease as well as the erosion volume. Thereafter, erosion depth for electrodes *E1* and *E2* slightly increases up to 5 *CCs* achieving depth values similar to those measured after 2 *CCs* (about 470 μm, figure 11). On the contrary, electrode *E4* cavity depth passes from 290 μm to 660 μm between 3 and 4 *CCs*, whilst the recess depth tends to remain almost constant thereafter. Electrode *E3* behaves differently, as the recess depth decreases from 1 to 2 *CCs*, then undergoes to a deepening after 3 *CCs*, whereas it remains almost constant at about 500 μm between 3 and 5 *CCs*. Qualitative correspondence was found between the amount of Hf detected on the nozzles inner surfaces and the deepening rate of the erosion cavity: massive HfO<sub>2</sub> deposits were found when the cavity depth increased significantly (figure 7(a)), while nozzle inner surfaces were found to be almost clean when the erosion volume and the recess depth decreased or remained almost constant (figure 7(b)). Only for electrode *E3* a limited amount of Hf was detected on the nozzle inner surface after 2 *CCs*, whilst the erosion volume decreased. Since *E3* underwent a strong deepening between 2 and 3 *CCs*,

this decrease in the erosion volume is related to the microstructure of the HfO<sub>2</sub> layer and thermally affected Hf (as already shown in figure 10), which were probably particularly affected by cracking and porosity at that stage.

These results show how the low repeatability of the erosion process, due to the complex interactions and phenomena taking place in the plasma chamber, is even increased by the process of formation of the natural concave recess, when starting with an initially plane emitting surface. The evolution of the recess shape, together with the erosion volume and nozzle inner surface analysis induce some considerations about the optimal initial shape that an emissive insert should be given when operating at high currents in PAC [10, 11]. Electrodes E1 and E2, between 2 and 5 CCs, maintained their cavity depth and erosion volume almost constant, while no or extremely limited Hf emission and deposition on the nozzle inner surface was detected, proving how the Hf volumes eroded during first 2 CCs could be removed from an optimized emissive insert. Due to this particular behaviour, they have been tested for an increased number of starts, in order to better study the evolution of the recess spontaneously established, and they have been considered as a reference point to start an experimental procedure for the optimization of the recess shape. The design of the emissive surface could be deduced from the analysis of the 3D topographies and mean profiles carried out for the considered phases.

#### *Increased number of cutting cycles*

Electrodes E1 and E2 were subjected to 11 CCs. They are both characterized by massive Hf ejection events after the first 5 CCs, in particular: the eroded volumes skip from 0.31 – 0.43 mm<sup>3</sup> to about 1 mm<sup>3</sup> and the maximum recess depth reaches a level of about of 0.7 mm. As shown in figure 11, the levels of eroded volume and maximum recess depth that electrodes E1 and E2 reach, in a stabilized manner, after 11 CCs are similar to those ones that electrodes E3 and E4 reached, with a non linear trend, after 5 CCs. They both reach the stabilization of the emissive surface morphological structure after 9 CCs.

#### **2.1.5 Behaviour of electrodes with initially optimized recess**

On the basis of the results obtained from tests on electrodes E1 and E2 after 5 CCs, two (non-trial) spherical recess shapes have been designed:

- from electrode E2 a spherical recess with an initial recess depth of about 500 µm and an initial recess volume of 0,43 mm<sup>3</sup> (electrode Es1);
- from electrode E1 a spherical recess with an initial recess depth of about 400 µm and an initial recess volume of 0,31 mm<sup>3</sup> (electrode Es2).

Both electrodes were subjected to subsequent CCs in order to find stabilization in the emissive surface morphology. After 5 CCs both electrodes reached the stabilization phase and were characterized by similar levels of maximum recess depth and eroded volume.

In particular, at the end of the test series, results were as follows (figures 12 and 13).

Electrode Es1 was characterized by:

- a reduction of the maximum recess depth (from 510  $\mu\text{m}$  to 421  $\mu\text{m}$ )
- a slight increase of the recess volume (from 0,43  $\text{mm}^3$  to 0,55  $\text{mm}^3$ )

Electrode Es2 was characterized by:

- a slight increase of the maximum recess depth (from 395  $\mu\text{m}$  to 432  $\mu\text{m}$ )
- a significant increase of the recess volume (from 0,31  $\text{mm}^3$  to 0,53  $\text{mm}^3$ )

The initial Hf emitter surface morphology of electrodes Es1 and Es2 closely reproduces the recess depth naturally created on electrodes E1 and E2 after 5 *CCs*. For this reason, electrodes Es1 and Es2 after 5 *CCs* and electrodes E1 and E2 after 10 *CCs* can be considered at the same service life stage; therefore, it is significant to evaluate differences between their resulting emission morphologies at that life stages, in order to highlight the influence of the emissive surface initial shape on the electrode behaviour during first *CCs*. Experimental evidences showed that both for electrode Es1 and Es2 the erode volume levels and the recess depth were significantly reduced with respect to the ones reached on E1 and E2 after 10 *CCs* (figure 14). Moreover, both eroded volume and maximum recess depth levels of Es1 and Es2 reached a similar value after erosion tests, although fresh electrodes were characterized by a slightly different initial shape of the spherical recess. This result enabled us to consider the recess shape obtained at this stage with electrodes Es1 and Es2 as a reference point to design the optimized spherical recess.

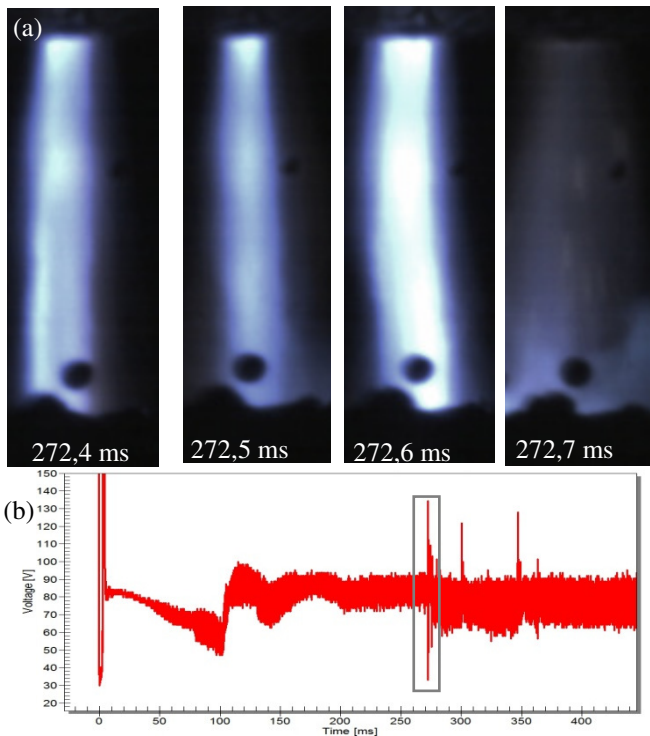


**Figure 1.** (a) Transferring arc images for a torch with 1,9 mm nozzle diameter and 3,5 mm shield diameter at 250 A (plasma/shield gas: O<sub>2</sub>/air) for the case of a new electrode with planar emission surface. (b) Electrode/nozzle voltage drop [V]; the gray box highlights the time interval related to the pictures showed in figure 1a. Taken from [16].

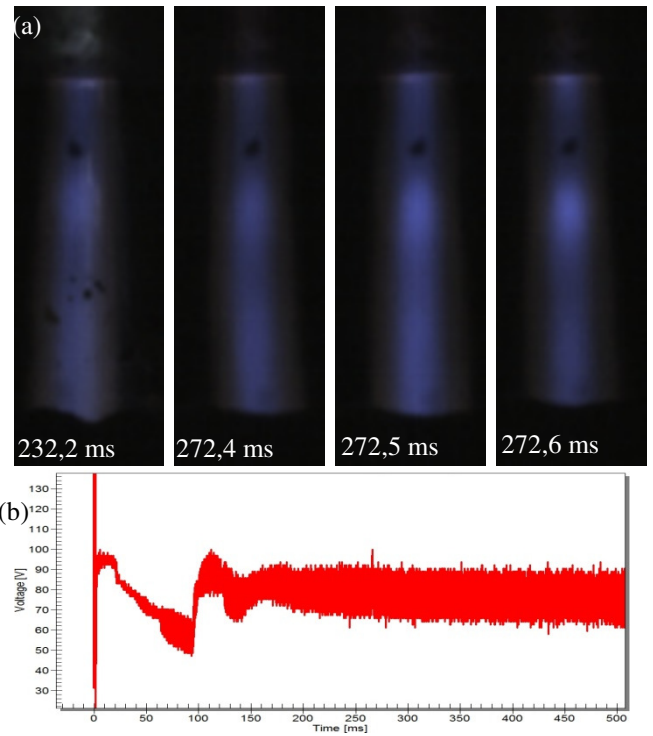


**Figure 2.** (a) Transferring arc images for a torch with 1,9 mm nozzle diameter and 3,5 mm shield diameter at 250 A (plasma/shield gas: O<sub>2</sub>/air) for the case of an electrode after 14 CCs (with initially planar emission surface) but with a new nozzle. Images acquired at 10000 fps and 1/200000 s shutter time, without any filtering. (b) Electrode/nozzle voltage drop [V]. Taken from [16].

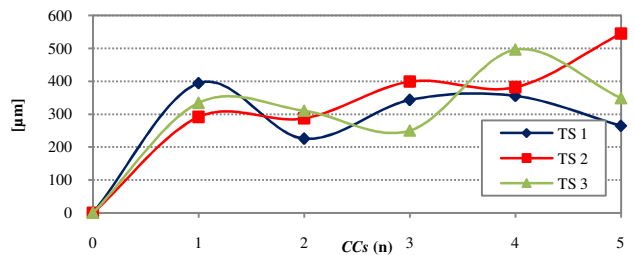


**Figure 3.** Cavity depth as a function of the number of CCs for three electrodes test series (TS). Taken from [16].

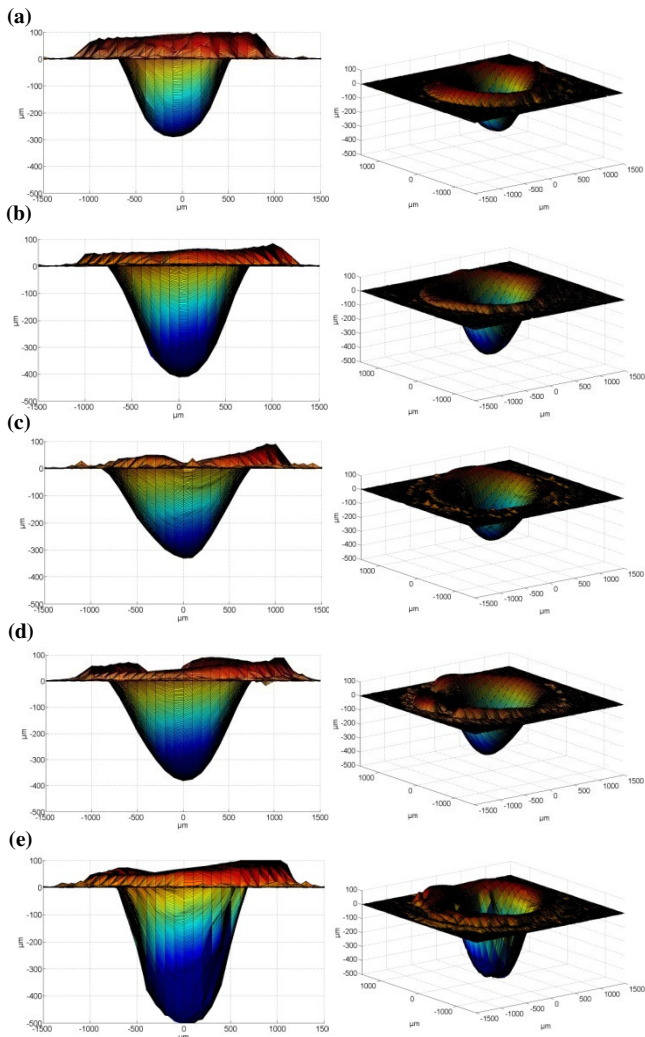


**Figure 4.** Different views of the electrode E1 topography after (a) 1 CC, (b) 2 CCs, (c) 3 CCs, (d) 4 CCs and (e) 5 CCs. Taken from [16].

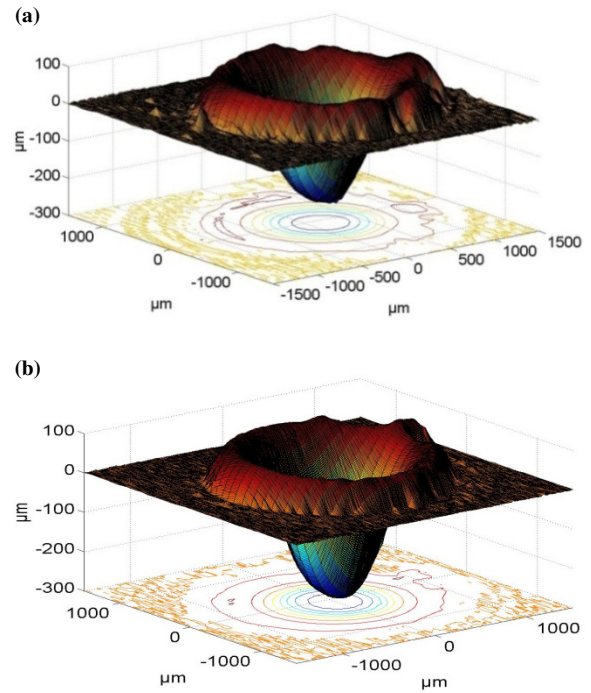


**Figure 5.** 3D topographies and contour map views of the emissive surface of electrode (a) E1 and (b) E2 after 1 CC. Taken from [16].

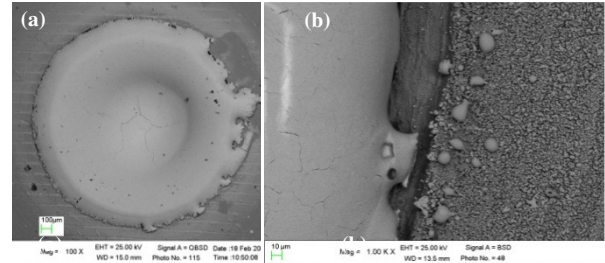


**Figure 6.** (a) SEM micrograph of electrode E1 after 1 CC and (b) particular of the finely dispersed  $\text{HfO}_2$  and droplets around the deposited hafnium. Taken from [16].

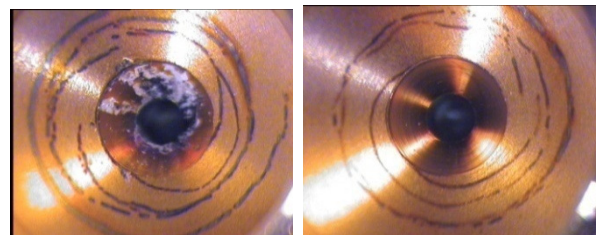


**Figure 7.** Stereo-microscopy images of the inner surfaces of nozzles associated with electrode E1 after (a) 2 CCs and (b) 3 CCs. Taken from [16].

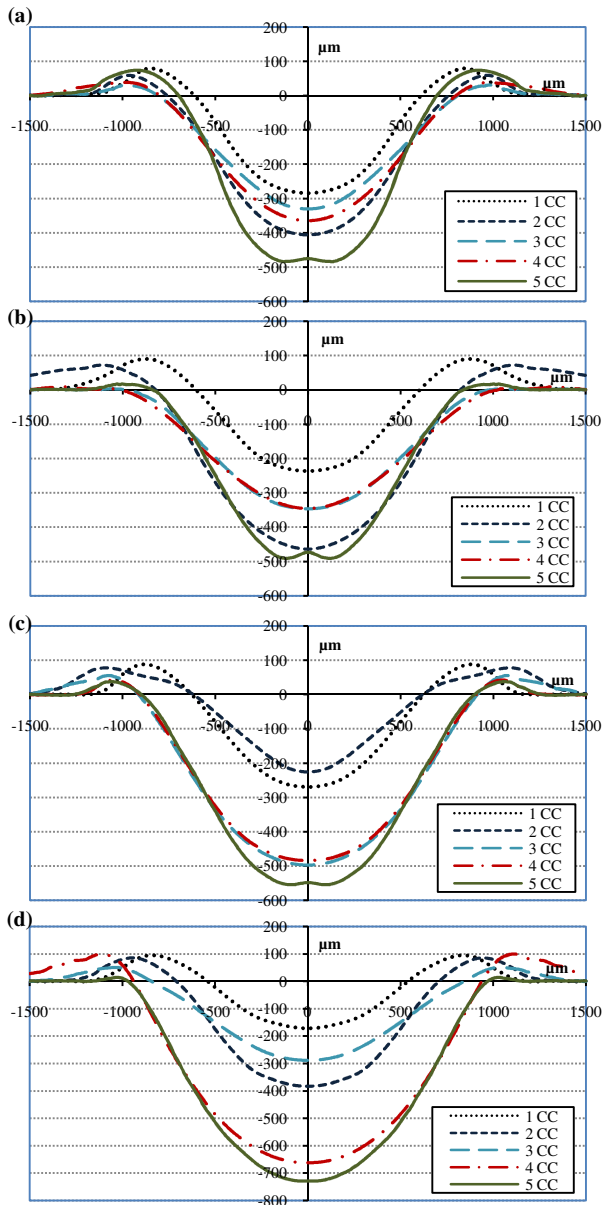


**Figure 8.** Trend of the cross sectional mean profiles, from 1 CC to 5 CCs, of the electrodes (a) E1, (b) E2, (c) E3 and (d) E4. Taken from [16].

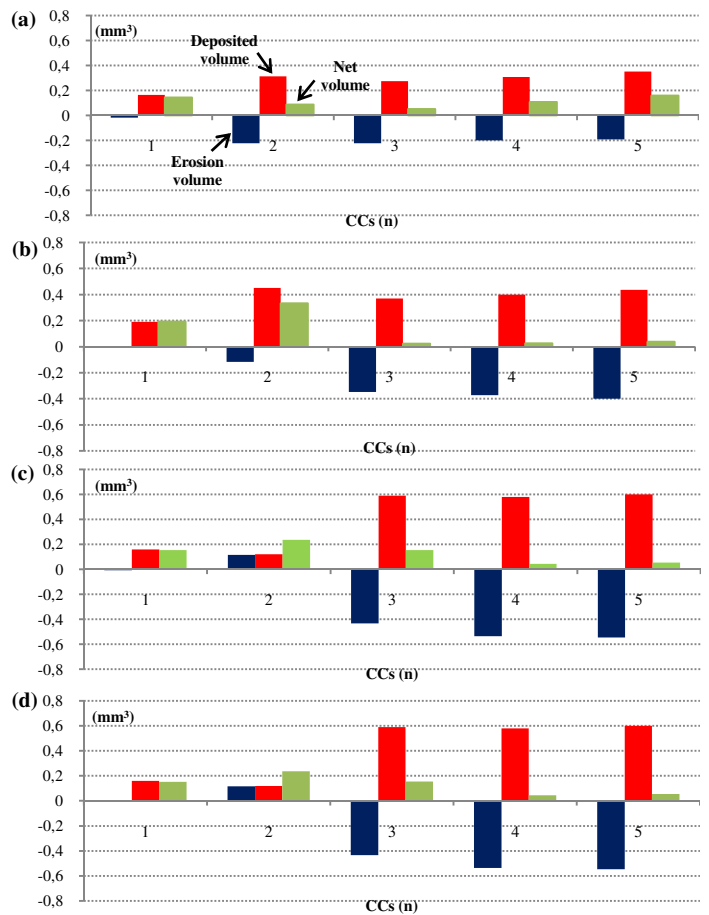


**Figure 9.** Trend of the calculated volumes, from 1 CC to 5 CCs, of the electrodes (a) E1, (b) E2, (c) E3 and (d) E4. The first column from the left is the erosion volume, the second one is the deposited volume and the third one is the net volume. Taken from [16].

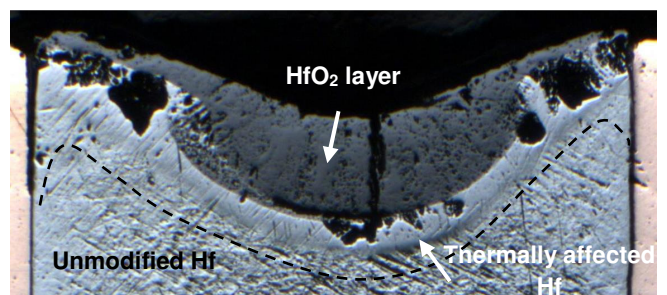


**Figure 10.** Cross sectional view of an Hf insert after 3 CCs, showing the typical microstructure comprising unmodified Hf, thermally affected Hf and HfO<sub>2</sub> layer. Taken from [16].

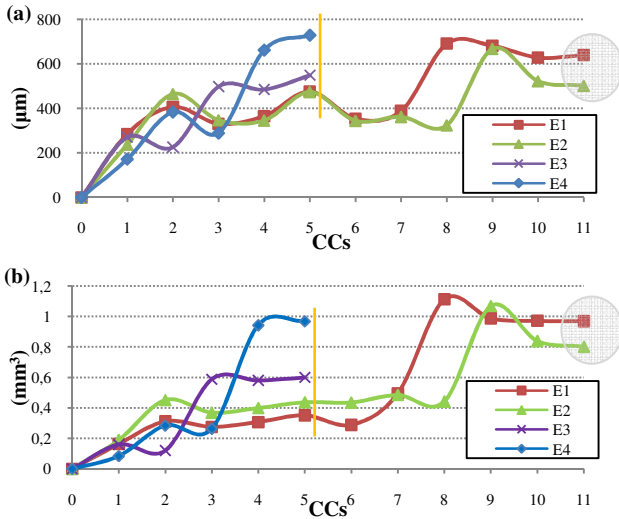


**Figure 11.** Trends of (a) the maximum recess depth and of (b) the calculated eroded volumes, as a function of the number of CCs, for electrodes with no initial recess. Taken from [16].

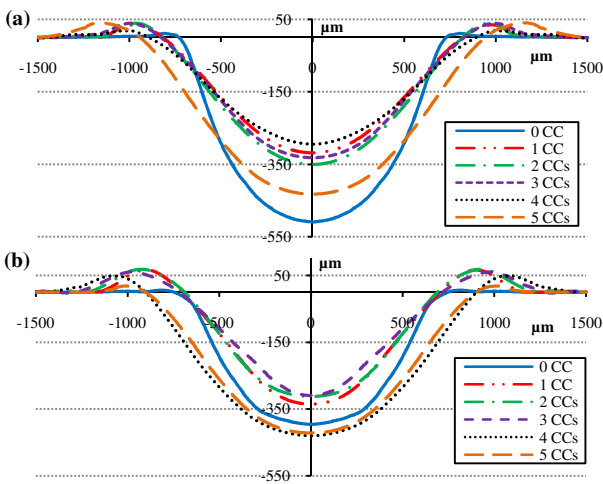


**Figure 12.** Trends of the cross sectional mean profiles, as a function of the number of CCs, for electrodes (a) *Es1* and (b) *Es2*. Taken from [16].

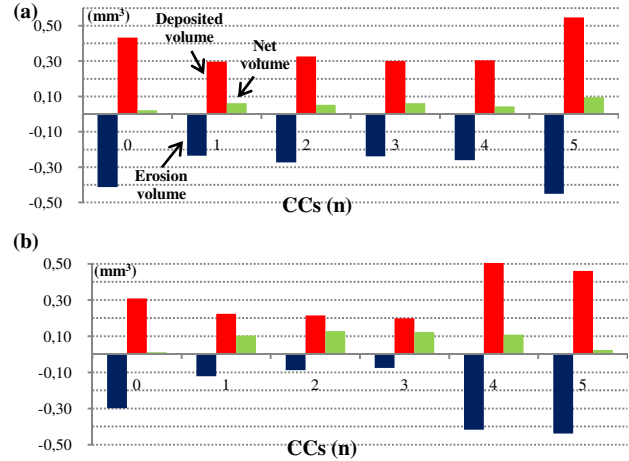


**Figure 13.** Trends of the calculated volumes, as a function of the number of CCs, for electrodes (a) *Es1* and (b) *Es2*. The first column from the left is the erosion volume, the second one is the deposited volume and the third one is the net volume. Taken from [16].

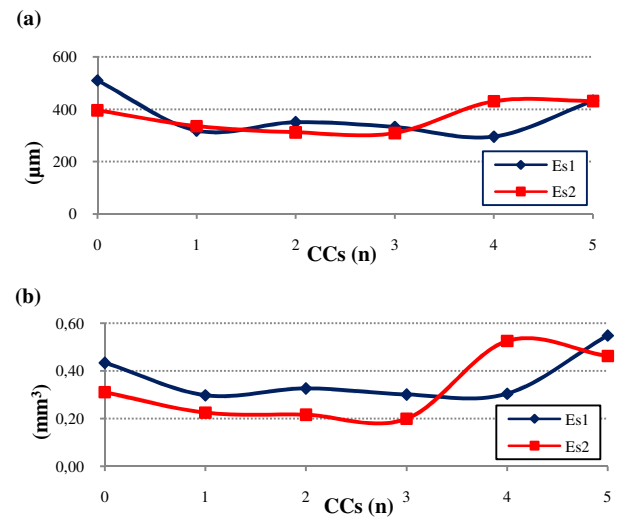


**Figure 14.** Trends of (a) the maximum recess depth and of (b) the calculated eroded volumes, as a function of the number of CCs, for electrodes *Es1* and *Es2*. Taken from [16].

## Conclusions and future developments

Studies described in chapter 2 were all devoted to improve plasma arc cutting torches performances in terms of electrode and nozzle service life. This challenge is crucial to allow the plasma cutting technology to make a significant step in innovation within its developmental curve and to obtain a competitive advantage over other competing technologies for the thermal break. The results obtained have allowed us to make great advances in understanding the erosion phenomena of the electrode at high operating current and plasma gas oxidizing and in the introduction of innovative technical solutions to limit the phenomena themselves, although this has not yet been able to fully understand what are the mechanisms underlying these phenomena

In particular, in the study presented in paragraph 2.1, the behaviour of high current electrodes in plasma arc cutting were investigated by means of morphological analysis during first cycles. An iterative experimental procedure for the optimization of the initial recess shape of the Hf insert have been validated, starting the investigation with an initially plane emission surface and defining subsequent optimization steps on the basis of the evolution of the recess depth naturally created during the first few *CCs*.

The process of cathode erosion at this stage was found to be only partially deterministic. Thus, 3D morphology of a set of electrodes (E1 - E4) was reconstructed after each of 5 cutting cycles. The results obtained during tests with electrodes characterized by an initially planar emission surface were a reference point for the design of two spherical recess shapes (Es1 - Es2), also tested on erosion during first cutting cycles. Results obtained from tests on electrodes Es1 and Es2 enabled us to identify optimal values for both the maximum recess depth and the erosion volume of the initial recess, for the specific geometrical and operative conditions under which erosion tests were accomplished.

Experimental evidences showed that an initial planar emission surface gives rise to massive Hf ejections during first *CCs*, inducing a preferred concave shape on the emitter, with consequent massive Hf deposition on the inner nozzle surfaces that negatively affect cut quality and nozzle service life; in patent literature, both these effects have been highlighted: as previously showed, by the abovementioned Hypertherm experimental procedure, but also in the Kabushiki Kaisha Komatsu patent “*Transferred Plasma Arc Torch*” - US 5214263 (May 25, 1993) [15]. In particular, the Komatsu patent highlights that any loss of axial-symmetry in the plasma chamber can negatively affect cut quality; experimental results reported in the patent are mainly based on an artificially induced loss of axial-symmetry of the electrode, by grinding out a portion of the tip of the electrode holder; but it is well known that the deposition on the nozzle inner surfaces of Hf-based products can raise similar consequences.

Moreover, the modified experimental procedure developed in the present work showed that the optimization of the initial recess shape of the Hf emitter surface not only minimizes the deposition of HfO<sub>2</sub> on the nozzle, as affirmed in [11], but positively affects the subsequent trend of the Hf erosion rate, improving electrodes service life on the whole.

Future developments will concentrate on implementing the new experimental procedure under different operating conditions, in order to study in detail the sensitivity of the optimal size of the spherical recess to changes in arc current and other operating parameters.

In conclusion, erosion phenomena that take place during different stages of electrodes service life at high currents were described without the pretence of clarifying the mechanisms underlying them. Up to now, the causes that produce such a strong erosion of the emitter surface are not exactly known and it would be an interesting topic for future work in this field.

## References

- [1] Nemchinsky V A and Severance W S 2006 What we know and what we know not about plasma arc cutting *J. Phys. D: Appl. Phys.* **39** R423-R438.
- [2] Nemchinsky V A and Showalter M S 2003 Cathode erosion in high-current high-pressure arc *J. Phys. D: Appl. Phys.* **36** 704-712
- [3] Nemchinsky V A 2003 Cyclic erosion of a cathode in high-pressure arcs *J. Phys. D: Appl. Phys.* **36** 1573-1576
- [4] Peters J, Yin F, Borges C F M, Heberlein J and Hackett C 2005 Erosion mechanism of Hf cathodes at high current *J. Phys. D: Appl. Phys.* **38** 1781-1794
- [5] V Colombo, A Concetti, E Ghedini, F Rotundo, S Dallavalle *Experimental analysis of the behaviour of high current electrodes in plasma arc cutting during first cycles* Plasma Sources, Science and Technology, Vol. 19 doi: 10.1088/0963-0252/19/6/065023 (2010)
- [6] M. S. Benilov, A. Marotta, *J. Phys. D: Appl. Phys.* 28 (1995) 1869.
- [7] D.R. Lide (Ed.), *CRC Handbook of Chemistry and Physics*, CRC Press, Boca Raton, 2009, p.4-97.
- [8] D. Eastman, *Phys. Rev B*, 2 (1) (1970) 1.
- [9] D.R. Holmes in: S.D. Cramer (Ed), S. Bernard (Ed.), Jr. Covino (Ed.), *ASM Handbook: Volume 13B: Corrosion: Materials*, ASM International, 2005, p.354
- [10] Luo L and Couch R W Jr 1992 Electrode for high current density plasma arc torch *Hypertherm Inc. Patent* US 5,310,988
- [11] Luo L and Couch R W Jr 1995 Electrode for plasma arc torch *Hypertherm Inc. Patent* US 5,464,962
- [12] Colombo V Concetti A Ghedini E Dallavalle and Vancini M 2009 High speed imaging in plasma arc cutting: a review and new developments, *Plasma Sources Science and Technology* **18** 1-24
- [13] Holmes D R 2005 Corrosion of Hafnium and Hafnium Alloys, *Corrosion: Materials*, Vol 13B, *ASM Handbook*, ASM International 354–359
- [14] *Gmelin Handbook of Inorganic and Organometallic Chemistry / Gesellschaft Deutscher Chemiker e.V. (GDCh)*, available from CrossFire Gmelin <http://info.crossfiregmelin.com/>, Elsevier Information Systems GmbH, last update 2010/01
- [15] Sakuragi S 1990 Transferred plasma arc torch *Kabushiki Kaisha Komatsu Patent* US 5,214,263
- [16] V Colombo, A Concetti, E Ghedini, F Rotundo, S Dallavalle *Experimental analysis of the behaviour of high current electrodes in plasma arc cutting during first cycles* Plasma Sources, Science and Technology, Vol. 19 doi: 10.1088/0963-0252/19/6/065023 (2010)

## Chapter 3

### High Speed Camera Imaging and Schlieren Imaging diagnostic in plasma arc cutting

Plasma modeling can be a very useful tool for the investigation and design of plasma arc cutting torches [2-5], but research still looks for an efficient link between simulation of the plasma arc and consistent prediction of *kerf* formation and cut quality; similarly to what has been recently done to relate spectroscopic measurements to cutting performance [6]. In this frame, diagnostics based on High Speed Imaging (HSI) can play an important role for investigating some of the fundamental phenomena typically occurring in PAC technology, such as:

- low-speed and high-speed dross formation outside of dross-free cutting window,
- anode attachment location with ultraviolet filtering,
- *kerf* formation mechanism with molten metal ejection,
- turbulence created by the interaction between the plasma jet and the surrounding atmosphere and by the secondary gas exiting the shield, through Schlieren imaging,
- cathode erosion with observation of the hafnium surface during different phases of a full operating cycle,
- shock wave location in the plasma jet as function of pressure conditions,
- pilot arcing and piercing phases[7-17, 25-26,30,32].

Most of the activities that I carried out in this field have been done in the framework of the research contract between the DIEM and Cebora Spa. My contribution initially consisted in carrying out a literature review on this topic. I also collaborated at several experimental studies in designing and carrying out experimental tests aimed at investigating phenomena with a strong industrial interest otherwise not investigable, involving members of the Group for Industrial Applications of Plasma of the University of Bologna and the members of R & D section of the Cebora Spa Company. I was also involved in the subsequent phase of interpreting obtained results in order to find a link between high speed images, oscilloscope waveforms and effects of the cutting torch behavior on cut quality and consumables wear. Some of the activities related to optimization of the performances of consumable electrode and nozzle, in terms of their service life, were carried out in collaboration with the Metallurgy Group of the Department SMETEC of the University of Bologna.

In a first stage, the high speed camera NAC Memrecam K3R (maximum resolution 1280x1024 pixels with an acquisition velocity of 1000 frame per second) for studying following phenomena, as detailed in paragraph 3.2:

- influence of different operating parameters (arc current, plasma gas inlet pressure and plasma gas swirl component inside the chamber) on the rotational motion of the arc attachment on the nozzle tip during the pilot arc phase;
- visualization of the cathode area (electrode) during a pilot arc through coaxial positioning of the torch with the axis of the high-speed camera to study phenomena that occur at different stages which form the pilot arc phase;
- study of the phenomena that occur during a non-destructive double arcing occurred under realistic conditions during the cutting of a mild steel plate of 20 mm thick using an operating current of 200 A and O<sub>2</sub>/air as plasma / secondary gas;
- study of the trajectory of solid particles coming from the plasma chamber, probably ejected from the hafnium emitter surface, during the pilot arcing phase;
- study of the influence of the centering of a torch consumable components (electrode, plasma gas diffuser, nozzle and shield) on the behavior of the plasma arc during the cutting of mild steel and stainless steel plates in the case of very thick plates (> 20 mm) and cutting currents above 120 A;
- study of hafnium massive ejection phenomena from the emission surface during the first cutting cycles of the service life of an electrode and study of the influence of the hafnium oxides depositions on the nozzle inner surfaces on the stability of the transferred arc.

The consumable components used during the tests described above were then subjected to microstructural, morphological and compositional characterization through optical microscopy, SEM + EDS and micro-Raman spectroscopy. In particular, we focused on the emission surface of the electrodes and on the side walls and on the tips of the nozzles in order to identify possible correlations between the behavior of the plasma arc, observed through high-speed camera, and the status of the analyzed areas.

In addition to the NAC Memrecam K3, cameras with greater acquisition speed (NAC MEMRECAM GX1 and NAC MEMRECAM GX3: maximum acquisition speed of 200000fps) have been used to study in detail the following phenomena:

- influence of various operating parameters (arc current, plasma gas inlet pressure and plasma gas swirl flow inside the chamber) on the rotational motion of the arc root attachment on the nozzle tip during pilot arcing phase;
- observation of the cathode (electrode) area during a pilot arc through coaxial positioning of the torch with the axis of the high-speed camera to study the differences in behavior during this phase of standard electrodes and electrode characterized by inserts achieved using sintered composite materials;
- study of the influence of the plasma gas swirl velocity component on the instability that characterized the cathodic attachment during the start-up transient phase;

- view of the plasma arc anodic attachment under transferred arc mode and study of the location and of the movement of the same under different operating conditions;

The high-speed cameras NAC Memrecam K3R (maximum resolution of 1280x1024 pixels with an acquisition speed of 10,000 fps) and NAC MEMRECAM GX3 (acquisition rate up to 200,000 fps) have been also used to study phenomena relating to:

- behaviour of the cathodic attachment during the pilot arc start up transient, in order to study the differences in behavior during this phase between electrodes at the beginning of their service life and used electrodes (as detailed in paragraph 3.3) and the influence of operating parameters and arc ignition methods (retract and high frequency pulse pilot arc ignition) on the duration and on the peculiarities of the transition itself;
- behaviour of the cathode arc attachment during the arc-on and arc-off transients of a transferred arc, the observation of the cathode area during the arc transfer mode was made possible through the use of a nozzle suitably modified;

High-speed imaging of the pilot arc transient phase in plasma arc cutting (PAC) has been carried out synchronizing the use of two high-speed cameras in conjunction with an optical system suitably designed for producing multiple synchronized views of the same phenomenon, as detailed in paragraph 3.4. Such imaging techniques have allowed a deeper understanding of the pilot arcing process, thanks to the simultaneous visualization of anode and cathode attachments and through the development of tomographic reconstruction of the pilot arc. This studies have been done in collaboration with P. Sanibondi [38].

The high-speed camera was also used with an optical system for imaging through Schlieren technique to study the interaction of the secondary gas with the plasma discharge with different geometries of the shield consumable on a mono-gas plasma torch. The development of statistical analysis methods to extract quantitative information from diagnostics through High-Speed Schlieren Imaging, in order to obtain a better understanding of phenomena related to the fluid dynamics in the area between the torch and the *kerf*, has been carried out. In particular, a code for calculating the mean, variance and Fourier transform of series corresponding to each pixel of the captured videos have been implemented in Matlab, as detailed in paragraph 3.5. This studies have been done in collaboration with P. Sanibondi [38].

### **3.1 Diagnostic based on high-speed video imaging and flow visualization techniques**

As previously mentioned, the plasma cutting technology are still many unsolved problems, and sometimes not even understood in their deepest nature. Therefore, use of diagnostic tools ever more accurate and sophisticated, it is essential to understand the phenomenology of plasma and the physics of the phenomena that characterize it, in order to overcome the technological issues and improve plasma arc cutting performances even more.

Diagnostic based on high-speed video imaging and flow visualization techniques has been already widely used to study many important phenomena in the plasma cutting, as will be detailed in the next section. The availability of tools for ever more sophisticated imaging also allows for ever more accurate studies on still poorly understood phenomena.

A recent diagnostic technique is based on the use of high-speed cameras (HSC), coupled with Schlieren photography, a special photographic technique that allows the visualization of density gradients in fluids.

These technologies are an important visual instrument to investigate the phenomena that characterize the plasma arc cutting, as they allow us to study phenomena that could not be investigated by a theoretical point of view or through computer simulations. Indeed, through the high-speed camera you can study phenomena that occur in very short time intervals, which would not be visible using standard cameras. The commonly used standard film provides a frame rate of 24 frames per second (fps), and is not capable of displaying phenomena whose characteristic time is less than  $1 / 24 \approx 0.04$  seconds.

The high-speed digital cameras, however, use CCD sensors that can capture images at high speeds. The latest models of high-speed camera allows time resolutions of less than 50 picoseconds, representing more than 20 billion frames per second.

The camera used in this study allows to take 10,000 frames per second and allows the visualization of phenomena such as the attack on the tip of the pilot nozzle, the transition of the pilot arc cathode attachment from the copper part of the electrode to the emitting area of the hafnium insert, the behaviour of the emitting area during different phases of the pilot arc, the double arcing non-destructive phenomena during the cutting phase, the mechanisms of erosion of the cathode, the movement of particles ejected from the surface of hafnium emitter, the dross formation, the effects of a non-perfect alignment of components, the location of the shock wave at the exit of the nozzle.

Only very recently, the use of Schlieren photography, coupled with high-speed recordings has made it possible to display the fluid turbulence that is created by the interaction between the plasma jet, the secondary gas and the surrounding atmosphere. The high-speed Schlieren movies provide qualitative information on the fluid dynamics of the plasma, but the statistical analysis of these films can also provide valuable quantitative information. It will be interesting to explore different methods of statistical analysis of data from a movie Schlieren high-speed, in order to find out what information can be extracted from video.

### **3.2 Literature analysis and first results on High Speed Imaging in Plasma Arc Cutting**

In the following section a review of the studies that have been accomplished through HS imaging and flow visualization techniques in PAC will be outlined. Because some of these results are not easy to access, below we give detailed description of the experiments and of the conclusions. Section 2.1 concerns the first studies that have been done for the visualization of the cutting front through HS imaging, with neutral and UV filters, and through Schlieren imaging. Section 2.2 presents some studies in which imaging techniques have been used to investigate several phenomena such as: the position and the geometry of the shock waves at the nozzle exit, the formation of dross, the anodic arc root attachment location and the double arcing. Section 2.3 is dedicated to studies of electrode erosion phenomena that have been accomplished through HS imaging. These sections are followed by a detailed description of new studies in which HS imaging has been used to investigate pilot arcing and piercing phases in PAC of mild steel (MS) and stainless steel (SS) plates with dual gas torches in various operating conditions, providing new insight of the process and highlighting some interesting phenomena. In particular, a study of the influence of different parameters on the rotation of the arc loop attachment on the nozzle tip during pilot arcing has been presented in section 4. Section 5 is devoted to a study of the cathode region phenomena during the different phases of pilot arcing and section 6 to a study of phenomena that take place during a non-destructive double arcing. In section 7 images with hafnium based particles ejected from the emitter surface during pilot arcing phase are shown. Finally, in section 8, two different sequences of images during piercing of MS and SS plates are presented.

### **Review on high speed imaging and flow visualization methods in plasma arc cutting**

#### **3.2.1 Visualization of phenomena that take place at the plasma cutting front**

The first study of phenomena related with plasma arc cutting, accomplished through high-speed photography and videography, has been an unpublished research [7] supported by Hypertherm Corp. and carried out by Potter and Settles in which the ejection of melted material from the *kerf* and the formation of dross during plasma cutting have been analyzed. The authors, using a commercial plasma system, obtained highly-magnified images with an acquisition speed of 30-500 frames/sec which show that dross formation is related to the wetting of the *kerf* edges by the molten ejecta, whence some of the melt is drawn into dross nodules by surface tension differences. This phenomenon has been observed in the case of both too high and too low cutting speeds with respect to optimum conditions. The authors also observed the presence of a dross-free interval of cutting speed values, where the melted material is ejected directly into the plasma jet without wetting the *kerf* edges.

In a subsequent unpublished research [8], again supported by Hypertherm Corp., Settles et al. used high-speed video imaging and flow visualization techniques with up to 1000 frames/second for investigating the liquid metal flow patterns, despite the intense illumination of the plasma jet during

plasma arc cutting, with different combinations of cutting speed, steel plate thickness, and plasma arc current.

The first published papers on the subject are those by Bemis and Settles [9-10], also supported by Hypertherm Inc., where, probably, some of the results presented convey the unpublished results of [7-8]. In [9] a study of the fluid-dynamic and plasma-dynamic mechanism involved in the formation of low-speed and high-speed dross has been carried out through the visualization of the plasma cutting front. A commercial plasma cutting system (Hypertherm HyDefinition™ HD-1070 System) in the 30 A configuration was used for cutting of 2.9 mm cold-rolled AISISAE 1008 mild steel plates with a highly-constricted oxygen plasma jet. Initially, visualization problems of image magnification, depth-of-field, illumination, and protection of the camera lens, due to the plasma arc peculiarities have been faced in order to observe physical phenomena related to dross formation.

Part of the research has been accomplished using a S-VHS videocamera shrouded to protect it from damage and fitted with a 50 mm focal-length lens and one or two 2X tele-extenders, capped with one of 7 different auxiliary “pinhole” apertures; excellent video results have so been obtained but with a time-resolution that was insufficient to suitably record phenomena typically related to plasma arc cutting. In a subsequent phase of the research, a Hycam II rotating-prism camera was employed: high-speed 16 mm films having a rating of ISO 160 with a 4:1 magnification ratio and a film speed of 1000 frames/sec have been obtained. This acquisition speed proved fit to obtain the suitable temporal resolution to study phenomena under investigation, slowing the process down by a factor of 42 compared to real-time observation. Also, when high image resolution was required, selected still frames were photographed on 35 mm colour film. The videotapes and high-speed films so obtained proved fundamental for studying the physical phenomena that take place during no-dross, low-speed and high-speed dross formation. Edge cutting was used in several experiments in order to observe phenomena that normally take place inside the *kerf*.

In the experimental setup, unlike industrial applications, the torch has been kept in a fixed position, while the workpiece is translated beneath it.

Some of the most relevant results taken from reference [9] will be presented here.

Figure 1 was obtained with the camera lens positioned below the torch and with metal motion toward the camera's point-of view while the plasma cutting torch is fixed; it shows a dross-free plasma cut characterized by a stable ejection of the molten material from the plasma cutting front directly into the plasma jet without wetting the sides of the *kerf*. Figure 2 shows an edge-cut characterized by low-speed dross formation. Here, the edge of the workpiece is on the plasma jet centerline, while the camera is set perpendicular to the plane defined by the metal edge and this centerline. The image clearly shows the formation of curved striations, the gap between the plasma jet and the *kerf* leading edge and a glow region that precedes the plasma jet.

Some images were obtained interposing a Schneider UV bandpass filter in the optical train in order to capture the emission of the molten iron oxide in the ultraviolet. Figure 3 shows the same experimental condition of figure 2, but it has been obtained through the interposition of a Schneider UV bandpass filter which blocks wavelengths longer than 405 nm and passes the near-UV band between 405 nm and the limit of glass transmission at approximately 280 nm. Most of the UV radiation comes directly from the plasma jet, with some reflection from the cut edge; anyway, the

region of self-luminance in the UV in the broad gap between the plasma jet and the *kerf* bottom leading edge has been interpreted by the authors as the anode attachment point of the plasma jet; the presence of a ionized path for current flow between the anode spot and the cathode through the plasma jet, is supposedly created by a hot spot of boiling metal positioned in the *kerf* bottom leading edge.

Furthermore, images were also obtained through a traditional lens-type Schlieren system employing a microsecond-flashlamp synchronized with the video camera. A vertical knife-edge cutoff was used to provide the best sensitivity perpendicular to the plasma jet axis. Because of the strong direct light emitted from the plasma jet, the authors made use of filters and masked the flashlamp, in order to increase the image contrast. Figure 4 shows an image of a dross-free plasma cutting obtained with the camera lens positioned on the side of the fixed torch and with the workpiece moving from right to left. It shows the turbulence created by the plasma jet in the mixing with the surrounding atmosphere and the turbulence above the workpiece created by the secondary gas flow exiting from the shield.

Figure 5 shows an image of a low-speed dross plasma cutting obtained with the same camera set-up of figure 4. It differs from the previous one for the presence of a forward spatter of small droplets that tend to attach to the bottom surface of the workpiece.

In conclusion, in this work the plasma cutting process was observed for the first time directly and with high spatial and temporal resolution. A dross-free cut has then been associated to a stable expulsion of molten material from the plasma cutting front; high-speed dross formation is induced by an unbalanced condition between the high ejecta flux and the geometrically-constrained cutting front, in addition to the wetting of the edges of the *kerf* by the melt; low-speed dross formation seems to be associated to a chaotic phenomenon subject to flow bifurcations leading to several metastable states of equilibrium. Ultraviolet imaging revealed the attachment location of the plasma arc on the *kerf* bottom leading edge through the strong radiation in the UV emitted from the anode spot for the presence of oxygen and iron ions. The Schlieren imaging technique showed turbulence created by the secondary gas flow and by the interaction between the plasma jet and the atmosphere underneath the workpiece.

In [10] again Bemis and Settles present more in-depth results obtained employing the ultraviolet imaging technique in order to study phenomena related to the anode attachment location of the plasma transferred arc during plasma arc cutting and its interaction with the molten metal at the leading edge of the *kerf*. Images have been taken in real cutting conditions of mild steel plates with oxygen as plasma gas. As in [9] the interposition of a Schneider UV bandpass filter enabled to capture emission in the ultraviolet. The ultraviolet imaging enabled to obtain better results with respect to imaging with visible light, using realistic cutting conditions. Different orientations of the camera lens with respect to the plasma jet have been used in order to better observe the location and the behaviour of the anode attachment of the plasma arc.

Figure 6 shows different images of the phenomenon under investigation in real cutting conditions. In particular, images of figures 6 (a)-(c), taken with the camera placed beneath the plate on the plasma jet axis, show the presence of both single (6-a and 6-c) and diffuse/multiple (6-b) anode root attachment points for the plasma arc; moreover figure 6-a shows that the anode attachment can be

also located on the melted material outside the *kerf*. In figures 6 d-e the camera is positioned perpendicularly to the cut direction and with an oblique angle from below the plate. In figure 6-d is visible how the high-velocity plasma jet convects away the anode jet below the plate; in figure 6-e the anode root attachment is located on the melted metal that is flowing out from the *kerf* and the anode jet is again convected below the plate. In conclusion, the authors showed that ultraviolet imaging can lead to a better understanding of some of the physical phenomena that rule plasma arc behaviour during cutting, even though the complete effects of formation and location of the anode attachment spot are yet to be fully understood.

### **3.2.2 Visualization of shock waves at the nozzle exit, dross formation, arc root attachment in the *kerf*, double arcing phenomena**

A few years after the first studies of Bemis and Settles had been reported, some more experiments [11-16], supported by the French company Air Liquide, used imaging techniques in order to visualize several phenomena concerning plasma arc behaviour in metal cutting. Particular emphasis was put on investigating the shock wave location at the nozzle exit, the influence of the cutting process parameters (arc voltage, cutting velocity and plasma gas inlet pressure) on the shock wave geometry at the nozzle exit, the dross formation on top and bottom of the plate, the positioning of the arc root attachment in the *kerf* and the formation of secondary arcs (double arcing).

#### *Shockwave location in PAC*

Even though what reported in various papers and Ph.D. theses [11-15] on the study of the jet shock wave location and shape at the nozzle exit is not strictly a time-dependent rendering of plasma cutting phenomena captured by high speed imaging, some results have been included in these review part of the paper since a fast acquisition camera with a shutter time of  $10^{-4}$  s has been used. In [12] and [13] Freton et al. present some simulation results for the plasma jet of a SAF NERTAJET HP120 cutting system and compare them with photographs (shown in figure 7) originally obtained by Air Liquide [11], for different values of the plasma inlet pressure (4.5, 5.5 and 6 atm, respectively), using a and a CCD camera equipped with a 105 mm lens, a grey filter OD3 and a shutter time of 1/10000 s.

Freton et al. in [12-13], commenting the Air Liquide photographs [11], explain that the line at  $z=0$  indicates the nozzle exit, that the bright area over  $z=0$  is supposed to be the reflection of the plasma jet on the nozzle side and that the succession of bright and dark areas under  $z=0$  is related to the supersonic behaviour of the jet: where the pressure is very low the plasma jet is not able to emit light and it appears dark; while where the pressure is much higher, the plasma jet appears very bright. These pressure waves are related to the adaptation (which cannot be obtained into the nozzle) of the chamber pressure to the atmospheric pressure. The Air Liquide photographs [11], reported in [12-13], also show that increasing the plasma inlet pressure, the first shock wave moves away from the nozzle exit, downstream the plasma jet. Freton et al. in [12-13], developing the plasma model, used a plasma inlet pressure of 4.5 atm, in order to have a direct comparison, on the shock wave location, between their computational results and the evidences rising from the plasma jet images [11]. In figure 8 the comparison between the Air Liquide photographs [11] and the

pressure field obtained from the computational model [12-13] is shown. In figure 8a the photograph of the plasma arc is referring to an inlet pressure of 4.5 atm and the laminar model shows a minimum pressure of about 0.4 atm. The model developed by Freton et al. [12-13] predicts a supersonic behavior of the plasma jet at the nozzle exit with a succession of pressure waves. The location of the underpressure and overpressure waves is well predicted by the model and corresponds to dark and bright zones detected experimentally. In figure 8b, the photograph of the plasma arc is referring to an inlet pressure of 5.5 atm; also, in this case the model correctly predicts the location of the shock and in correspondence to an increase of inlet pressure, the model predicts a shift of the shockwave downstream the plasma jet, as shown by the Air Liquide photographs [11]. In conclusion, the study reported in [12-13] showed a good agreement between the model prediction and the shock wave location detected experimentally.

Subsequent studies, concerning the influence of the cutting process parameters (arc voltage, cutting velocity and plasma gas inlet pressure) on the structure, the geometry and the dimension of the shock wave at the nozzle exit, were published by Girard et al in [14] and in the Ph.D. thesis by Girard [15]. An Air Liquide OCP 150 system with a Nertajet HP 120 power supply was used as plasma cutting system. A CCD camera (PHOTRON FASTCAM PCI 10k, with  $512 \times 480$  pixels and recording 30–10 000 fps) was set perpendicularly to the cutting trajectory, as shown in figure 9, in order to visualize the shock wave and to measure the distance between the nozzle exit and the top of the plate. This camera was coupled with a Macro zoom COMPUTAR MLH 10× and, in order to maximize the number of active pixels, its acquisition rate was set at 250 fps. For all experiments, the arc current was 60 A, the plate thickness 10 mm and the plasma gas was O<sub>2</sub>. Other cutting parameters varied between 130 and 150V for the arc voltage, between 50 and 140 cm min<sup>-1</sup> for the torch velocity and between 4.0 and 6 atm for the plasma gas pressure. Figure 10, published only by Girard in her Ph.D. thesis [15], shows the results obtained with a cutting velocity of 70 cm/min, a plasma inlet pressure of 5.5 atm and an arc voltage that varies from 130 V to 150 V. At the top of the picture, the bright area is supposed to be the reflection of the arc on the nozzle side. The formation of a shock wave is visible at the nozzle exit and it is characterized by a succession of bulges and pressure nodes. The very bright and luminous area at the nozzle exit has been interpreted as an overpressure wave, so that the first pressure node is located after 1.5 mm. The distance between the nozzle exit and the top of the plate increases with increasing arc voltage, but it has no influence on the shock wave geometry. Nevertheless, it was not possible to measure the total length of the arc, because images acquired by Girard [15] and reported in figure 10 don't show the position of the anodic arc root attachment. Girard [15] highlights that the axis of the plasma jet is not vertical and she explains this distortion as the result of some kind of nozzle damaging. She also affirms, on the basis of some other experiments, that the jet axis displacement can sometimes be oriented towards the *kerf* front and not always towards the opposite side as in figure 10. Figure 11, presented once again only by Girard in [15], shows results obtained with a variation of cutting speed from 50 to 130 cm/min, with an arc voltage of 130 V and a plasma gas inlet pressure of 5.5 atm; decreasing the cutting speed and using a stand-off control system with constant nozzle-workpiece voltage drop, the distance between the nozzle exit and the top of the plate decreases: this result is assumed to be due to the fact that with a low cutting speed the arc root attachment is positioned in the lower region of the *kerf*. Nevertheless, Girard could not demonstrate that the total length of the arc keeps constant at different cutting speed, because images acquired through the CCD camera didn't show the anodic arc root attachment.

Figure 12, published in [14] and taken from Girard's Ph.D. thesis [15], shows results obtained with an arc voltage of 140 V, a cutting speed of 70 cm/min and a plasma gas inlet pressure that varies from 4 to 6 atm, in order to study its influence on the geometry and the dimension of the shock wave. While results reported in figures 10 and 11 showed that a change in arc voltage (between 130 and 150 V) and in cutting speed (between 50 and 130 cm/min) does not affect the shock wave shape, the results reported in figure 12 demonstrated that the oxygen inlet pressure strongly influences the structure of the underexpanded jet. Indeed, the experiment showed that increasing the plasma gas inlet pressure from 4 to 6 atm, the torch end approaches the plate; once again, it is not possible to demonstrate a change in the total length of the plasma jet. The images reported in figure 12 also show that increasing the plasma gas inlet pressure, the luminous zone at the nozzle exit, corresponding to a straight shock wave, increases its length and its brightness; moreover, Girard highlights in [15] that the first overpressure node (indicated in the images with white broken lines) moves downstream from the nozzle exit for increasing plasma gas inlet pressure; this phenomenon being indicative of an increase of the distance between two pressure nodes.

#### *Dross formation in PAC*

In her Ph.D. thesis [15] Girard presented also a series of images obtained during a study concerning the influence of operating parameters on cut quality in terms of dross formation on the sides of the *kerf*. The imaging experimental set-up is shown in figure 9 and it is without filtering. Taken from [15], figure 13 shows the formation of molten metal droplets on the top of the plate. The reported operating conditions are those that minimize dross formation during cutting at the bottom of a 10 mm mild steel plate, with oxygen as plasma gas.

The experiments reported in [15] also highlighted that the chemical composition of mild steel can slightly influence the mechanism of dross formation.

#### *Arc root attachment in the kerf in PAC*

The anodic arc root attachment has been studied by Girard et al. through the same CCD camera that they used in the abovementioned experiments [14-15] and results have been published both in Girard's Ph.D. thesis [15] and by Girard et al. in [16]. Current intensity and plate thickness have been fixed at 60A and 10 mm, respectively; arc voltage, torch velocity and inlet pressure of oxygen have been operated in the range, 130 V-150 V, 50 cm/min-140 cm/min and 4.0 -6 atm, respectively. The experimental set-up is presented in figure 14 and shows how the camera is integral with the torch and positioned obliquely with respect to the plate, to better visualize the arc root attachment inside the *kerf*; an acquisition speed of 250 fps has been selected to obtain the maximum active pixels on the CCD camera. An acquisition speed of 3000 fps has been selected for those experiments aimed at studying the stability of the arc.

Figure 15, published in [16] with results taken from Girard's Ph.D. thesis [15], shows a cutting initiated on the edge of a workpiece. In image 15a, the arc is piercing the plate and the presence of the melted material ejected on the top of the plate is shown. In image 15b, the piercing of the edge of the plate is completed, the torch is still immobile and a widened cavity with a molten pool on the

bottom of the edge of the plate can be seen. In image 15c, the torch is in motion and it is possible to see the formation of the *kerf* and molten metal droplets under the plate that will cool down as dross. Moreover, in [15] Girard highlights the presence of some small and very bright spots on the top edge of the *kerf* (image 15c), that she interprets either as melting metal droplets or anodic arc root attachments. To better study the influence of arc parameters (arc voltage, cutting speed and plasma inlet pressure) on the arc root attachment position, neutral filters have been interposed between the plasma jet and the camera lens. Figure 16, published both in [15] and [16], shows the comparison between filtered and non filtered images of the arc root on the cut front surface. In the case of filtered signal, the arc shows a luminous area that could be explained either as a hot spot on the cut-front surface or as radiation emitted by a concentration of metallic vapour in the plasma jet; both phenomena being probably related to the position of the anodic arc root attachment.

The authors also point out that, for cutting speed over 90 cm/min, a second luminous spot can be observed close to the top of the cut-front surface, probably due to anode spot oscillation or to a double attachment of the arc root. As a conclusion, the authors finally affirm that, even if the anodic root attachment slightly moves toward the top of the plate increasing arc voltage and cutting speed and decreasing plasma gas mass flow rate, the arc root position doesn't seem to be strongly influenced by operating conditions and that the anode spot looks always close to the middle depth of the *kerf* wall. On the other side, Nemchinsky in [1], comparing the results published in [15-16] with some results that he had obtained in the same operating conditions using a set of thermocouples positioned at different depths aside of the *kerf*, highlights that both experiments show how arc voltage and plasma gas flow rate have no influence on the position of the arc root attachment while for increasing cutting speed the anode spot moves toward the top of the plate.

#### *Double arcing phenomena in PAC*

Girard, in her Ph.D. thesis [15], shows some images, obtained during her investigation of the influence of the plasma gas inlet pressure on the geometry of the shock wave, which are characterized by the presence of secondary arc discharges (double arcing), as shown in figure 17. During those experiments, the abovementioned secondary arc discharges appeared mainly when the nozzle was not new or even damaged and when the plasma inlet pressure was lower than 4 atm. Both these conditions can be related to a lower stability of the arc and to a consequently higher probability of arc attachment on the nozzle wall, inducing double arcing.

### **3.2.3 Visualization of cathode erosion phenomena**

More recently, a paper by Heberlein et al. [17] brought high speed imaging investigation again at the attention of the PAC scientific community with a detailed study of the erosion mechanism of hafnium cathodes at high current levels. Also this work has been supported by Hypertherm Inc.: its results are closely related to some important Hypertherm patents [18-19] and demonstrate the reason for the industrial success in reducing electrode wear. Experiments were accomplished through a commercial plasma cutting system (Hypertherm HT2000) with oxygen and nitrogen as plasma gases, with total flow rate near 38 slpm and an arc current of 200 A; maximum current density is

about  $10^8 \text{ A/m}^2$ . While in the studies presented in the previous paragraphs the experimental set-up was characterized by realistic cutting conditions, in this case a water-cooled rotating ring simulating the anode-plate has been used.

Two different camera systems have been used: a laser strobe system capable of very short exposure time (100 ns) but slow repetition rate (30 frames  $\text{s}^{-1}$ ) and a high framing rate camera. The laser strobe system, manufactured by Control Vision, consists of a 337 nm nitrogen laser, CCD camera, image intensifier, video recorder and a system controller; it proved to be particularly suitable for obtaining good images of the cathode surface during arc operation. The high framing rate camera is a Kodak 4540 Ektapro Highspeed Motion Analyzer with a maximum framing rate of 40 000 fps and it has been used in imaging of electrode erosion during arc shutdown transients. In their experiments the authors set an acquisition speed of 9000 fps, with a consequent resolution of  $128 \times 256$  pixels. A Questar telescopic lens has been used with both acquisition systems in order to obtain a magnification of the cathode, while neutral density filters have been used in order to reduce the brightness of the arc and to protect the camera. The observation of the cathode surface during torch operation was accomplished by designing and operating a modified nozzle with two viewing ports, positioned at opposite sides, at an angle of  $45^\circ$  with respect to the torch axis; each port has an axis centred on the hafnium insert and a diameter of about 2.5 mm, as shown in figure 18; sapphire windows have been suitably cemented into the ports to avoid flow disturbance on the inside nozzle wall; moreover, during operation the shield gas flow cup was removed. The viewing angle of  $45^\circ$  implies the presence of the round view port in images and an elliptical shape of the hafnium insert, as shown in figure 19. The erosion of hafnium cathodes has been analyzed in the three phases that compose a real cutting process and that are characterized by different erosion mechanisms. According to the authors, erosion is mainly related to the ejection of molten hafnium droplets during changes in plasma conditions (in particular during start-up, shut-down and during the changing of gas flow), due to imbalances of the forces acting on the molten surface.

The first phase of the cutting process, called by the authors “plasma start phase”, is characterized, after arc ignition, by the motion of the arc root attachment from the electrode copper holder to the centre of the hafnium insert and by the consequent expansion of the arc root on the entire emitter surface. In experiments done by the authors, the total time of the arc root expansion is about 0.2 s, as shown in figures 20 and 21; simultaneously, the arc current increases with a slope-up and reaches the operating level about 0.8 s after arc ignition, while plasma pressure changes from a pre-flow level (a mixture of oxygen and nitrogen) to a cut-flow level about 0.7 ms after arc ignition. As shown in figure 21, the arc root expansion is completed before the arc current reaches its steady value. During the arc root expansion, droplets of hafnium can be ejected from the molten pool that is formed on the emitter surface. In their experiments the authors observed three different ejections during this time interval; in particular, the first ejection takes place immediately after arc ignition, the second one 0.35 ms after arc ignition and the third ejection event corresponds to the instant in which the plasma gas flow changes from the pre-flow level to the cut-flow level. Figures 21c and 21d show the second and third ejection observed through the laser strobe camera, while figure 22 shows three ejection events observed during the start-up phase. The authors also observed that the first ejection has no correlation with the type and the flow rate of pre-flow and cut-flow gases, while the second and the third ejection decrease with the reduction, during the pre-flow phase, of the flow rate of oxygen and nitrogen, respectively.

The second phase of the cutting cycle, called by the authors “steady running phase”, is characterized by arc current, nozzle pressure and voltage reaching their steady values; it starts with a change of plasma gas from pre-flow to cut-flow and finishes when the cut is completed. As said, the authors report that this phase starts 0.7 ms after arc ignition, while steady state is reached about 2 ms after arc ignition. During this phase the authors measured an arc root diameter of 1.8 mm for a 200A current, while no ejection phenomena were observed and the acquired images showed a very stable molten pool.

The third phase of the cutting process which has been investigated is the “arc shutdown phase”. The authors studied two different shut-down configurations: the first one is characterized by a slow decrease of the arc current through a ramp-down of about 150 ms; the second one is characterized by a sudden extinction of the arc (in about 1 ms) through the emergency stop mechanism. The authors observed that in the first case very few ejection events take place while in the second configuration large particles are ejected from the molten pool, immediately after arc extension, as shown in figure 23. The authors also investigated the type and amount of hafnium particles ejected during the arc operation with a mass collection system composed of a suitably modified nozzle and of a collection rod. Particles deposited on the rod during the start phase (more particles with a much smaller diameter) and the fast current shutdown (fewer particles with larger diameter and greater size distribution) show significant differences.

In conclusion, the direct observation of the cathode emitter surface without substantially interfering with normal arc behaviour, enabled the authors to study the physical phenomena of hafnium erosion during different phases of the cutting process.

Finally, it must be said that part of the results described above has been presented by Joachim Heberlein during the 2007 *International Round Table on Thermal Plasma Fundamentals and Applications* in Sharm El Sheikh [20]: his work was dealing more generally with erosion phenomena in thermionic cathodes: they require the use refractory materials which can reach temperatures above 3000 K without much evaporation to deliver the electrons for the arc. For the case of very high current densities, as in PAC, Heberlein showed some HSC movies highlighting the abovementioned erosion effects during arc shutdown as a result of an imbalance between the fluid dynamic drag forces, the ion current pressure, the electromagnetic pressure and the surface tension, with consequent ejection of liquid metal droplets.

## **New developments**

### **3.2.4 Experimental setup and HSC operating conditions**

In the previous paragraphs, several studies have been presented, in which HSC diagnostics have been used to investigate significant phenomena related to PAC. New studies [21-22] have been accomplished by some of the authors of this paper in order to better understand the plasma arc behavior during different phases of the pilot arcing, the phenomena that take place during non-destructive double arcing and the influence of the axial symmetry of the torch consumables on the

piercing process. The most significant results obtained will be reported in next paragraphs. A NAC Memrecam K3R HS camera has been used, with a 180 mm focal-length lens, protected by a sacrificial neutral filter, at a distance of 1 m from a Cebora (HQC164 for the range 25-120 A and HQC 254 for the range 120-250 A) plasma torch, joined with a digital oscilloscope (LeCroy LT374M). Figures 24 and 25 show a picture and a schematic of the experimental set-up, respectively. The synchronization of data acquisition has allowed to time-correlate the images captured by the HSC with the oscilloscope waveforms of voltage and current. In particular, high speed imaging has allowed to investigate pilot arc behaviour in different operating conditions (some of them not realistic when compared with a real ignition and transfer phase in PAC) and double arcing phenomena under operating conditions fit for fictitiously induce them; a correlation between arc instabilities and arc voltage oscillations as well as between arc shapes and pressure and current transients has been evidenced.

One of the reasons behind the study of non-realistic pilot arcing phases is aimed at a future investigation of the positive and negative impact of possibly keeping the pilot arc on after discharge shutdown at the end of a cutting phase; this procedure, when optimized under operating conditions probably different from the ones customarily used during conventional pilot arcing, might have some positive effect in reducing the amount of electrode erosion induced by thermal transients in the hafnium insert. On the contrary, it might have also the drawback of an undesired level of thermal stress and material damage on the electrode and nozzle. For what concerns this paper we will concentrate only on the search for a stable and non erratic pilot arcing condition to be further investigated on even longer time scale for the abovementioned reasons.

The HSC positioning with respect to the torch has been suitably defined for every experiment, taking into account to the particular phenomenon under investigation. In all the experiments the camera is fixedly mounted on a holder which allows setting its distance from the torch and its inclination with respect to the plane of the workpiece. During both pilot arcing and piercing the torch is in a fixed position with respect to the camera even tough stand-off distance is set using a pantograph with a CNC control.. Some experiments have been accomplished in real operating conditions typical in PAC, while some others have been accomplished with non standard set up for the consumables and for the operating conditions, in order to induce and monitor particular phenomena.

Pilot arcing images have been obtained in the absence of the torch shield cup (without secondary gas) in order to observe the arc loop attachment on the nozzle tip. Pilot arcing duration has been extended with respect to real cutting conditions in order to fully observe arc loop attachment phenomena. Since the typical arc loop attachment point moves along the nozzle faster than the maximum fps of the camera, its set-up has been selected, for all pilot arcing experiments, with 10000 fps and 1/200000 s shutter time, which is the maximum acquisition speed that the camera is able to achieve. In all experiments, the auxiliary lighting has been used only in the setting phase in order to optimize each focusing procedure, while the images have been captured without any filtering.

### 3.2.5 Effects of different operating parameters on pilot arc behavior

A study of the influence of different parameters on the rotation of the arc loop attachment on the nozzle tip during pilot arcing has been carried out through a series of experiments at different operating conditions, investigating the effect of changing pilot arc current level, plasma gas flow rate and its swirl strength. For each experiment a high speed movie has been done. An oblique upward viewing angle from underneath the nozzle tip has been set for the camera, in order to observe the arc loop attachment in every area of the nozzle tip with a tridimensional effect.

#### *Effects of arc current level*

The influence of current level on the pilot arcing in different operating conditions and in different torch configurations has been studied setting a current waveform with two different current levels: a first phase at 45A, with a second phase at 25A. At higher current level the pilot arc shows an increase of both its cross section and of its visible light emission; the pilot arc loop attachment is characterized by an enhanced random jumping mode; even so it is still possible to identify a rotation pattern around the nozzle tip. During the lower current phase, the arc cross section and its visible light emission are clearly reduced, while movement of the arc loop attachment is continuous and with lower rotation frequency with respect to the higher current phase. Figure 26a shows images of a pilot arc at 45 A, while figure 26b highlights the arc behavior during a subsequent current slope-down to 25A; figure 26c shows images of that same pilot arcing during the lower current phase; all sequences are at constant time intervals of 0.2 ms, 0.7 ms and 0.2 ms, respectively. The comparison between the series of images of figures 26a and 26c shows differences in pilot arc shape and behavior, while the images of figure 26b show the gradual change in pilot arc shape and behavior during the transient. Figure 26d shows the current waveform during pilot arcing, the correspondence between every image and the waveform being identified by the vertical lines.

#### *Effects of plasma gas flow rate*

Three high speed imaging experiments with different plasma gas flow rates have been carried out. All other operating parameters and the torch configuration have been kept as in the experiments reported in paragraph 4.1. This comparative analysis has shown that the plasma gas flow rate has an opposite effect on the movement of the pilot arc loop attachment on the nozzle tip with respect to the arc current level. In fact, an increase in flow rate brings to the reduction of the pilot arc rotational speed on the nozzle tip. Figures 27a, 27b and 27c show three sequences of pilot arcing images at 25 A, corresponding to three levels of plasma gas flow rate: 21 slpm, 28 slpm and 36 slpm, respectively. A comparison between images highlights a gradual decrease of the rotational speed of the arc loop attachment from figure 27a to figure 27c; the rotational speeds have been evaluated analyzing the single frames for the three cases and the frequencies are about 2000 Hz, 1000 Hz and 400 Hz, respectively.

### *Effects of swirl strength*

Two experiments have been carried out, under the same operating conditions (25 A), but with two plasma gas diffusers differing from one to another for the number and diameter of their holes, in order to obtain different swirl strength conditions for the plasma gas flow. The first diffuser had three 0.4 mm diameter holes (higher swirl strength), while the second one had six 0.8 mm diameter holes (lower swirl strength). Figure 28 illustrates the case of higher swirl strength: 24 frames of the high speed film, at a constant time interval of 0.5 ms, show how the arc loop attachment experiences an entire 360° rotation along the nozzle tip without any erratic or discontinuous moving. The total time for a complete rotation of the arc around the nozzle tip is 11.5 ms. Figure 29 illustrates the case of lower swirl strength: this case is characterized by erratic and discontinuous movements of the arc attachment on the nozzle tip. Figure 29 considers the same overall time interval of Figure 28; however, in this case, the frames are selected on a non constant time interval basis to highlight the discontinuous movement of arc attachment and the permanence time of the arc attachment in a specific point of the nozzle tip. It is also interesting to note that in this case the arc loop attachment experiences an incomplete (180°) rotation on the nozzle tip.

### **3.2.6 Cathode surface images during pilot arcing**

Visualization of the cathode surface during pilot arcing was accomplished by positioning the torch and the camera lens on the same horizontal axis. Four different experiments have been carried out in the same operating conditions. The experiments differ from one to another for the use of different focal ratio in the camera set-up, with the aim of showing at best different phenomena that take place in the various phases of pilot arcing; this induces a need of focusing on different regions of the inner plasma chamber or on the tip of nozzle. Realistic conditions for cutting of mild steel plates with 250 A and O<sub>2</sub>/air as plasma/secondary gas have been used. As above-mentioned, the experiments have been accomplished without the torch shield cup (with no secondary gas), in order to observe the arc loop attachment on the nozzle tip. The first three pilot arcing experiments have been accomplished using a torch nozzle with a 1.9 mm diameter of the orifice, while a modified one has been used for the last experiment for the detection of molten hafnium particles ejected from the emissive surface during current stop. For every experiment, the images captured by the HSC have been time-correlated to the oscilloscope waveform of arc current.

### *Images of the pilot arc moving out of the nozzle*

Images of figure 30a were obtained with focal ratio f/16 and they show the arc been blown out of the nozzle by the plasma gas flow [1] after the low current (25 A) initiation of the arc discharge between cathode and nozzle by means of a short HF pulse. In this phase the arc root on the cathode moves from the copper holder of the electrode to the centre of the emitter surface. This process is critical in terms of hafnium cyclic erosion processes, since the arc root, on its track, removes particles of the hafnium oxide solid layer that has formed after the last arc switch-off. In the meantime, the anodic arc root moves from the region of the nozzle that is closest to the electrode to the nozzle tip. The arc must rapidly exit the nozzle not to wear its internal surface. The best compromise between these two opposite needs has to be found in terms of optimization of current

waveform. Another important factor in this process is the swirl component in the plasma flow: the presence of a high swirl component in the plasma gas velocity induces a longer helicoidal track of the arc root attachment on the nozzle internal surface with respect to the case of a low swirl component of the plasma gas, so increasing the residence time of the arc inside the nozzle before the arc is blown out of it. Images of figure 30a highlight the swirling motion of the arc exiting the nozzle, due to the swirl component of the plasma flow. Figure 30a at 0.6 ms accounts for an arc attachment that still hasn't reached the centre of the cathode, even with already stabilized current level, and, therefore, is invisible. Figures 30b and 30c show the waveforms of current and electrode-nozzle voltage corresponding to the recorded pilot arcing phase. The link between every image and the waveform is shown by the vertical lines that appear in some points of the current graph. The first peak value of the arc current corresponds to the instant in which the arc is ignited while the increase in the voltage can be associated to the increasing of the arc axial length.

#### *Images of the emitter surface during pilot arcing*

Images of figure 31a were obtained with focal ratio  $f/32$  and they refer to the phase in which the arc has already exited the nozzle, creating a loop protruding out of it. This particular set-up of the camera lens is aimed at focusing on the emitter surface during this phase of pilot arcing. Some bright areas on the emitter surface between the arc root and the copper older of the electrode appear in some frames of the images of figure 31a. They are to be interpreted as electron emission spots on the molten hafnium surface of the electrode. The sequence of frames shows that the movement of those bright areas is ruled by the drag of the swirling plasma gas flow. Figure 31b shows the waveform of arc current during the end of its initial transient phase and while reaching its stationary value, with reference to the instant in which images of figure 31a have been captured.

#### *Images of the arc loop attachment on the nozzle tip*

Images of figure 32a were obtained with focal ratio  $f/5.6$ ; these HSC operating conditions do not allow a clear view of the electrode surface (unlike figures 29a, 30a and 31a) being aimed at obtaining information on the conditions on the nozzle tip in the time interval in which the arc has already exited the nozzle and the current has reached a stationary level around 45 A. The operating conditions and the torch configuration used in this experiment are the same used for the experiment reported in figure 29; in fact, frames reported in figure 32a also show an intermittent motion of the arc loop attachment on the nozzle tip. The particular positioning of the camera lens with respect to the torch has allowed to see how the intermittent root attachment of the pilot arc induces the formation of dark dots on the nozzle tip, even though the arc maintains its non-moving and localized attachment on the same point for less than 0.4 ms. Figure 32b shows details of the time interval to which images of figure 32a are related. Figure 33 shows SEM images of the tip of the nozzle used in this experiment, clearly showing the presence of some points in which the copper has suffered damages due to the arc root attachment.

### *Images of molten hafnium particles ejected from the emissive surface during current stop*

Images of figure 34a were obtained with focal ratio  $f/5.6$ ; torch head geometry differs from the one of the three previously mentioned experiments for the presence of a modified nozzle with a 2.5 mm diameter of the orifice, used to observe a wider portion of the plasma chamber in line of sight between the electrode external surface and the nozzle wall. These two experimental conditions were aimed at obtaining a suitable focus both on the emissive surface of the electrode and on the region between electrode and nozzle. This solution has proved to be particularly suitable for studying phenomena that take place during the pilot arcing shutdown transient; in particular, images obtained during this experiments show both the detachment from the hafnium molten pool of molten hafnium particles and their trajectories. Figure 34b shows the arc current waveform corresponding to images of figure 34a. The time correlation between HS images and current waveform shows that the detachment of molten hafnium particles from the emissive surface begins when the arc current drops to zero (as already described in [17] for arc shut-down) with current going from 25A to 0A in less than 0.1ms; on the contrary, in real cutting conditions, current goes from the operating level to zero through a slope-down whose length is dependent on the type of operating conditions set for the cutting process. Even if the experimental observation reported in [17] refers to a real cutting process and it is accomplished by means of viewing ports on the nozzle in order to see cathode surface during arc operation, results showed an hafnium ejection very similar to the one of figure 34a, with a considerable amount of large particles leaving the emissive surface in the case of a very fast rump-down of the arc current. Moreover, the HS images of figure 34a show that centrifugal forces due to the plasma gas swirling motion play a leading role both in the stability of the hafnium molten pool on the emissive surface during the final transient of the arc current and in determining the trajectories of molten hafnium particles ejected from the emissive surface.

The electrode used in the experiment reported in figure 34a was not a new one in order to avoid the effects of first ignition erosion phenomena that, especially at high current levels, are stronger than erosion mechanisms taking place during the rest of the electrode service life. On the contrary, the nozzle used in this experiment was at its first cutting cycle, in order to have the possibility of analyzing only hafnium collected on the internal surfaces of the nozzle.

Referring to the test reported in figure 34a, a morphological analysis shows that both the solidification morphology of the emissive surface (figure 35) and the deposition morphology of the particles collected on the nozzle internal surface (figure 36) maintain the directionality of molten hafnium centrifugal motion. Moreover, EDS analysis on the electrode used in the test reported in figure 34a, confirms the presence of hafnium oxide on the electrode emissive surface. Also, a morphological analysis of the hafnium pellet cross-section of the electrode, performed through optical microscope and through SEM in back-scattered electron (BSE) imaging, shows the presence of three different regions:

- one region of pure hafnium;
- one region of re-melted hafnium, rich in oxygen in solid solution;
- one region of hafnium dioxide ( $\text{HfO}_2$ ).

It must be remarked that being not new the electrode used in the experiment reported in figure 34a shows a morphological structure of its cross section which is strongly affected by the operating conditions in which it has previously worked. These results are not presented here with pictures.

### **3.2.7 Images of non-destructive double arcing during the transferring phase**

Figures 37, 38 and 39 show images of a realistic phase of arc transferring during the piercing of a MS plate 20 mm thick at 200 A and O<sub>2</sub>/Air as plasma/secondary gas, respectively. Gas flow rates and torch stand-off have been set to increase the probability of double arcing taking place during piercing. The sequence of images shows different phenomena that can be associated to the double arcing. The arc, which normally connects cathode and workpiece, is then split in two parts: one connecting the electrode and the nozzle and the other connecting the nozzle and workpiece. In particular green vapours and silver grey vapours appearing in some of the image frames can be correlated to copper (nozzle orifice) and hafnium (electrode) vapour emissions, respectively. The emission of copper vapours can be related to the consequences of arc attachment on the nozzle and on the shield, explaining also the presence of erosion marks on both of them after such a non-destructive double arcing, lasting only few milliseconds. The evidence of hafnium vapours exiting the nozzle could be related to a greater erosion of the hafnium insert in case of double arcing due to arc root attachment instability on the electrode emissive surface. The hypothesis of arc root attachment instability is also supported by the evidence in some of the frames of figures 38 and 39 of traces of solid particles (probably hafnium oxide) exiting the nozzle. Some other image frames show the presence of an arc attachment on the nozzle, the arc having disappeared from its usual position along the torch axis. All phenomena observed can explain the dreadful consequences of double arcing on consumables and torch safeness, under particular operating conditions [1]. Images captured by the HSC have been time-correlated to the oscilloscope waveform of arc voltage drop between the electrode and the nozzle, as shown in Figure 40. This correlation shows that HS images associated to the time interval where double arcing phenomena take place correspond to the presence of uninterrupted spikes in the oscilloscope waveform of arc voltage. This correspondence leads to a hypothesis of correlation between arc instability and arc voltage oscillations. According to this hypothesis the arc voltage between electrode and nozzle can be assumed as an indicator of arc stability.

In particular, the time interval between 250 ms and 300 ms, during which the waveform of arc voltage shows different types of oscillations, can be divided into three consecutive parts, each with different typical phenomena. In the first time interval (from 272 ms to 273,9 ms) the waveform of electrode-nozzle voltage shows two peaks, corresponding to images with continuous emissions of grey blue vapours associated to hafnium vapour emissions, as shown in figure 40. In the second time interval (from 274.1 ms to 276 ms), the oscilloscope waveform of electrode-nozzle voltage shows continuous spikes, corresponding to images in which the arc disappears from the nozzle exit region, as shown in figure 41. Moreover, a transient time zone can be evidenced before the continuous spikes one (from 274.1 ms to 274.7 ms), during which HS images show hafnium vapours emissions with arc instabilities and pronounced emission of solid particles. In the third time interval (from 276.1 ms to 278 ms), the oscilloscope waveform of electrode-nozzle voltage shows

the transient phase from the continuous spike tract to the subsequent stable phase, during which, as shown in the HSC images of figure 39, the arc gradually returns to be stable.

This detailed analysis of the correspondence between instabilities of the electrode-nozzle voltage and plasma behaviour, leads to a hypothesis of correlation between arc voltage isolated peaks and hafnium vapours emission and between arc voltage continuous spikes and arc attachment on the nozzle and the shield, respectively.

Non-destructive double arcing phenomena during piercing probably occur as a consequence of the deposition of a small amount of hafnium oxide on the nozzle orifice wall, inducing a local increase of the radial electric field and an increase in the probability of double arcing. When double arcing occurs, rapid [ $<1$  ms] evaporation of the hafnium oxide with vapour emission from the nozzle restores the previous and normal arc behaviour. Due to their very short duration the described phenomena can assume a non-destructive character.

### **3.2.8 Tracking of ejected particles from the nozzle orifice**

Figure 41 shows two consecutive pilot arc images in which the presence of a flying solid particle is clearly visible in two different positions; probably, a hafnium oxide particle ejected from the electrode emissive insert [17]. In fact, during the arc starting transient, particles of the hafnium oxide layer that covers the cold re-solidified hafnium emitter can be removed on the track of the arc attachment that first moves from the periphery of the insert to its centre [1] and then expands on the emitter surface during the gradual increase of the arc current. The observed particle emission takes place 5.7 ms after the arc ignition; the time-correlation of the image with the oscilloscope waveform shows that in that instant the current has finished its initial transient phase and it is reaching, through a slope-up, its stationary value of about 45 A.

An estimate of the solid particle velocity is possible comparing two consecutive frames. The calculation can be done with two different methods, leading to comparable results. With the first method the length of the particle trail (constant in the two frames) must be multiplied by the reciprocal of the shutter time set for image acquisition; while, with the second method the distance between the two particle trails in the consecutive frames must be multiplied by the number of frames per second set for image acquisition. Both methods give a resulting particle velocity of about 720 m/s.

Figure 42 also shows a sequence of images taken during pilot arcing; in this case, the torch head is characterized by the presence of a torch shield cup and of a secondary gas flow. In this sequence of images characterized by real pilot arcing duration (less than 1 ms), the typical arc loop attachment, with a “double discharge” appearance, can be seen. Moreover, the image for  $t=0.6$  ms shows a solid particle ejected from the nozzle orifice, once again probably coming from cracking of the solid layer of  $\text{HfO}_2$  on the emitter during pilot arcing [1] and on a shorter time-scale than the one typical for the ejection of liquid metal droplets during transients [17]. The calculated particle velocity is about 1350 m/s.

### 3.2.9 Piercing phase

In a plasma arc torch consumable head components (namely, electrode, nozzle, secondary swirl ring, retaining cap and shield) systematically deteriorate over time. The alignment of these components within the torch is critical to ensure stability and axial symmetry of plasma arc jet and consequently a reasonable consumable life and a suitably satisfying cut quality. In piercing of plates thicker than 20 mm, with current level higher than 120 A, the alignment of torch consumables plays an important role in attaining a suitable protection of shield and nozzle from the negative effects of splattered molten metal ejected from the deepest regions of the initiated hole. Figure 43 shows the piercing phase of a 15 mm thick SS slab, when a high level of alignment (in the order of magnitude of 0.025 mm of maximum relative non-alignment between shield and electrode, for example) for the torch head components is attained. Even though at  $t=400$  ms the piercing phase is concluded, in figure 43 frames are reported up to 1200 ms in order to show the multiple arc root attachments on vaporized conductive metal from dross formation in the range 400-600 ms [21]. Figure 44 shows some images of a piercing (initiated at  $t=0$  but reported only from  $t=146.8$  ms) of a MS slab 40 mm thick when using non-perfectly aligned torch head components; this leads to an off-axis discharge that upon interaction with the workpiece induces the ejection of molten metal sideways and on the shield surface.

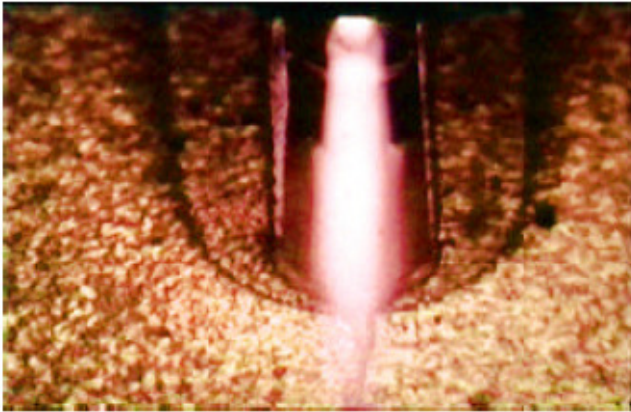


**Figure 1.** Image of a dross-free plasma cut, viewed from below, trailing the torch. (Taken from [9]).

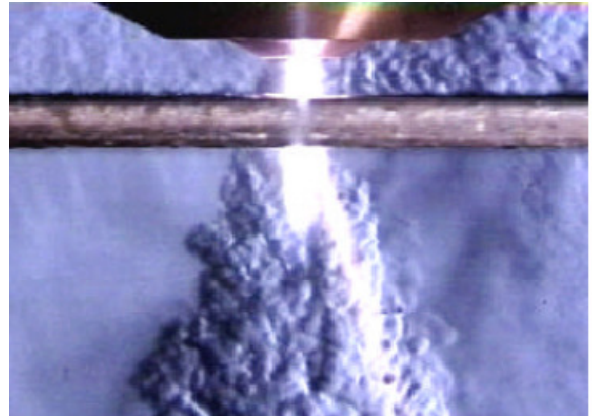


**Figure 4.** Schlieren image of dross-free plasma cutting. (Taken from [9]).

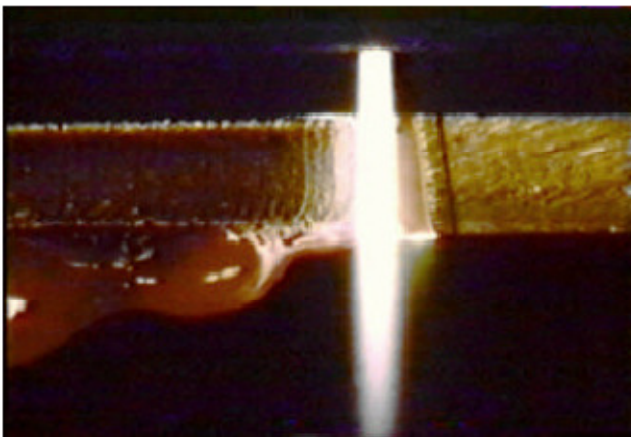


**Figure 2.** Image of an "edge cut" with low-speed dross formation. (Taken from [9]).

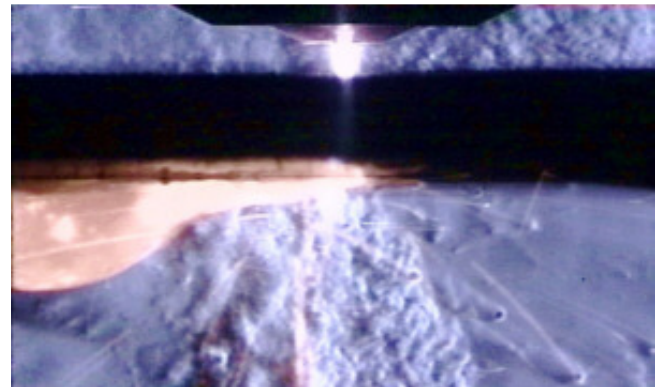


**Figure 5.** Schlieren image of plasma cutting with low-speed dross. (Taken from [9]).



**Figure 3.** Ultraviolet image of an "edge cut". (Taken from [9-10]).

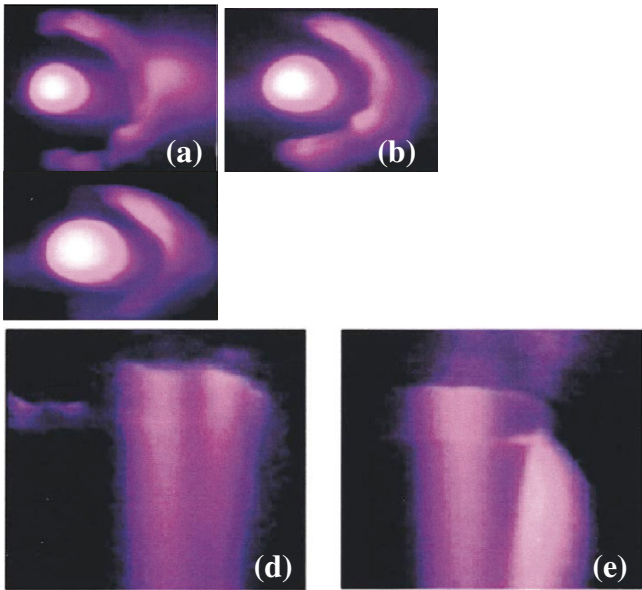


**Figure 6.** Ultraviolet images of the plasma-arc cutting process: (a) low-speed on-axis view (anode outside *kerf*), (b) on-axis view at normal cutting speed (anode inside *kerf*); (c) high-speed on-axis view (anode inside *kerf*); (d) under-plate oblique view (anode inside *kerf*), and (e) under-plate oblique view (anode outside *kerf*). (Taken from [10]).

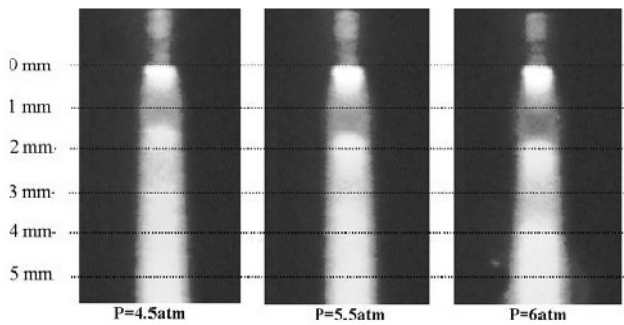


**Figure 7.** Photographs of the plasma jet for different plasma inlet pressures. (Taken from [12-13]).

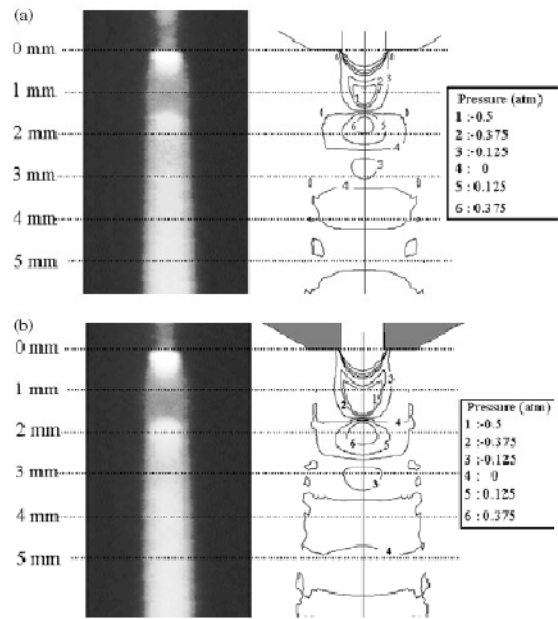


**Figure 8.** Comparison between photograph of the plasma jet and pressure field obtained from the model at an inlet pressure of (a) 4.5 atm and (b) 5.5 atm. (Taken from [12-13]).

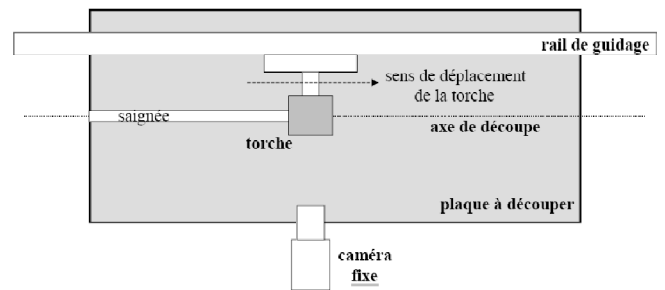


**Figure 9.** Experimental set-up with the camera fixed and perpendicular to the torch trajectory, aimed to visualize the shock waves. (Taken from [14-15]).

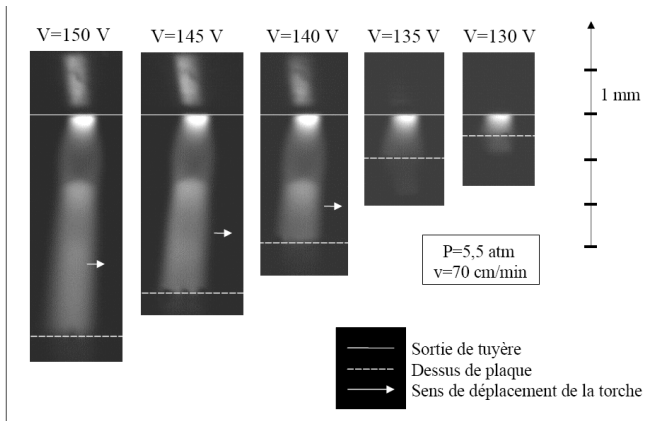


**Figure 10.** Shock wave geometry for different arc voltage values. (Taken from [15]).

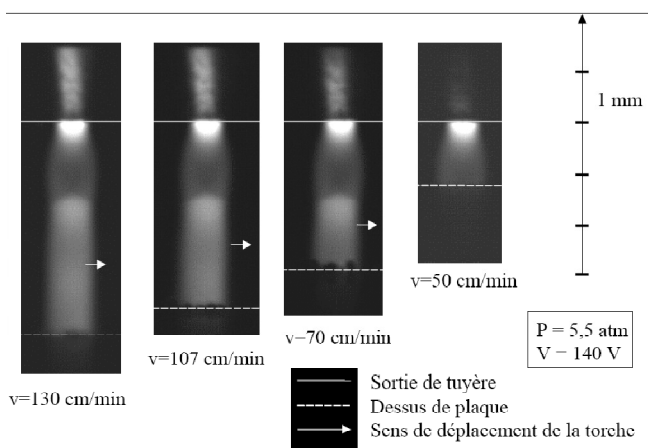


**Figure 11.** Shock wave geometry for different cutting speed values. (Taken from [15]).

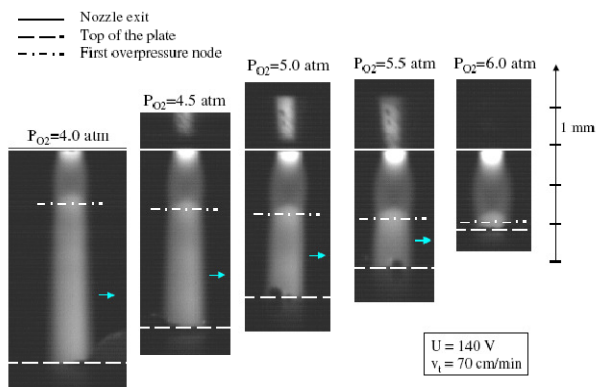


**Figure 12.** Shock wave geometry for different plasma inlet pressure values. (Taken from [14]).

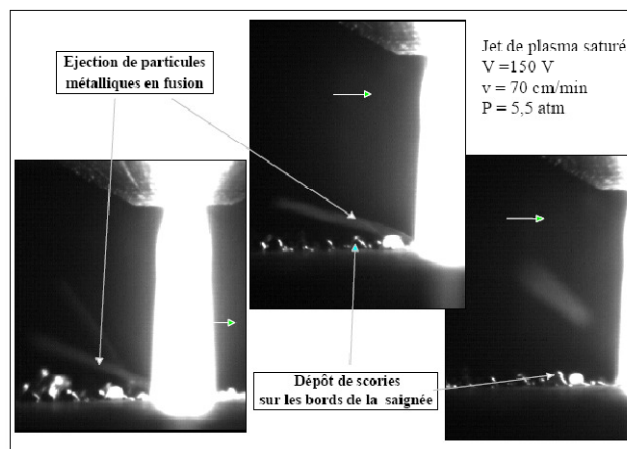
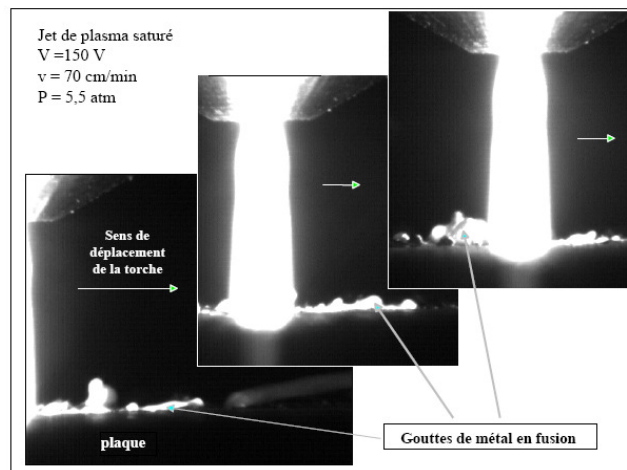


**Figure 13.** Plasma jet and melting metal droplets. (Taken from [15]).

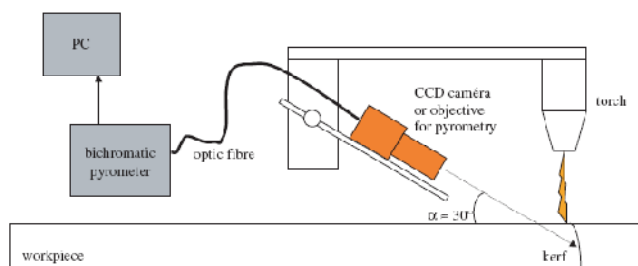


**Figure 14.** Experimental set-up with the camera integral with the torch and oblique positioned, aimed to visualize the anodic arc root attachment. (Taken from [16]).

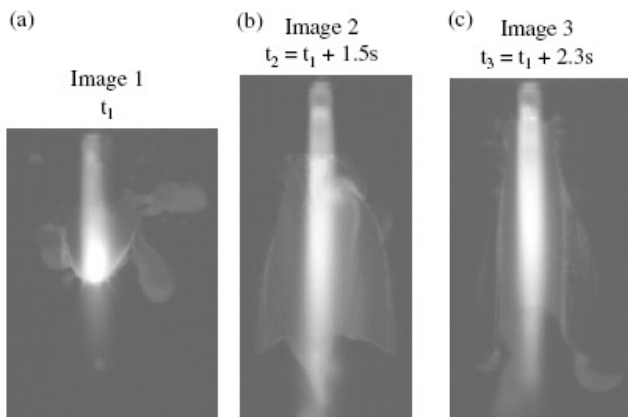


**Figure 15.** Arc images during (a) edge piercing of the plate, (b) completed the edge piercing the torch is still motionless and (c) cutting. (Taken from [16]).

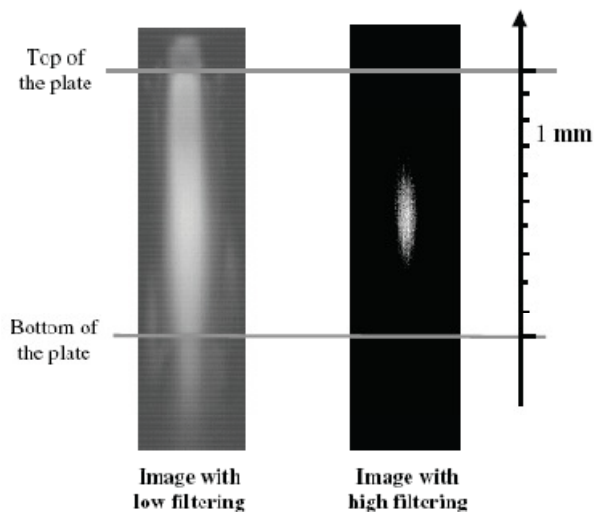


**Figure 16.** Arc root images on the cut front surface with low filtering and with high filtering. (Taken from [15-16]).

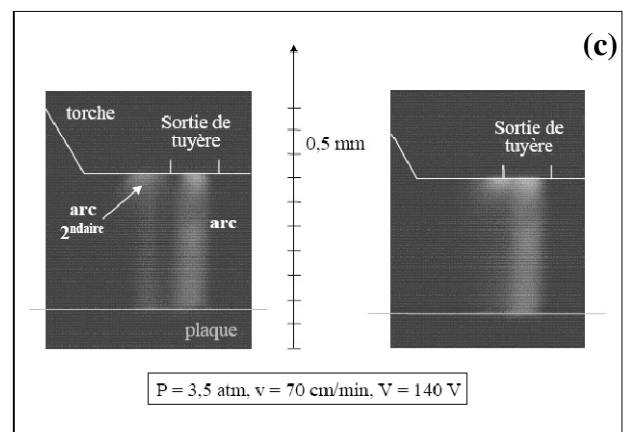
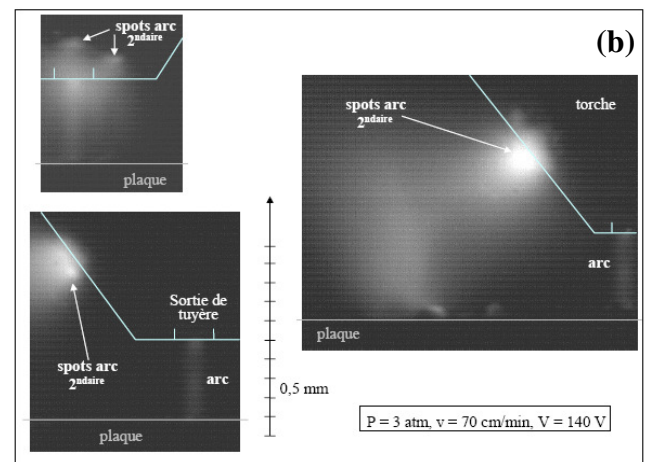
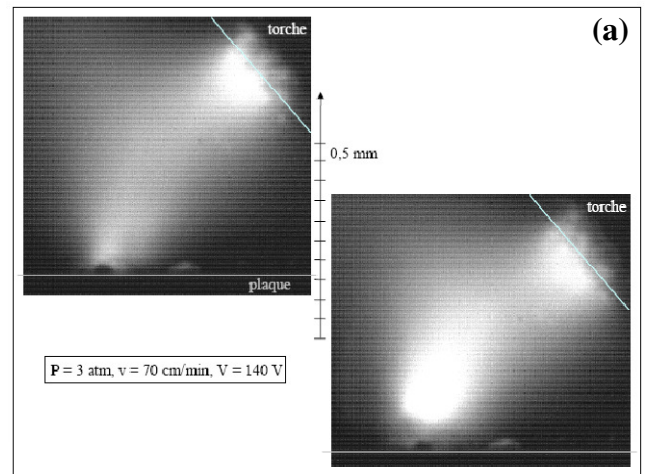


**Figure 17.** Images of secondary arcs with a plasma inlet pressure of (a-b) 3 atm and (c) 3.5 atm. (Taken from [15]).

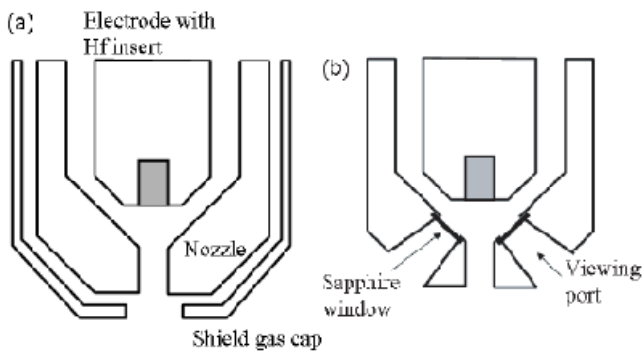


**Figure 18.** Standard nozzle (a) and nozzle modified for cathode visualization (b). (Taken from [17]).

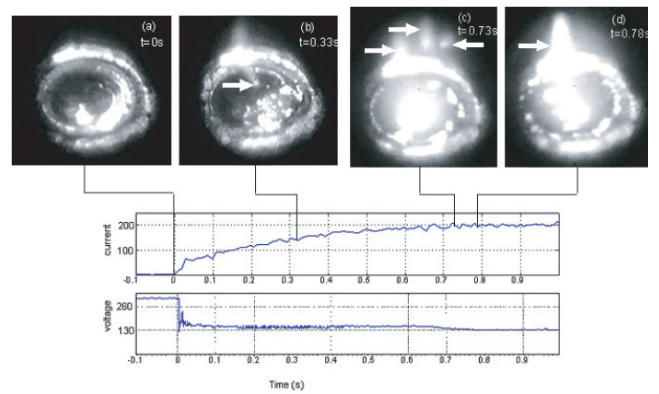


**Figure 21.** Current and voltage traces during start-up correlated with the first and third ejection events. (Taken from [17]).

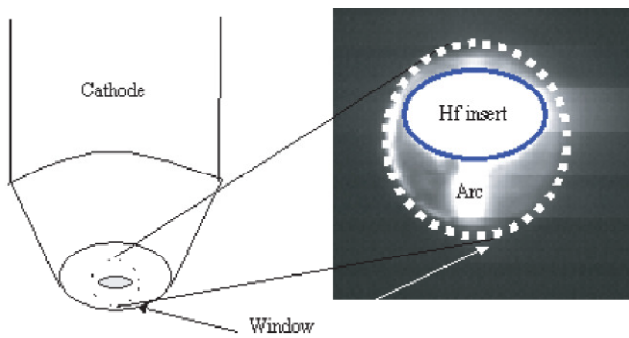


**Figure 19.** Cathode viewing angle and sample image with elliptical Hf insert. (Taken from [17]).

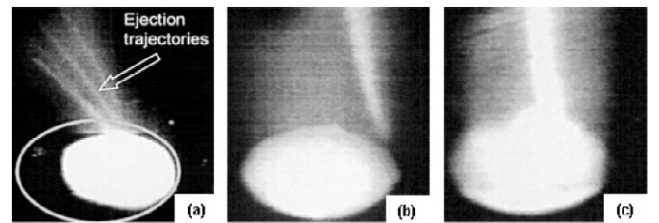


**Figure 22.** Start-up droplet ejection events, first ejection (a), second ejection (b) and third ejection (c). (Taken from [17]).

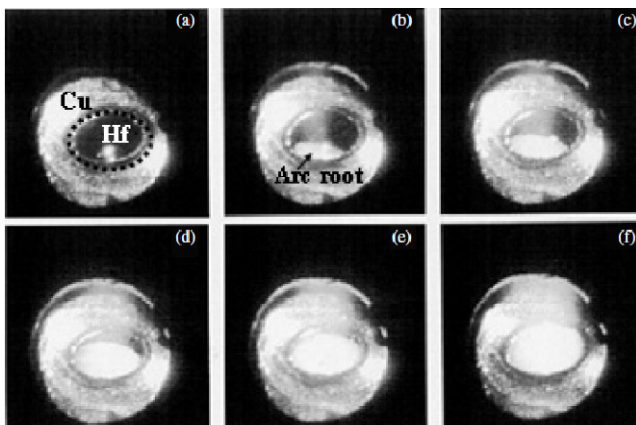


**Figure 20.** Arc root expansion on the hafnium surface. (Taken from [17]).

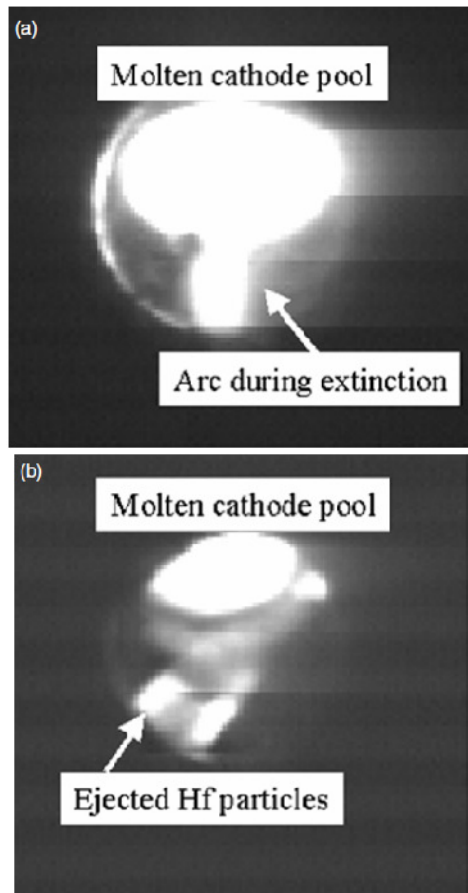


**Figure 23.** Cathode behaviour during shutdown with fast current ramp-down; (a) is just before arc extinction and (b) shows ejected particles shortly after extinction. (Taken from [17]).

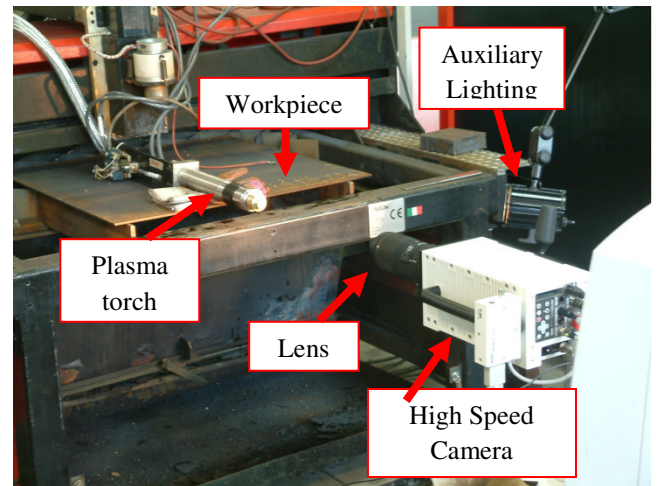


**Figure 24.** Picture of the experimental setup for high speed imaging of pilot arcing. In these experiments the axis of the lens is perfectly aligned with the axis of the torch, in order to observe the arc inside the nozzle.

Taken from [25].

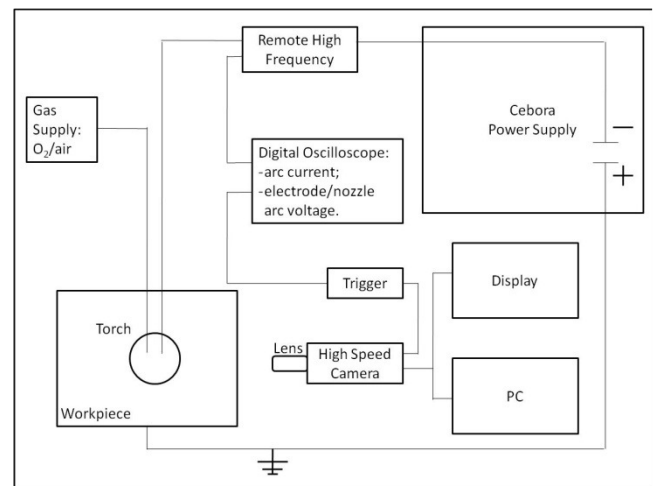


**Figure 25.** Schematic of the experimental setup for high speed imaging. Taken from [25].

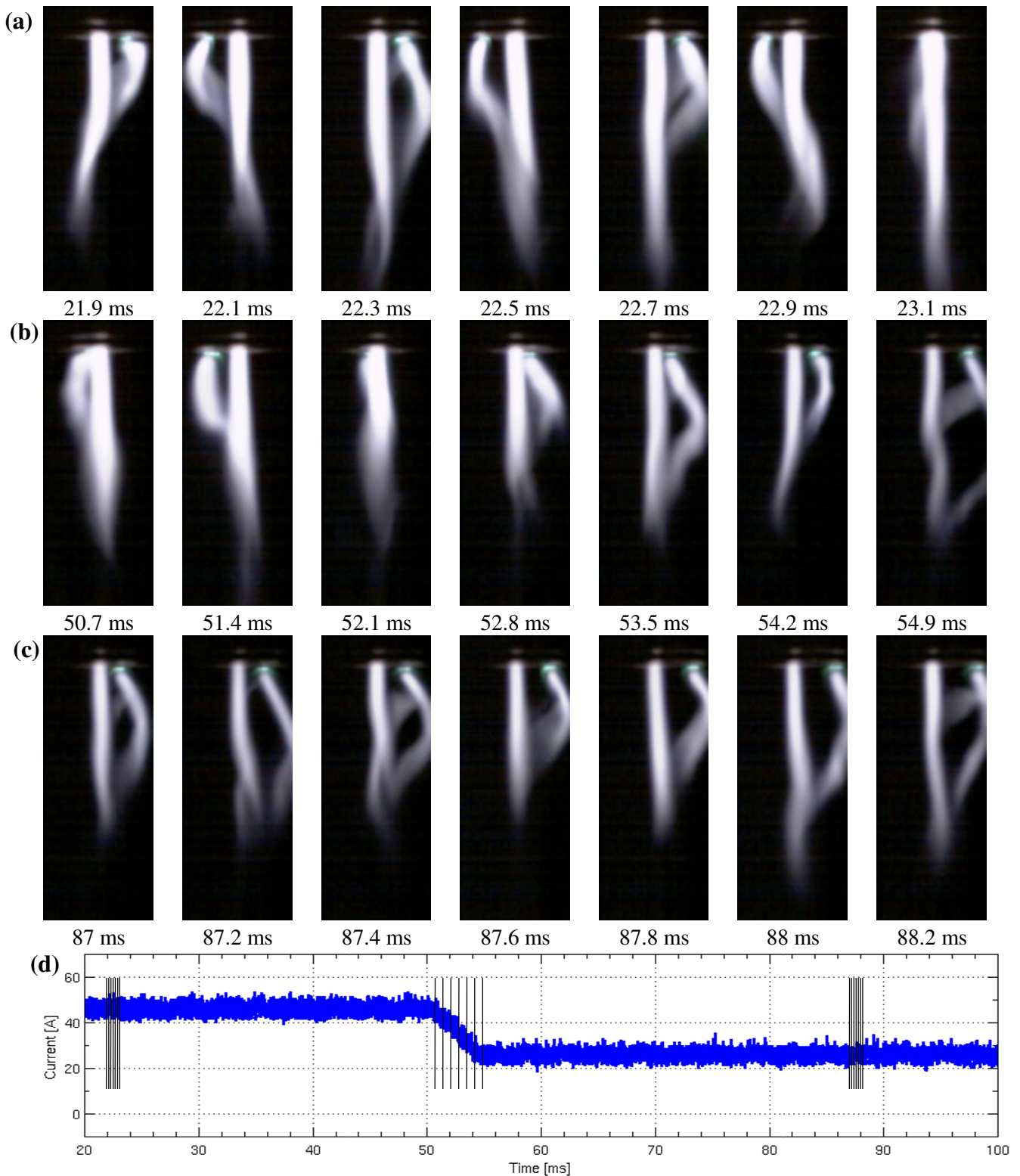


**Figure 26.** Pilot arc images for a torch with 1.9 mm nozzle diameter (pilot arc plasma gas: air), (a) at 45A and at constant time intervals of 0.2 ms, (b) during current slope from 45A to 25A and at constant time intervals of 0.7 ms, (c) at 25A and at constant time intervals of 0.2 ms. Images acquired at 10000 fps and 1/200000 s shutter time without any filtering. (d) Images are time-correlated to the oscilloscope waveform of arc current; every vertical line on the arc current graph shows the time-correlation between images and waveform. Taken from [25].

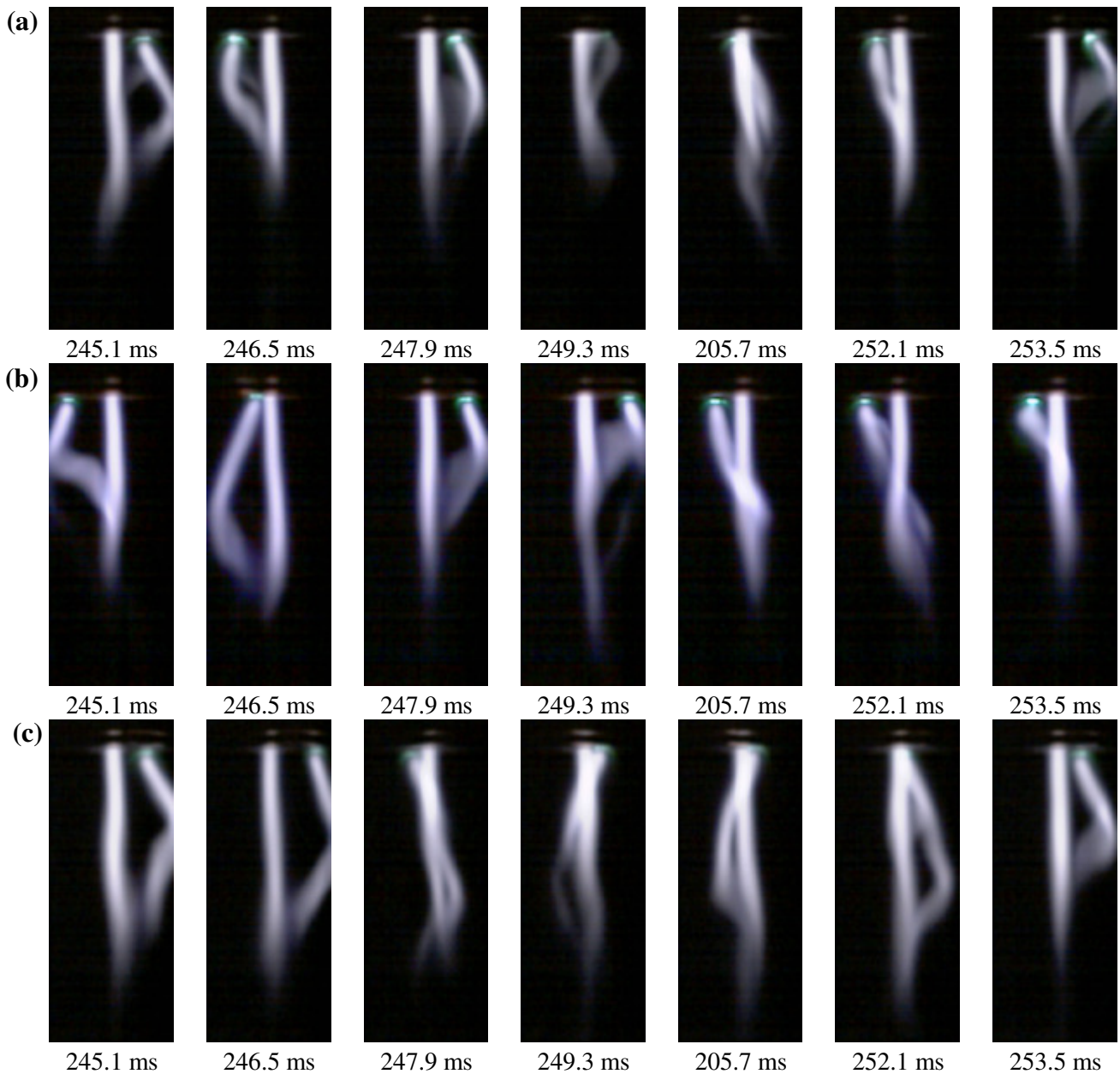


**Figure 27.** Pilot arc images at constant time intervals of 1.4 ms for a torch with 1.9 mm nozzle diameter at 25 A with plasma gas flow rate (pilot arc plasma gas: air) of about: (a) 21 slpm, (b) 28 slpm, (c) 36 slpm.

Images acquired at 10000 fps and 1/200000 s shutter time without any filtering. Taken from [25].

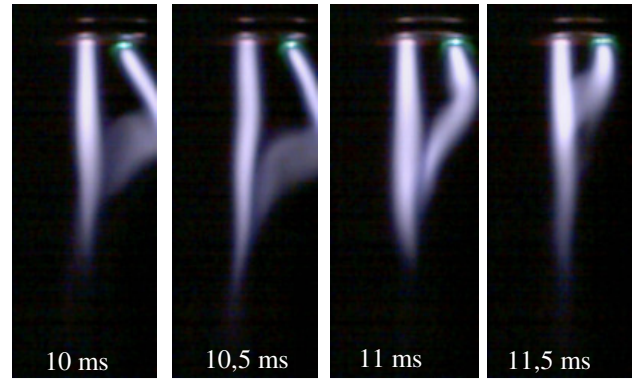
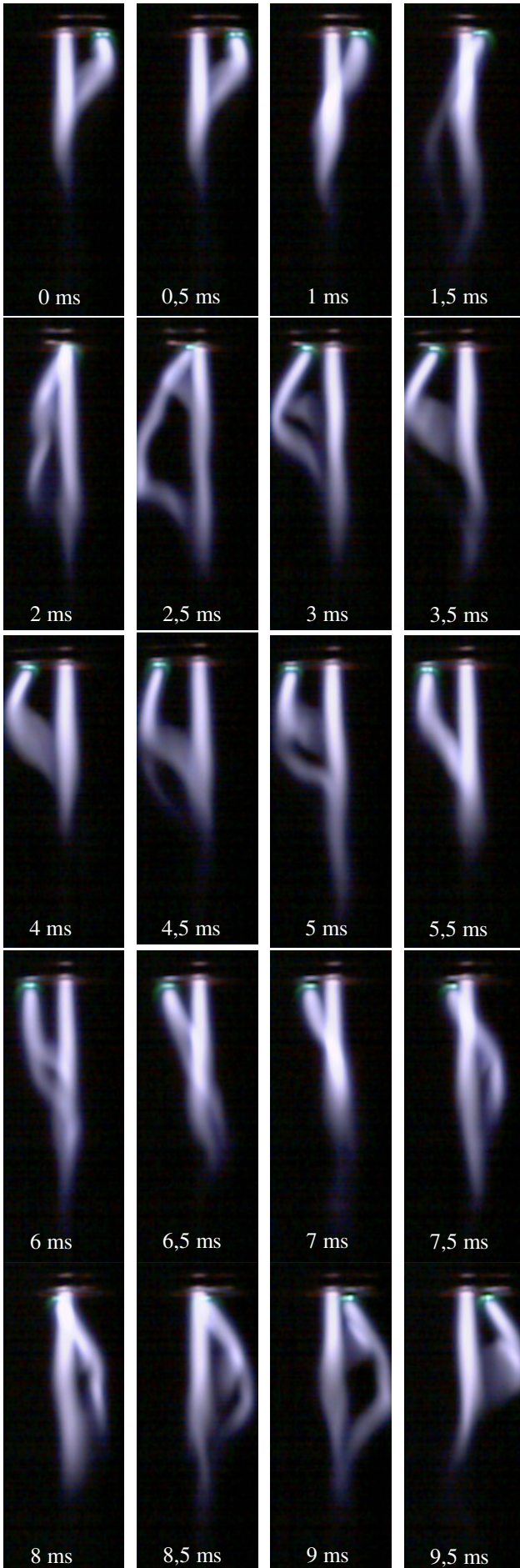


**Figure 28.** Pilot arc images at constant time intervals of 0.5 ms for a torch with 1.9 mm nozzle diameter, at 25A (pilot arc plasma gas: air). Images acquired at 10.000 fps and 1/200000 s shutter time without any filtering. The image at  $t=0$  ms describes pilot arcing 166.6 ms after ignition. Taken from [25].

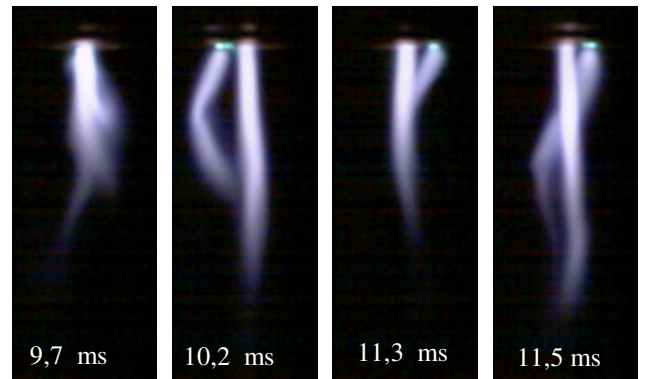
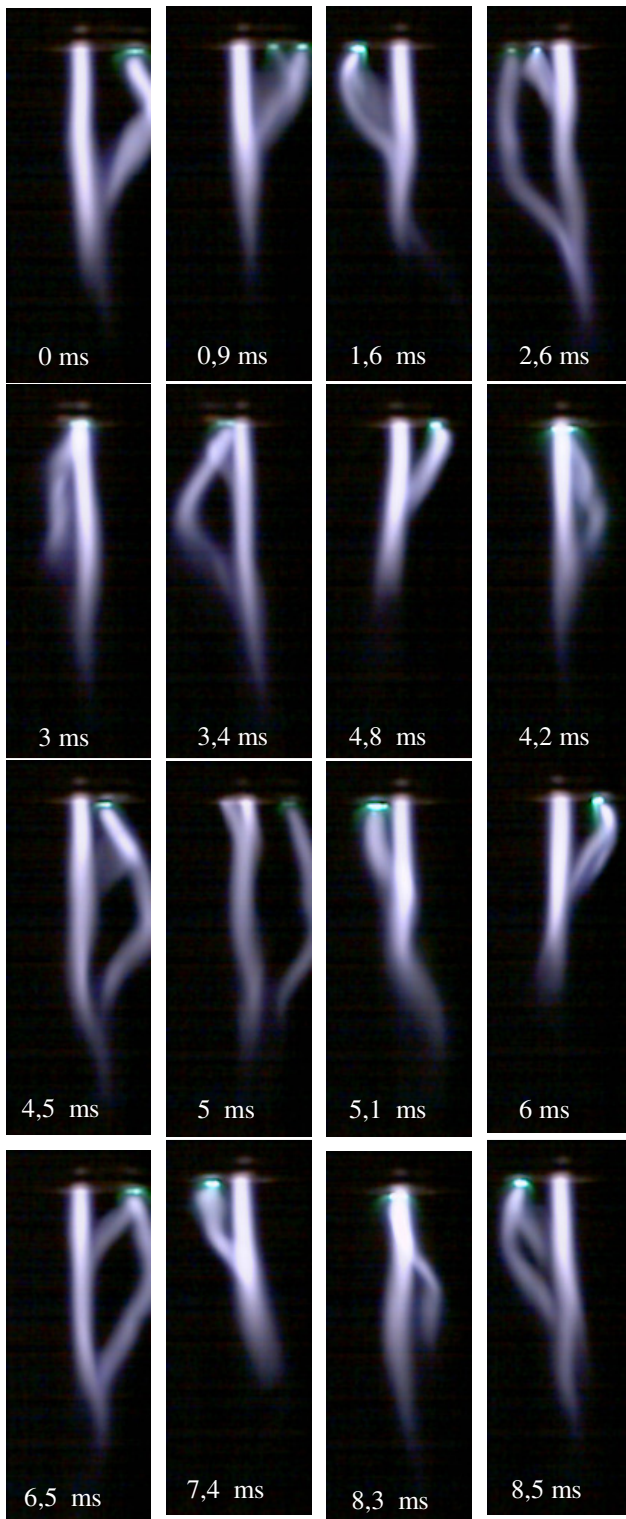


**Figure 29.** Pilot arc images at different time intervals for a torch with 1.9 mm nozzle diameter, at 25A (pilot arc plasma gas: air). Images acquired at 10000 fps and 1/200000 s shutter time without any filtering. The image at t=0 ms describes pilot arcing 243 ms after ignition. Taken from [25].

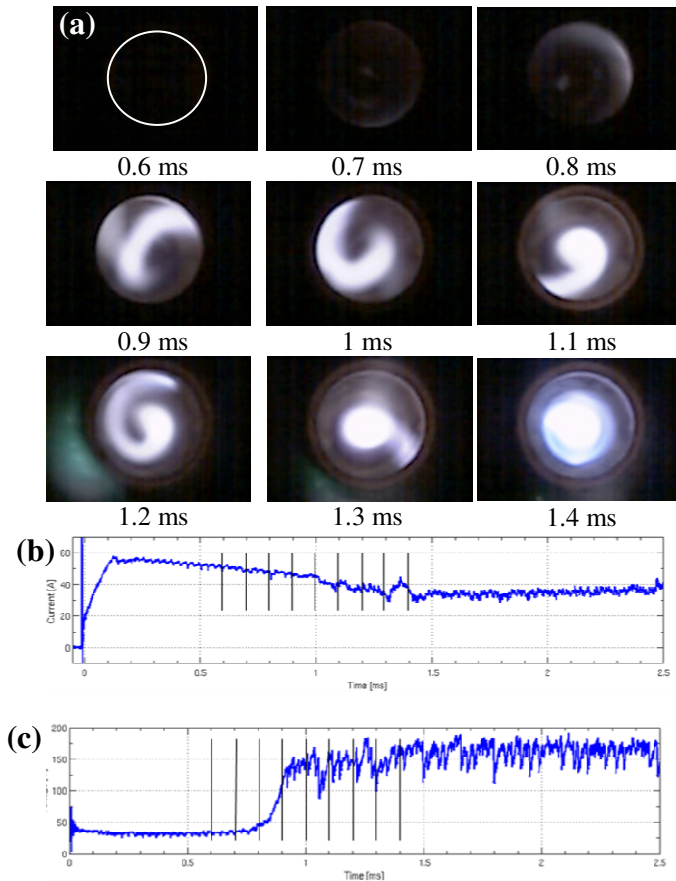


**Figure 30.** (a) Sequence of pilot arc images for a torch with 1.9 mm nozzle diameter, during an arc current transient subsequent to arc ignition (pilot arc plasma gas: air). The axis of the torch is coincident with the axis of the camera lens. Images are acquired at 10000 fps and 1/200000 s shutter, time without any filtering. Images are time-correlated to the oscilloscope waveform (b) of arc current and (c) arc voltage between electrode and nozzle. Every vertical line on the arc current graph shows the time-correlation between images and waveform. In the first image frame the position of the shield hole is shown.

Taken from [25].

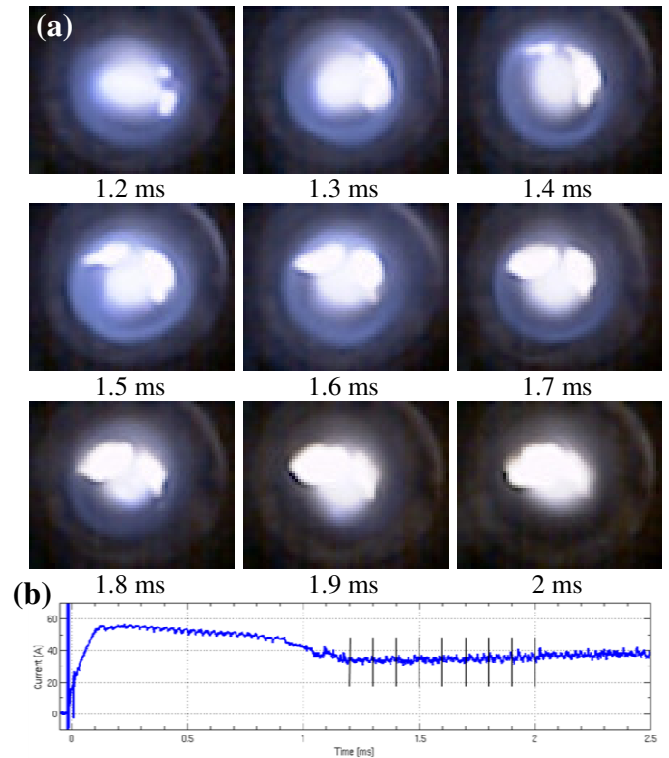


**Figure 31.** (a) Sequence of pilot arc images for a torch with 1.9 mm nozzle diameter (pilot arc plasma gas: air). The axis of the torch is coincident with the axis of the camera lens. Images are acquired at 10000 fps and 1/200000 s shutter, time without any filtering. (b) Images are time-correlated to the oscilloscope waveform of arc current. Every vertical line on the arc current graph shows the time-correlation between images and waveform. Taken from [25].

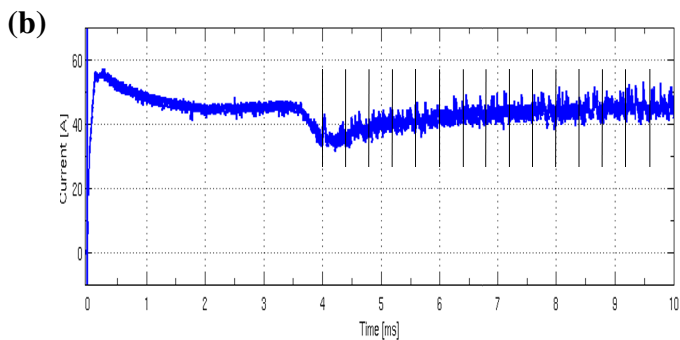
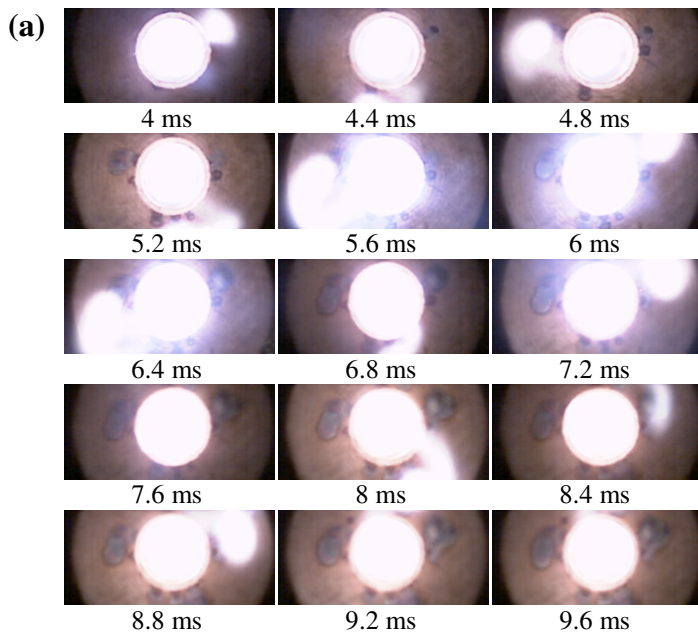


**Figure 32.** (a) Pilot arc images at constant time intervals for a torch with 1.9 mm nozzle diameter, at about 45 A (pilot arc plasma gas: air). The axis of the torch is coincident with the axis of the camera lens. Images are acquired at 10000 fps and 1/200000 s shutter, time without any filtering. (b) Images are time-correlated to the oscilloscope waveform of arc current. Every vertical line on the arc current graph shows the time-correlation between images and waveform. Taken from [25].

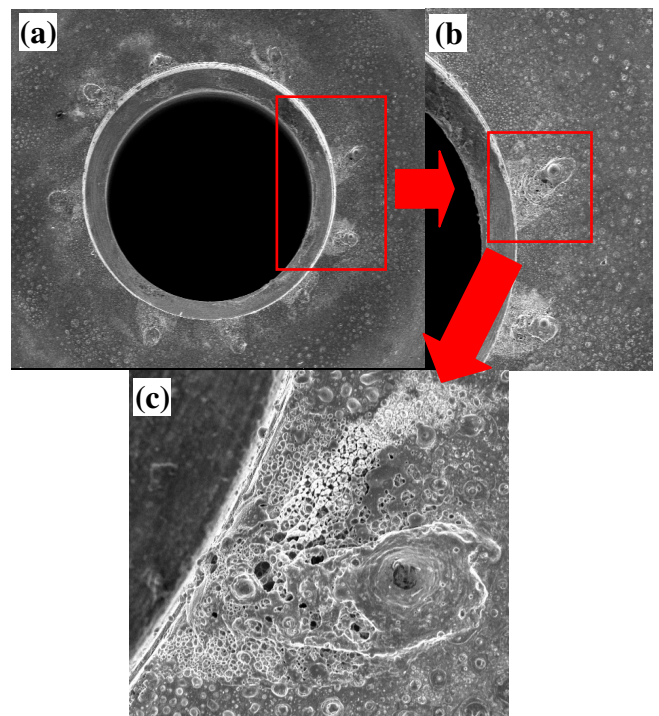


**Figure 33.** SEM images of the nozzle tip, after pilot arcing of figure 32, with gradually increasing magnification level: (a) 50X, (b) 100X and (c) 600X. Taken from [25].

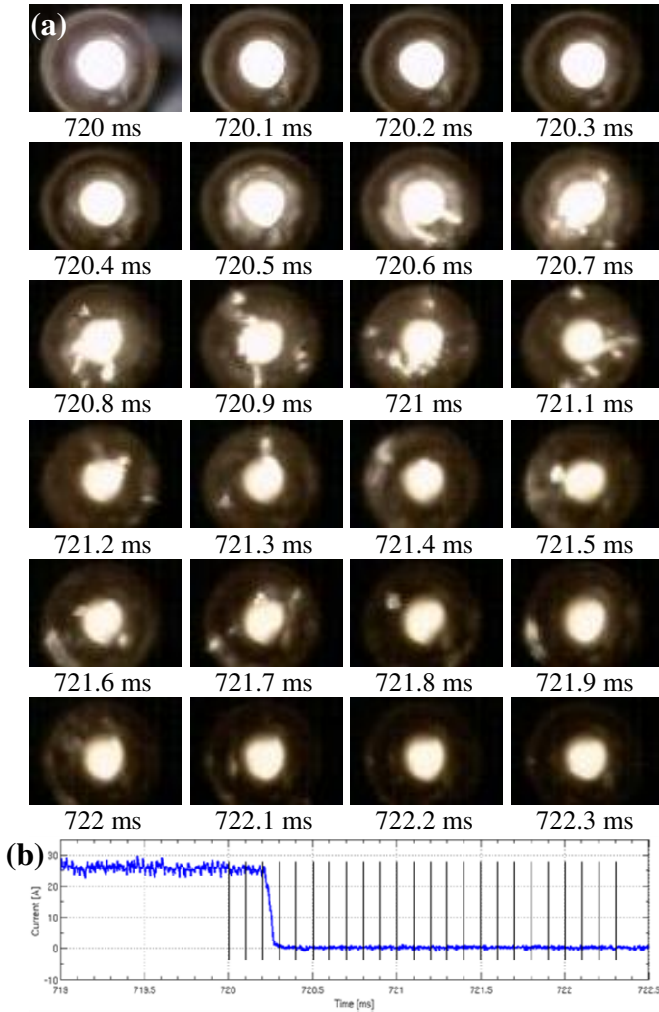


**Figure 34.** (a) Sequence of pilot arc images for a torch with 2.5 mm nozzle diameter, during arc current shutdown from 25A to 0A (pilot arc plasma gas: air). The axis of the torch is coincident with the axis of the camera lens. Images are acquired at 10000 fps and 1/200000 s shutter, time without any filtering. (b) Images are time-correlated to the oscilloscope waveform of arc current. Every vertical line on the arc current graph shows the time-correlation between images and waveform. The electrode used was not at its first ignition. Taken from [25].

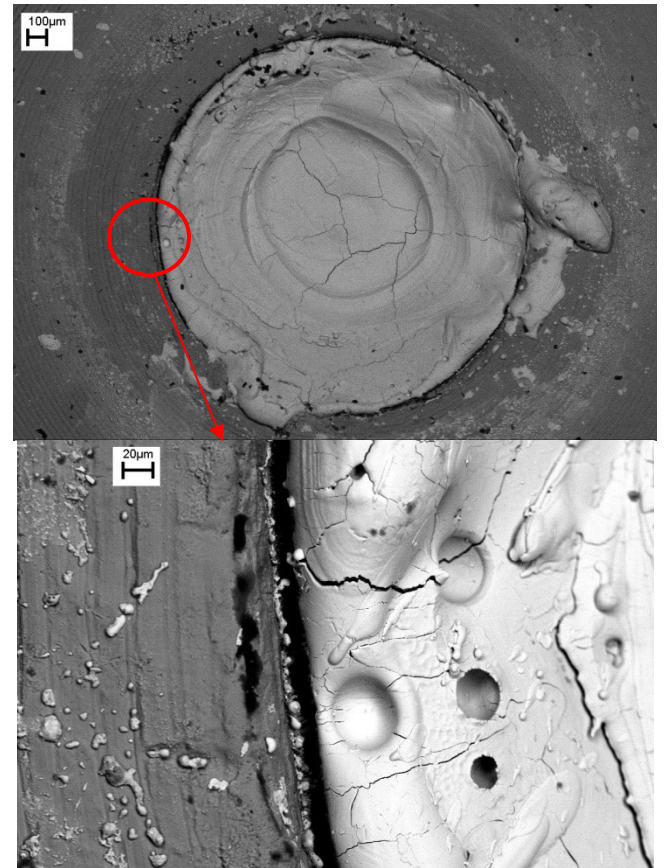


**Figure 35.** SEM image at two different magnification levels of the emitter surface (right) and of the interface between hafnium and copper (left), after pilot arcing of figure 34. Taken from [25].

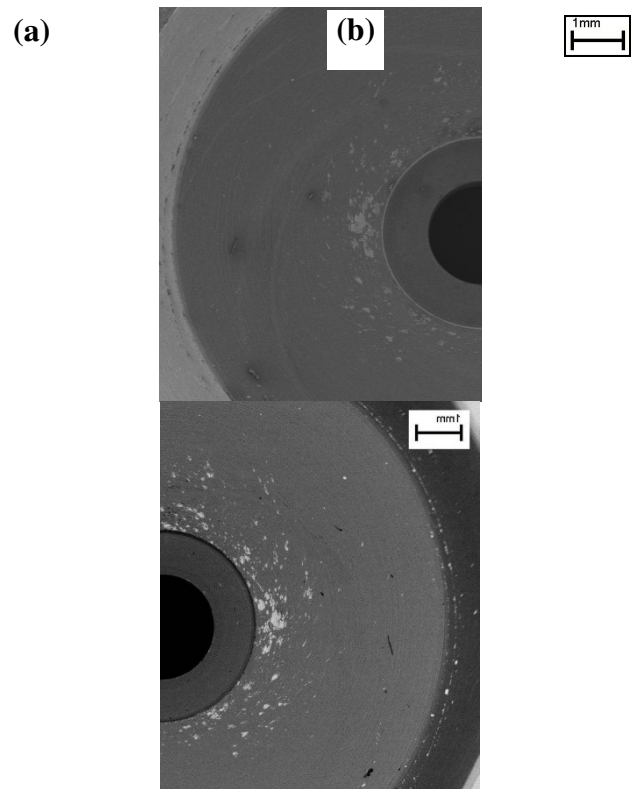


**Figure 36.** SEM of the internal surface of the nozzle with collected erosion particles in (a) secondary electron (SE) imaging and (b) back-scattered electron (BSE) imaging, after pilot arcing of figure 34. Taken from [25].

Taken from [25].

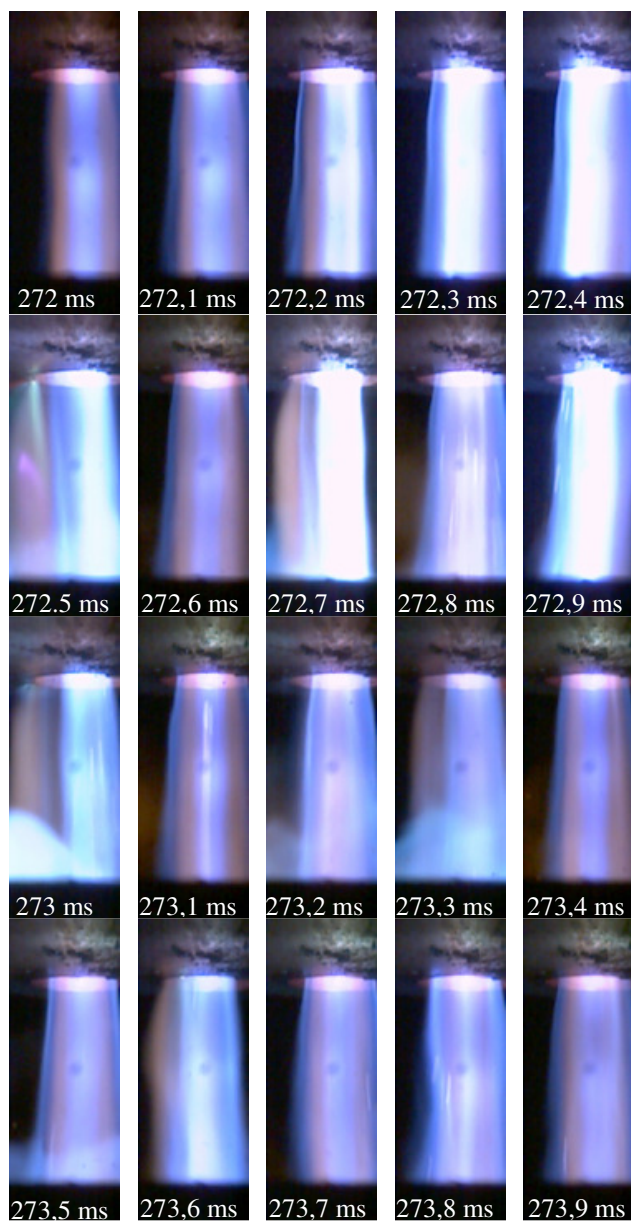


**Figure 37.** Transferring arc images, in the time interval 272-273,9 ms, for a torch with 1.6 mm nozzle diameter and 3 mm shield diameter, at 200 A (plasma/shield gas: O<sub>2</sub>/air). Images acquired at 10000 fps and 1/200000 s shutter time, without any filtering.

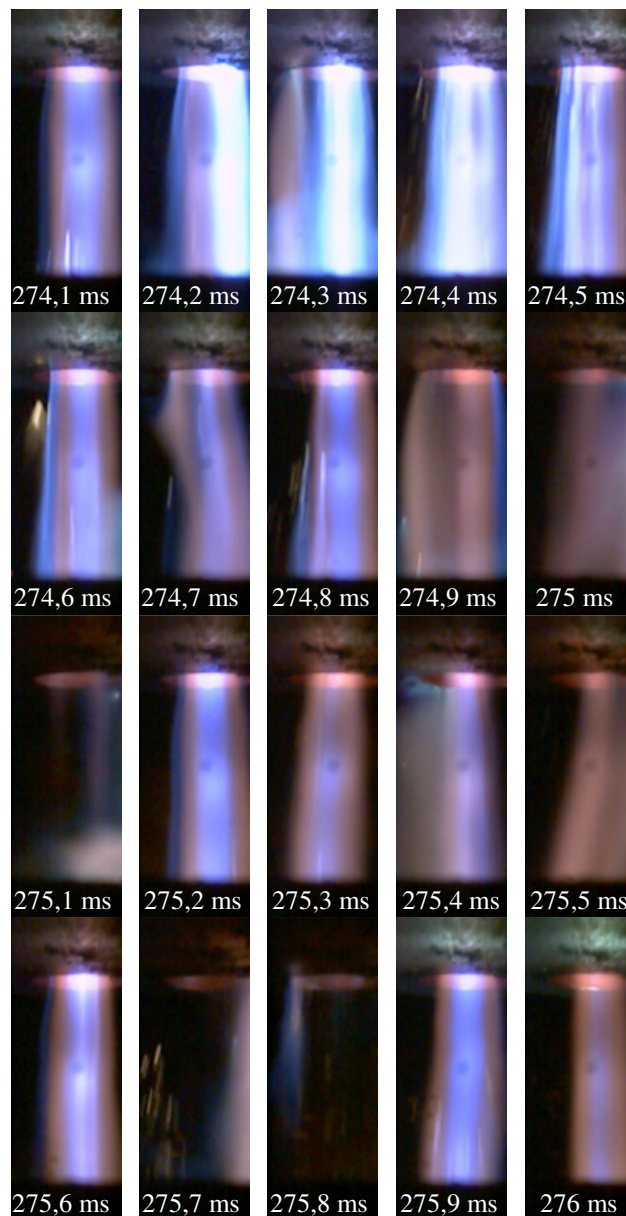


**Figure 38.** Transferring arc images, in the time interval 274.1-276 ms, for a torch with 1.6 mm nozzle diameter and 3 mm shield diameter, at 200 A (plasma/shield gas: O<sub>2</sub>/air). Images acquired at 10000 fps and 1/200000 s shutter time, without any filtering.

Taken from [25].

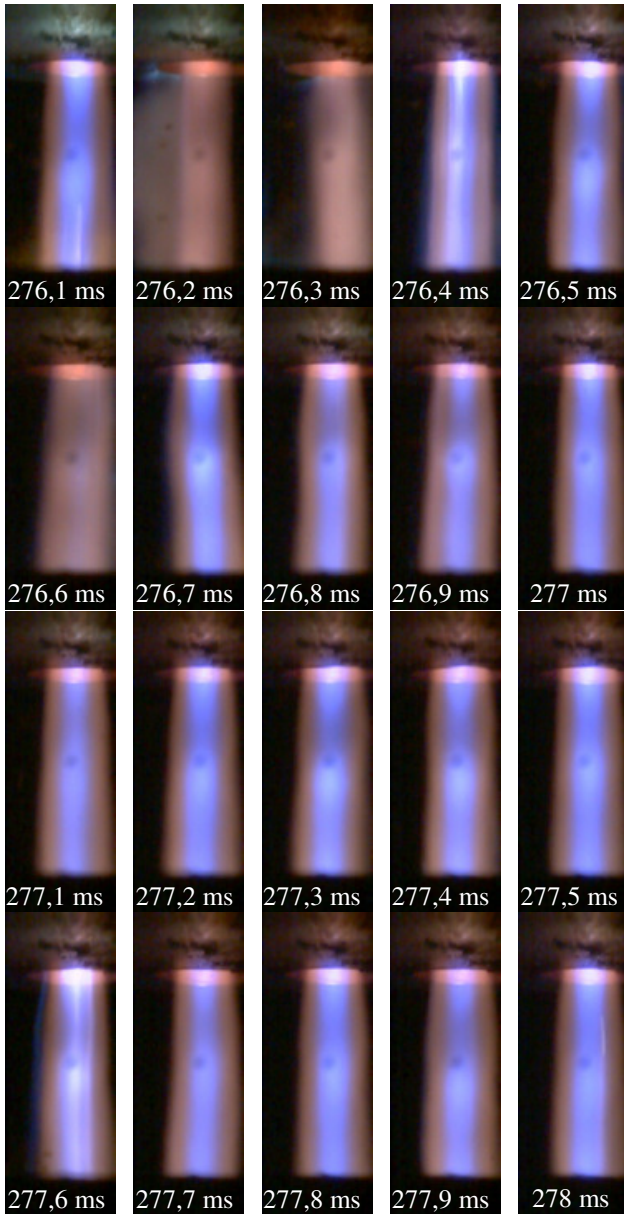


**Figure 39.** Transferring arc images, in the time interval 276.1-278 ms, for a torch with 1.6 mm nozzle diameter and 3 mm shield diameter, at 200 A (plasma/shield gas: O<sub>2</sub>/air). Images acquired at 10000 fps and 1/200000 s shutter time, without any filtering. Taken from [25].

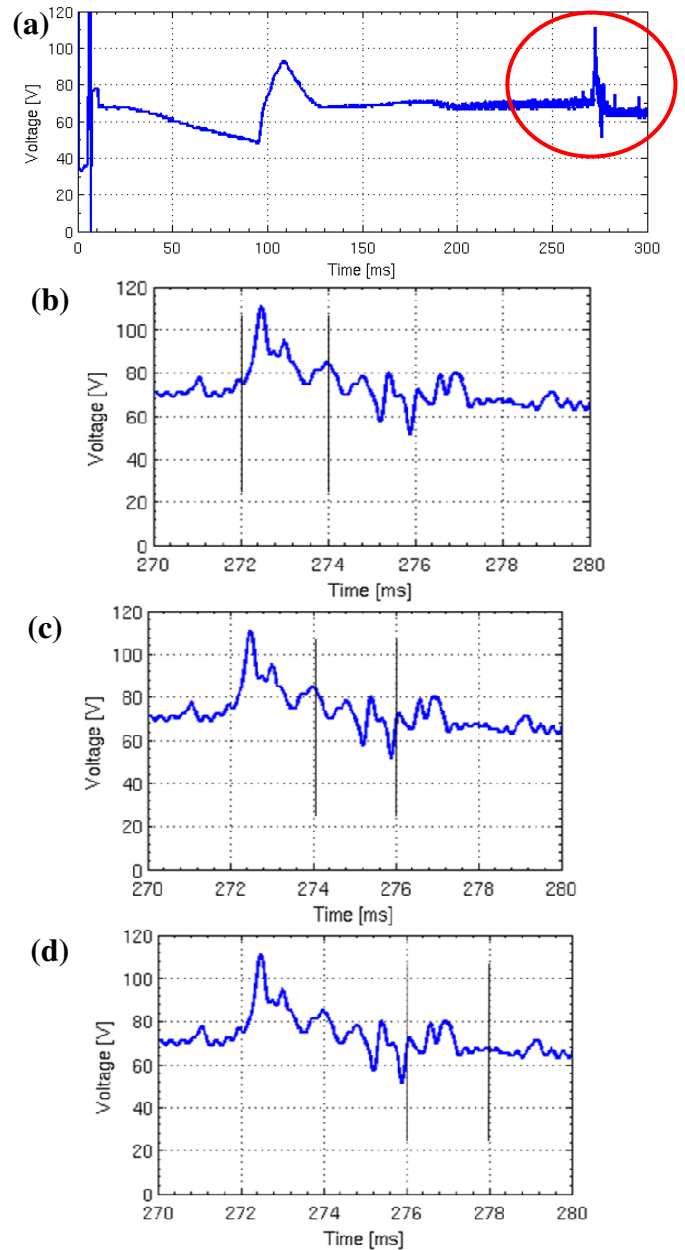


**Figure 40.** (a) Oscilloscope waveform of electrode-nozzle voltage related to the test whose results are reported in figures 40, 41 and 42. (b-d) The vertical lines on the voltage waveforms show the time correlation between the voltage waveform and the images of figures 40, 41 and 42, respectively. Taken from [25].

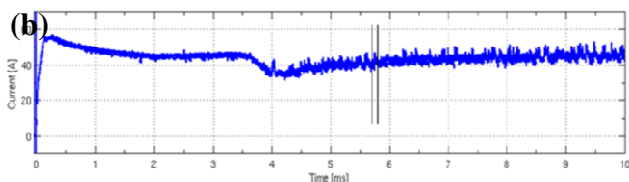
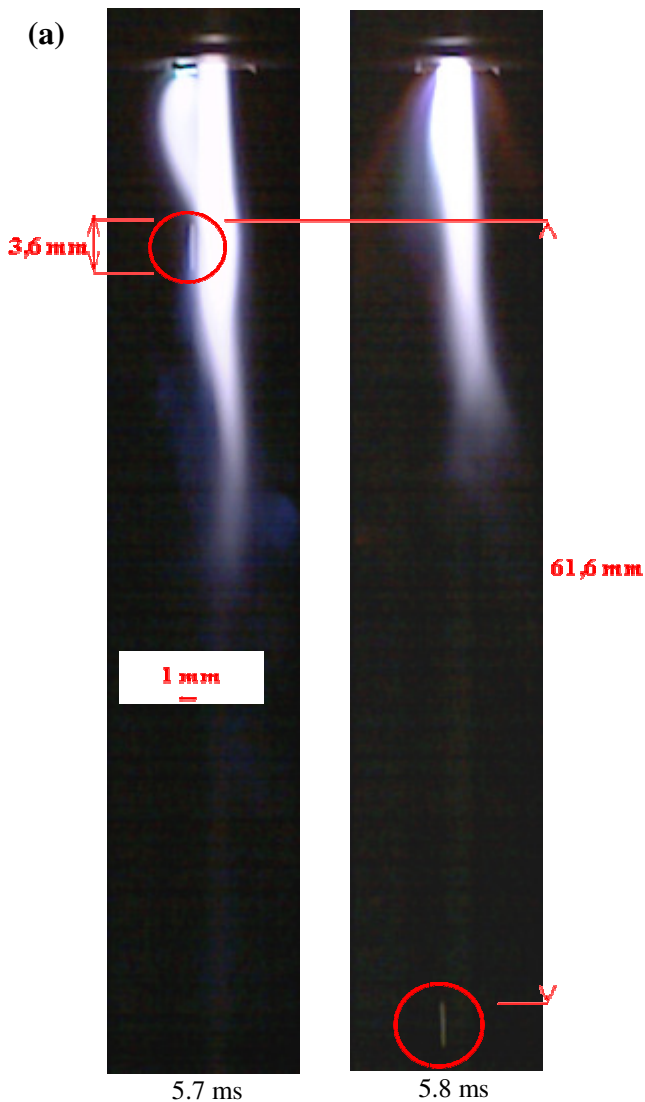


**Figure 41.** (a) Pilot arc images in two consecutive time steps in which a particle (most probably hafnium oxide from the emitter insert), ejected from the nozzle orifice (1.9 mm diameter, 45 A, pilot arc plasma gas: air) at about 720 m/s, is clearly visible in two different positions. Images acquired at 10000 fps and 1/200000 s shutter time, without any filtering. Images are time-correlated to the oscilloscope waveform of arc current. (b) Every vertical line on the arc current graph shows the time-correlation between images and waveform.

Taken from [25].

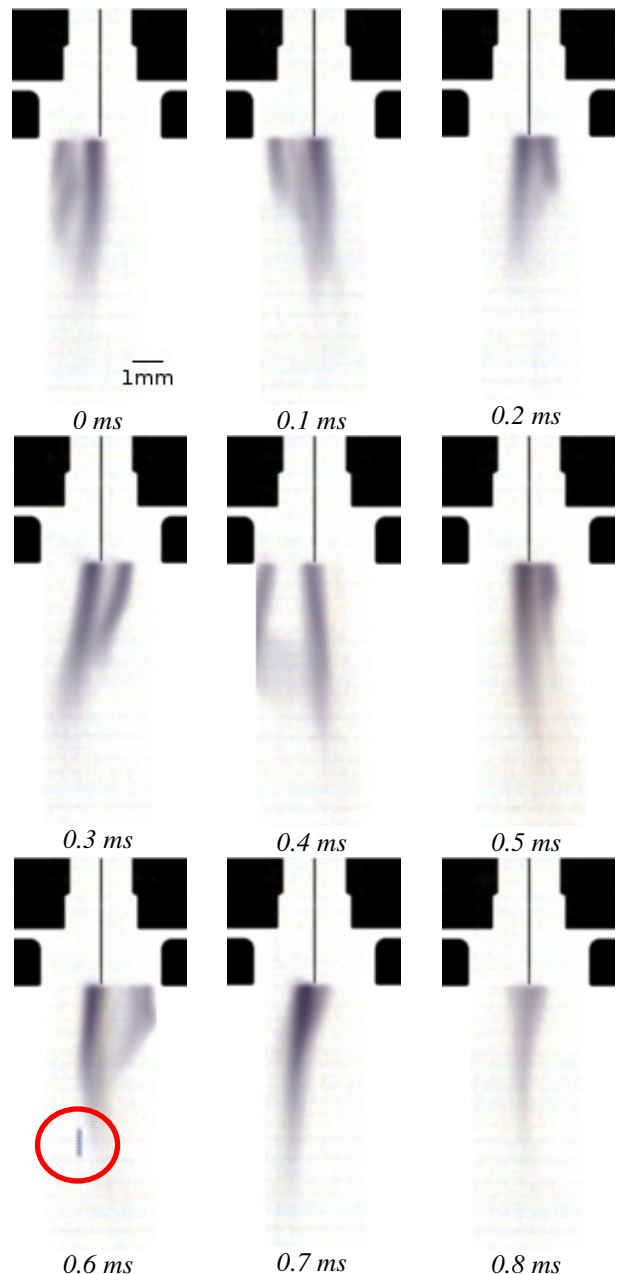


**Figure 42.** Pilot arc images at different time steps for a torch with 1.9 mm nozzle and 3.5 mm shield diameter, at 25 A (pilot arc plasma/shield gas: air/air). The  $t = 0$  ms frame is the first noticeable after ignition. Nozzle and shield are partly sketched in black with torch axis. Images are acquired at 10000 fps and 1/200000 s shutter time without any filtering. (Taken from [21]).

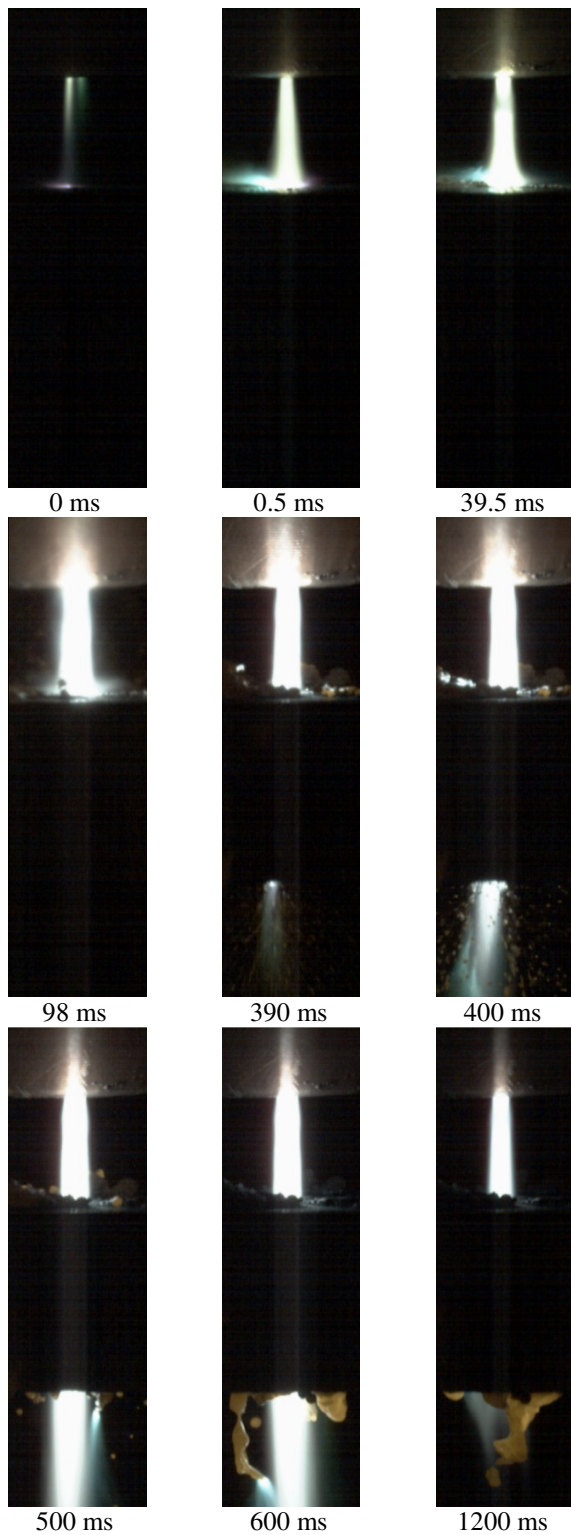


**Figure 43.** Piercing of a 15 mm SS slab (1.6 mm nozzle, 120 A, pilot arc plasma/shield gas:  $N_2/N_2$ , cut plasma/shield gas:  $H35/N_2$ ; 1000 fps, 1/20000 shutter time). Multiple arc root attachment on vaporized conductive metal from dross formation

can be seen in the time range 400-600 ms. (Taken from [21]). Taken from [25].

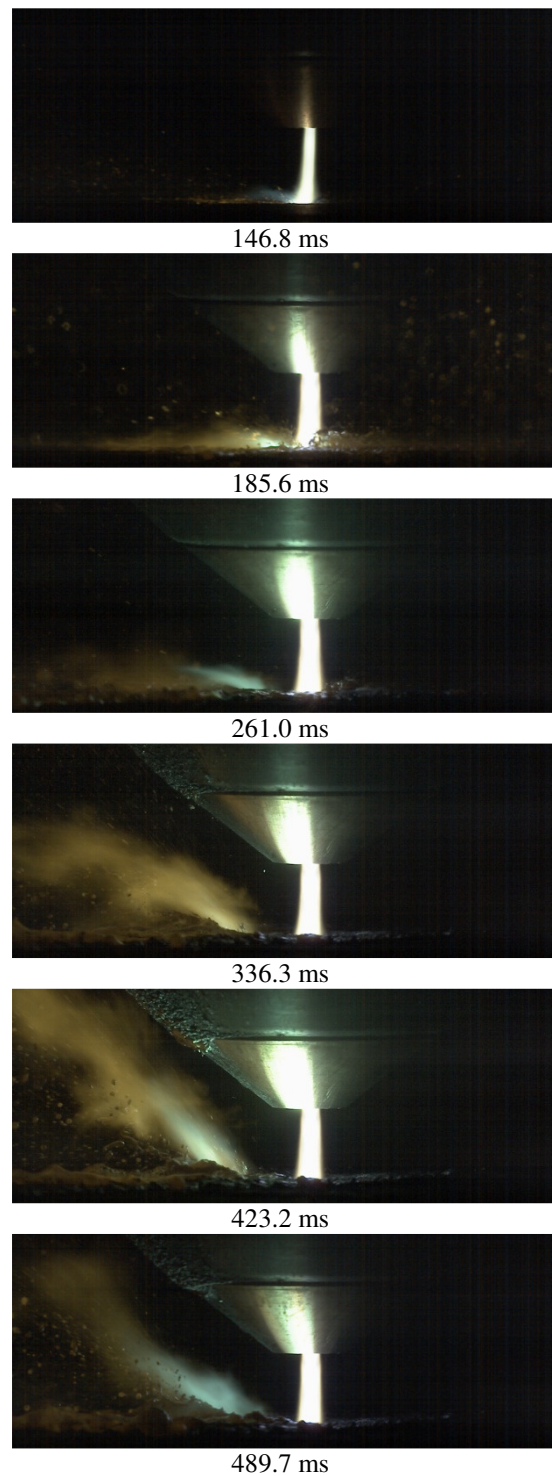


**Figure 44.** Piercing of a 40 mm MS slab using non-perfectly aligned torch head components: 1.9 mm nozzle, 250 A, cut plasma/shield gas:  $O_2/air$ , 1000 fps, 1/20000 shutter time. Taken from [25].

### **3.3 High speed imaging investigation of transition phenomena in the pilot arc phase in Hf cathodes for PAC**

Several studies [1, 17, 24] have been accomplished in order to understand phenomena that induce Hf erosion in different phases of the PAC operative cycle. More recently, high speed camera (HSC) imaging has also been used [25-26] to investigate pre-cut phases in PAC analysis, providing new insight into the process and highlighting some interesting phenomena related to plasma arc behaviour during pilot arc.

Research activities on PAC cathodes in the past were based mainly on try and error procedures rather than on deep insight into physical processes, resulting in a large number of patents; this fact induces a strong need for understanding the physical reasons behind successful industrial solutions that, due to patenting rules and strategies, are often not fully described or scientifically based.

The behaviour of Hf cathodes has been investigated with high speed camera (HSC) imaging techniques during the low current pilot arc phase, to highlight phenomena that take place during the transition from insulating, non-emissive, cold to conductive, emissive, hot for the Hf-based material used in electrodes for plasma arc cutting (PAC) of mild steel plates. The different behaviour during start-up phases of new or used electrodes has been considered. Such phenomena have been partially described on physical bases in the past but can now be fully seen and analyzed using diagnostics. Conclusions can be drawn concerning the particular conditions in which heat transfer transients in the cathode tip during PAC pilot arc take place; giving additional useful information for future design oriented simulation of such phenomena in different geometric and operating conditions, with the final aim of optimizing cathode expected service life.

The arc start-up phase consists of several stages. First, a high frequency signal breaks down electrode-nozzle gap, as shown in figure 3.3.1(a). After that, a relatively low-current (say 20A) pilot arc between electrode (negative) and nozzle (positive) is established. The arc column is blown out from the nozzle, forming an arc loop attachment on its tip, as shown in figure 3.3.1(b) and 3.3.1(c). Up to this stage, the arc (pilot arc) works in non-transferred mode. The aim of the pilot arcing phase is to provide a conductive medium in the nozzle-workpiece gap. When this extended loop touches the workpiece, the electronic control system in the generator isolates the nozzle and the main arc between electrode and workpiece is established in a transferred mode, as shown in figure 3.3.1(d). Main arc starts with some relatively low current, which is then increased up to the desired operational value.

Traces of the arc on the cathode surface show that the arc initially starts at the copper holder and then moves to the holder-emissive insert boundary. From there, it should reach its final position at the centre of the insert. New electrodes are characterized by a surface of smooth metallic Hf, while the used ones, after being exposed to the high temperature oxidizing atmosphere, are characterized by a surface layer in the order of 500  $\mu\text{m}$  of hafnium oxide ( $\text{HfO}_2$ ). It has been suggested in [1] that start-up erosion has its origin in difficulties for the arc to move from this boundary region of the emitter towards its centre. This is especially true for used electrodes, where the arc moves along the thin layer of hafnium oxide, which has cooled down and solidified after the previous arc cycle. The reason for this difficulty being that solid hafnium oxide (unlike its liquid phase) is a very poor heat and electricity conductor. It was hypothesized [1] that there is some mechanism, with which the arc can either

remove or melt this solid film; that mechanism being related to start erosion. Also, it was suggested that there is some kind of natural speed with which the heat wave moves into the insulating layer and melts it without catastrophic erosion.

It is known from experiments [17] and patent literature [18,27] that a gradual increase in the arc current in coordination with a gradual increase in the gas flow rate while switching the arc on decreases erosion.

It is evident, therefore, that some portion of the start erosion takes place during the transferred mode, where the current reaches its highest value. However, it is not clear which portion of the total start erosion takes place during the pilot arcing phase and how its characteristics affect it. Any experimental data that can shed light on these problems are highly desirable.

It can be foreseen that the way the arc reaches its final position at the centre of the cathode is very important for erosion phenomena. Therefore, it is important to know the mechanism and the time scale that leads the emitter surface from solid to melting phase. For example, if the pilot arcing phase produces relatively low erosion during the hafnium layer conversion, the process of transferring the arc from pilot to the main arc could be artificially delayed to reduce start erosion. Shortening or artificial delay of process of changing pilot into main arc can be done based on valuable information that can be obtained from high speed imaging. In particular, we are interested in how the arc, initially located at the holder-emissive insert boundary, ends up to be relocated on the centre of the emissive surface. According to [1], mismatch of this relocation process with the arc current increase could lead to high start erosion.

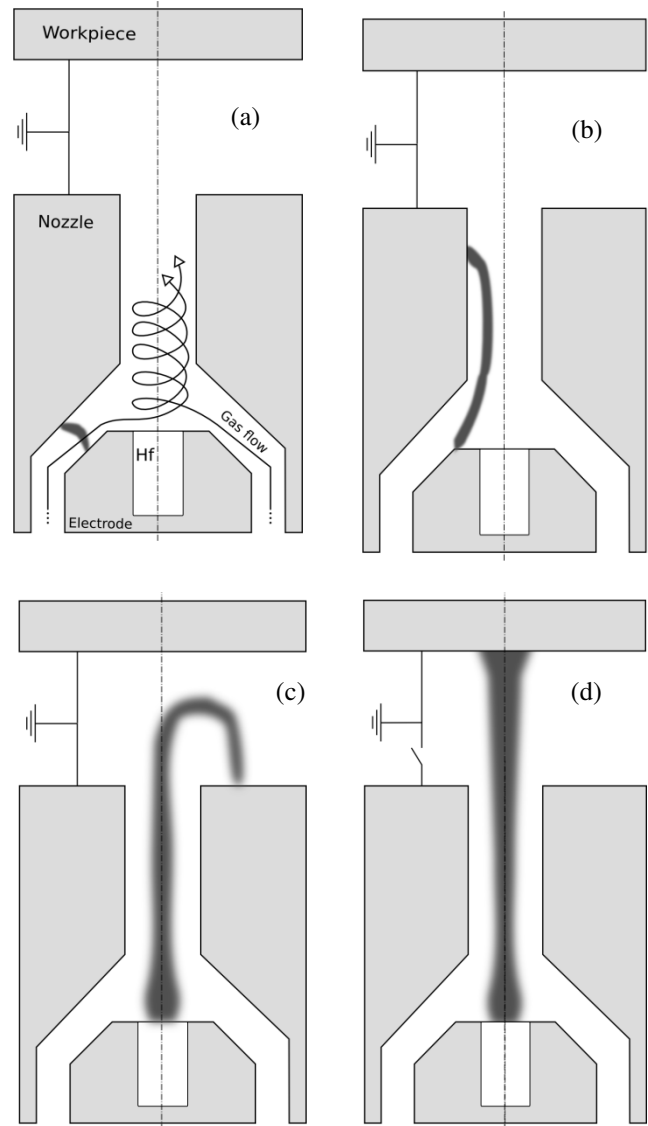


**Figure 3.3.1.** Start-up stages in a PAC process: (a) high frequency pulse; (b) blow-out of the arc; (c) pilot arc non-transferred mode; (d) transferred mode. Taken from [30].

The aim of this work is to investigate time and space evolution of the arc attachment during pilot arc phase. In particular, we are interested in investigating the characteristic time scale for the solid hafnium oxide layer to be converted into a molten film enabling the arc root attachment to stabilize itself at the centre of the emissive surface, with respect to the typical behaviour of fresh electrodes.

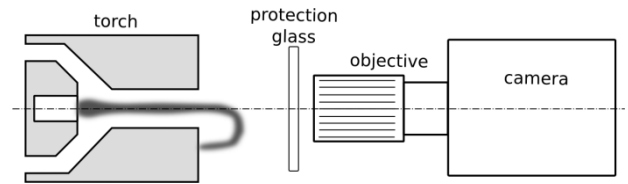


**Figure 3.3.2.** Sketched scheme of the visualization setup for high speed imaging of pilot arcing. Taken from [30].

### 3.3.2 Experimental set-up

#### *Plasma torch set-up*

During experimental tests a Cebora S.p.A. plasma cutting system has been used; comprising the power supply Plasma Prof 264 HQC, equipped with the remote high frequency unit HV18 and the Gas Console PGC1-2 for manual gas settings, together with the multi-gas plasma torch CP251G. The system can operate in the current range 25-250A in controlled current mode. Experiments have been accomplished under operative conditions typically used in cutting of MS plates thicker than 20 mm, with air as both plasma and shield gas. In the considered pilot arc phase the arc current is fixed at 25 A; the signal of the voltage drop between the electrode and the nozzle has an average value of 150 V with fluctuations of about  $\pm 30$  V. The tested electrodes use a press fit Hf insert with a diameter of 2 mm working in association with a nozzle with a 1.9 mm orifice diameter.

#### *Visualization set-up*

A NAC Memrecam GX-1 camera has been used, with a maximum acquisition speed of 200 000 fps and a 180 mm focal-length lens, protected by a sacrificial neutral filter, at a distance of about 0.5 m from the plasma torch, joined with a digital oscilloscope (LeCroy LT374M).

Visualization of the cathode surface during pilot arc was accomplished by positioning the torch and the camera lens on the same horizontal axis and in the absence of the torch shield cup (without secondary gas) in order to observe the arc loop attachment on the nozzle tip, as shown in figure 2. The camera set-up has been selected, for all pilot arc experiments, with 100 000 fps and 1/200 000 s shutter time, in order to achieve the best compromise between a suitable camera acquisition speed and a suitable image resolution. In all experiments auxiliary lighting has been used only in the setting phase, in order to optimize each focusing procedure, while the images have been captured without any filtering.

### *Pilot arc phase description*

Pilot arc duration has been extended compared to real ignition and transfer phases typical for PAC processes in automated cutting applications, where the torch operation and handling are managed by a pantograph with Computer Numerical Control (CNC). However, this duration can be considered realistic for manual cutting applications, for which the time interval between pilot arc ignition and arc transfer to the work-piece can be highly variable. In manual applications, moreover, the cutting process is characterized by a shut-down transient that cannot be managed through optimized current and pressure waveforms, usually aimed at reducing the arc-off erosion. Therefore, any means of reduction of arc-on erosion phenomena through the optimization of the plasma arc behaviour during the start-up transient is very important. The study of the cathode attachment behaviour and of the consequent erosion phenomena occurring during pilot arcing phases can be quite interesting for the optimization of consumable service life in cutting systems for manual applications.

Moreover, the study of pilot arcing phases which might be non-realistic, on time scale, for PAC processes in CNC applications, is aimed at the possible investigation of the impact of keeping the pilot arc on after discharge shutdown at the end of a cutting cycle. This procedure, when optimized under operating conditions probably different from the ones customarily used during conventional pilot arc, might have some positive effect in reducing the amount of electrode erosion induced by

thermal transients in the hafnium insert. On the contrary, it might have also the drawback of an undesired level of thermal stress and material damage on the electrode and nozzle.

### *Test cases*

The behaviour of the cathode arc root attachment during the abovementioned phases has been studied for three electrode emitter surface conditions:

- new electrode with planar emission surface
- new electrode with initially concave emission surface

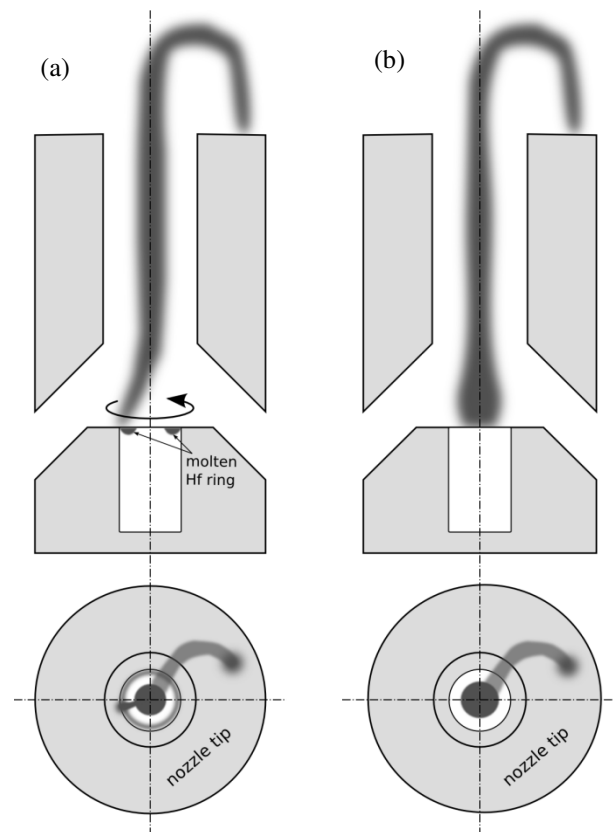


**Figure 3.3.3.** Side and top view schematic of the PAC torch in the two start-up pilot arc phases: (a) rotation of the cathodic arc root on the insert periphery; (b) stable centred arc root. Taken from [30].

- used electrode with a recess spontaneously established on the emission surface after a few cutting cycles.

The second emitter surface type has been included in the study since it is well known that, to avoid the negative effects induced by a natural deepening of the concave pit in an Hf insert initially flat, the emission surface can be otherwise shaped with a concave recess [28], so neatly removing a volume of first few starts, also badly conditioning the subsequent erosion process. When used in a torch, this solution accounts for a minimal deposition of emissive material on the nozzle, so reducing nozzle wear and double arcing phenomena, together with an increase in arc stability and cut quality.

### **3.3.3 Results**

The use of a very high acquisition speed of 100 000 fps and camera positioning in front of the nozzle, enabled to observe the early instants of the pilot arcing phase and the cathode arc root motion on the emitter surface. Literature results on this topic are limited [17] and take into account phenomena in a time scale of hundreds of milliseconds; the results presented in this paper are on a time scale about two orders of magnitude lower.

The experimental camera recordings for the three conditions of the electrode emitter surface that have been studied show that the pilot arc process is characterized by two subsequent phases. In the first one, the cathode arc root rotates on the periphery of the emitter surface, as shown in figure 3.3.3(a). This phase is also characterized by the emission of Hf vapours. In the second phase, the cathode attachment is no more rotating at the periphery of the emitter surface and the arc column stabilizes at its centre, as shown in figure 3.3.3(b). The transition from the first pilot arc phase to the second one occurs as a sudden event during which the cathode attachment progresses very fast to the centre of the emitter surface, almost as a collapse, with consequent emission of Hf vapours and, for the case of used electrode, also with the ejection of molten particles.

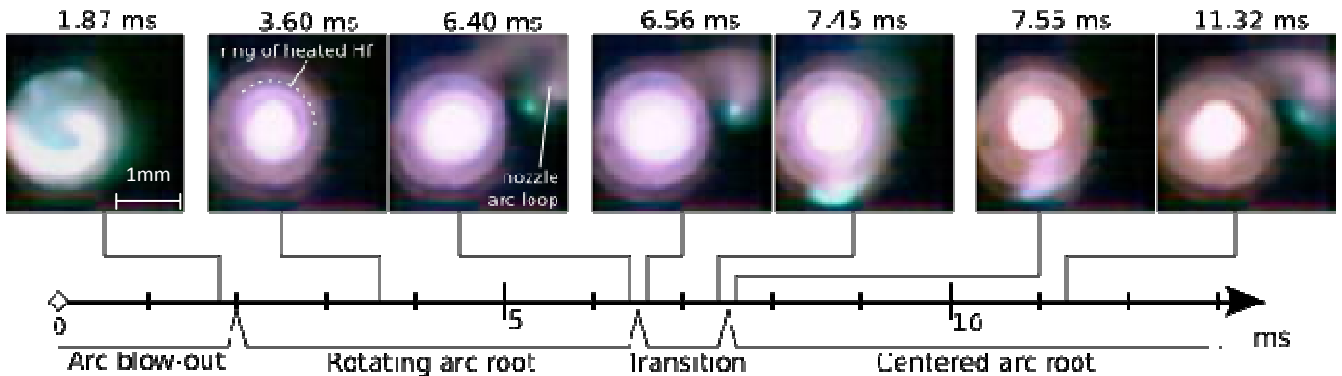


**Figure 3.3.4.** Pilot arc images, at different time intervals, for the case of a new electrode with an initially planar emission surface with spatial scale of 1 mm on the nozzle tip plane (supplementary video fig\_4.avi). Taken from [30].

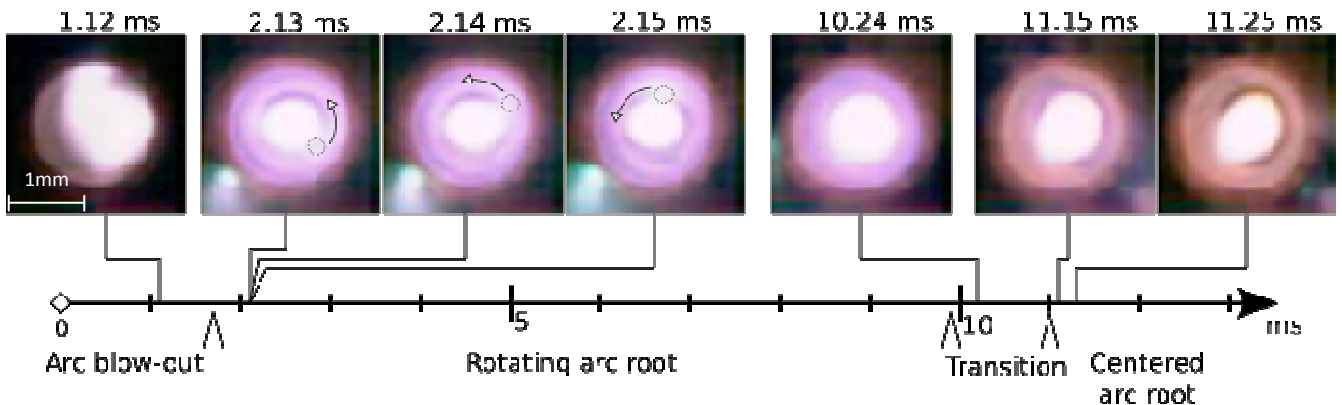


**Figure 3.3.5.** Pilot arc images, at different time intervals, for the case of a new electrode with an initially concave emission surface with spatial scale of 1 mm on the nozzle tip plane (supplementary video fig\_5.avi). Taken from [30].

Taken from [30].

#### *New electrode with planar emission surface*

Selected frames for the case of a new electrode with planar emission surface are shown in figure 3.3.4. The high frequency signal occurs at  $t = 0$  ms; then the arc is blown out from the nozzle in about 2 ms. The frame at  $t = 1.87$  ms shows the arc column deflected by the swirl component of the gas while it is blown out from the nozzle. After that, the cathode arc root starts to rotate at the periphery of the hafnium insert, creating a heated ring of molten hafnium as shown for  $t = 3.60$  ms. The arc appears brighter and unstable just about  $t = 6.56$  ms and a transition occurs from the first pilot arc phase to the second one, with the emission of gray-blue hafnium vapours. The transition event ends at  $t = 7.55$  ms and the second pilot arc phase follows. In this first case, the transition event appears to be smooth and non traumatic, with only minor emission of hafnium vapours and no perceptible ejection of droplets.

#### *New electrode with concave emission surface*

Selected frames for the case of a new electrode with initially concave emissive surface are shown in figure 3.3.5. The arc is blown out from the nozzle in about 1.8 ms and the rotation of the cathode arc root is shown for three consecutive frames starting at  $t = 2.13$  ms. The transition event occurs at about  $t = 10$  ms; about 3.5 ms later with respect to the previous case, probably due to the bigger surface involved in an initially concave shaped emitter.

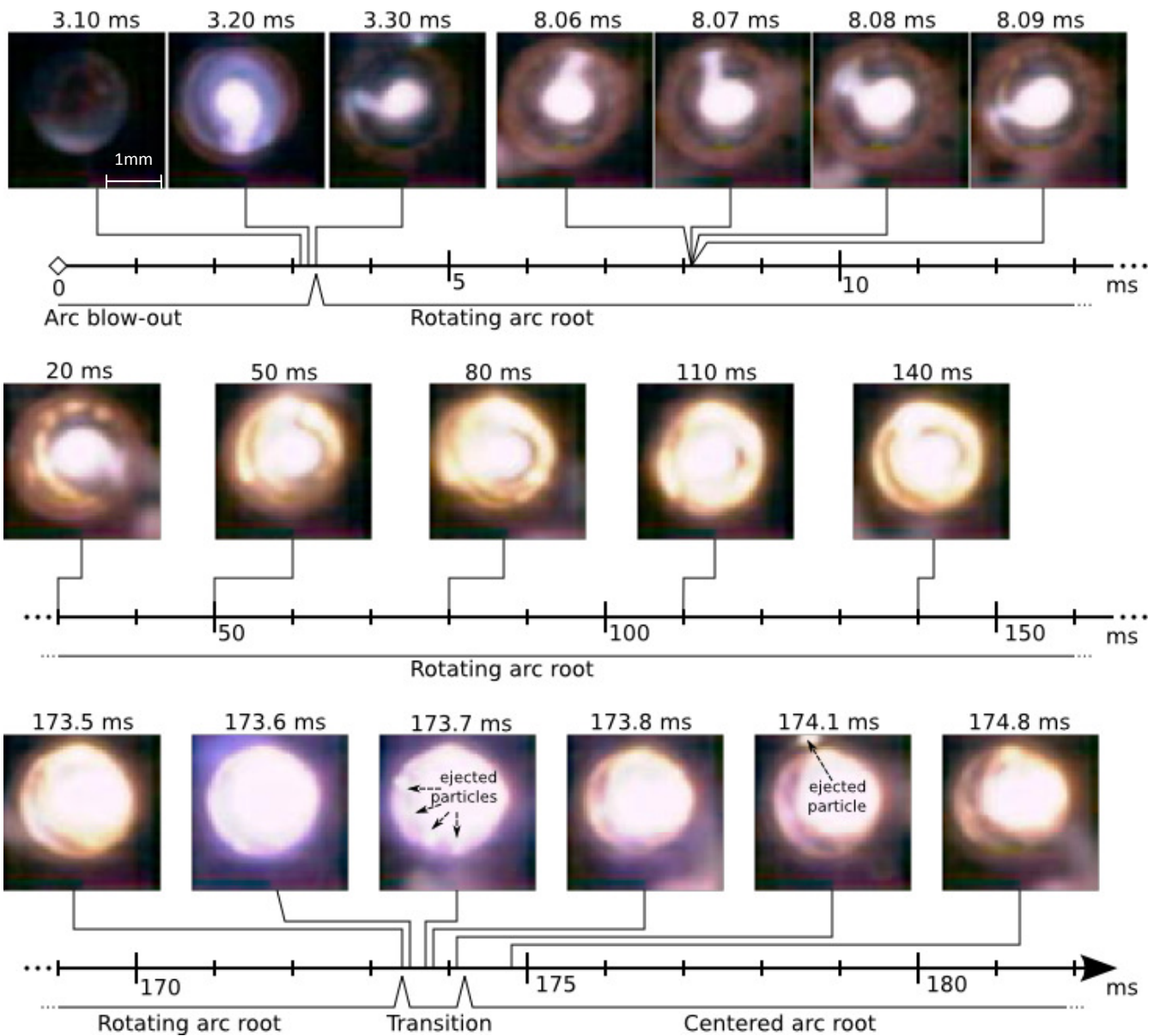


**Figure 3.3.6.** Pilot arc images, at different time intervals, for the case of used electrode with spatial scale of 1 mm on the nozzle tip plane (supplementary videos fig\_6a.avi, fig\_6b.avi and fig\_6c.avi). Taken from [30].

The comparison between the behaviour during pilot arc of these two electrodes with different emitter surface conditions shows that both reach the stable condition with the arc column at the centre of the emitter surface in less than 12 ms, with a smooth transition event between the first and the second phase and without massive ejection of melted Hf based particles. Tens of tests performed with this type of electrodes confirm this result, with only slight fluctuations on the time scale of the transition from phase one to phase two, when using the same operating conditions.

#### *Used electrode*

Selected frames for the case of a used electrode with a recess spontaneously established on the emission surface are shown in figure 3.3.6. The arc is blown out from the nozzle in about 3 ms. The cathode arc root rotates at the periphery of the hafnium insert for a longer time with respect to the

previous cases, up to  $t = 174.5$  ms. During the first pilot arc phase the cathode arc root attachment heats the annular layer of  $\text{HfO}_2$ , which becomes brighter and brighter. At about  $t = 173.5$  ms the transition occurs from the first pilot arc phase to the second one. In this case, the transition event is characterized by massive ejection of emitter material droplets and vapours. At  $t = 173.7$  ms a massive ejection of droplets occurs; most of them will hit the inner surface of the nozzle. In the  $t = 174.1$  ms frame, a droplet exiting the nozzle is shown. The transition event ends at about  $t = 174.5$  ms and the second pilot arc phase follows.

The fluctuations of the measured electrode nozzle voltage is induced by several phenomena, such as arc attachment motion on the nozzle tip, arc length variations in the post nozzle region and background noise; so, it is not possible to clearly identify the probable additional effect due to the ejection of Hf based droplets or the effect of the transition events. A much more evident correlation between some fluctuations on the voltage signal and the deposition of small amounts of hafnium oxide on the nozzle orifice wall has been shown in [25] by some of the Authors, for a transferred mode condition.

### **3.3.4 Comments on the results**

The comparison of the behaviour during pilot arc of electrodes with different emission surfaces shows that the new ones, both with or without the initially shaped emission surface, are characterized by a quite short (less than 12 ms) transient towards stabilization of the arc column at the centre of the Hf surface with a smooth transition event without massive ejection of melted Hf based particles. Used electrodes, on the contrary, are characterized by a quite long (almost 175 ms) transient phase with massive ejections.

This experimental evidence, summarized in figures 3.3.4-3.3.6, can now support and integrate the qualitative explanation given in [1] for the correlation between a decrease in the erosion rate and a sufficiently gradual increase in arc current during the starting transient. In fact, the presence of a peripheral and rotating attachment of the arc to the Hf based emissive surface and the critical heating transient for used electrodes, as shown by high speed imaging, can be related to the mechanism [1], which indicates the importance of heating and melting the solid layer of hafnium oxide.

Unlike hypothesis [1], where it was suggested that the hot spot moves radially towards the insert centre, images show that hot cathode attachment during the above mentioned first phase rotates along a relatively narrow ring at the insert periphery. It is likely that the width of this ring gradually increases while the final phase of this ring expansion progresses very fast, almost as a collapse.

#### *Thermal diffusion*

The difference between new and used electrodes on the duration of the first pilot arc phase is probably due to several factors, like the shape of the recess, the condition of the copper surrounding the insert and the depth of the recess. However, in the Authors' opinion, the main factor influencing the duration of that first phase is the value of thermal properties of the emitter, which suggests how fast the

material can be heated by the arc in the cathode spot. Thermal diffusivity, inversely proportional to the heat diffusion time, is defined as:

$$\alpha = k/(\rho C_p)$$

where  $k$  is the thermal conductivity,  $\rho$  the density and  $C_p$  the specific heat. Thermal properties for Hf and HfO<sub>2</sub> can be found in [29], leading to the estimation of  $\alpha(\text{Hf}) = 1.4 \cdot 10^{-5} \text{ m}^2/\text{s}$  and  $\alpha(\text{HfO}_2) = 5.1 \cdot 10^{-7} \text{ m}^2/\text{s}$ . The ratio  $\alpha(\text{Hf})/\alpha(\text{HfO}_2)$  is about 25; this being roughly in the same order of magnitude of the ratio between the duration of the first pilot arc phase for used and fresh electrode; that being about 20.

#### *Pilot arc transition in real cutting*

Our study showed that, for the set of conditions here investigated, the arc root attachment relocates from the periphery of the new insert to its centre in a relatively short time (about 10 ms), which is significantly shorter than the time of transferring from pilot (low current) to the transferred (high current) mode. Therefore, the arc attachment meets the transferring event already being at the electrode centre. On the contrary, in the case of used electrodes, pilot arc time for stabilization of the arc at the centre of the emitter is substantially longer (about 175 ms). Due to this characteristic time, it is possible that the melting process of the hafnium oxide layer is not completed at the moment of the transferring event, when the current ramps up to its typical level for cutting, with possible major effect on start-up erosion.

### **3.4 Multiple View and Tomographic Reconstruction of Pilot Arcing Transients**

High-speed imaging of the pilot arc transient phase in plasma arc cutting (PAC) has been carried out synchronizing the use of two high-speed cameras in conjunction with an optical system suitably designed for producing multiple synchronized views of the same phenomenon. Such imaging techniques have allowed a deeper understanding of the pilot arcing process, thanks to the simultaneous visualization of anode and cathode attachments and through the development of tomographic reconstruction of the pilot arc.

During the start-up phase, a low-current (25 A) pilot arc is ignited between the cathode and the nozzle by means of a short high-frequency pulse; the pilot arc is subsequently blown out of the nozzle by the gas flow. Deeper understanding of the non-transferred start-up transient can provide useful information on consumables wear.

#### **3.4.1 Experimental set - up**

In this paper we report some new results obtained with an imaging apparatus composed by two high-speed cameras, a Nac Memrecam K3R and GX3 (180-mm and 200-mm focal-length lens), by an optical system with four plane mirrors and by a digital oscilloscope (LeCroy LT374M) synchronizing the start acquisition time of both cameras. Experiments were carried out with the Cebora multi-gas plasma torch CP251G. In a first set-up (Fig. 3.4.1a), one camera, focusing on the cathode surface along the axis of the torch; while the other one can capture the arc loop attachment on the nozzle tip from two side-view points. In a second set-up (Fig. 3.4.1b), both cameras are used to capture the pilot arc behavior outside of the nozzle from three points; a three dimensional tomographic reconstruction [31] of the arc has then been accomplished.

#### **3.4.2 Results**

On this basis, the behavior in time of the anodic attachment during the pilot arcing phase could eventually be fully investigated, also highlighting the spot location and the rotation frequency. Some selected results will be here presented. Fig. 3.4.2 shows the axial view focused on the cathode surface together with the synchronized side views showing the behavior of the arc loop attachment on the nozzle tip; the high frequency impulse being at  $t=0$ , the first frame in which the anodic attachment becomes visible in side views is at  $t=1$  ms; the behavior of the cathodic attachment seen by the axial view has been previously described in [30]. For  $t=1.2$  ms, Hf vapors emissions from inside the plasma chamber are visible. For  $t=5.3$  ms, the left side view shows a double anodic attachment, which is hidden in the right side visualization; it is can also be put in correlation with the two bright spots evidenced by the axial view. For  $t=7.7$  ms, massive Hf vapors emissions are shown on both views and can be related to the transition event described in [30].

In Fig. 3.4.3a, three synchronized images of the pilot arc are shown; Fig. 3.4.3b shows the slices of the reconstructed total emissivity field on four planes located at different heights along the torch axis; Fig 3.4.3c shows the three-dimensional total emissivity field reconstructed using images of Fig. 3.4.3a and

visualized by a single iso-contour surface and volume rendering method, to qualitatively show the arc shape.

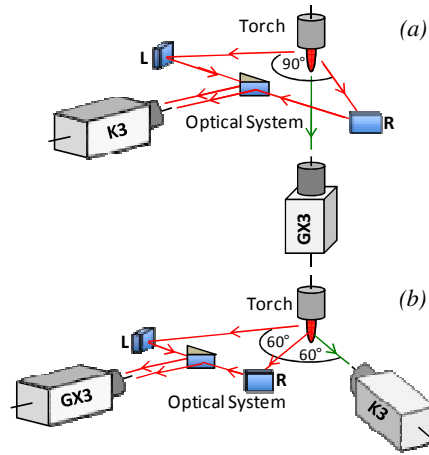


**Fig. 3.4.1:** Scheme of the (a) first experimental set-up and of the (b) second experimental set-up. Taken from [36].

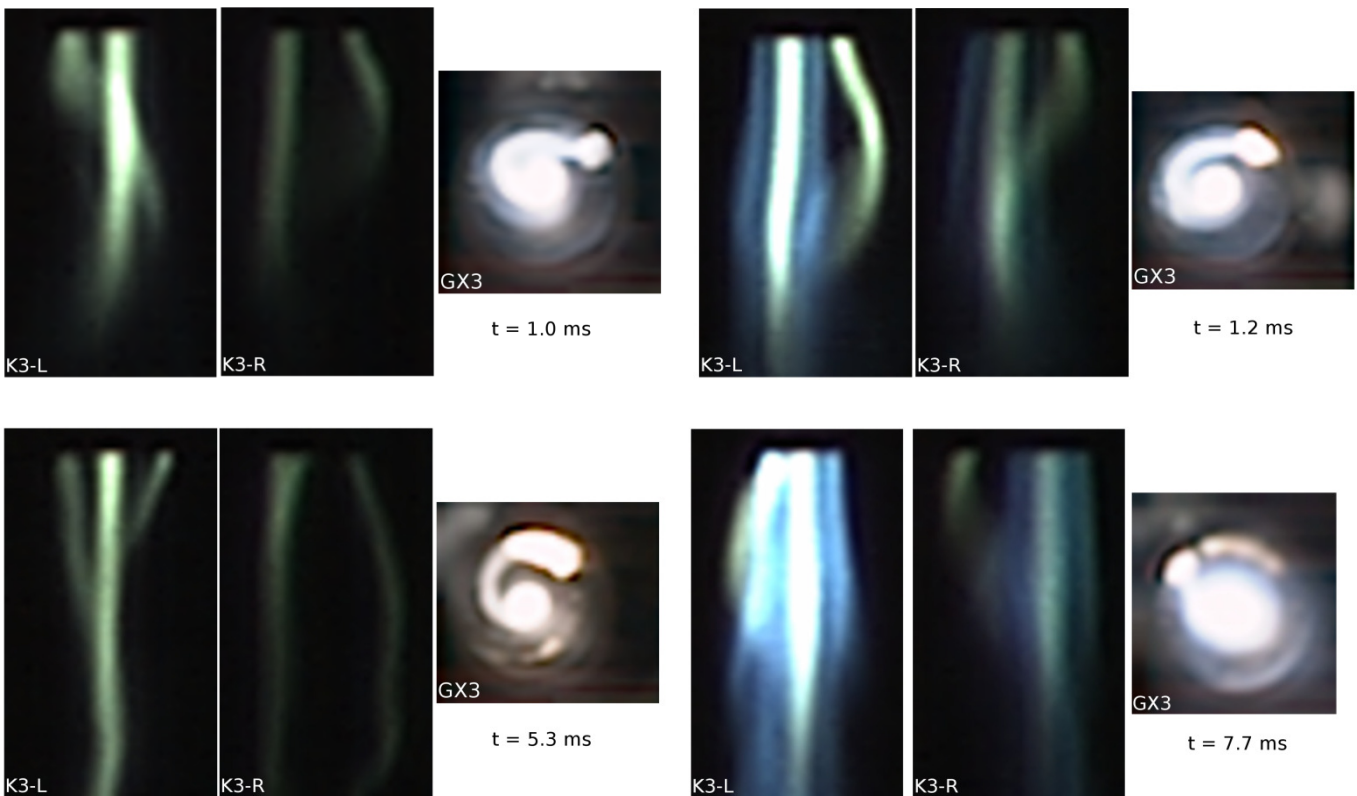


**Fig. 3.4.2.** Side and axial views of the pilot arc at different time steps. Images acquired at 10'000 fps (K3) and 100'000 fps (GX3) and 1/200'000 s shutter time, without any filtering. Taken from [36].

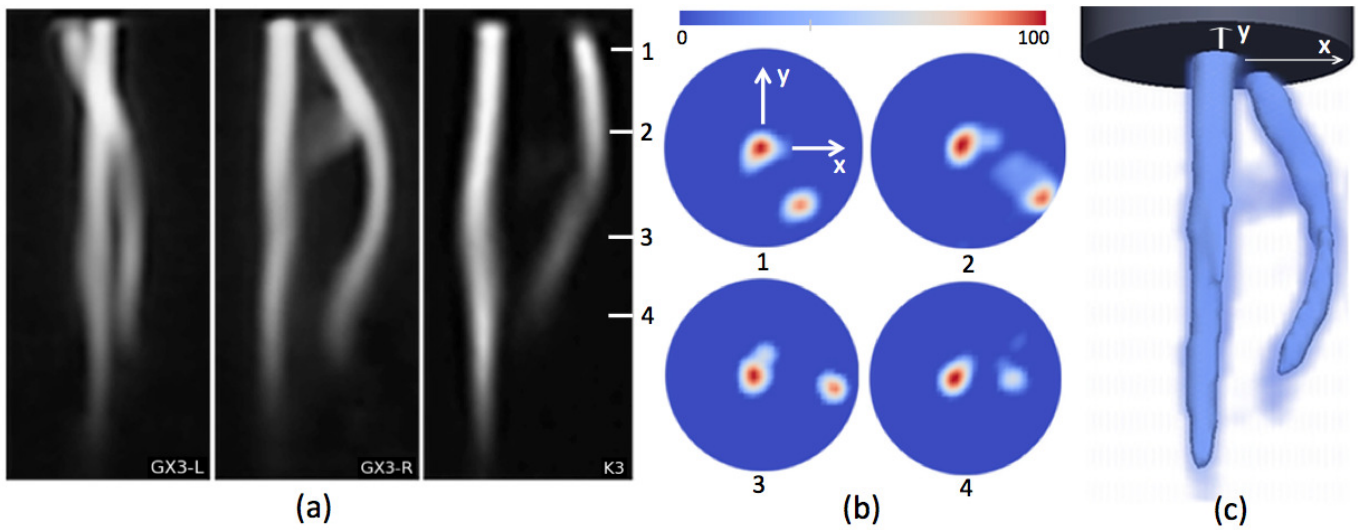


**Fig. 3.4.3.** (a) Synchronized images of the pilot arc acquired at 10'000 fps and 1/200'000 s shutter time, (b) total emissivity field slices at different heights and (c) three-dimensional reconstructed emissivity field. The GX3-R line of sight lies on the y-axis. (emissivity has been normalized for each slice). Taken from [36].

### 3.5 Schlieren Imaging experimental set-up

Schlieren photography was invented in 1864 by German physicist August Toepler to study the supersonic motion. Since then, the Schlieren photography has found widespread use in the aviation industry to see the air flow around the aircraft. This technique makes it possible to photograph the density gradients in a fluid, resulting in gradients of its index of refraction [35].

In fact, when in a fluid there is a refractive index gradient, the rays of light passing through it are deflected. The refractive index depends on many parameters such as composition, temperature and density of the medium. Also, its value changes significantly if a gas is ionized.

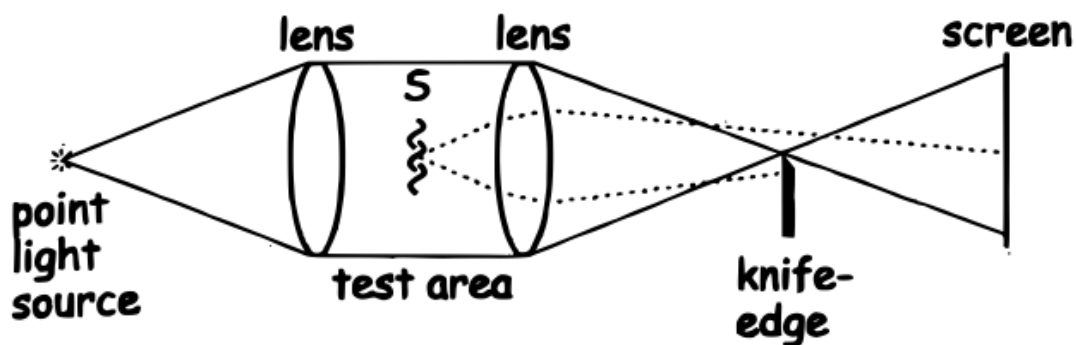


**Fig. 3.5.1** Diagram of an apparatus for Schlieren photography with point light source. Taken from [35]

Figure 3.5.1 is a schematic of an ideal Schlieren apparatus, which uses a point light source. Even if a real Schlieren apparatus is significantly different from that shown in the diagram, to consider the ideal system is still very useful for understanding the principles of Schlieren photography. In this scheme, the light rays are emitted isotropically from the light source and subsequently collimated by a lens that produces a beam of parallel rays. This beam passes through the object to be tested (S) and then meets a second lens that focuses the rays to a single point, where a knife-edge is placed. After that point, the rays are reversed and produce an inverted image of the object S on the screen. In absence of the knife-edge, the screen cannot display transparent objects present in the test area.

However, if in the focal point of the second lens is introduced the knife-edge, the latter blocks part of the rays refracted by the object S. Since these rays are deflected from their original direction, they do not converge at the focal point, but instead are focused towards neighbouring points. The figure illustrates very clearly the action of the knife-edge on the refracted rays. In fact, the beams deflected upwards illuminate a point on the screen, whereas the beams deflected downward meet the knife and cannot proceed to the screen. The point of the screen where the beam was supposed to come will therefore be dark.

So it's clear that, depending on the orientation of the blade, the image on the screen will be different. The knife blocks only those rays that are refracted perpendicular to the plane of its blade. A vertical knife shows only the horizontal density gradients because the horizontal component of the gradient

deflects the rays only laterally but not through it without causing changes in brightness. Conversely, a vertical knife may show only the horizontal density gradients. Depending on the physical phenomenon in question is therefore very important to choose the proper orientation of the knife.

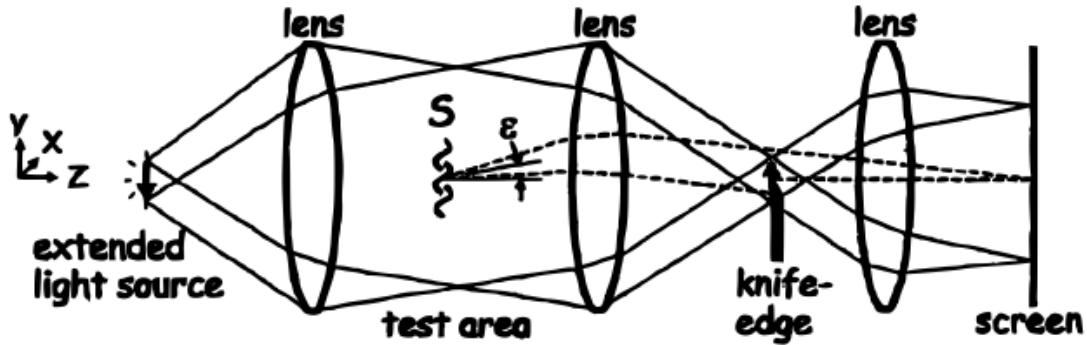


Fig. 3.5.2 Diagram of an apparatus for Schlieren photography with extended light source. Taken from [35]

Using a point light source is an ideal case. A more realistic case is the one with a light source extended in space (fig. 3.5.2). In this system a third lens downstream of the knife is used to focus an inverted image of the test area on the screen. The plane of the light source and the plane of the knife-edge are a pair of optically conjugated planes, as they are the plane of the screen and the plane of the test. This implies that an image of the light source is focused on the plane of the knife, as well as an image of the object S is projected on the screen. The image obtained on the screen with this apparatus is a grey-scale image.

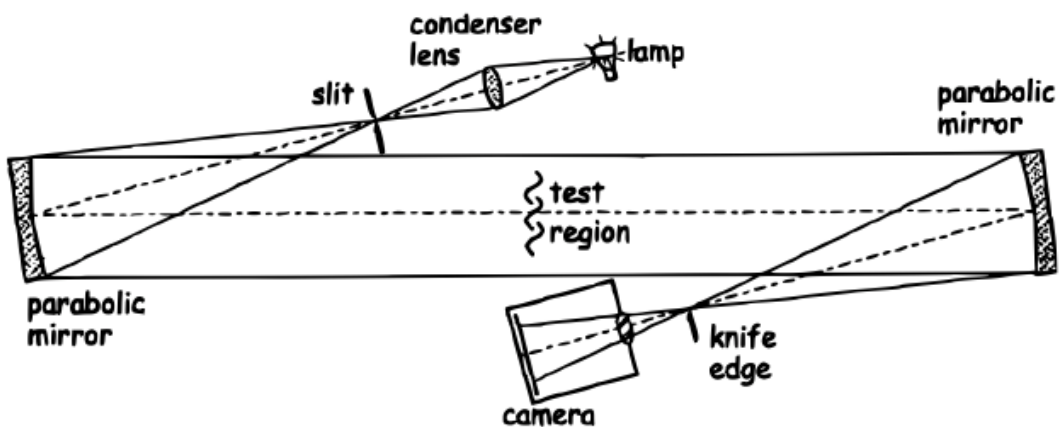


Fig. 3.5.3 Diagram of an apparatus for Schlieren photography: Z-type configuration. Taken from [35]

The experimental apparatus that was set-up for the accomplished studies was characterized by parabolic mirrors arranged in a Z-setup, as shown in figure 3.5.3. In this system, a non-coherent light beam produced by a 450W Xenon lamp is collimated by a lens on a small slit. Next, a parallel beam is produced by two parabolic mirrors tilted in opposite directions. The test area is located between two

mirrors, which are positioned at a distance of  $2f$  from each other, where  $f$  is the focal length of the mirror.

In designing the Schlieren apparatus for the tests it was necessary to take into account a fundamental characteristic of the physical phenomenon being analyzed: the arc plasma is characterized by a strong light and a very high density gradient. Schlieren photography must have a beam of intensity comparable to that of the phenomenon to observe to get a satisfactory quality image. It was subsequently chosen as light source a Xenon arc lamp, 450W of power. In addition, the slit was adjusted to its maximum opening allowed in order to ensure the highest level of brightness and trying to create an illumination as uniform as possible.

The knife was positioned to cover 50% of the source image. In this way, you create a situation symmetrical to the positive and negative density gradients. To observe the plasma is not necessary to push to the limits the sensitivity of the instrument, because there is a strong plasma density gradient and thus the Schlieren effect is very pronounced.



**Fig. 3.5.4** Picture of the experimental Schlieren setup.

For the acquisition of images, the high speed camera NAC Memrecam K3R HS was used, combined with a lens with focal length 180 mm. The high-speed camera used is capable of recording color images with resolutions up to  $1280 \times 1024$  pixels at 1,000 frames per second, but lower resolution can go up to 10,000 frames per second.

A preliminary study has been carried out with cutting torches with no plasma ignited. The cold flow exiting the torch at supersonic velocity creates density variation that can be detected with Schlieren imaging. In figure 3.5.5, the flow obtained with different operating conditions of the torch has been reported. Shock diamonds can be clearly seen when plasma gas is used. In figure 3.5.6, the turbulence pattern created by the flow of a cutting torch in pilot arc phase can be seen. Using different knife-edge orientations it is possible to highlight vertical and horizontal components of the density gradient in the flow. In figure 3.5.7, a Schlieren image of a cutting torch during the cutting phase of a mild steel plate has been reported. Strong turbulence can be seen in the upper part of the workpiece that disturb the arc.

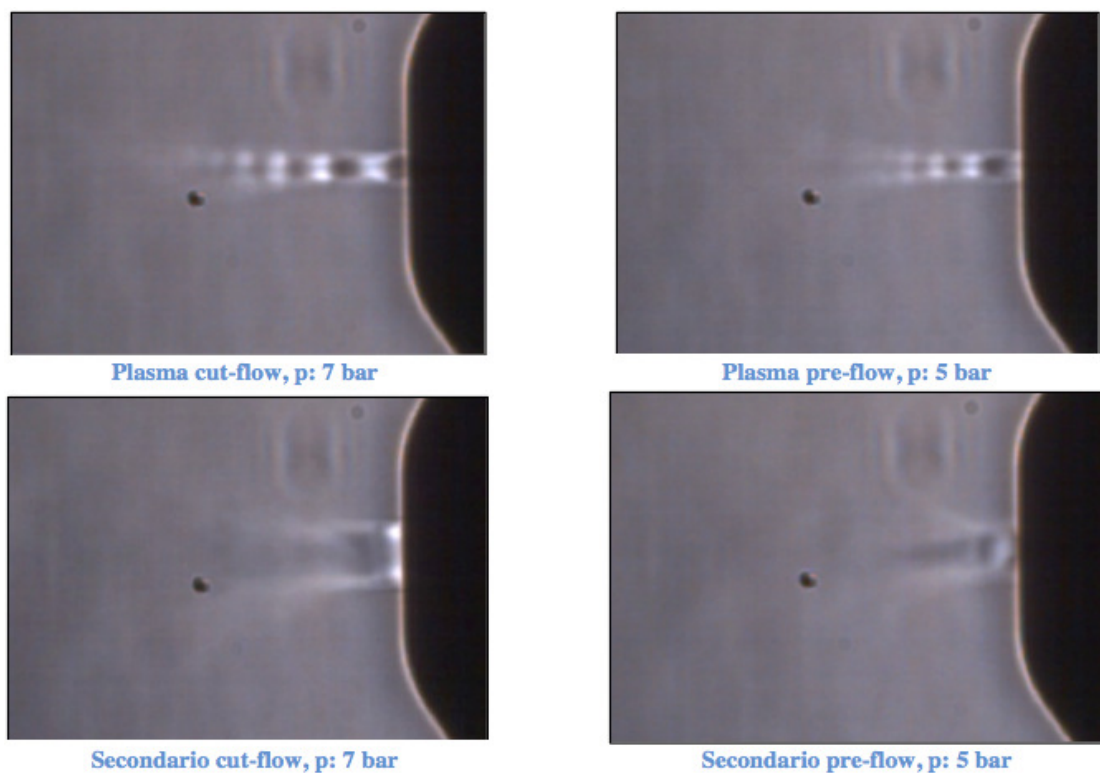


**Fig. 3.5.5** Schlieren images of the supersonic flow at the cutting torch nozzle outlet with no plasma power – Acquisition at 5000 fps. Horizontal knife-edge.



**Fig. 3.5.6** Schlieren images of the flow at the cutting torch nozzle outlet during pilot arc phase – Acquisition at 5000 fps. Horizontal knife-edge.



**Fig. 3.5.7** Schlieren images of the flow at the cutting torch nozzle outlet during pilot arc phase – Acquisition at 5000 fps. Vertical knife-edge.

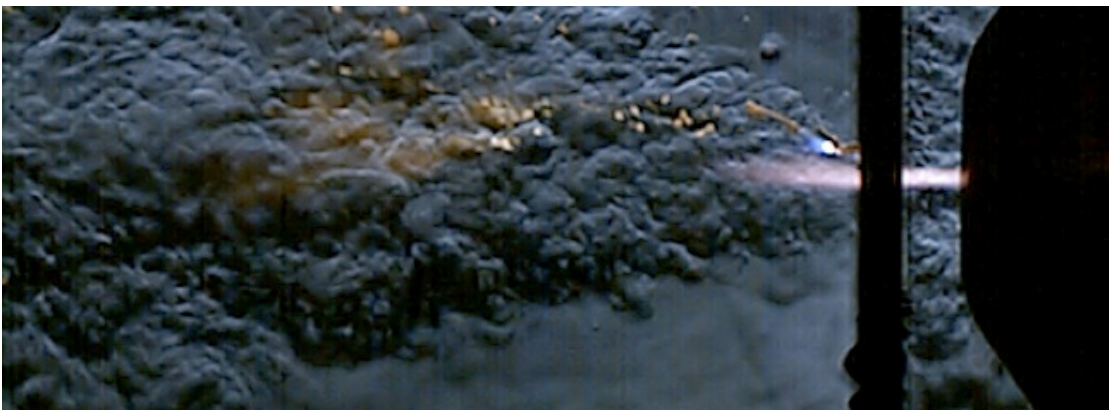


**Fig. 3.5.8** Schlieren images of the flow at the cutting torch nozzle outlet during cutting phase – Acquisition at 4000 fps. Vertical knife-edge.

### **3.6 Statistical Analysis of High-Speed Schlieren Imaging in PAC**

The interaction of plasma gas with the surrounding atmosphere in plasma arc cutting (PAC) has been investigated using high-speed Schlieren imaging. The time-series corresponding to the recorded intensity of each pixel have been post-processed using statistical analysis. Two different methods that highlight the time variation of the amplitude of the fluctuations in the density field have been compared: the windowed standard deviation and the GARCH approach. Whereas a mean-variance analysis can provide at most time-averaged results, GARCH can model the instantaneous variation of the luminous signal, thus providing new insights on the time evolution of the turbulence around the arc.

The high-definition cut requires high power density and high velocity in the plasma jet [1]. Increasing attention has been given to fluid-dynamic instabilities in the fringes of the arc, where the plasma gas (usually O<sub>2</sub> for mild steel cutting) mixes with the air coming from both the surrounding atmosphere and the secondary gas, creating strongly fluctuating turbulence patterns [32]. Optical methods like Schlieren and shadowgraphs have proven to be effective in order to visualize these patterns, mainly because they can be associated with high-speed image recording [25]. The Schlieren method is based on the angular deflection undergone by light rays when passing through a region characterized by refractive index gradients [33].

#### **3.6.1 Experimental set-up**

In this work the abovementioned Schlieren Z-type setup connected with a high-speed camera (NAC K3) is used to visualize a 25 A arc discharge of a CEBORA manual torch, cutting a 2 mm mild steel workpiece, using O<sub>2</sub> both for primary and secondary gas.

#### **3.6.1 Results**

The video at 10,000 fps has been post-processed using two statistical methods. In the first one, the “windowed standard deviation”, the raw video was divided into 25 frames sub-videos. Each of these was collapsed in a unique frame, where the value of each pixel represents the standard deviation of its corresponding 25 values in the sub-video. A 400 fps video was then constructed using the post-processed frames. The 25-frame window was chosen as a compromise between time-resolution and accuracy of the estimated standard deviation. Since most of the values were truncated due to overexposure of the film, the calculated standard deviation was adjusted hypothesizing an underlying Gaussian distribution. In the second method, the GARCH analysis [34], the intensity of each pixel was extracted frame-by-frame from the raw movie, yielding a time series of values. Each time series was normalized to zero mean and unit variance and fitted with an AR(1) + GARCH(1,1) model, interpreting each value as the sum of a deterministic trend plus a random noise drawn from a Gaussian distribution with time-dependent variance. For each frame, the value of each pixel in the raw video can be substituted with the value of its corresponding GARCH volatility, the standard deviation of the Gaussian noise, yielding a video representing the instantaneous turbulence in the plasma flow. In Fig.

3.6.1 results from windowed standard deviation method and the GARCH analysis have been reported for different time steps together with the corresponding non-processed Schlieren images.

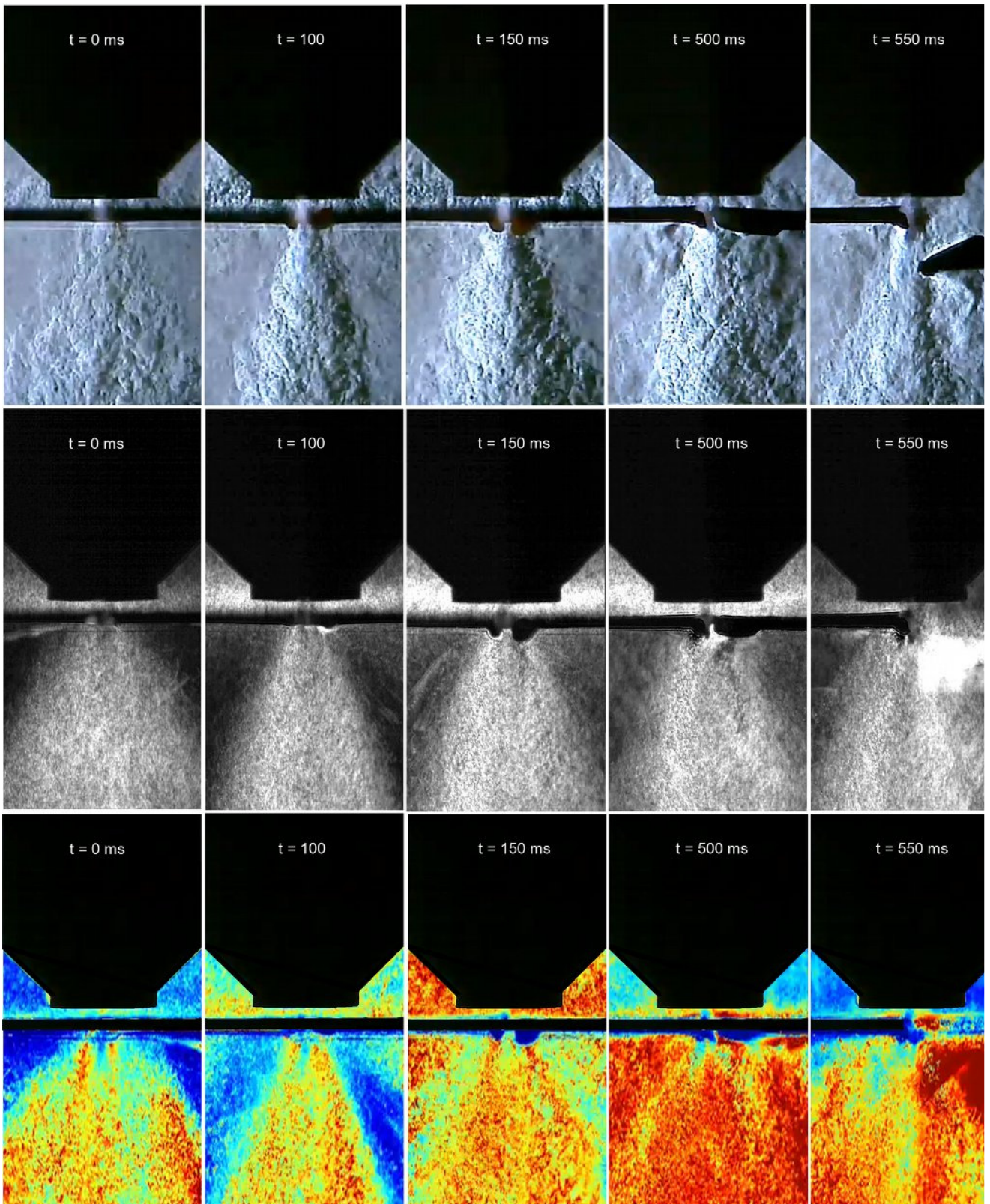


**Fig. 3.6.1.** Schlieren field (top), windowed standard deviation of the Schlieren field (middle) and GARCH volatility of the Schlieren field (bottom) at different time steps during realistic cutting conditions. The scale for the windowed standard deviation is set from black (low) to white (high). The scale for GARCH volatility is set from blue, which means low volatility, to red, which means high variance of the Gaussian noise. Taken from [37].

## **Conclusions and future developments**

Results presented in chapter 3 show that HS imaging can be a useful tool for a deep understanding of phenomena taking place in PAC and that are typically characterized by a very small time scale (less than 1 ms). Results coming from this kind of investigation are mostly qualitative; still, they can give important additional information on solving problems that have been otherwise investigated mainly from the theoretical or computational point of view. They can help in optimizing the design of torch components, of process characteristics and of plasma operative conditions (e.g. cathode erosion mechanism, double arcing, effect of anode attachment location, dross formation, effects of non perfectly aligned torch head components, etc.).

In paragraph 3.2, some new HS imaging results have been presented, enabling to study phenomena that cannot be investigated with other diagnostic methods. Pilot arc loop attachment on the nozzle tip, motion of the pilot arc from the electrode copper holder to the hafnium emitter surface, behaviour of the emitter surface during different phases of the pilot arcing, non-destructive double arcing during plate piercing, motion of solid hafnium based particles ejected from the emitter surface have been investigated.

In paragraph 3.3 a work has been presented in which the behaviour of the arc during pilot arc phase was explored. During this phase, cathode attachment relocates from the periphery of the emitting insert to its centre. It was found that characteristic time of arc transition from the first pilot arc phase to the stable second pilot arc phase is quite different in case of new and used electrodes. For the operating conditions explored, this time was about 10 ms for new electrode, whereas it was about 175 ms for a used electrode. Arc attachment stabilization at the centre of the emitter surface was also different for the case of fresh and used electrodes: rapid and smooth for the new inserts, characterized by a long rotation of the arc attachment at the insert periphery with the subsequent very fast (almost explosive-like) occupation of the centre of the insert for the used ones. We didn't notice any significant difference in behaviour between flat and concave emitter surfaces of new electrodes. These results indicate the presence of a significant ejection of Hf-based material from the emitter surface during pilot arc phase, when the melted hafnium oxide ring widens toward the centre of the emissive surface and enables the arc to relocate itself.

In paragraph 3.4, high-speed imaging of the pilot arc transient phase has been carried out synchronizing the use of two high-speed cameras in conjunction with an optical system suitably designed for producing multiple synchronized views of the same phenomenon. Such imaging techniques have allowed a deeper understanding of the pilot arcing process, thanks to the simultaneous visualization of anode and cathode attachments and through the development of tomographic reconstruction of the pilot arc.

Paragraph 3.5 showed results obtained investigating fluid dynamic instabilities in PAC using statistical analysis of high speed Schlieren images. The presented results are only an initial stage that allowed to study the possibility of transforming into quantitative data the typically qualitative information achievable with the schlieren technique.

Future developments in this field of research will concentrate on the still open issues, like HS imaging of the behavior of arc root attachment in the *kerf* region during plasma arc piercing and cutting in various operating conditions. This argument has been touched in the past by Bemis and Settles using ultraviolet imaging during [9-10], by Girard [15] in real cutting conditions but on a limited range of workpiece thickness and, more recently, by Nemchnisky and Severance [1] under a more conventional experimental approach that uses thermocouples.

Further developments will also aim at defining an efficient link between simulations of the plasma arc, experimental evidences coming from HS imaging and a consistent prediction of *kerf* formation and cut quality; similarly to what has been recently done to relate spectroscopic measurements to cutting performance.

For what concern the study of the electrode erosion phenomena, obtained results showed that the behaviour of the plasma arc and of the emitter surface during pilot arc should be considered for the reduction of hafnium erosion phenomena, especially when designing plasma arc systems for manual cutting applications. Further studies should be devoted to study these phenomena in different process operating and torch geometry conditions. In particular, it would be interesting to investigate the sensibility of start-up behaviour of used electrodes at various different stages of their service life and using a non oxidizing gas.

For what concern the high speed schlieren imaging technique, future developments will allow to apply these methods to real cases to obtain quantitative information on axial symmetry and stability of the arc, showing how even slight imperfections of the nozzle caused by erosion or non perfect alignment can influence arc symmetry and stability, and on the interaction between the plasma jet and the secondary gas, for different secondary gas injections.

## References

- [1] Nemchinsky V A and Severance W S 2006 What we know and what we know not about plasma arc cutting *J. Phys. D: Appl. Phys.* **39** R423-R438.
- [2] Freton P, Gonzalez J J, Gleizes A, Camy Peyret F, Caillibotte G and Delzenne M 2002 Numerical and experimental study of a plasma cutting torch *J. Phys. D: Appl. Phys.* **35** 115--131.
- [3] Colombo V, Dallavalle S, Ghedini E, Masini G, Russo D and Vancini M 2006 2D And 3D fluidynamic and plasma characterization of DC transferred arc plasma torches for metal cutting *J. of High Temp. Mat. Proc.* **10** 379-392.
- [4] Ghorui S, Heberlein J V R and Pfender E 2007 Non-equilibrium modelling of an oxygen-plasma cutting torch *J. Phys. D: Appl. Phys.* **40** 1966–1976.
- [5] Colombo V, Concetti A, Dallavalle S, Ghedini E and Vancini M 2008 Understanding plasma fluid dynamics inside plasma torches through advanced modeling *IEEE Transaction on Plasma Science* **36** 389-402.
- [6] Peters J, Barlett B, Lindsay J and Heberlein J 2008 Relating spectroscopic measurements in a plasma cutting torch to cutting performance, *Plasma Chem. Plasma Process.* **28** 331-352.
- [7] Potter K C and Settles G S 1996 Flow Visualization of Dross Formation in Plasma Cutting of Steel *49<sup>th</sup> Annual Meeting of the Division of Fluid Dynamics* (Syracuse, NY, USA, November 1996).
- [8] Lillis M M, Settles G S, Miller J D and Dodson-Dreibelbis L J 2000 High speed imaging of dross formation in plasma cutting of steel plate *American Physical Society, 53<sup>rd</sup> Annual Meeting of the Division of Fluid Dynamics* (Washington, DC, USA, November 2000).
- [9] Bemis B L and Settles G S 1998 Visualization of liquid metal, arc, and jet interactions in plasma cutting of steel sheet *8<sup>th</sup> Inter. Symp. on Flow Visualization* (Sorrento, Italy, September 1998).
- [10] Bemis B L and Settles G S 1999 Ultraviolet Imaging of the Anode Attachment in Transferred-Arc Plasma Cutting *IEEE Transaction on Plasma Science* **27** 44-45.
- [11] Camy-Peyret F, Durox D, Scouflaire P, Candel S and Delzenne M 2001 Etude experimentale d'un jet plasma d'arc de découpe *5<sup>eme</sup> journées sur les fluctuations des arcs* (Toulouse, France) (CPAT, Université Paul Sabatier, Toulouse, France) pp I.29–32.
- [12] Freton P 2002 Etude d'un arc de découpe par plasma d'oxygène. Modélisation – expérience *PhD Thesis* (Université Paul Sabatier, Toulouse III, France).
- [13] Freton P, Gonzalez J J, Camy Peyret F and Gleizes A 2003 Complementary experimental and theoretical approaches to the determination of the plasma characteristics in a cutting plasma torch *J. Phys. D: Appl. Phys.* **36** 1269-1283.

- [14] Girard L, Teulet P, Razafinimanana M, Gleizes A, Camy-Peyret F, Baillot E and Richard F 2006 Experimental study of an oxygen plasma cutting torch: I. Spectroscopic analysis of the plasma jet *J. Phys. D: Appl. Phys.* **39** 1543-1556.
- [15] Girard L 2004 Caractérisation expérimentale d'une torche de découpe dans l'oxygène: étude du jet de plasma et de l'interaction arc-matériau *PhD Thesis* (Université Paul Sabatier, Toulouse III, France).
- [16] Girard L, Teulet P, Razafinimanana M, Gleizes A, Camy-Peyret F, Baillot E and Richard F 2006 Experimental study of an oxygen plasma cutting torch: II. Arc-material interaction, energy transfer and anode attachment *J. Phys. D: Appl. Phys.* **39** 1557-1573.
- [17] Peters J, Yin F, Borges C F M, Heberlein J and Hackett C 2005 Erosion mechanisms of hafnium cathodes at high current. *J. Phys. D: Appl. Phys.* **38** 1781-179.
- [18] Luo L, Sanders N A and Couch R W Jr, Process and apparatus for reducing electrode wear in a plasma arc torch, Hypertherm inc. patent US 5,166,494, 24 November 1992.
- [19] Couch R W Jr, Sanders N A, Luo L, Lu Z, Backander P and Sobr J, Electrode for high current density plasma arc torch, Hypertherm Inc. patent US 5,310,988, 10 May 1994.
- [20] Heberlein J 2007 Observations on thermionic cathode erosion *International Round Table on Thermal Plasma Fundamentals and Applications* (Sharm El Sheikh, Egypt, January 2007).
- [21] Colombo V, Concetti A, Dallavalle S, Ghedini E and Vancini M 2008 High Speed Imaging of Pilot Arcing and Piercing in PAC *IEEE Transaction on Plasma Science* **36** 1042-1043.
- [22] Colombo V, Concetti A, Dallavalle S, Fazzioli R, Ghedini E and Vancini M 2008 High Speed Imaging of Pilot Arcing and Piercing in PAC *ISFV-13 – 13<sup>th</sup> International Symposium on Flow Visualization and FLUVISU12 – 12<sup>th</sup> French Congress on Visualization in Fluid Mechanics* (Nice, France, July 2008).
- [23] Kim S J and Heberlein J 2008 Quantifying instabilities of a plasma cutting arc through analysis of Schlieren images *35<sup>th</sup> International Conference on Plasma Science-ICOPS 2008* (Karkruhe, Germany, June 2008).
- [24] Colombo V, Concetti A, Ghedini E, Rotundo F and Dallavalle S 2010 Experimental analysis of the behaviour of high current electrodes in plasma arc cutting during first cycles, submitted to *Plasma Sources Science and Technology*
- [25] Colombo V, Concetti A, Ghedini E, Dallavalle S and Vancini M 2009 High speed imaging in plasma arc cutting: a review and new developments, *Plasma Sources Science and Technology* **18** 1-24
- [26] Kavka T et al. 2009 Anode processes during pilot arcing in cutting torch, *19th International Symposium on Plasma Chemistry - ISPC19* (Bochum, Germany)
- [27] Hardwick S F 2004 Process for operating a plasma arc torch *Innerlogic Inc.* US 6,677,551

- [28] Luo L and Couch R W Jr 1997 Electrode for plasma arc torch *Hypertherm Inc. Patent US* 5,601,734
- [29] Touloukian Y S (Ed.) 1967 *Thermophysical Properties of High Temperature Solid Materials Vol. 4*, (New York: The Macmillan Company)
- [30] Colombo V, Concetti A, Ghedini E and Nemchinsky V 2010 High-speed imaging investigation of transition phenomena in the pilot arc phase in Hf cathodes for plasma arc cutting *Plasma Sources Sci. Technol.* 19 065025
- [31] Mishra D, Muralidhar K and Munshi P 1999 A robust mart algorithm for tomographic applications *Numerical Heat Transfer, Part B: Fundamentals* 35:4 pp. 485-506.
- [32] S. Kim, J. Heberlein, J. Lindsay and J. Peters, "Control of fluid dynamic instability in oxygen plasma arc cutting" Proceedings of ISPC 19, Bochum, 2009.
- [33] L. Prevosto, G. Artana, B. Mancinelli, e H. Kelly, "Schlieren technique applied to the arc temperature measurement in a high energy density cutting torch" *Journal of Applied Physics*, vol. 107, 2010, pag. 023304.
- [34] T. Bollerslev, "Generalized Autoregressive conditional Heteroskedasticity", *Journal of Econometrics*, vol. 31, 1986, pag. 307-327.
- [35] G. S. Settles, "Schlieren and shadowgraph techniques", 2001, Springer-Verlag, Berlin Heidelberg, New York
- [36] V Colombo, A Concetti, E Ghedini, P Sanibondi, M Gherardi, M Bodelli and G Cantoro *High-Speed Imaging in PAC: Multiple View and Tomographic Reconstruction of Pilot Arcing Transients* Submitted for publication on IEEE Trans. Plasma Sci, 6th Triennial Special Issue on Images in Plasma Science.
- [37] G Cantoro, V Colombo, A Concetti, E Ghedini, P Sanibondi, F Zinzani *Statistical Analysis of High-Speed Schlieren Imaging in PAC* Submitted for publication on IEEE Trans. Plasma Sci, 6th Triennial Special Issue on Images in Plasma Science.
- [38] Sanibondi P 2011 Modelling , diagnostics and transport properties of thermal plasmas for industrial applications *PhD Thesis* (Alma Mater Studiorum Università di Bologna, Italy).

## Part II

### RF induction coupled plasma torches

This technology has its roots in 1961, year of publication of the article "Induction-coupled plasma torch" by Thomas Reed [1], where is described a method to create to thermal plasma, stable at atmospheric pressure, by means of an instrument, schematically illustrated in Figure 2.1, composed of a quartz tube confinement, a gas diffuser, an electric generator and a coil. Nowadays architecture has undergone some variations, particularly relating to materials used, but the operating principle has remained unchanged.

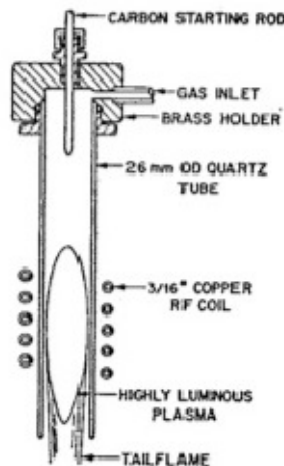


**Figure 2.1** Scheme of the Reed's torch. Taken from [1]

#### Working principle

The plasma is a result of the inductive coupling between the gas introduced into the quartz tube and the electromagnetic field generated by the radio frequency current flowing in a coil coaxial with the tube. When introducing the gas in the torch it is not, however, conductive; it is then necessary to trigger the ignition of the plasma discharge in order to create an initial plasma core which is then sustained by coupling with the electromagnetic field. Becoming conductive, in fact, the gas allows the formation of eddy currents within itself induced by the electromagnetic field due to the current flowing within the coil. These induced currents give power to the plasma through the Joule heat, in an area determined by the so-called skin effect, supporting the plasma discharge and compensating for the heat exchanges with the external area that take place by conduction, convection and radiation.

## **Plasma discharge ignition**

As mentioned in the previous paragraph, a non-ionized gas is unable to conduct and therefore it cannot be coupled with an electromagnetic field; it is therefore necessary to free some charge carriers. Already in [1] this problem had been reported; it was important enough to be considered, together with the stabilization of the plasma discharge, the parameter which determined the success of the experiments.

Ignition techniques commonly used are:

- Heating of a conductor. This method, described in [1], consists in introducing a rod, made by a conductive and refractory material, in the coil area; the rod is heated and becomes able to emit electrons, due to the Joule effect, and to increase, due to the thermionic effect, the temperature of the plasma gas by conduction and convection, thereby increasing its electrical conductivity;
- low pressure break-down. For the ignition, the plasma chamber is maintained at low pressure (eg 0.1 Torr); in these conditions the electrons mean free path of the introduced gas increases, enabling them to accumulate sufficient energy from electric field, so as to generate an ionization cascade. Once you have obtained this initial plasma core, the pressure can be increased up to its operational value;
- Pointed conductor. Near the tip of a conductor immersed in a high-frequency electromagnetic field, the field lines converge, giving rise to high gradients of electrical conductivity in a very small space. This leads to the ignition of a spark resulting in the ionization of the gas;
- Tesla coil. By means of a high potential source coupled with a sharp probe placed inside the torch, it is possible to generate an electric discharge characterized by sufficient energy to ignite the plasma.

## **RF torch operation parameters**

Over the years, various studies were conducted on the operation of inductively coupled plasma sources; one of the most comprehensive investigation was proposed in 1985 by Maher Boulos in [2]. In this article, as well as a computational modeling of the phenomena that take place inside the torch, the analysis of the influence of some parameters on the physical and geometrical behavior of the torch is presented. This study is based on the approximation and the mathematical modeling proposed in 1968 by Freeman and Chase [3]; they assumed that the plasma can be considered as a cylindrical load characterized by uniform temperature and electrical conductivity and that the temperature between the plasma and the confinement tube wall varies linearly between the values of temperature in these two zones. A schematic of this model is shown in Figure 2.2

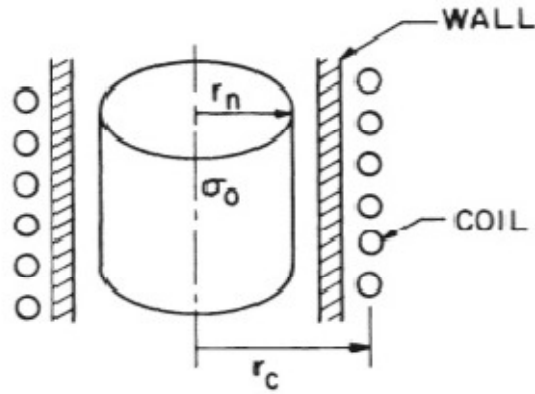


**Figure 2.2** Scheme of the model proposed by Freeman and Chase. Taken from [2]

### *Skin depth*

In a plasma immersed in an electromagnetic field eddy currents are generated that supply power to the plasma itself due to the Joule effect; experimentally it was observed that they are located in the outer zone of the plasma, from which the heat is then transferred by conduction and convection.

Assuming that the plasma is similar to a cylindrical load, the power transfer due to the inductive coupling with the electromagnetic field takes place in a cylindrical shell whose thickness is related to the current frequency and to the plasma physical properties. This thickness is called *skin depth*,  $\delta$ :

$$\delta = \frac{1}{\sqrt{\pi \xi_0 \sigma f}} \quad (2.1)$$

In 2.1  $\xi_0$  shows the plasma magnetic permeability, similar to that of vacuum,  $\sigma$  its the electrical conductivity and  $f$  is the induction current frequency. It can be seen that with the decrease of the frequency an increased thickness of the area of heat transfer to the plasma takes place with a consequent more uniform temperature distribution.

This localized power transfer results in a temperature peak dislocated from the torch axis, as shown in Figure 2.3 when operating with argon as plasma gas.

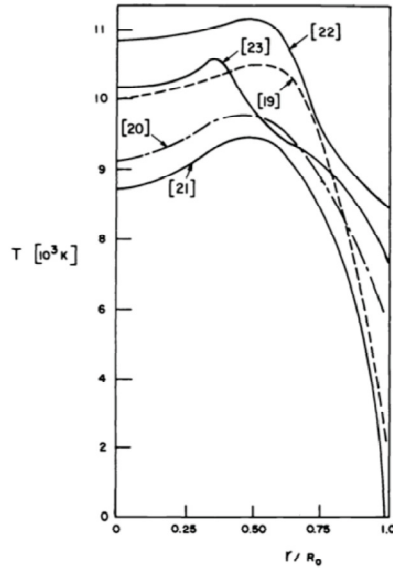


**Figure 2.3** Radial trend of the plasma temperature. Taken from [2].

This phenomenon is a direct consequence of the fact that eddy currents in plasma, being induced, circulate in opposite directions with respect to the coil currents. This means that an electromagnetic field opposite to the one that generated them is created, so as to shield the most internal part of the plasma, where then the transferred power is practically null. In Figure 2.4 the trend of the induction magnetic field into the confinement tube in the cases of presence or absence of the plasma is shown.

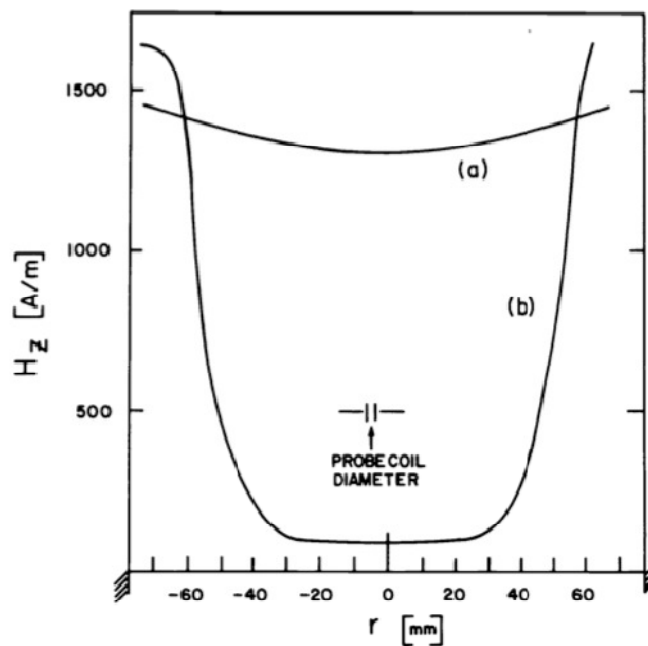


**Figure 2.4** Trend of the induction magnetic field into the confinement tube in the cases of presence (b) or absence (a) of the plasma. Taken from [2]

Finally, it was shown that the plasma gas strongly influences the maximum temperature and its distribution inside the torch. In Figure 2.5 it is shown as the maximum temperature is subjected to strong variation with the variation of the gas. In Figure 2.6 we see that in the case of oxygen as plasma gas the peak of temperature is along the torch axis, while for argon it is displaced.

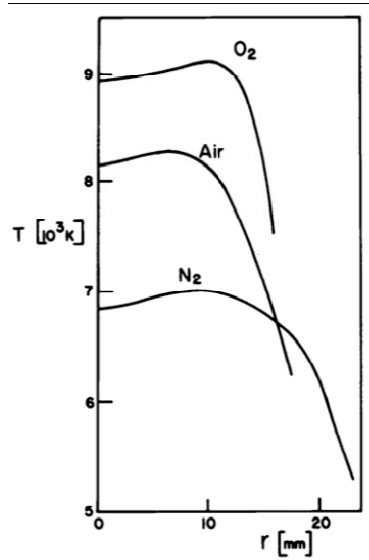


**Figure 2.5** Radial trend of the temperature for different gases. Taken from [2]

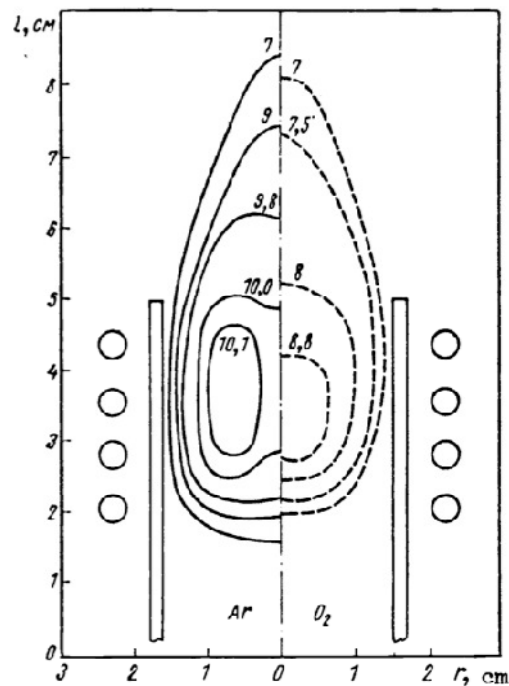


**Figure 2.6** Plasma temperature field when using argon (left) and oxygen (right). Taken from [2].

### Coupling efficiency

This parameter is an indicator of the efficiency of the coupling between the electromagnetic field and the plasma, it is expressed as the ratio between the power effectively transferred to the plasma and the reactive power available. Denoted by  $\eta_c$ , it is a function of two parameters.

$$\eta_c = f\left(\frac{r_n}{r_c}, k\right) \quad (2.2)$$

The first parameter is the ratio between the radius of the idealized plasma cylinder and the radius of the induction coil circumference, while the second one is expressed as:

$$k = \sqrt{2} \frac{r_n}{\delta} \quad (2.3)$$

In 2.3, the term  $\delta$  indicates the skin layer depth. The k term is representative of the geometric characteristics of the tube confinement, of the physical characteristics of the and of the chosen operation mode. The relationship between the coupling efficiency and these parameters is shown in figure 2.7.

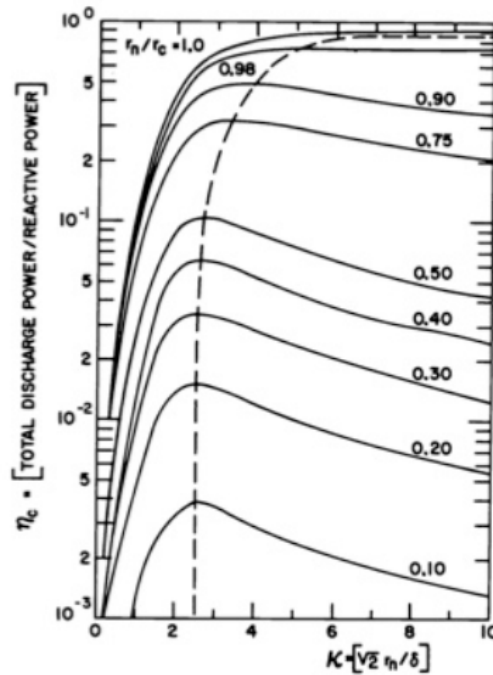


**Figure 2.7** Coupling efficiency of an inductively coupled plasma source. Taken from [2].

From figure 2.7 we see that the fixed geometry of the system, that is the ratio between the radii of the tube and the coil, has maximum efficiency for k values between 2 and 4; moving to higher values of k when the ratio between the radii increases. This means that when the plasma size goes toward the dimension of the coil, the thickness of the skin layer should be progressively smaller, at

least in proportion to the increasing radius of the plasma. This result can be obtained, with the same physical characteristics, by using a higher frequency of the induction current. It can be also seen that when the ratio between the considered radii goes toward the unit, the coupling efficiency tends to the maximum value, however, there is an upper limit above this ratio, given by the thermal resistance of the material of the confinement tube.

*Minimum sustaining power*

In order to sustain a stable plasma it is necessary to provide power; the least amount of energy necessary for this purpose is highly dependent on the type of gas used, on the pressure inside the torch and on the frequency at which the induction current work. The trend of the minimum sustaining power is shown in Figure 2.8.

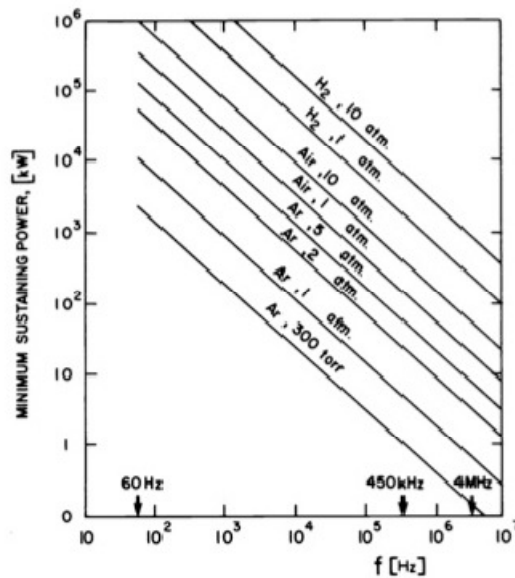


**Figure 2.8** Minimum sustaining power of a plasma discharge for different gases. Taken from [2].

It is known as the minimum sustaining power is facilitated by low pressures because, as previously described, when these conditions take place the mean free path of the electrons is increases, making it easier to ignite the electronic avalanche that creates the plasma. Moreover, high frequencies of the induction current reduce the minimum sustaining power. Finally we see that this parameter is closely linked to the used gas; due to the special advantages offered by argon, depending on its low thermal conductivity and specific heat, it is commonly chosen as the gas for the plasma ignition, it is subsequently replaced with the operation gas, if different, once reached a stable operating condition.

### Magnetic pinch

The magnetic pinch phenomenon, or magnetic compression, is at the basis of the formation of recirculation eddies in the area of the plasma. If we consider valid the hypothesis given by Freeman and Chase for which the plasma is comparable to a cylindrical metallic conductor, assuming that the coil is composed of distinct rings coaxial with the confinement tube, the density of the current induced in the plasma by an external electric field can be expressed as:

$$\bar{J} = \sigma \bar{E} \quad (2.3)$$

The magnetic field acts only in the axial direction. Along the torch axis, because of the shielding produced by the skin effect, the magnetic field has almost no value, while in the area of the skin layer it takes maximum values, giving rise to Lorentz forces non-negligible, expressed by 2.4.

$$\bar{F}_L = \bar{J} \times \bar{B} \quad (2.4)$$

It follows then that the Lorentz force is directed towards the torch axis, as a vector product of the magnetic field directed downward axially, and of the induced current density, for the Lenz law, directed in the opposite verse compared to the current that generated it, but with the same direction.

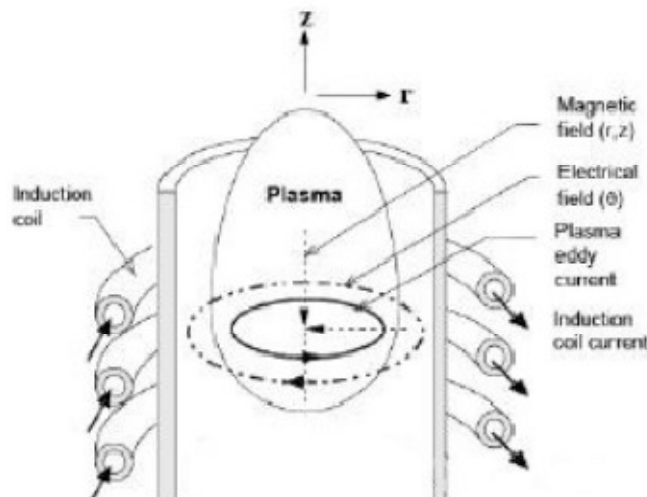


**Figure 2.9** Schematic of the magnetic pinch model. Taken from [2].

To maintain the radial balance of forces it is necessary that the Lorentz force is opposed by another force characterized by equal magnitude and opposite direction; this will be due to the pressure field in the plasma, which has its maximum value along the torch axis.

The magnetic pressure has a negligible effect on the overall pressure in the torch, but not on its fluid dynamics. For high plasma gas flow rates significant variations are not experienced, but with reduced plasma gas flow rates the creation of vortices takes place in plasma zone, as shown in Figure 2.10.

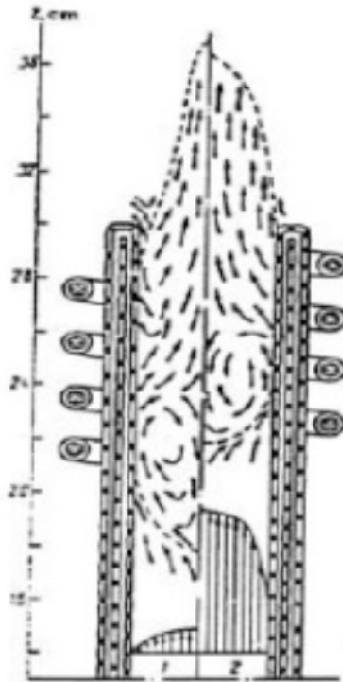


**Figure 2.10** Velocity vectors in the plasma zone. Taken from [2].

### *Energy balance*

From the energy balance of the system for the inductive coupling plasma source can be derived an expression of the overall efficiency,  $\eta$ , of this technology; this is defined as the ratio between the energy available in the form of enthalpy at the torch exit and the energy supplied from the electric generator. The overall efficiency of this system varies in the range of 40-60% and is closely linked to geometric parameter  $r_p/r_c$ , the ratio between the radii of the plasma discharge and of the induction coil.

In figure 2.12 a graphical representation of the energy balance is shown, it is known that the losses to the generator of alternating current have an almost constant trend and expected independent from the geometry of the torch, covering approximately 20% of the energy supplied to the system. Losses associated with transmission of energy and the ohmic into the induction coil are strongly reduced when the geometric parameter goes toward the unit, due to the improved efficiency of the coupling. Similar trend characterize the losses in the inductive coil with a dielectric. It should also be taken into account, however, that part of the energy made available to the plasma is transferred to the walls of the confinement tube through conduction, convection and radiation; as shown in Figure 2.11, this fraction increases as the factor geometry increases, due to the reduction

of the distance between the hot plasma and the torch walls. For a value of  $r_n/r_c$ , actually achievable, equal to 0.7 it is possible to obtain efficiencies close to the 50%; as mentioned above, this value is limited by the thermal resistance of the components, in particular of the confinement tube of the torch.

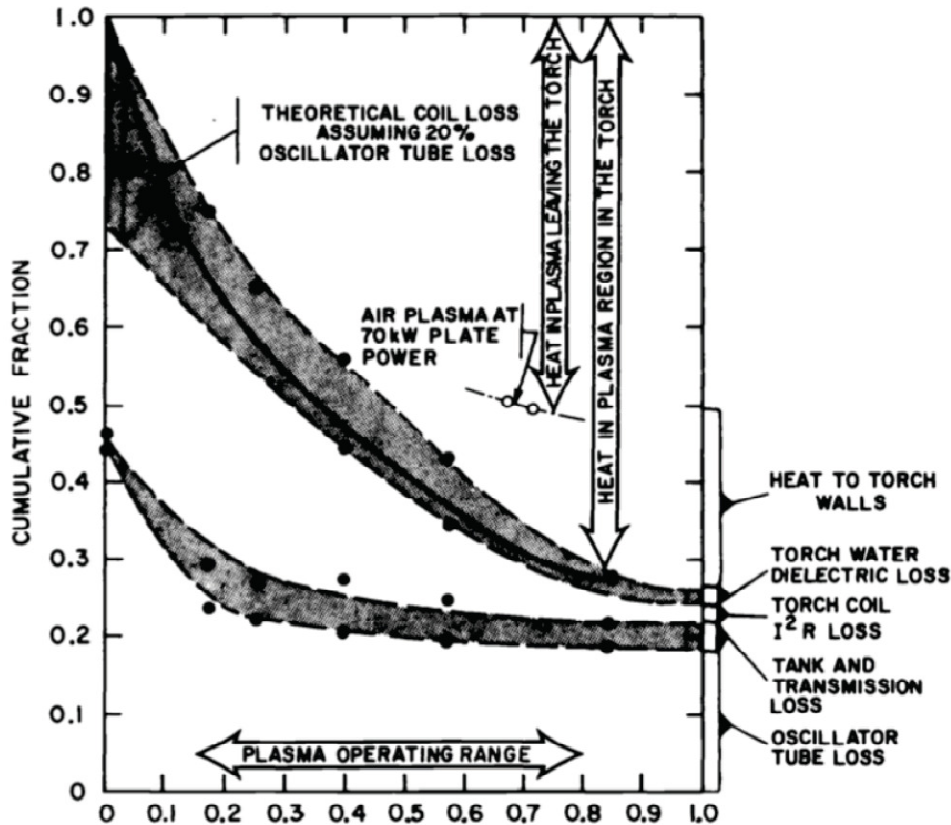


Figure 2.11 Scheme of the energy balance into the RF plasma system. Taken from [2].

### Modern architecture of the RF torch

In Figure 2.1 the basic model of the inductively coupled plasma torch, proposed in 1961 by Reed in [1], the architecture and the principle of operation, over the years, have not undergone much evolutions, if not linked to increasing the temperature obtainable in the plasma and the operating power. As previously mentioned, the critical element of the torch is the confinement tube, originally thought in quartz and cooled by the same plasma gas that was introduced sideways in the chamber with a tangential component.

Figure 2.12 shows the different methods adopted for the stabilization of the plasma discharge, and and the cooling, by convection and conduction, of the wall itself, by means of gases introduced and directed in different ways. In 1983, a group of researchers at the Los Alamos National Laboratory coordinated by Hollabaugh developed an architecture of the confinement tube able to allow the

increase of the plasma temperature and the synthesis of silicon carbide nanoparticles [4]. The scheme of the process is shown in Figure 2.12.

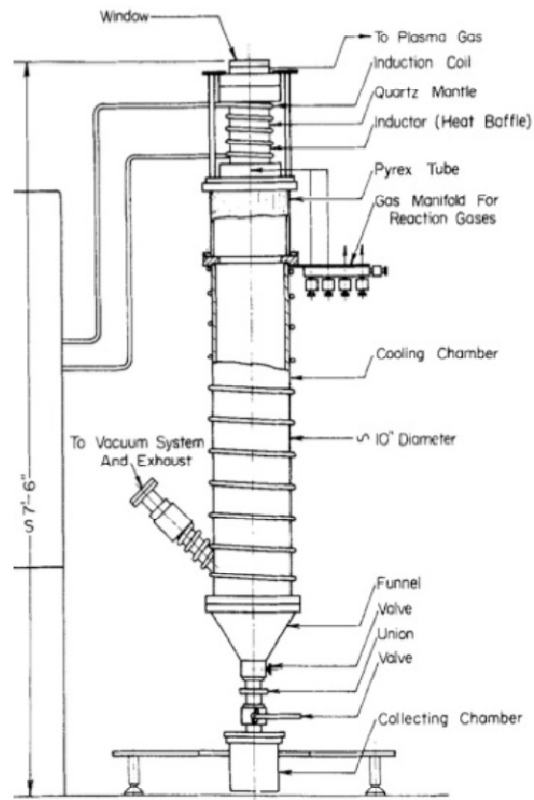


**Figure 2.12** System used by Hollabaugh for the production of SiC nanopowders. Taken from [4]

They added on the inside wall of the containment tube made of silica, some copper stripes in order to protect the tube from radiation. Furthermore, these stripes would had act like transformers, improving the coupling between the electromagnetic field and the plasma. Figure 2.13 shows the confinement tube which they developed.

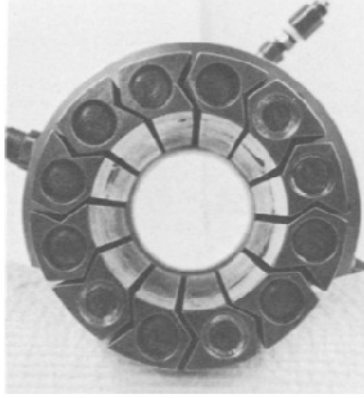


**Figure 2.13** Confinement tube proposed in [4].

This architecture, however, had two critical issues: the copper strips, introduced to increase the coupling efficiency, actually reduced it and also make it impossible to operate the torch with any gas, due to the reactivity of the copper.

These critical issues were solved by a patent filed in 1993 by M. Boulos and J. Jurewicz [5] in which the use of a containment tube made of a sintered ceramic material (silicon nitrate, boron, aluminum or alumina) is claimed, characterized by high thermal conductivity, electrical resistivity and thermal shock resistance.

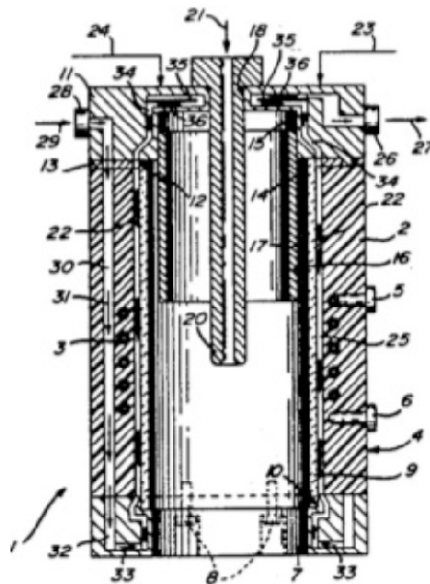


**Figure 2.14** Architecture of the plasma torch proposed in [5].

As shown in Figure 2.14, the claimed torch is composed by the following components:

- a ceramic cylindrical body (2) with high thermal conductivity;
- an copper induction coil (3), cylindrical and coaxial, internally cooled with water and drowned in the torch
- a plasma confinement tube (9) of ceramic material with high thermal conductivity, high electrical resistivity and high thermal shock resistance, with an outer diameter slightly smaller than the inside diameter of the torch body (2)
- a gas distributor (11) fixed to the top of the torch body (2) which allows the introduction of at least one gas into the torch
- a nozzle for the plasma exit (7) with a cylindrical body and connected to the torch.

The most important element introduced by this patent is the annular chamber (25) of a thickness of about 1 mm that is created between the cylindrical body (2) and the confinement tube (9): here there is a high-velocity water flow in order to obtain high values of the heat transfer coefficient to ensure proper cooling of the plasma confinement tube (9). The effectiveness of the cooling can produce plasma discharges characterized by increased power and temperatures lower with gas flow rates lower with respect to other design architectures. This solution enables to obtain increased enthalpic levels of the gases at the torch exit, that can be used for possible downstream processes.

Other components mentioned in the patent but not specifically introduced in the claims:

- an intermediate tube (16) in quartz to allow the introduction of a plasma gas and a sheath gas;
- a powder injection probe (20), transported by a carrier gas, cylindrical and coaxial with the intermediate tube (16), the confinement tube (9), the torch body (2) and the coil (3).

This architecture, which allowed to increase the operating power up to 1 MW, is still used and adopted and in particular produced from the Tekna Company, the world's leader company in the production of inductively coupled plasma sources.

### **The Inductively Coupled Plasma System installed at the UNIBO - DIEM laboratories**

The Inductively Coupled Plasma System installed in the DIEM laboratories of the University of Bologna and used to perform the experimental studies subsequently described comprises a Tekna PL-35 torch operating since December 2003 and whose design is in accordance with the principles claimed in the abovementioned patent [5].

## References

- [1] *Reed*, Journal of applied physics 32 5 (1961) 821.
- [2] *Boulos*, Pure & applied chemistry 57 9 (1985) 1321.
- [3] *Freeman, Chase*, Journal of applied physics 39 1 (1968) 180.
- [4] *Hollabaugh et al.*, Journal of materials science 18 (1983) 3190.
- [5] *Boulos*, US 5200595 (1993).

## Chapter 1

### Thermal plasma in-flight waste treatment

The problem of the waste disposal is taking in Italy and elsewhere in the world an ever-increasing importance. The growing production of waste materials and the increasing difficulty that the traditional strategies encountered in the collection and disposal process of waste are at the base of this problem. The plasma-assisted technologies, given the high temperatures that they can reach, are a powerful tool in this field, since they allow to treat hazardous waste making it possible their reuse in the building industry.

Most of the activities that I carried out in this field have been done in the framework of the Emilia Romagna regional projects ENVIREN - ENVironmental REgional Network and LITCAR Laboratory (*Laboratorio Integrato Tecnologie e Controllo Ambientale nel Ciclo di Vita dei Rifiuti*) . My contribution consisted in taking part in experimental studies focused on using plasma technology aimed at treating and utilization of waste, especially slag and fly ash coming from the incineration of municipal waste, liquid waste from the remediation of contaminated sites and different fractions of Waste from Electrical and Electronic Equipment (WEEE). In particular, experimental tests consisted in the treatment of materials by induction plasma source consisting in an induction plasma torch, a reactor, a graphite substrate or crucible, a powder injector.

In paragraph 1.1 an experimental study done in the framework of the LITCAR Laboratory is presented. In this work fluorescent lamps glass powders, sieved in two particle size ranges, have been subjected to thermal plasma in-flight treatment by injection into the discharge of a Tekna PL-35 plasma torch and reaction chamber as part of a source operated at 3MHz with a maximum power of 25kW, with Ar as plasma and carrier gas and N<sub>2</sub> as sheath gas. The sieved powders and the plasma treated ones have been characterized by powder XRD and particle size analysis in order to verify if the plasma treatment can induce modification in the mineralogical and physical characteristics. The spherical shape of the particles have been analyzed by scanning electron microscopy. Moreover, this technique has allowed to verify if the plasma treatment can induce modification of the (qualitative) chemical composition of the powder. Results for various operating conditions and injection probe positions are presented. The spherical powders have been then introduced in thermoplastic polymer (polypropylene) in place of glass spheres usually used, and the results are compared to each others. The samples are characterized by mechanical tests (flexural strength) and microstructural analysis (SEM) in order to verify the differences in materials properties obtainable by mean of conventional and plasma assisted processes.

In paragraph 1.2, an experimental study done in the framework of the ENVIREN project is presented. In this work a process of treatment, inertization and deposition on a graphite substrate and in graphite crucibles of fly ash and bottom ash coming from the Reggio Emilia incinerator through induction thermal plasma (Induction Coupled Plasma Torch) was carried out.

In particular, several experimental tests have been carried out to study the technical feasibility and the performances of different processes for the vitrification of bottom ashes and fly ashes from

incinerator on graphite substrates and into graphite crucibles placed in the reaction chamber during treatment.

The alternative procedures studied are the following:

- introduction of a mixture containing powder to be treated and SiO<sub>2</sub> powders into the plasma discharge, using a dispersion probe, and subsequent deposition of them on a substrate of graphite placed inside the reaction chamber;
- introduction of the powders to be treated into the plasma discharge through a dispersion probe and subsequent deposition of them in a molten pool of SiO<sub>2</sub> contained into a graphite crucible placed inside the reaction chamber;
- preparation of a mixture of powders to be treated and SiO<sub>2</sub> powders in the graphite crucible and subsequent treatment of the same by entering the crucible in the reaction chamber.

I also managed the acquisition and the activities of characterization and testing of a system for the injection of suspended nano-metric size particles and liquid inside the RF induction torch.

## **1.1 RF thermal plasma treatment of waste glass and its reutilization in composite materials**

Inductively coupled plasma torches (ICPTs) are successfully used as high-temperature sources in a wide range of applications, such as spheroidization and purification of both metallic and ceramic powders. However, the effectiveness of these processes strongly depends on a large number of parameters, including the torch operating conditions and the type and characteristics of the injected powders. This causes the try and fail approach to be expensive and difficult to carry out. In this frame, numerical modelling represents a useful tool that may help in the design and optimization of these processes. Recently, a new 3D FLUENT-based model for the evaluation of the trajectory and thermal history of particles injected, by means of an injection probe, together with a carrier-gas, into ICPTs working at atmospheric pressure has been presented by some of the Authors [1-4]. In this model, the gas injection section of an industrial Tekna Plasma Systems Inc PL-35 plasma torch, which is characterized by two different sets of 8 and 18 circumferentially distributed injection points with a diameter of 0.8 mm for the tangential plasma gas and the axial sheath gas, respectively, can be modelled without geometry simplifications, and the powder carrier gas, which is introduced axially in the plasma region by means of an injection probe, is also considered. In this paper we present a novel RF thermal plasma assisted process where the design of the experiment has been carried out on the basis of results previously obtained from numerical simulation for different types and characteristics of the injected particles. This plasma technology has been applied to powdered glass coming from the dismantling of fluorescent lamps. The end of life lamps are classified among the waste of electric and electronic equipment (WEEE) which contain dangerous substances, while, after their dismantling and claiming treatment, the resulting glass is not dangerous. Fluorescent lamps glass powders are subjected to thermal plasma in-flight treatment by injection into the discharge of a Tekna PL-35 plasma torch and reaction chamber as part of a source operated at 3MHz with a maximum power of 25kW, with Ar as plasma and carrier gas and N<sub>2</sub> as sheath gas. The sieved powders and the plasma treated ones have been characterized by powder XRD and particle size analysis in order to verify if the plasma treatment can induce modification in the mineralogical and physical characteristics. The spherical shape of the particles have been analyzed by scanning electron microscopy. Moreover, this technique has allowed to verify if the plasma treatment can induce modification of the (qualitative) chemical composition of the powder.

The spherical powders have been then introduced in thermoplastic polymer (polypropylene) in place of glass spheres usually used, and the results are compared to each others. The samples are characterized by mechanical tests (flexural strength) and microstructural analysis (SEM) in order to verify the differences in materials properties obtainable by mean of conventional and plasma assisted processes.

### **1.1.2 Pre-treatment of waste glass and chemical-physical analysis**

Fluorescent lamps glass powders are sieved in two particle size ranges  $75 < x < 125 \mu\text{m}$  (1P) and  $38 < x < 75 \mu\text{m}$  (2P). The sieved powders have been characterized by laser size analyzer (Malvern Mastersizer hydro 2000S) and by scanning electron microscopy analysis (SEM) (Philips XL 30 coupled with energy dispersion spectroscopy (EDS) EDAX 9900) on samples coated with a thin

Au/ Pd film, to determine the qualitative chemical composition of the powder (confirmed also by ICP (Philips, VARIAN 200)) and to verify if plasma treatment can induce modification in its physical and chemical characteristics. The  $75 < x < 125 \mu\text{m}$  sieved powder shows a particle size distribution with two fractions, one with a maximum between  $60\text{-}300 \mu\text{m}$ , and another centered on  $20 \mu\text{m}$ . The  $38 < x < 75 \mu\text{m}$  sieved powder shows a particle size distribution mainly corresponding prevalently to a Gaussian curve centered between  $20\text{-}200 \mu\text{m}$ , with a significant presence of fraction between  $0.7\text{-}20 \mu\text{m}$ .

### **1.1.3 Inductively coupled thermal plasma treatment of waste-glass**

Waste-glass powders have been treated within a laboratory scale RF thermal plasma source. The raw particles have been injected from top of the plasma torch, along its axis and in the plasma region by means of a water cooled injection probe has been set in a suitable axial position with respect to induction coil in dependence on powder sample and powder flow rate, in accordance with results of plasma behavior obtained by means of a 3D numerical simulation code developed at the University of Bologna and with the final aim of minimizing powder loss on plasma containment tube and chamber [1-4]. The treated powders have been collected at the bottom of the first chamber (reactor, 1C) as well as at the bottom of the second chamber (cyclone, 2C) (Fig. 1.1.1).

The plasma treated powders have been characterized by powder XRD (Philips PW 3710 with Ni-filtered  $\text{CuK}\alpha$  radiation) in the  $5\text{-}70 2\theta$  range and particle size distribution in order to verify if the plasma treatment can induce modification in the mineralogical and physical characteristics. The spherical shape of the particles and the qualitative chemical composition of the powder have been demonstrated by scanning electron microscopy analysis to verify if the plasma treatment can induce modification. By means of powder diffraction technique, the unaltered amorphous nature of the plasma treated powders have been confirmed. As regards particle size analysis, the fraction under  $20 \mu\text{m}$  visible in the  $75 < x < 125 \mu\text{m}$  sieved powder, disappears, independently by the chamber, and the Gaussian curve is more narrow and centered in the range of  $50\text{-}250 \mu\text{m}$  and  $50\text{-}200 \mu\text{m}$ , for reactor and cy-clone, respectively. This curve confirms the effectiveness of this thermal treatment. In the  $38 < x < 75 \mu\text{m}$  treated powder the spheroidization process eliminates completely the fraction between  $0.7\text{-}20 \mu\text{m}$  by the treatment in chamber 1, while after the treatment in chamber 2 forms a significant fraction between  $5\text{-}20 \mu\text{m}$ . From this analysis appears that the powder in the coarse particle size range gives a more homogeneous and narrow particle size distribution and consequently a more effective spheroidization process. The effectiveness of the plasma treatment in order to obtain a spheroidized powder has been evaluated by SEM analysis. From the micrographs appears evident that the powders with higher particle size (1P) (Fig. 1.1.3) are more homogeneous with respect to the finer ones (2P) (Fig. 1.1.2) and in particular for the larger powder the treatment in the second chamber (2C) produces a more regular spherical shape than the first chamber (1C). The dimensions of the main spheres are between  $60$  and  $130 \mu\text{m}$  for this samples, confirming the starting particle size of  $75 < x < 125 \mu\text{m}$ . The finer powders show a less homogeneous distribution of the spheres confirming the larger Gaussian curve characteristic of particle size distribution.

The dimensions of the spheres after the treatment in chamber 1 are in the range  $10\text{-}90 \mu\text{m}$ , while after the chamber number 2 are less than  $10 \mu\text{m}$ . Moreover, the SEM technique allows obtaining by means of energy dispersion spectroscopy (EDS) a qualitative chemical composition of the

spheroidized powders compared with the untreated ones. Results of this analysis show that the more significant effect of plasma treatment is related to a decrease of potassium and sodium, both in reactor and cyclone products, due to their high volatilization capability, explaining the mass balance loss between raw and treated material.

#### **1.1.4 Reuse of purified and spheroidized waste glass in thermoplastic polymers.**

The sieved and plasma treated glass powders have been introduced in a polymer matrix as reinforcement by means of mixer (Haake Rheocord) at 180°C for 15 min at 20 rpm. The chosen matrix has been polypropylene (PP). The PP used in this paper is for injection moulding because it is the kind of PP usually added with glass particles as reinforcement in order to modify the physical-mechanical properties. The mixtures behavior has been compared to PP mixed with industrial glass spheres (SVPP). The spherical powders appear to be homogeneously dispersed in the polymer matrix, as evidenced by SEM analysis (Fig. 1.1.4). An index of the material workability had been determined by the torque (N/m) measurement. The flexural strength of the samples, prepared according to ASTM D790 (80X10X3 mm<sup>3</sup>), has been measured by Instron and the fracture surfaces have been analyzed by SEM: the results obtained are summarized in Table 1.1.2. As regards workability, the addition of plasma treated powders does not modify significantly this property not causing flow problem during their processing. The same table shows that both the samples with un-treated powders are characterized by values of  $\sigma_{\text{yielding}}$  which are lower than the standard one; while both the samples, which show higher spheroidization rate by SEM analysis (1C2P and 2C1P), are characterized by higher values of mechanical properties. SEM analysis (Figure 1.1.4) confirms the higher mechanical property of these two samples as a result of an improved interface between the particle reinforcement and the PP matrix with respect to the addition of untreated powders. This improved inter-face is a consequence of the spherical geometry of particles, favoring the wet-ability with respect to the case of irregular particles. In this last case the presence of sharp edges worsens the adhesion between reinforcement and matrix.

Plasma gas and flow rate	Argon – 12 slpm
Sheath gas and flow rate	Nitrogen – 60 slpm
Carrier gas ad flow rate	Argon – 5 slpm
Tip of injection probe position	3 cm within coil region
Powder feeding rate – sample one (75-135 $\mu\text{m}$ )	16.7 g/min
Powder feeding rate – sample two ( 35-75 $\mu\text{m}$ )	16.7 g/min
Plate power	32 kW
Chamber pressure	14 kPa
<b>Table 1.1.1.</b> Experimental conditions for plasma treatment of in-flight waste-glass powders. Taken from [23-24]	

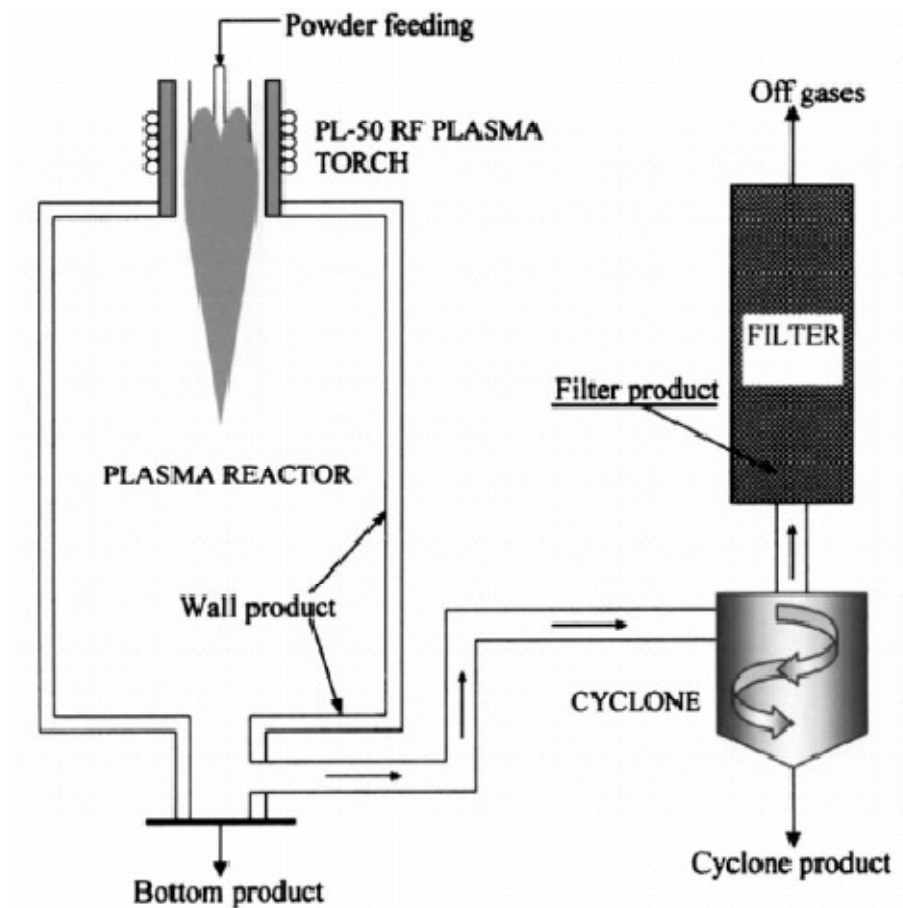
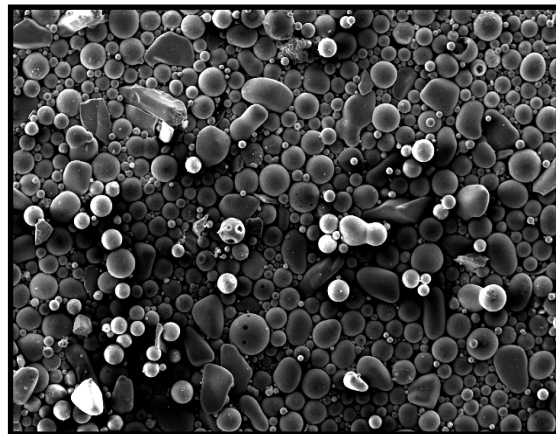


**Figure 1.1.1** Schematic illustration of inductive plasma reactor system (modified from [5]).



— 50  $\mu\text{m}$ .

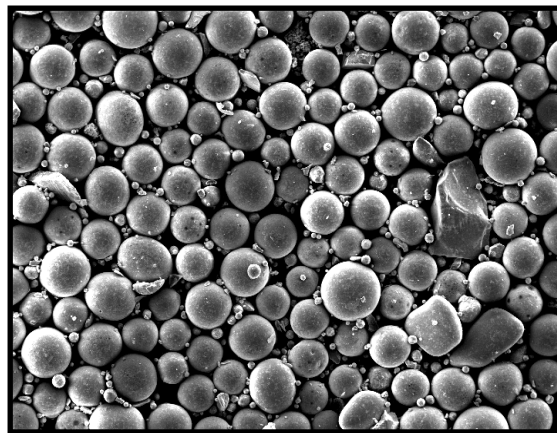


— 50  $\mu\text{m}$ .

**Figure 1.1.2** SEM morphologies of the 2P powder raw (left) and after plasma treatment (right) as obtained in the first chamber (reactor). Taken from [23-24]

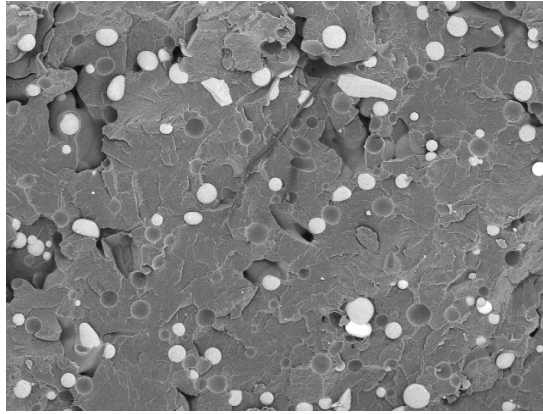


— 50  $\mu\text{m}$ .



— 50  $\mu\text{m}$ .

**Figure 1.1.3** SEM morphologies of 1P sample powder raw (left) and after plasma treatment (right) as obtained in the second chamber (cyclone). Taken from [23-24]

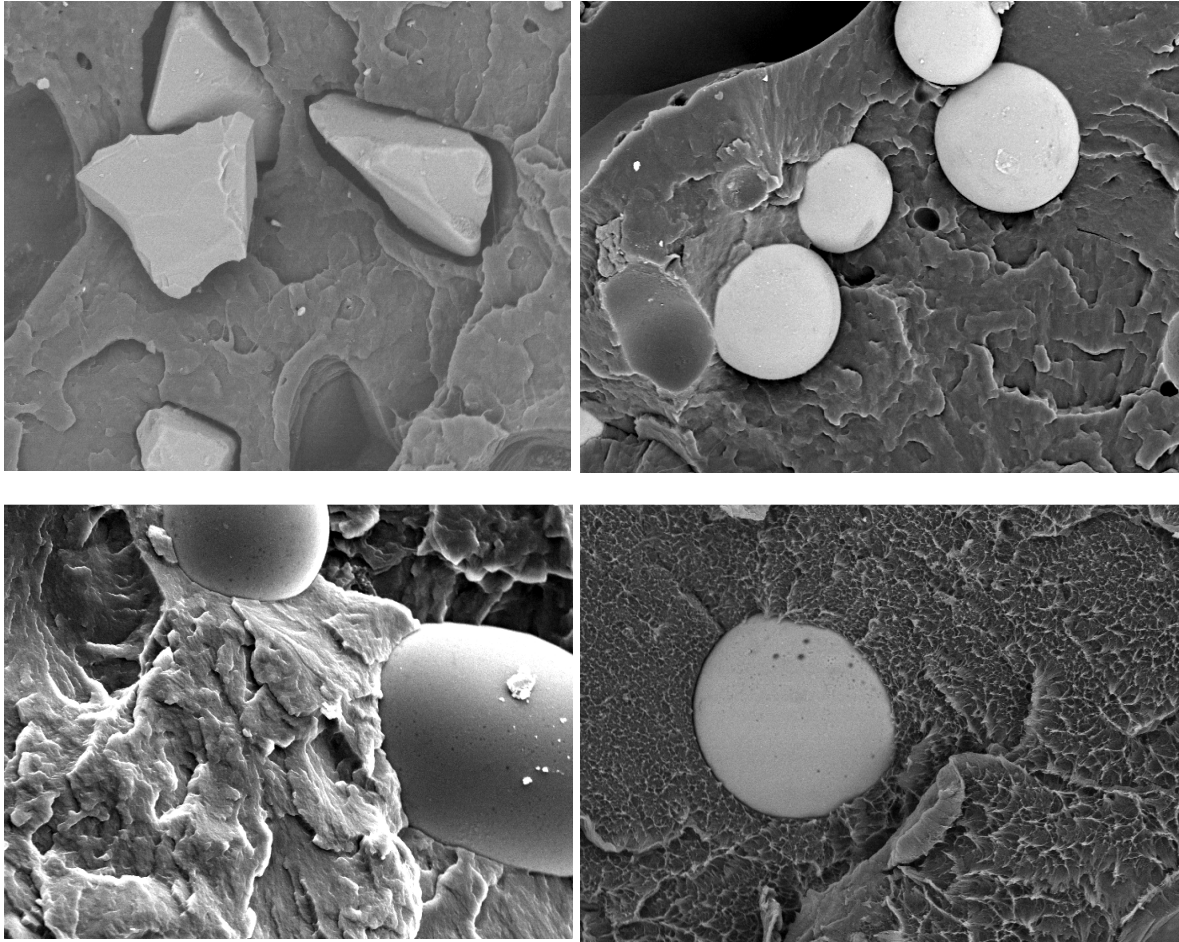


0,5 mm

**Figure 1.1.4** SEM micrograph showing the spheres distribution in the PP matrix. Taken from [23-24]

Samples	Torque (N/m)	$\sigma_{\text{yielding}}$ (MPa)
svpp	2,4	22,9
75pp	2,6	20,9
pp1c1p	2,6	22,9
pp2c1p	2,7	23,4
38pp	2,8	22,4
pp1c2p	2,4	23,4
pp2c2p	2,8	21,4

**Table 1.1.2.** Mechanical and workability properties of the PP mixed with the industrial glass spheres (SVPP) and with the raw (75PP and 38PP) and plasma treated waste-glass ones. Taken from [23-24]



— 10  $\mu\text{m}$ .

**Figure 1.1.5** SEM micrographs (500X) of PP reinforced with raw and plasma treated waste-glass samples. Taken from [23-24]

## **1.2 RF thermal plasma vitrification of incinerator bottom and fly ashes with waste glasses from fluorescent lamps**

The problem of the waste disposal is taking in Italy and elsewhere in the world an ever-increasing importance because of the growing production of waste materials and the increasing difficulty that the traditional collection and disposal strategies encountered in the process. In this field, new European regulations have been introduced that attempt to modify and modernize the strategies used in waste management: faced with a restriction of materials that can be put in landfill and more control on the impact that these ones have on the environment, which results in a disincentive to their use, there is an emphasis on practices of reuse, recycling and recovery of raw materials. When these practices are not feasible, in any case the incineration is preferred to the use of landfill disposal because it reduces the waste volume and can be joined to incinerators. Therefore, to reduce the amount of municipal solid waste deposited in landfill, in recent years we are witnessing the construction of a number of incineration plants.

The practice of incineration, however, presents some critical aspects: the fumes produced during treatment and waste production. These compounds are the ashes from the combustion of waste that are collected or at the bottom of the furnace ("bottom-ash ") or in gas phase filtration ("fly-ash"). In particular, the "fly-ash "with their compact dimensions, the heavy metal content and products resulting from partial and incomplete combustion of the constituents of the waste (polycyclic aromatic hydrocarbons, polychlorinated biphenyls, benzene, heavy metals and dioxins), are very hazardous to health. In fact, the most recent regulations require special attention to this detail and require the use of methods and technologies in order to ensure a high level protection of environment and public health.

Usually this waste, which require disposal in landfills, are previously immersed in cement to reduce the dispersion of pollutants in the environment. Recently, however, the idea of reusing these wastes as raw materials in the construction field has been introduced. To enable this transformation from waste to new raw material is necessary to study and implement processes that make inert harmless these ashes: the way is to melt the powder and then cool them quickly to obtain a solid glassy. For the physical characteristics of these materials, heat sources at high temperature are necessary and plasma-assisted technologies, given the high temperatures that can reach, are a powerful tool in this field, as shown by many studies already carried out [6-7].

High plasma temperatures enable to destroy complex molecules and to encapsulate the toxic elements in a non-leaching glass or ceramic matrix, obtaining non-hazardous wastes with large volume reductions [6-9].

The first ideas of making use of thermal plasma technology for waste processing go back to the early-1970's during the energy crisis period [6,7]. As the etymological origin of the own word indicates, "crisis" is synonymous of analysis and different measures were introduced to change something that hadn't worked properly before. It was during these years when society was concerned over resources scarcity, and where, for the first time, great developments of alternative energy forms took place. As a consequence, debates grew over the technical feasibility and

economic viability of new alternative energy sources, and the possibility of using plasma technology as a recovery source was considered for the first time [8-10]. Since then, many investigations came off, and in the 1980's thermal plasma technology evolved significantly by the strong drive for high-performance materials and the growing need for new material-processing technologies [11]. Some of these advances induced Japan, due to their limited land mass, to install in the early-1990's the first commercial facility for the treatment of municipal solid waste incineration ash.

Waste treatment has become one of the main problems of our age, as traditional waste repositories, such as landfills and ocean dumpsites, become less and less available. Because of the ability of the plasma to vaporize anything and to destroy any chemical bond, plasma technology has become a valid and effective alternative to the treatment of wastes [12-15].

Different plasma technologies and other thermal treatments have been already used to vitrify incinerator bottom ash [16] as well as incinerator fly ash [17], but there has been no one reported with the RF thermal plasma source yet.

Actually, DC plasma arc generators are considered a better alternative rather than AC ones for hazardous waste treatment, because of less flicker generation and noise, a more stable operation, better control, a minimum of two electrodes, lower electrode consumption, slightly lower refractory wear and lower power consumption [18]. Nevertheless, inactivity periods are expected due to the electrodes routine maintenance. Moreover, reactive gas cannot be used with some categories of electrodes, whereas with the Inductively Coupled Plasma Torches (ICPTs), since the plasma gas does not come in contact with electrodes, possible sources of contamination are eliminated and a wide range of operating conditions including inert, reducing and oxidising, and other corrosive atmospheres are allowed for their operation. For these reasons, and for the flexibility showed when different operating conditions (powder, gas flow, injected material) are changed, ICPTs can be considered as a valid alternative for the treatment of wastes.

Therefore, the main objective of this work was to investigate the feasibility of using a RF thermal plasma source technology to treat hazardous incinerator residues, adding fluorescent lamps glass powders to produce a single-phase amorphous glass, and to characterize the obtained glassy material in terms of leaching behaviour.

Experimental tests for the vitrification of hazardous incinerator residues (bottom and fly ashes) coming from incinerator with the addition of coarse scraps and powders of glass from dismantled fluorescent lamps[10] have been carried out with a laboratory scale radiofrequency (RF) thermal plasma in different operating conditions and with different experimental set-up, in order to identify the optimal conditions for the achievement of non hazardous slags.

The basic principle of the RF plasma source vitrification process consists in the powder injection from the top of the plasma torch, along its axis and in the plasma region by means of a water cooled injection probe. During these experiments, treated powders have been collected in a graphite crucible in order to obtain a final glass deposit that can be further characterized.

In a first phase of the accomplished experimental procedure, glass scraps were collected into a graphite crucible and exposed to the plasma heat flux, resulting in a melted batch. In a second

phase, the incinerator ashes were injected as powders in the plasma discharge and in-flight treated, with subsequent deposition into the crucible containing the melted glass. In order to assess the minimum concentration of glass needed to achieve non-hazardous slags, several experimental tests have been carried out with different amounts of injected ashes, for a constant content of glass scraps introduced in the crucible. The obtained samples were characterized by scanning electron microscopy analysis (SEM), energy dispersion spectroscopy (EDS), X-ray diffraction (XRD) and leaching tests. The latter showed that toxic elements were completely encapsulated in the glass matrix, with release values below the law limits. Results of this work demonstrate the feasibility of bottom and fly ash vitrification in a batch of glass scraps from dismantled fluorescent lamps and can also provide useful insights for the optimization of vitrification processes carried out by the more widespread arc plasma furnaces.

### 1.2.1 Experimental set-up

#### *Hazardous incinerator residues*

Bottom and fly ashes used during this work came from an Energy Waste plant in Reggio Emilia, which processes approximately 51,000 ton of municipal solid waste per year.

Morphological characterization of bottom and fly ashes have been carried out before treatment with the scanning electron microscopy (SEM) (Philips XL 30 coupled with energy dispersion spectroscopy (EDS) Oxford INCA-350). These analysis showed that both compositions are characterized by the presence of glass formers as main components: Si, Ca, Al. The bottom-ashes have a highest percentage of Na, K and Cu, while fly ashes are characterized by a high concentration of P, Ti, V, Zn and Cr.

Crystalline phase analysis of both residues have been carried out by X-ray diffraction (XRD), and confirm the results obtained with the previous characterization tests. Percentage compositions of both samples are shown in Tables 1 and 2.

P.F.	Na <sub>2</sub> O	MgO	Al <sub>2</sub> O <sub>3</sub>	SiO <sub>2</sub>	P <sub>2</sub> O <sub>5</sub>	K <sub>2</sub> O	CaO	TiO <sub>2</sub>	MnO	Fe <sub>2</sub> O <sub>3</sub>	PbO	ZnO	Cu <sub>2</sub> O
1,7	2,21	4,5	12,97	32,69	2,63	1,62	34,27	1,48	0,14	5,52	0,32	0,26	0,11

**Table 1.2.1.** percentage composition of bottom ashes by XRD

	Na <sub>2</sub> O	MgO	Al <sub>2</sub> O <sub>3</sub>	SiO <sub>2</sub>	P <sub>2</sub> O <sub>5</sub>	K <sub>2</sub> O	CaO	TiO <sub>2</sub>	MnO	Fe <sub>2</sub> O <sub>3</sub>	PbO	ZnO	Cu <sub>2</sub> O
1,97	9,31	4,11	11,57	21,47	2,70	2,89	40,31	2,79	0,12	2,77	0,25	0,45	0,06

**Table 1.2.2.** percentage composition of fly ashes by XRD

### *Fluorescent lamps*

Fluorescent lamps represent about 70% of the total consumption of electrical lighting in Italy; also in the United States about 620 million of fluorescent lamps are discarded annually [19]. These lamps are a particular kind of discharge lamp, in which the light is generated by a fluorescent material and they are constituted mainly by glass and small amount of Hg, inert gas (generally argon) and phosphorous. During the accomplished experiments, the fluorescent lamps glass scraps undergo a high temperature process that allow to vaporize the total mercury content. Therefore, after the plasma treatment, the resulting glass is not dangerous and can be classified as CER 19 12 05 [20].

### *RF plasma source*

The experimental setup used in this work is shown in Figure 1.2.1. The laboratory scale RF thermal plasma source includes: radio frequency plasma torch, model Tekna PL-35 (with ceramic confinement tube for operation up to 30kW); 25 kW LEPEL unit RF power supply working at 3 MHz; a control console Tekna Plasma Systems (Sherbrooke, Quebec, Canada) RF-CS-30 with gas flowmeters for operation with Ar, Ar/H<sub>2</sub> or any other auxiliary gas (Air, N<sub>2</sub>, O<sub>2</sub>); Tekna Plasma Systems external cooling system; Tekna Plasma Systems powder feeder PF-400, from where particles are injected in the plasma discharge; adjustable water-cooled arm to put the graphite crucible inside the reactor chamber. This steel device, generally used for ash vitrification purposes, helps to regulate the distance between the exit of the torch nozzle and the crucible from 104mm (highest position) to 134mm (lowest position).

### **1.2.3 Plasma treatment**

The operating conditions used during each experimental test are shown in Table 3. In the first one, bottom ashes and fluorescent lamps glass powders have been injected in the plasma discharge at the same time and with the same percentage (50%), whereas in the second one, the same test has been carried out using fly ashes instead of bottom ashes. The main operating parameters for both experiments are very similar, using argon as a fluidization gas in the fly ash treatment to improve the powder flow rate at the exit of the powder feeder.



**Fig.1.2.1.** Picture of the experimental set-up

	<i>BOTTOM ASH</i>	<i>FLY ASH</i>
Plasma gas and flow rate	Argon – 15 slpm	Argon – 15 slpm
Sheath gas and flow rate	Argon – 50 slpm, Hydrogen 10 slpm	Argon – 50 slpm, Hydrogen 10 slpm
Carrier gas and flow rate	Argon – 5 slpm	Argon – 3 slpm
Fluidization gas and flow rate	-	Argon – 2 slpm
Distance exit torch nozzle - crucible	13,4 cm	13,4 cm
Ash quantity	50g	100g
Powder feeding rate	5,6 g/min	7,2 g/min
Plate power	23,4 kW	22,75 kW
Chamber pressure	13,5 kPa	13,5 kPa
Exposure time	20 minutes	20 minutes

**Table 1.2.3.** Experimental conditions for plasma treatment of in-flight bottom and fly ashes with waste-glass powders

### 1.2.4 Characterization of the obtained glassy slags

In both experiments, the glassy slag obtained after the treatment, has been crushed to powder in order to make possible the characterization of their chemical composition with the scanning electron microscopy (SEM) combined with energy dispersive X-ray spectrometry (EDS). SEM micrographs suggest that in both cases the main matrix is formed by the typical glass phase, with a certain quantity of small metallic spheroidized particles (Fig. 1.2.2). EDS analysis have been carried out (Fig. 1.2.3) to confirm results obtained with the SEM analysis. Similar peaks of main glass formers, such as Si, Ca and Al can clearly be seen in both graphs of Fig. 1.2.3. The Na and Ti peaks, can be related to the different original composition of bottom and fly ashes.

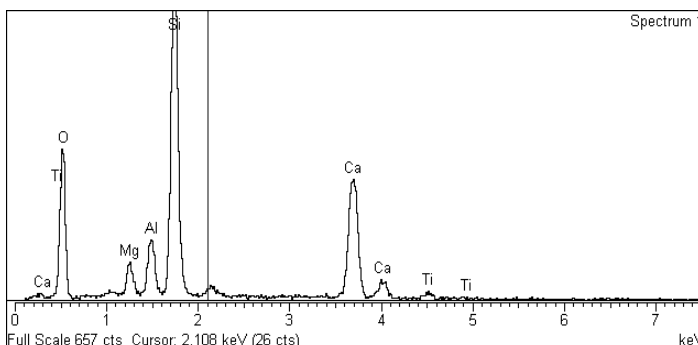
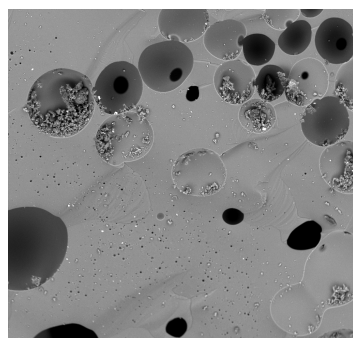
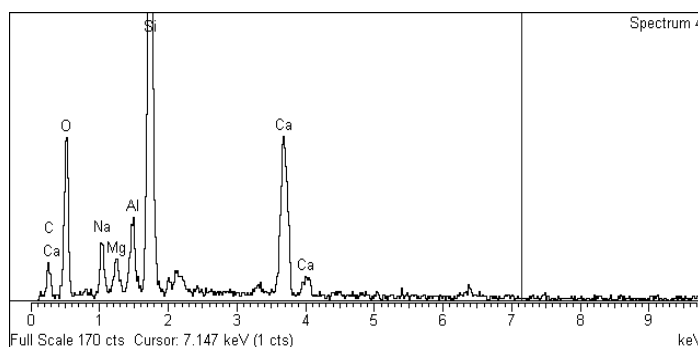
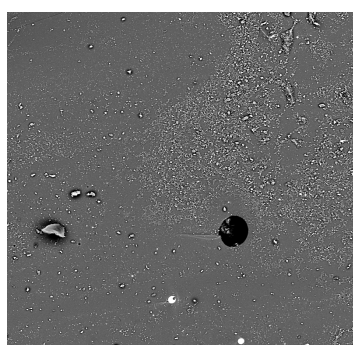


**Figure 1.2.2.** SEM morphologies of (a) bottom ash glassy slags and (b) fly ash glassy slag

**Figure 1.2.3.** EDS spectra of (a) bottom ash glassy slags and (b) fly ash glassy slag

XRD data given in Figures 1.2.4 and 1.2.5 confirm the typical broad band of amorphous nature glasses, where crystalline phases have not been formed.

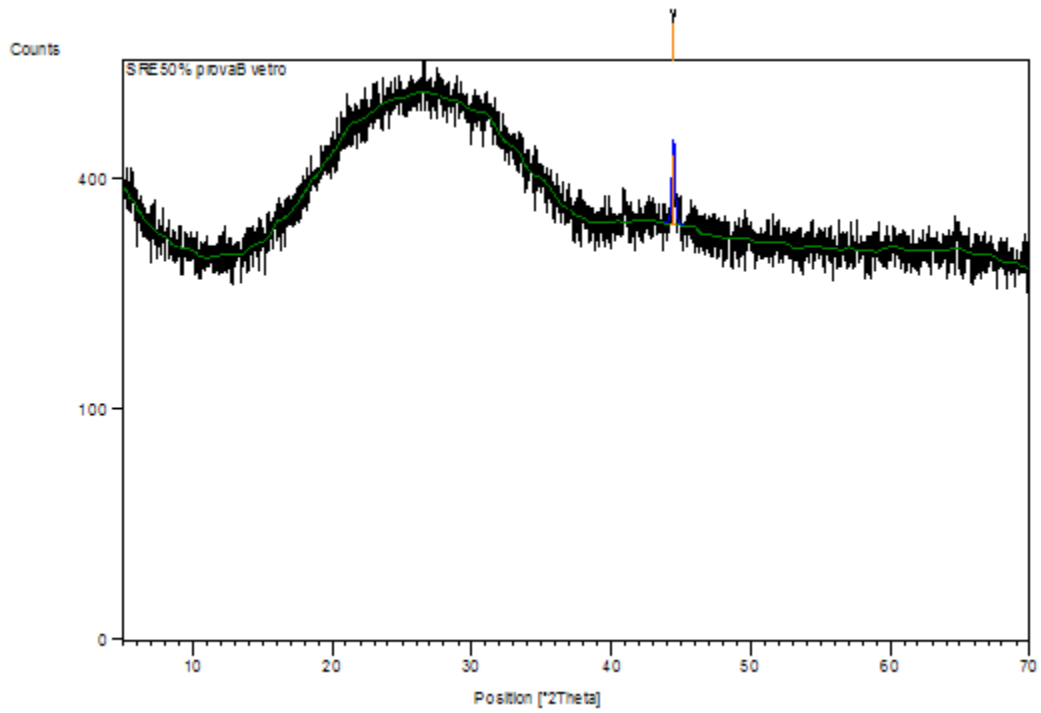


**Figure 1.2.4** XRD graph of the plasma treated bottom ash glassy slags

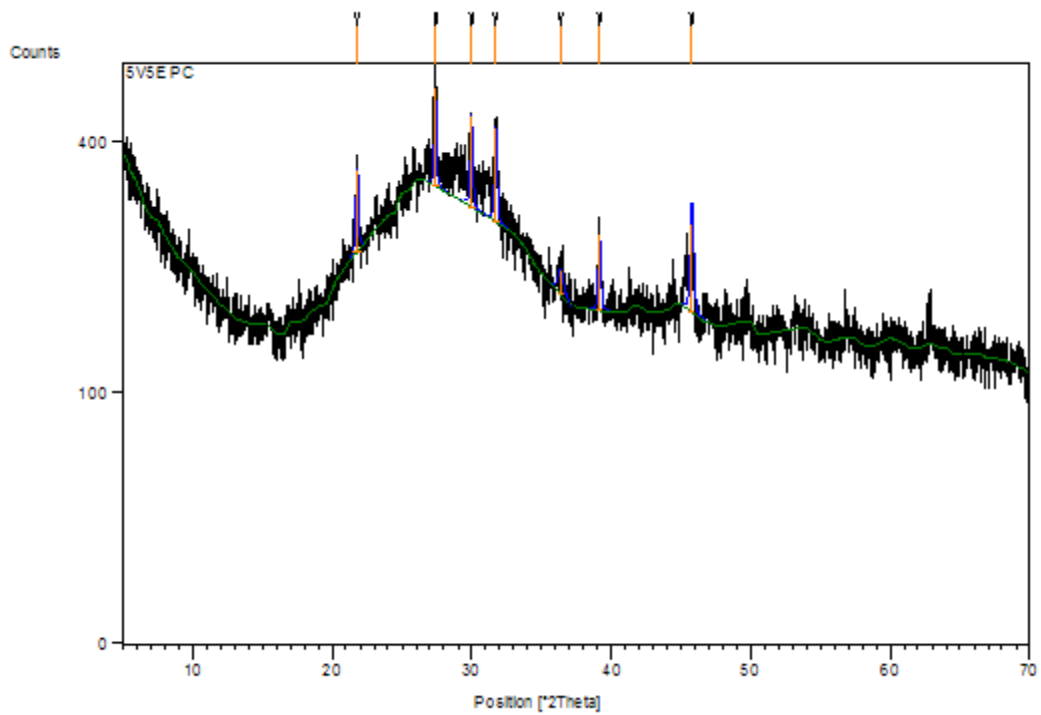


**Figure 1.2.5** XRD graph of the plasma treated fly ash glassy slags

Before the final leaching tests, and in order to confirm the chemical composition of each sample after the plasma treatment, chemical analysis have been accomplished (Table 1.2.4). These results confirm once again the glassy nature of the treated hazardous incinerator residues. The Pb disappearance and the great Zn decrease are also interesting data.

Oxide	Bottom ash treatment %	Fly ash treatment %
SiO <sub>2</sub>	47,70	46,70
CaO	15,30	25,80
Br	13,50	10,70
Al <sub>2</sub> O <sub>3</sub>	7,14	8,05
Na <sub>2</sub> O	5,59	2,20
Fe <sub>2</sub> O <sub>3</sub>	5,09	0,573
MgO	2,19	2,71
K <sub>2</sub> O	0,932	0,335
P <sub>2</sub> O <sub>5</sub>	0,807	0,354
TiO <sub>2</sub>	0,618	1,61
As <sub>2</sub> O <sub>3</sub>	0,270	0,182
SO <sub>3</sub>	0,238	0,127
BaO	0,213	0,352
CuO	0,142	-
ZnO *	977	199
MnO *	499	385
Cr <sub>2</sub> O <sub>3</sub> *	450	486
SrO *	384	661
Cl *	355	-
NiO *	263	254
Zr *	112	193
V <sub>2</sub> O <sub>5</sub> *	76	165
RbO <sub>2</sub> *	-	28
<b>Total</b>	<b>98,69</b>	<b>95,90</b>
* Measured in ppm		
<b>Table 1.2.4</b> Chemical composition of glassy slags coming from bottom/fly ashes treatment		

Compliance leaching test results for hazardous residues derived glass are given in Table 1.2.5. In order to determine the risk category of the discharge, the UNI ISO 10802 rule includes the procedure to carry out a leaching test. Every single metallic element must be below the law limit indicated by the Waste Acceptance Criteria (WAC). Table 1.2.5 demonstrates that the concentrations of heavy metals in leachates were below the law limits (Tab 5 DM, decree passed by the Italian Government 03/08/2005) [21-22], and these results evidence that plasma treated hazardous incinerator residues are suitable for disposal to inert waste landfill. Furthermore, the relatively low leachable level of the elements that constitute the crystal lattice (Al, Na and Si) guarantee a high-resistant glass material.

	<i>Cu</i>	<i>Mn</i>	<i>Ba</i>	<i>Zn</i>	<i>Cr</i>	<i>As</i>	<i>Ni</i>	<i>V</i>	<i>Al</i>	<i>Na</i>	<i>Si</i>
WAC	5 ppm	Nd	10 ppm	5 ppm	1 ppm	0.2 ppm	1 ppm	nd			
Bottom	4,54	0,185	0,304	0,150	0,026	0,019	0,88	0,133	5,27	12,1	0,72
Fly	0,366	0,29	2,170	0,075	0,051	0,061	0,032	0	21,1	31,2	4,14

**Table 1.2.5** Compliance leaching test for bottom/fly ash glassy slags

## **Conclusions and future developments**

The accomplished studies demonstrated the effectiveness of the use of inductively coupled plasma torches (ICPTs) as high-temperature sources for the treatment and the value increasing of hazardous wastes for different applications. Despite this, the upscaling of these processes for their industrial application is still far.

Results showed in paragraph 1.1 confirms the higher mechanical property of the obtained samples as a result of an improved interface between the particle reinforcement and the PP matrix with respect to the addition of untreated powders. This improved interface is a consequence of the spherical geometry of particles, favouring the wet-ability with respect to the case of irregular particles. In this last case the presence of sharp edges worsens the adhesion between reinforcement and matrix.

The process that has been proposed still needs to be fully investigated with the final aim of optimizing plasma operating conditions with respect to plasma/sheath gas type, to raw powder average dimensions and most of all to carrier gas flow rate which might have strong impact on spheroidization rate (the ratio of number of spherical particles as determined under optical microscopy over the total number of particles in the treated sample). Also the degree of evaporation of waste-glass particles during plasma treatment will have to be considered in a future analysis. Furthermore, from the characterisation of the obtained materials appears evident that it is not necessary a stronger milling process ( $38 < x < 75 \mu\text{m}$ ) in order to obtain workability and mechanical properties values comparable to those characteristic of PP added with industrial spheres. This represents an environmental and economical advantage.

Results presented in paragraph 1.2 showed that the use of crucible instead of substrates allowed to increase the percentage quantity of collected powders and to effectively create a molten pool, moreover the use of  $\text{SiO}_2$  demonstrated to be necessary to obtain a uniform glassy scarp. Finally, the effectiveness of vitrification of hazardous incinerator residues (bottom and fly ashes) with a laboratory scale radiofrequency (RF) thermal plasma source have been demonstrated. The process also allows the waste fluorescent lamps dismantling . EDS and XRD analysis show the glassy nature of the obtained samples, and from the leaching tests appears evident that concentrations of heavy metals are surely below the law limits.

Future developments will imply the optimization of the operating conditions and of the experimental set-up, in order to increase the process efficiency in terms of duration and cost of the treatment process. The proper optimization of the lab-scale process will then be a necessary precondition for implementing the next phase of scaling-up of the process for industrial applications.

## References

- [1] D. Bernardi, V. Colombo, E. Ghedini, A. Mentrelli, T. Trombetti, *European Physical Journal D*, **28**, pp. 423-433 (2004).
- [2] D. Bernardi, V. Colombo, E. Ghedini, A. Mentrelli, T. Trombetti, *IEEE Transactions on Plasma Science*, **33**, pp. 424-425 (2005).
- [3] D. Bernardi, V. Colombo, E. Ghedini, A. Mentrelli, *IEEE Transactions on Plasma Science*, **33**, pp. 426-427 (2005).
- [4] D. Bernardi, V. Colombo, E. Ghedini, A. Mentrelli, *Pure and Applied Chemistry*, **77**, pp. 359-372 (2005).
- [5] M.I. Boulos, R. Ye, T. Ishigaki, J. Jurewicz, P. Proulx, *Plasma Chemistry and Plasma Processing*, **24**, no. 4, pp. 555-571 (2004).
- [6] Camacho, Salvador L. ; “Refuse Converting Method and Apparatus Utilizing Long Arc Column Forming Plasma Torches”, (1973) U.S Patent Number 3779182
- [7] Camacho, Salvador L., Louis J. Circeo, Jr. ; “Apparatus and Method for the Recovery of Fuel Products from Subterranean Deposits of Carbonaceous Matter Using a Plasma Arc”, (1978) U.S Patent Number 4067390
- [8] Melosi, Martin V. ; “Coping with Abundance: Energy and Environment in Industrial America” Temple University Press, Philadelphia (1985)
- [9] Feldman, David Lewis ; "How Far Have We Come?" (1995) *Environment*, May, 16-24
- [10] Betz, Kenneth W. ; "Remembering the Energy Crisis," (1998) *Energy User News*, December, 4-6
- [11] Boulos, M. I. ; “Thermal plasma processing”, *IEEE Trans. Plasma Sci.* **19** (1991) 1078–1089
- [12] J. Heberlein, A. B. Murphy; “Thermal plasma waste treatment”, (2008) *J. Phys. D: Appl. Phys.* **41** 053001
- [13] D. A. Counts, B. D. Sartwell, S. H. Peterson, R. Kirkland, N. P. Kolak; “Thermal Plasma Waste Remediation Technology: historical perspective and current trends”, (1999) U.S. Naval Research Laboratory Report NRL/MR/6170-00-8835
- [14] M. I. Boulos, P. Fauchais, E. Pfender; “*Thermal plasmas - fundamental and applications*”, Plenum Press, New York (1994)
- [15] T. W. Cheng, J. P. Chu, C. C. Tzeng, Y. S. Chen; “Treatment and recycling of incinerated ash using thermal plasma technology”, (2002) *Waste Management* **22**(5) 485-490

- [16] Barbieri, L., Lancellotti, I., Pellacani, G.C. ; “Vitrification of municipal waste incinerator bottom ash and product properties”, (1998), Proceedings of XVIII International Congress on Glass, The American Ceramic Society, 21-30
- [17] Boccaccini, A.R., Schawohl, J., Kern, H., Schunck, B., Rincon, J.M., Romero, M. ; “Sintered glass ceramics from municipal incinerator fly ash”, (2000), *Glass Technology* **41**, 99-105
- [18] Gomez, E., Amutha Rani, D., Cheeseman, C.R., Deegan, D., Wise, M., Boccaccini, A.R.; “Thermal Plasma Technology for the Treatment of Wastes: A Critical Review” (2008) *Journal of Hazardous Materials* **161** (2-3) 614-626
- [19] Aucott, M., McLinden M., Winka M. ; “Release of Mercury from Broken Fluorescent Bulbs” *Journal of the Air & Waste Management Association* (2004)
- [20] V. Colombo, A. Concetti, E. Ghedini, F. Andreola, L. Barbieri, E. Fabbri, I. Lancellotti, P. Pozzi. (2007). RF Thermal Plasma Treatment of Waste Glass: Design of the Experiment with 3D Modelling and Glass Reutilization in Composite Materials. *18th International Symposium on Plasma Chemistry Abstract and Full-Papers CD*. 18th International Symposium on Plasma Chemistry - ISPC18. Kyoto University, Japan. 26-31 august 2007.
- [21] Italia. Ministero dell’Ambiente e della Tutela del Territorio. Decreto Ministeriale 3 agosto 2005. “Criteri e procedure di ammissibilita' dei rifiuti nelle discariche”, in conformita' a quanto stabilito dal decreto legislativo 13 gennaio 2003, 36, *Gazzetta Ufficiale* **201**, 30 agosto 2005.
- [22] Centioli, D., Comans, Rob N.J., Gaudino, S., Galas, C., Belli, M. ; “Leaching tests: useful tools for the risk assessment of contaminated sediments” (2008) *Ann Ist Super Sanità* **44** (3) 252-257
- [23] V. Colombo, E. Ghedini, G. Masini, D. Russo, F. Andreola, L. Barbieri, E. Fabbri, I. Lancellotti, P. Pozzi. (2006). RF Thermal Plasma Treatment of Waste Glass and its Reutilization in Composite Materials. *High Technology Plasma Processes 9 - HTPP9, St. Petersburg*
- [24] V. Colombo, E. Ghedini, G. Masini, D. Russo, F. Andreola, L. Barbieri, E. Fabbri, I. Lancellotti, P. Pozzi. (2006). *Journal of High Temperature Material Processes*, 10, 2, 207

## **Chapter 2**

### **Scaling-up of ICP technology for continuous production of Metallic nanopowders for Battery Applications**

During my Ph.D. I collaborated at the European research project SIMBA - “Scaling-up of ICP technology for continuous production of Metallic nanopowders for Battery Applications” – Call identifier: FP7-NMP-2008-2.1-2 where the University of Bologna participated as leader in the work-package on the modelling of induction plasma sources.

I was involved on the fluid-dynamic simulations of lab-scale ICPT systems used by the project partners for the lab-scale experimental tests whose results will be used for the design of a new reaction chamber for the optimization of nanopowder synthesis process at the laboratory scale. This studies have been done in collaboration with P. Sanibondi [1]. In the following paragraphs some of the obtained results have been reported.

#### **2.1 The SIMBA project**

Although nanotechnology, and particularly the development of nanoparticles-based materials, has advanced rapidly in recent years, industrial production techniques have not kept pace. At this point there is a substantial need for safe production facilities, enabling the synthesis of large amounts of metallic nanoparticles with controlled and uniform quality (particle size, particle size distribution, chemical composition, etc.). The SIMBA project will respond to this need by developing an industrial production line including on-line monitoring systems, assuring at the same time a high quality of the synthesized product as well as safety for the operating personnel and surrounding environment. The nano-structured materials of interest for this project are silicon and silicon-based alloyed nanoparticles, which have a huge potential as anode material in battery applications.

The production technology proposed is the Inductively Coupled Plasma (ICP) technique, which generates a high temperature thermal plasma discharge at atmospheric pressure. Since most of the ICP processes currently available are batch processes, the core of this project is the transfer of the ICP towards an industrial scale permitting the continuous production of a wide range of semiconductor or metallic (alloyed) nanoparticles. In order to achieve this, major scientific breakthroughs are required such as the incorporation of a novel on-line functionalization technique, the design of an industrial powder injection system to ensure a continuous production, on-line monitoring techniques to ensure quality and safety and advanced modelling of the particle trajectories in the ICP plasma.

The resulting industrial production line will provide maximum production efficiency by virtue of fully automated and controlled feeding of raw materials and optimal reactor processing including evacuation of the processed powders. An additional advantage of this industrial line will be the recovery and recycling of excess precursor components and gases. The overall objective of this project is to transfer the ICP processing knowledge and technology investigated at a lab-scale (10-100 g/h) to an industrial scale apparatus for the continuous production of tailored oxygen-free Si-based nanopowders at a production rate between *1 and 10 kg/hour*.

The *modelling* of the plasma flow dynamics and particle trajectories will permit to define the process at different scales, to predict the influences of the main process parameters and to design an optimum reactor chamber to increase the flow of particles for collection.

## 2.2. Characterization of the lab-scale ICPT system at EMPA

### *Evaporation rate of the Si precursor*

One of the most important technologic issues for the scaling up of the nanopowder production is the evaporation of the precursor. Especially when the precursor is solid, the energy subtracted to the plasma by the heated powders can be enough to cool down the plasma discharge (loading effect) and cause a technological limit in the evaporation process. This is a know issue from experimental point of view but a modelling approach to this problem gives new insight in how it could be avoided.

Several simulations have been carried out with different types of Silicon powder precursors and different powder feed rates. Two distributions of commercial powders have been used: Keyvest powders (mean diameter = 14µm) and Brodmann powders (mean diameter = 33µm), as shown in figure 2.2.1. PSD for these powders are shown in figure 2.2.1. Computation have been carried out for these operating conditions reported in table 2.2.1.

Power coupled (kW)	Sheath gas	Central gas	Feed gas	pressure	f(MHz)
10 kW – 20 kW	60 Ar + 6 H <sub>2</sub>	12 Ar	6.5 Ar	400 mbar	3-13.56

Table 2.2.1: operating conditions considered for accomplished computations

A bigger precursor will have a higher thermal inertia but it will result in a lower loading effect with respect to a smaller precursor: thus, it is difficult to find which one will results in a higher evaporation rate. Simulations have been carried out for these two types of precursor, for different powers coupled to the torch (from the usual value of 10 kW up to the unrealistic value of 20 kW) and different precursor feed rates (from 1 to 5 g/min), as shown in figure 2.2.2. For powder feed rate higher than 2 g/min no complete evaporation can be achieved even with the unrealistic power of 20 kW. For the case at 10kW, Brodmann powders generally have higher evaporation rate than

Keyvest powders, except for precursor feed rate lower than 1 g/min where the loading effect still doesn't create a cold central channel with plasma temperature below the evaporation temperature of Silicon (figure 2.2.3). For the unrealistic power of 20 kW, the Keyvest powders have higher evaporation rate for the whole range of powder feed rate considered. The evaporation efficiency, defined as the ratio between the evaporation rate and the precursor feed rate, for different precursor types and different values of power coupled to the torch, is shown.

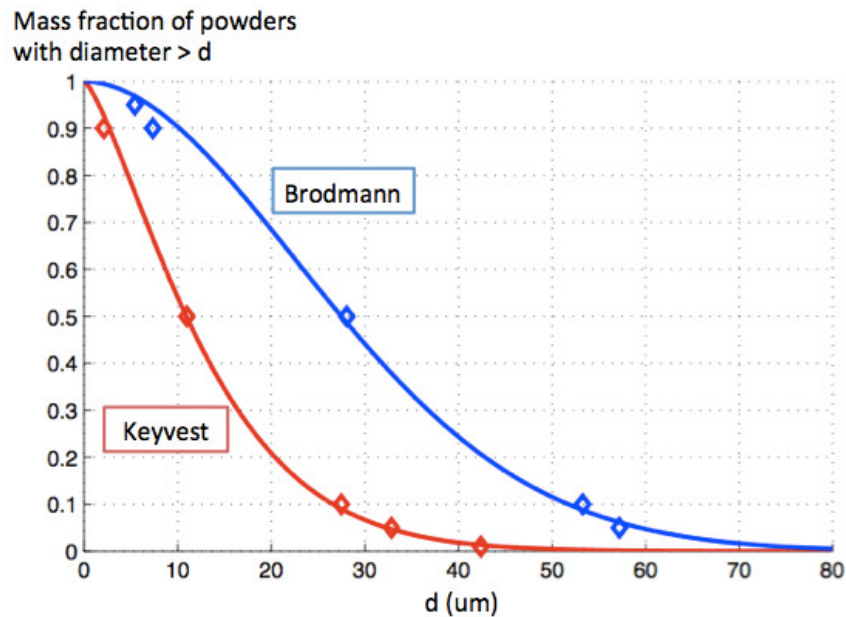


Fig. 2.2.1 Particle size distribution of Keyvest and Brodmann powders.

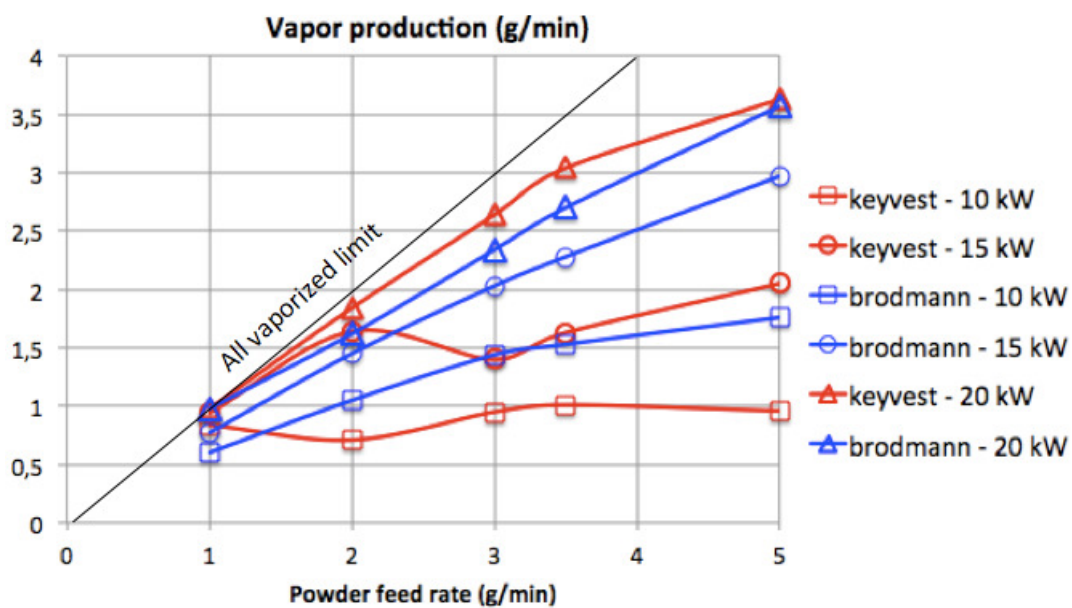
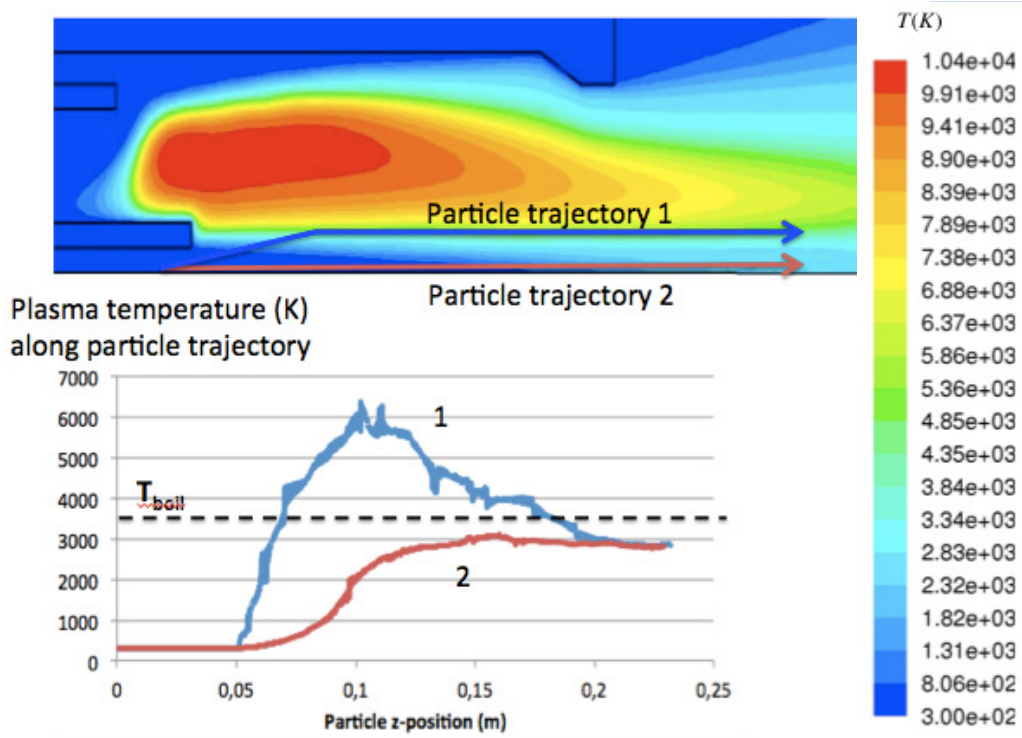
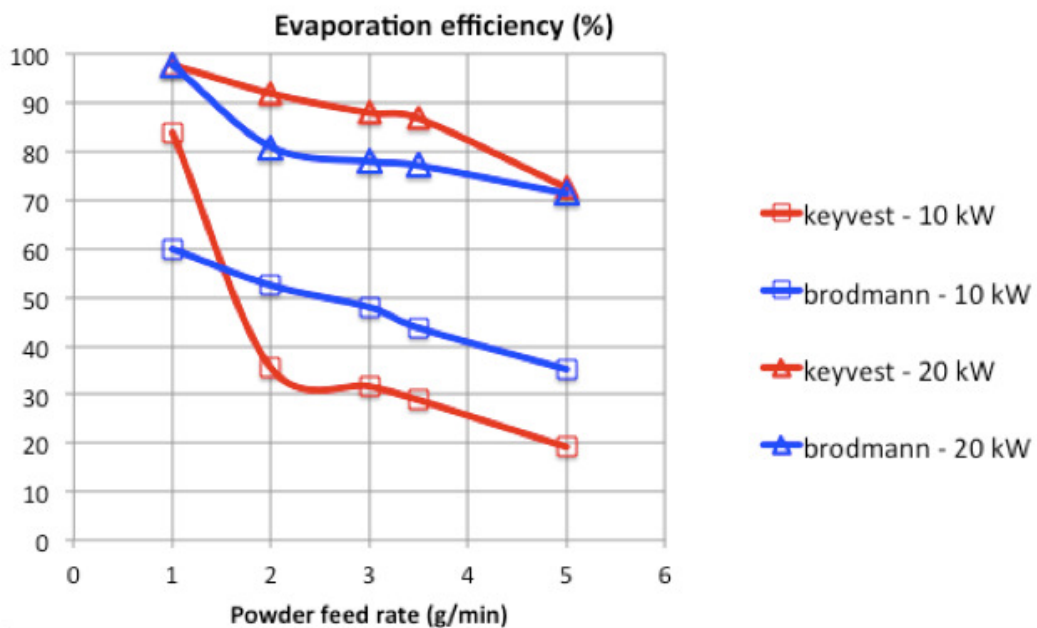


Fig. 2.2.2 Evaporation rate as a function of powder feed rate for different types of precursor and different values of power coupled to the plasma torch.



**Fig. 2.2.3** Temperature field inside the torch in presence of a strong loading effect with two sketched particle trajectories (top); Particle temperature along particle trajectory for a particle passing in the hot plasma region, part. 1, and a particle passing through the cold central channel, part. 2, (bottom).



**Fig. 2.2.4** Evaporation efficiency defined as evaporation rate/precursor feed rate for different precursor types and different values of power coupled to the torch.

### 3D simulations of PL35 torch without injection probe

The idea behind was to inject powder in the hottest part of the plasma for improving heat transfer and evaporation yield or from the bottom to increase the residence time of the precursors in the plasma. For this reason, 3D simulations of PL35 torch without injection probe and a subsequently investigation on the temperature field at the torch outlet (as shown in figure 2.2.5) under different operating conditions (figures 2.2.6, 2.2.7 and 2.2.8) have been carried out.

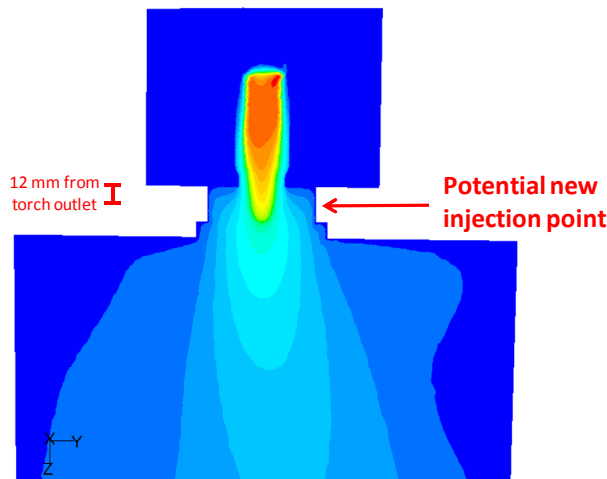


**Figure 2.2.5** Considered position, as potential new injection point, at the torch outlet

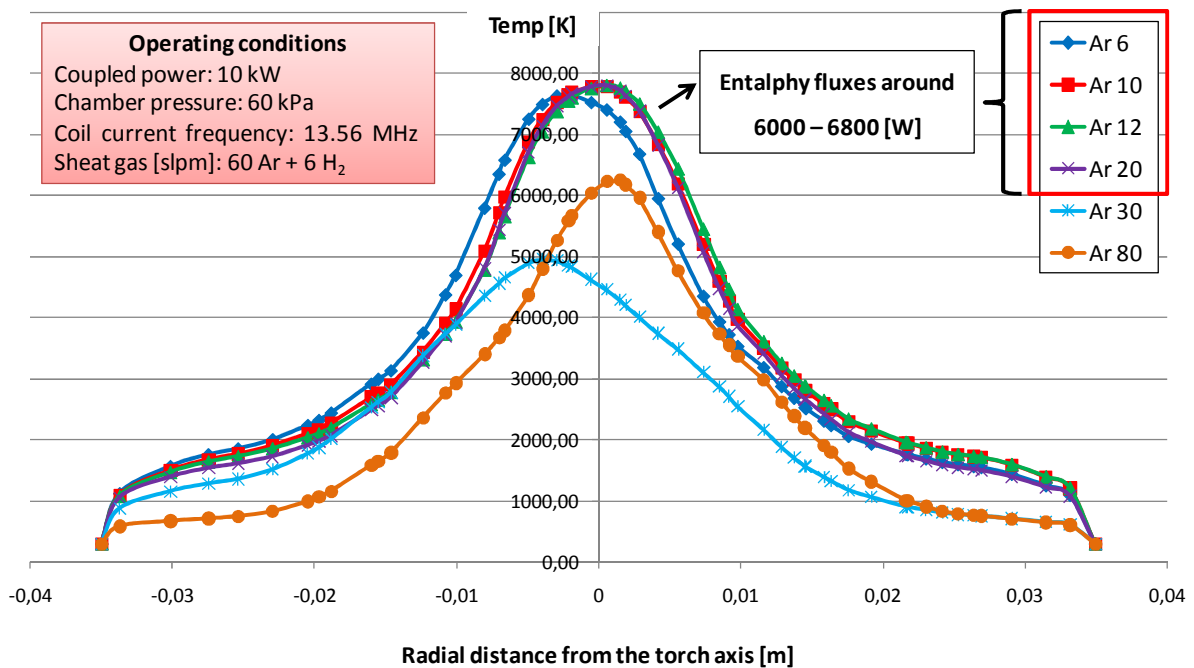


**Figure 2.2.6** Influence of the plasma gas flow rate [slpm] on the temperature radial profile at the new injection point

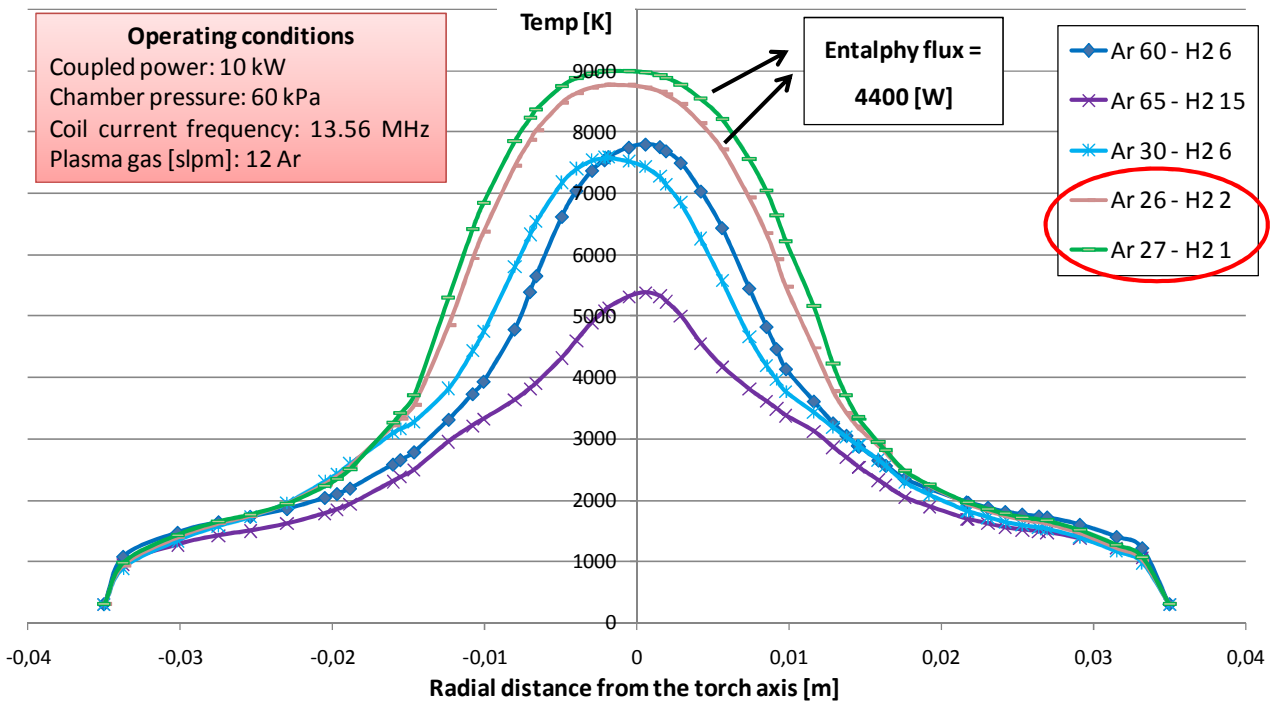


**Figure 2.2.7** Influence of the sheat gas flow rate [slpm] and composition on the temperature radial profile at the new injection point

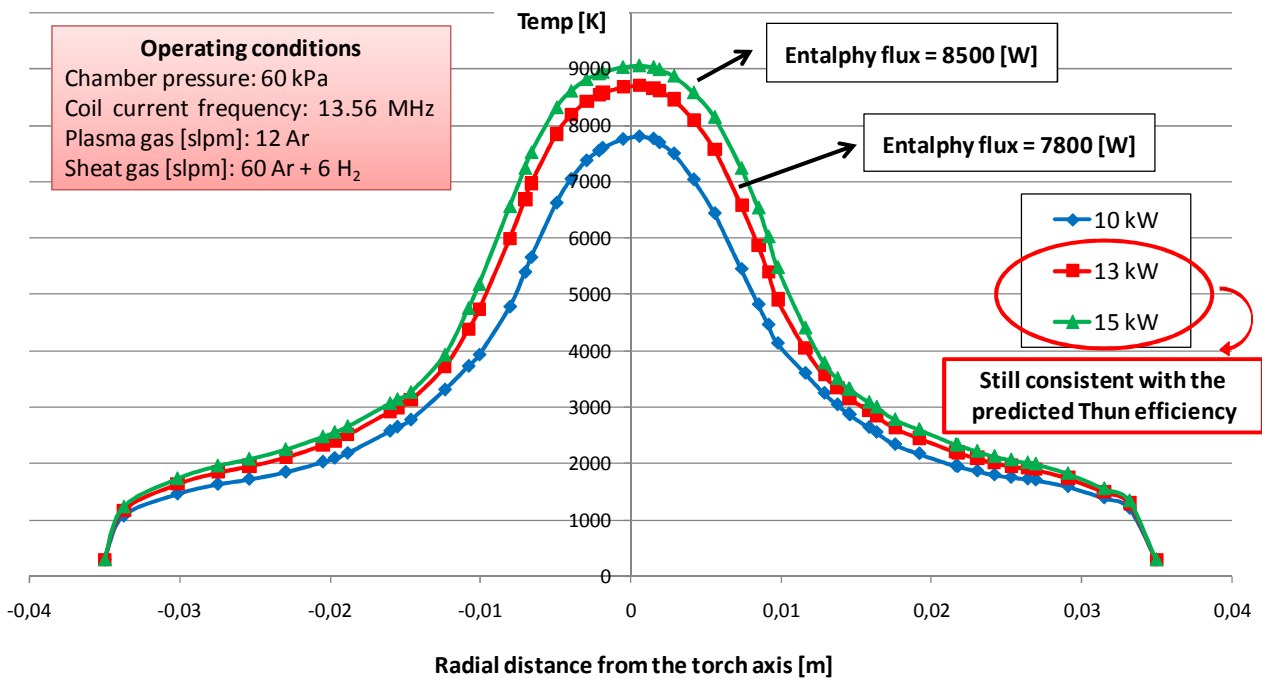


**Figure 2.2.8** Influence of the coupled power [kW] on the temperature radial profile at the new injection point

These preliminary calculations were done in order to understand what happens without the injection probe in the considered position and to identify the operating conditions that maximize the discharge temperature profile at the new injection point with the final aim of identifying some reference conditions to start thinking about a different injection method.

The increase of the plasma gas flow rate gives rise to a proportional increase of the plasma gas tangential component, that leads to:

- an increase of the turbulence in the upper region of the torch; this turbulence increase can significantly modify the velocity field in that region ;
- an increase of the discharge non-axial symmetry.

These phenomena can lead to a displacement of the discharge, very difficult to predict a priori on the basis of the operating conditions. Simulative results show that, in the considered operating conditions, a significant displacement of the discharge takes place with a plasma gas flow rate higher than 20 slpm.

In addition to the radial temperature profile, we could also consider the enthalpy flux at the new injection point, in order to identify the operating conditions that give rise to the best compromise between these two parameters and other design constraints.

## **Conclusions and future developments**

The shown results deal with the characterization of the ICP systems currently used by the project partners. These results will be key inputs for a subsequent phase of designing of a reactor optimized for the nanopowders synthesis and for the up-scaling of the lab-scale process.

A new set of simulations could be useful to evaluate different designs of the reaction chamber in order to identify the optimal solution for avoiding recirculating flows inside the plasma chamber obtaining optimized particle diameter distributions and vapour consumption field.

Moreover, results obtained from simulations of the PL35 torch without injection probe could be an interesting starting point for evaluating alternative solutions for the powders injection.

The estimation of the effect of frequency on particle evaporation, through simulations at 13.56 MHz and 3 MHz for different powder types and different powder feed rates, will be a crucial task for the up-scaling of the lab-scale process. The coil current frequency is, in fact, an important design parameter for the up-scaling of the lab-scale process because it has a strong effect on power distribution inside the plasma torch. Lower frequency induces a more uniform power distribution, which may result in less cooling of the plasma discharge by particle loading. The EMPA system operates at 13.56 MHz but the same torch could be used also with lower frequency, down to about 3 MHz.

In order to increase the value of the critical feed rate for a given process, the use of a dispersion probe to inject the precursor has been suggested by Tekna Plasma Systems: this particular type of torch injects powders with a cone of dispersion realized by means of a secondary gas injected at high velocity near the probe tip through micro-sized holes. It would be interesting to estimate the effect of such technology in the evaporation of Si solid precursor of fixed diameter.

## References

- [1] Sanibondi P 2011 Modelling , diagnostics and transport properties of thermal plasmas for industrial applications *PhD Thesis* (Alma Mater Studiorum Università di Bologna, Italy).